

MICROSCALE APPROACHES TO THE
DESIGN AND OPTIMISATION OF
EQUILIBRIUM CONTROLLED
BIOCONVERSIONS

Murni Binti Halim

A thesis submitted for the degree of
Doctor of Philosophy
to
University College London

Department of Biochemical Engineering
University College London
Torrington Place
London
WC1E 7JE
2012

‘I, Murni Binti Halim, confirm that the work presented in this thesis is my own.
Where information has been derived from other sources, I confirm that this has been
indicated in the thesis.’

ABSTRACT

The widespread use of biocatalysis in industry will require conversions to achieve high space-time yields. For many next generation bioconversions the low thermodynamic equilibrium constant of reactions currently limits their industrial implementation. This thesis aims to establish a series of generic microscale methods for the rapid evaluation of process options to enhance the yield of such equilibrium-controlled bioconversions. These are evaluated based on the asymmetric synthesis of chiral amino alcohols by the CV2025 ω -transaminase (ω -TAm) from *C. violaceum* DSM30191. Using 50 mM each of L-Erythrulose (Ery) as substrate and S- α -methylbenzylamine (MBA) as amino donor the standard yield of the product 2-amino-1,3,4-butanetriol (ABT) is just 26 % (mol.mol⁻¹). This reaction produces acetophenone (AP) as a by-product which is also inhibitory to the CV2025 ω -TAm.

Microscale methods to evaluate four process options for increasing the bioconversion yield were established each operating at 300 μ L volume. The first option involves screening of alternative amino donors to the widely-used MBA. The second couples ω -TAm with an alcohol dehydrogenase (ADH) to convert the inhibitory AP by-product into the non-inhibitory (R)-1-phenylethanol (a glucose dehydrogenase (GDH) is also present to facilitate co-factor recycling). The third approach involves physical *in-situ* product removal (ISPR) of the volatile AP by operation at reduced pressure in a 96-well vacuum manifold. The final approach involves ISPR using polymeric resins, such as the AmberliteTM XAD series, for selective adsorption of AP from the bioconversion medium. For the particular reaction studied here, use of alternative amino donors such as isopropylamine (IPA) enabled a 2.8-fold increase in the reaction yield to 72 % (mol.mol⁻¹) while the second enzyme system, though more expensive to

implement, achieved a 3.8-fold increase in yield and almost quantitative conversion (98 % (mol.mol⁻¹)).

Each of the microscale methods was subsequently implemented as process options in an automated micro-scale process sequence linking biocatalyst production, bioconversion and product analysis. The high throughput potential of the methods was then illustrated using a focused library of ten novel ω -TAMs from various strains. The bioconversion rates and yields of each enzyme were evaluated using a range of alternative amino donors. This highlight one novel ω -TAM, able to utilise L- α -serine as amino donor at improved yield than the CV2025 ω -TAM. This opens up the possibility of engineering whole cell TAM biocatalysts where the normally expensive amino donors are synthesised *in vivo* by normal amino acid metabolism starting from simple, cheap substrates. The microscale methods also enabled rapid optimisation of bioconversion conditions using the second enzyme system. This identified the possibility of reducing by 40-fold the standard concentrations of the co-factor recycling enzymes thus reducing the contribution of the enzymes to the overall Costs of Goods (CoG).

Overall, this work has established an efficient and generic microscale approach to aid bioprocess design and specifically to help increase the yield of equilibrium-controlled bioconversions. The bioconversion rates and yields for the optimised reaction systems were subsequently verified for preparative scale bioconversions.

ACKNOWLEDGEMENTS

It would not have been possible to write this doctoral thesis without the help and support of the kind people around me, to only some of whom it is possible to give particular mention here.

First and foremost I want to thank my supervisor Professor Gary J. Lye. It has been an honour to be his Ph.D. student. I appreciate all his contributions of time, ideas, advice and support to make my Ph.D. experience productive and stimulating. The joy and enthusiasm he has for his research was contagious and motivational for me, even during tough times in the Ph.D. pursuit. I thank also my Ph.D. advisors, Dr. Martina Micheletti and Dr. Frank Baganz for their invaluable advice, help and support during the project.

Above all, I would like to thank my loving husband, Mohd Salleh and my 3 years old son, Adam Rayyan for their faithful support and great patience at all times. My parents, brothers and sisters have given me their unequivocal support throughout, as always, for which my mere expression of thanks likewise does not suffice.

I gratefully acknowledge the funding sources that made my Ph.D. work possible. I was funded by the Ministry of Higher Education (MOHE), Malaysia and International Islamic University Malaysia (IIUM), Malaysia.

I also thank all staff of the Department of Biochemical Engineering, University College London (UCL) for their support and assistance since the start of my previous postgraduate study, MSc Biochemical Engineering in 1997.

My time at UCL was made enjoyable in large part due to the many friends and groups that became a part of my life. I am most grateful to Leonardo Rios and Chuanjie Du for all the collaborative research we did together and making the hard times in the lab become more enjoyable. I would also like to thank all my colleagues and friends at Biochemical Engineering, UCL including Phattaraporn Morris, Homam Al-Bahrani, Raha Rahimi Fard, Shahina Ahmad, Ehsan Esbati, Christopher Grant, Subhas Pradhan, Amanatuzzakiah Abd Halim, Maria Francisca Villegas, Panwanjee Payongsri and Dawid Dreszcz for their kindness, friendship and support.

Also, I acknowledge and would like to thank Elena Pallari for her valuable contributions in the *in-situ* product removal using adsorbent resins studies and Dr. Julio Martinez for the useful information provided on the novel ω -transaminases used in this research.

Last, but by no means least, I thank my friends in Malaysia, United Kingdom, and elsewhere for their support and encouragement throughout. For any errors or inadequacies that may remain in this work, of course, the responsibility is entirely my own.

CONTENTS

Section		Page
	ABSTRACT	3
	ACKNOWLEDGEMENTS	5
	CONTENTS	7
	LIST OF FIGURES	14
	LIST OF TABLES	21
	NOMENCLATURE AND ABBREVIATIONS	23
<hr/>		
1.	INTRODUCTION	27
1.1.	DEVELOPMENT OF CHIRAL PHARMACEUTICALS	27
1.2.	BIOCATALYSIS	32
1.2.1.	Industrial Biocatalysis	32
1.2.2.	Biocatalysis Processes	36
1.3.	CHIRAL AMINES	41
1.4.	TRANSAMINASES (TAMs)	45
1.4.1.	Introduction to TAM	45
1.4.2.	Classification of TAMs	46
1.4.3.	Structure of ω -TAM	47
1.4.4.	ω -TAM for Investigation	47

1.4.5.	ω -TAm Bioconversions	49
1.4.6.	Reaction Mechanism of ω -TAm	51
1.4.7.	Range of Potential of Amino Donors and Amino Acceptors	52
1.4.8.	Asymmetric Synthesis and Kinetic Resolution	56
1.4.9.	ω -TAm Bioconversion Process Challenges	56
1.4.9.1.	ω -TAm Thermodynamic Equilibrium	57
1.4.9.2.	Substrate and Product Inhibitions	58
1.4.10.	Possible Strategies for Improving Reaction Performances	59
1.4.10.1.	<i>In situ</i> product removal (ISPR) methods	59
1.4.10.2.	Alternative Amino Donor	63
1.4.10.3.	Addition of Excess Substrate	63
1.4.10.4.	Auto-Degradation of By-product	63
1.4.10.5.	Enzymatic Cascade / Second Enzyme Reactions	63
1.5.	MICROSCALE HIGH-THROUGHPUT EXPERIMENTATION	64
1.5.1.	Conventional Microwell Plate Platform	64
1.5.2.	Automation Microscale Platform	66
1.6.	AIM AND OBJECTIVES OF THE PROJECT	69

2.	MATERIALS AND METHODS	72
2.1.	Materials	72
2.1.1.	Reagents and suppliers	72
2.1.2.	Media preparation	72
2.1.3.	Agar Plate Preparation	73
2.1.4.	Antibiotic Solution	73
2.1.5.	Glycerol Stocks	74
2.1.6.	Transaminase plasmids	74
2.2.	FERMENTATIONS	75
2.2.1.	Shake Flask Fermentations Using LB Media	75
2.2.2.	Shake Flask Fermentations Using 2xTY Media	76
2.2.3.	7.5 L New Brunswick Bed-batch Fermentation	76

2.3.	BIOCATALYST PREPARATION	77
2.3.1.	Whole Cell and Lysate Forms	77
2.3.2.	Purified Enzymes (His ₆ -tag Purification)	77
2.3.3.	Alcohol Dehydrogenase (ADH)	79
2.3.4.	Glucose Dehydrogenase (GDH)	80
2.4.	SYNTHESIS OF PRODUCT AND DERIVATIZING REAGENT	80
2.4.1.	Chemical Synthesis of ABT Product Standard	80
2.4.2.	Enzymatic Synthesis of ABT	81
2.4.3.	Synthesis of Derivatizing Reagent	82
2.5.	BIOCONVERSION REACTIONS	82
2.5.1.	Microscale Experimental Platform	82
2.5.2.	Preparative Scale Bioconversions	84
2.5.3.	Second Enzyme Reaction	84
2.5.4.	Reduced Pressure Reaction	85
2.5.5.	ISPR Resin Adsorption Isotherms and Bioconversions	86
2.5.6.	Automated Microscale Bioconversion Processes	88
2.6.	ANALYTICAL METHODS	90
2.6.1.	Dry Cell Weight (DCW) Measurement	90
2.6.2.	Optical Density Measurements for Biomass Quantification	90
2.6.3.	Bradford Assay Total Protein Quantification	91
2.6.4.	Purified Enzyme Quantification by UV Absorbance	91
2.6.5.	SDS-PAGE Electrophoresis	91
2.6.6.	HPLC Methods	93
2.6.7.	Mass Spectrometry	94
<hr/>		
3.	MICROSCALE QUANTIFICATION OF ω- TRANSAMINASE KINETICS	95
3.1.	INTRODUCTION	95
3.2.	AIM AND OBJECTIVES	97

3.3.	ω-TRANSAMINASE PRODUCTION AND LYSATE PREPARATION	97
3.3.1.	CV2025 ω -TAm Production at Shake Flask and 7.5 L Bioreactor Scales	97
3.3.2.	Characterization of CV2025 ω -TAm Synthesis	101
3.3.3.	Influence of Pyridoxal 5' Phosphate (PLP) Addition	103
3.3.4.	Stability of Stored and Fresh Cells Lysate	105
3.4.	IDENTIFICATION OF LEAD ω-TRANSAMINASE AND INITIAL BIOCONVERSION CONDITIONS	107
3.4.1.	Activity of His-tagged (PQR801) and non His-tagged (PQR800) CV2025 ω -TAm	107
3.4.2.	Activity Determination at Laboratory and Microwell Scales	109
3.4.3.	Influence of pH	110
3.5.	L-ERYTHRULOSE (ERY) BIOCONVERSION KINETICS	113
3.5.1.	Kinetic Profile of CV2025 ω -TAm Bioconversion	113
3.5.2.	Influence of Biocatalyst Form: Clarified Lysate and Whole Cells	114
3.6.	SUMMARY	117

4.	MICROSCALE PROCESS OPTIONS TO INCREASE ω-TAm BIOCONVERSION YIELDS	119
4.1.	INTRODUCTION	119
4.2.	AIM AND OBJECTIVES	120
4.3.	STANDARD CV2025 ω -TAM BIOCONVERSION KINETICS AND YIELD	121
4.4.	EVALUATION OF ALTERNATIVE AMINO DONORS	122
4.5.	SECOND ENZYME SYSTEM	128
4.6.	PHYSICAL ISPR METHOD: OPERATION AT	133

	REDUCED PRESSURE	
4.7.	PHYSICAL ISPR METHOD: APPLICATION OF ADSORBENT RESINS	136
4.7.1.	Equilibrium Adsorption Isotherms	139
4.7.2.	CV2025 ω -TAm Bioconversions with ISPR by Adsorptive Resins	143
4.8.	SUMMARY	146
<hr/>		
5.	AUTOMATION AND PARALLEL OPERATION OF MICROSCALE PROCESS OPTIONS	148
5.1.	INTRODUCTION	148
5.2.	AIM AND OBJECTIVES	149
5.3.	CHARACTERISATION OF ω -TRANSAMINASE LIBRARY	150
5.3.1.	Parallel <i>E.coli BL21 (DE3) Gold</i> Batch Growth Kinetics	150
5.3.2.	Quantification of ω -TAm and Host Cell Protein Production	152
5.4.	BIOCONVERSION AUTOMATION PLATFORM DESIGN AND DEVELOPMENT	155
5.4.1.	Overview of the Tecan Platform	155
5.4.2.	Preliminary Bioconversion Automation Platform Evaluation	156
5.5.	PARALLEL EVALUATION OF ALTERNATIVE AMINO DONORS	157
5.6.	OPTIMIZATION OF SECOND ENZYME REACTION CONDITION	163
5.6.1.	Parallel CV2025 ω -TAm Bioconversions with Second Enzyme Reaction Using Alcohol Dehydrogenase (ADH) from <i>Lactobacillus Kefir</i>	163
5.6.2.	Parallel CV2025 ω -TAm Bioconversions with a Second Enzyme Reaction Using Alcohol Dehydrogenase (ADH)	166

	from <i>Thermoanaerobium Brockii</i>	
5.6.3.	Economic Considerations of Second Enzyme Reactions	169
5.7.	PARALLEL EVALUATION OF REDUCED PRESSURE REACTION	170
5.7.1.	The Design of Reduced Pressure System Automation Platform	170
5.7.2.	Parallel CV2025 ω -TAm Bioconversions at Reduced Pressure	171
5.8.	SUMMARY	176
<hr/>		
6.	PREPARATIVE SCALE VERIFICATION OF MICROSCALE BIOCONVERSION KINETICS	178
6.1.	INTRODUCTION	178
6.2.	AIM AND OBJECTIVES	179
6.3.	VERIFICATION OF OPTIMISED SECOND ENZYME REACTION CONDITIONS	179
6.4.	VERIFICATION OF THE USE OF ALTERNATIVE AMINO DONORS AND ω -TRANSAMINASES: L- α -SERINE AS AMINO DONOR	184
6.4.1.	Transamination of Ery Using L- α -serine by BSU09260_1971 ω -TAm in Clarified Lysate Form	184
6.4.2.	Transamination of Ery Using L- α -serine by BSU09260_1971 ω -TAm in Purified Form	187
6.5.	CONFIRMATION OF ABT PRODUCT SYNTHESIS	190
6.6.	SUMMARY	191
<hr/>		
7.	CONCLUSIONS AND FUTURE WORK	193
7.1.	SUMMARY OF PROJECT ACHIEVEMENTS	193

7.2.	FUTURE WORK	196
-------------	--------------------	------------

8	REFERENCES	198
----------	-------------------	------------

Appendix I	CALIBRATION PLOT OF BIOMASS IN FUNCTION OF OD₆₀₀	215
-------------------	------------------------------------------------------------------------	------------

Appendix II	BRADFORD ASSAY CALIBRATION	216
--------------------	-----------------------------------	------------

Appendix III	HPLC STANDARD CALIBRATIONS AND CHROMATOGRAMS	217
---------------------	---------------------------------------------------------	------------

Appendix IV	TECAN SCRIPTS	224
--------------------	----------------------	------------

Appendix V	MASS SPECTROMETRY CHROMATOGRAMS	242
-------------------	----------------------------------------	------------

LIST OF FIGURES

- Figure 1.1.** The chemical structures of (S)-ibuprofen and (S)-ketoprofen drugs.
- Figure 1.2.** Top 5 cardiovascular drugs in 2002.
- Figure 1.3.** Distribution of worldwide-approved drugs according to chirality character in the period 1983–2002.
- Figure 1.4.** (a) Multistep chemical and (b) protecting group-free biocatalytic strategies in an aldo reaction.
- Figure 1.5.** Complex drug compounds with multiple chiral centres and the biocatalytic step(s) associated with the development of each synthetic route.
- Figure 1.6.** Comparison of the old (chemical) and the new (enzyme) process for the hydrolysis of penicillin G.
- Figure 1.7.** Time-dependence of equilibrium and kinetically controlled processes catalysed by enzymes.
- Figure 1.8.** Classification of biocatalytic processes with enzymes as biocatalysts.
- Figure 1.9.** Examples of peptidomimetic drugs.
- Figure 1.10.** Kinetic resolution in the esterification reaction of racemic mandelic acid with optically active (-)-menthol to a pair of diastereomeric esters.
- Figure 1.11.** Reaction scheme of the kinetic resolution via ω -TAm starting with racemic (rac) amines is limited by 50 % maximum yield.
- Figure 1.12.** Reaction scheme of the asymmetric synthesis of prochiral ketones via ω -TAm with theoretically a 100% yield if the equilibrium can be shifted appropriately.
- Figure 1.13.** Structure of the protease inhibitor drug NelfinavirTM.

- Figure 1.14.** Ribbon structure of homodimeric ω -TAm from *V. fluvialis* JS17.
- Figure 1.15.** Two-Binding Site Model of ω -TAm from *V. fluvialis* showing (a) binding of the amino donor and (b) the binding of the amino acceptor.
- Figure 1.16.** General reaction scheme of a TAm reaction where an amino group is transferred to a carbonyl group.
- Figure 1.17.** Reaction scheme of the ω -transamination (ω -TAm) bioconversion between (S)- α -methylbenzylamine (MBA) and pyruvate to acetophenone (AP) and L-Alanine in the presence of co-factor pyridoxal 5'-phosphate (PLP).
- Figure 1.18.** Schematic representation of the ping pong bi-bi ordered reaction mechanism used of ω -TAm.
- Figure 1.19.** Schematic diagram of ω -transamination. E-PLP and E-PMP represent a complex between ω -transaminase and pyridoxal 5-phosphate and a complex between ω -transamination and pyridoxamine phosphate respectively.
- Figure 1.20.** Transketolase catalysed condensation of glycolaldehyde with β -hydroxypyruvate to yield L-erythrulose with the evolution of carbon dioxide.
- Figure 1.21.** Reaction scheme of ω -transamination in biphasic system. Image reproduced from Shin and Kim (1997).
- Figure 1.22.** Diagram representation of individual microwell formats.
- Figure 1.23.** Capabilities framework for the industrial adoption of high-throughput technologies.
-
- Figure 2.1.** Cap for 96-microwell plate used for bioconversions.
- Figure 2.2.** Preparative scale worktable layout used for ω -TAm bioconversions with second enzyme system (Section 6.3) and L- α -serine alternative amino donors (Section 6.4).
- Figure 2.3.** Diagram of system used for bioconversion at reduced pressure.
- Figure 2.4.** Tecan Genesis robotic platform.
-

- Figure 3.1.** Reaction yield scheme of the CV2025 ω -TAm catalyzed transamination between (S)- α -methylbenzylamine (MBA) and pyruvate to acetophenone (AP) and L-Alanine in the presence of co-factor, pyridoxal-5-phosphate (PLP).
- Figure 3.2.** Growth kinetic profiles for *E.coli* BL21 (DE3) Gold cells containing plasmid pQR801 in a 2 L shake flask and a 7.5 L bioreactor fermentation scales with fed-batch operation.
- Figure 3.4.** SDS-PAGE gels showing intracellular expression of CV2025 ω -TAm in cellular extracts of *E. coli* BL21 (DE3)-Gold cells.
- Figure 3.5.** Bioconversion kinetics of CV2025 ω -TAm clarified lysates obtained from 2 L shake flask and 7.5 L bioreactor fermentation (Section 3.3.1)
- Figure 3.6.** Bioconversion kinetics using either fresh or stored clarified CV2025 ω -TAm lysates (6 months at -80°C).
- Figure 3.7.** Bioconversion kinetics of CV2025 ω -TAm clarified lysates prepared using plasmids pQR 800 (non His-tagged) and pQR801 (His-tagged).
- Figure 3.8.** Bioconversion kinetics for CV2025 ω -TAm clarified lysate performed in glass vials and 96-well glass microplate formats.
- Figure 3.9.** Effect of pH on the initial rate of AP production by clarified CV2025 ω -TAm lysate and whole cells of *E. coli* with plasmid pQR801 expressing CV2025 ω -TAm.
- Figure 3.10.** Reaction yield scheme of the CV2025 ω -TAm catalyzed transamination between (S)- α -methylbenzylamine (MBA) and L-erythrulose (Ery) to acetophenone (AP) and 2-amino-1,3,4-butanetriol (ABT) in the presence of co-factor pyridoxal-5-phosphate (PLP).
- Figure 3.11.** Bioconversion kinetics using CV2025 ω -TAm clarified lysate with Ery as amino acceptor.
- Figure 3.12.** Bioconversion kinetics of CV2025 ω -TAm in whole cell and clarified lysate forms.

Figure 4.1. Overview of potential process options to increase the yield of equilibrium-controlled ω -TAm bioconversions.

Figure 4.2. Process options investigated in this work at microwell scale to overcome thermodynamic and equilibrium limitations of the

CV2025 ω -TAm bioconversion.

- Figure 4.3.** Quantification of product inhibition effects by AP.
- Figure 4.4.** Effect of alternative amino donors on ABT product formation kinetics for the profile of CV2025 ω -TAm clarified lysate bioconversions of Ery with alternative amino donors (Section 4.4).
- Figure 4.5.** Influence of second enzyme system on ω -TAm bioconversion kinetics.
- Figure 4.6.** ω -TAm bioconversion kinetics using the second enzyme system at increased buffer concentrations.
- Figure 4.7.** Average water evaporation kinetics across a 300 μ L plate operated at 30 °C under reduced pressure and 5 torr pressure.
- Figure 4.8.** Mathematical equations for prediction of evaporation rate constant.
- Figure 4.9.** ω -TAm bioconversion kinetics for operation at reduced pressure.
- Figure 4.10.** Equilibrium adsorption isotherms on XAD 7 resin.
- Figure 4.11.** Equilibrium adsorption isotherms on XAD 1180 resin
- Figure 4.12.** Equilibrium adsorption isotherms on XAD 16 resin.
- Figure 4.13.** Influence of ISPR adsorbent resin selection on ω -TAm bioconversion kinetic profiles performed with three ISPR adsorption resins XAD 7; XAD 1180; XAD 16 system (Section 4.7.2) and ω -TAm whole cell standard reaction (Section 3.5.2).
-
- Figure 5.1.** Batch growth kinetics for *E.coli* BL21 (DE3) Gold strains each expressing different ω -TAm plasmids cultured in 2xTY media.
- Figure 5.2.** SDS-PAGE analysis showing expression of the library of novel ω -TAm enzymes compared to the CV2025 ω -TAm (pQR801).
- Figure 5.3.** Detail of the robotic platform used for ω -TAm bioconversions with alternative amino donors (Section 5.5) and second enzyme system (Section 5.6).
- Figure 5.4.** Comparison of automated and manual microwell methods for bioconversion kinetics of CV2025 ω -TAm (pQR801).

- Figure 5.5.** Summary of measured bioconversion kinetics of the ω -TAm library on the microscale automation platform (Section 5.5) using alternative amino donors.
- Figure 5.6.** Bioconversion kinetics of CV2025 ω -TAm (pQR801) using the second enzyme system with various ratios of ADH, GDH and glucose (as described in Table 5.2).
- Figure 5.7.** Bioconversion kinetics of CV2025 ω -TAm (pQR801) using the second enzyme reaction with ADH from *Lactobacillus kefir* and Glucose limitation on the microscale automation platform (Section 5.6.1).
- Figure 5.8.** Bioconversion kinetics of CV2025 ω -TAm (pQR801) using second enzyme reaction with various ratios of ADH, GDH and glucose (as described in Table 5.2).
- Figure 5.9.** Detail of the robotic platform used for CV2025 ω -TAm standard bioconversions with reduced pressure system using a Te-VacS vacuum separator (Section 5.7).
- Figure 5.10.** Microwell evaporation kinetics of water at 23 °C in the automated reduced pressure system (Section 5.7).
- Figure 5.11.** Bioconversion kinetics of CV2025 ω -TAm (pQR801) performed at reduced pressure on microscale automated platform and manual method.
-
- Figure 6.1.** Comparison of preparative scale (Section 6.3) and automated microwell platform (Section 5.6.1) for bioconversion kinetics of CV2025 ω -TAm (pQR801) with second enzyme reaction using ADH from *Lactobacillus kefir*.
- Figure 6.2.** Reaction scheme of the BSU09260_1971 ω -TAm from *Bacillus subtilis* (pQR960) catalysed transamination between L- α -serine and L-erythrulose (Ery) to β -hydroxypyruvic acid and 2-amino-1,3,4-butanetriol (ABT) in the presence of co-factor pyridoxal-5-phosphate (PLP).
- Figure 6.3.** Comparison of preparative scale (Section 6.4.1) and automated microwell platform (Section 5.5) for bioconversion kinetics of BSU09260_1971 ω -TAm (pQR960) in clarified lysate form with L- α -serine as an alternative amino donor.
- Figure 6.4.** SDS-PAGE gel showing expression of the BSU09260_1971 ω -transaminase in cellular extracts of *E. coli* BL21 (DE3)-Gold cells.

Figure 6.5. Preparative scale bioconversion kinetics of purified BSU09260_1971 ω -TAm (pQR960) using L- α -serine as amino donor.

Figure A.I.1. Calibration graph of biomass in $\text{g}_{\text{dcw}} \cdot \text{L}^{-1}$ as a function of OD_{600} (Section 2.6.2).

Figure A.II.1. Standard graph for Bradford assay of BSA concentration as a function of OD_{595} (Section 2.6.3).

Figure A.III.1. Calibration graph of L-Erythrulose (Ery) concentration as a function of HPLC area (Section 2.6.6).

Figure A.III.2. HPLC chromatogram of Ery. The peak retention time is at 11.63 min. (Section 2.6.6).

Figure A.III.3. Calibration graph of derivatized 2-amino-1,3,4-butanetriol (ABT) concentration as a function of HPLC area (Section 2.6.6).

Figure A.III.4. HPLC chromatogram of derivatized ABT (Section 2.6.6). The peak retention time is at 8.9 min.

Figure A.III.5. Calibration graph of derivatized L- α -Serine concentration as a function of HPLC area (Section 2.6.6).

Figure A.III.6. HPLC chromatogram of derivatized L- α -Serine (Section 2.6.6). The peak retention time is at 7.3 min.

Figure A.III.7. Calibration graph of Pyruvate concentration as a function of HPLC area (Section 2.6.6).

Figure A.III.8. HPLC chromatogram of pyruvate (Section 2.6.6). The peak retention time is at 10.43 min.

Figure A.III.9. Calibration graph of Acetophenone (AP) concentration as a function of HPLC area (Section 2.6.6).

Figure A.III.10. HPLC chromatogram of AP (Section 2.6.6). The peak retention time is at 7.28 min.

Figure A.III.11. Calibration graph of (R)-1-phenylethanol concentration as a function of HPLC area (Section 2.6.6).

Figure A.III.12. HPLC chromatogram of (R)-1-phenylethanol (Section 2.6.6). The peak retention time is at 6.45 min.

Figure A.III.13. Calibration graphs of (S)- α -Methylbenzylamine (MBA) concentration as a function of HPLC area (Section 2.6.6).

- Figure A.III.13.** HPLC chromatogram of MBA (Section 2.6.6). The peak retention time is at 3.4 min.
- Figure A.IV.1.** Parallel evaluation of alternative amino donors (Section 5.5).
- Figure A.IV.2.** Optimization of second enzyme reaction condition (Section 5.6).
- Figure A.IV.3.** Parallel evaluation of reduced pressure reaction (Section 5.7).
- Figure A.IV.4.** Bioconversion reactions samples centrifugation step prior HPLC analysis (Sections 5.5, 5.6 and 5.7).
- Figure A.V.1.** Chemical ionization (CI) mass spectrometry analysis for reaction mixture with ABT produced from CV2025 ω -TAm bioconversion of MBA and Ery with second enzyme reaction using ADH from *Lactobacillus kefir* (Section 6.3).
- Figure A.V.2.** Chemical ionization (CI) mass spectrometry analysis for reaction mixture with ABT produced from BSU09260_1971 ω -TAm bioconversion of L- α -serine and ERY (Section 6.4.1)

LIST OF TABLES

Table 1.1. Specificity of CV2025 ω -transaminase towards various amino donors. Image reproduced from Kaulmann et al. (2007).

Table 1.2. Specificity of CV2025 ω -transaminase towards various amino acceptors. Image reproduced from Kaulmann et al. (2007).

Table 1.3. Examples of industrial *in situ* product removal research. Image reproduced from Lye and Woodley (1999).

Table 2.1. Composition of the LB-glycerol medium used in *E. coli* fermentations for expression of ω -transaminases obtained from plasmids pQR800 and pQR801.

Table 2.2. Composition of the 2xTY medium used in *E. coli* fermentations for expressions of ω -transaminases obtained from plasmids pQR426, pQR813, pQR956, pQR960, pQR978, pQR985, pQR1010, pQR1014, pQR1017, pQR1019.

Table 2.3. List of ω -TAm novel library.

Table 2.4. His₆-tag enzyme purification buffers used for affinity purification (Section 2.3.1.2).

Table 2.5. The chemical and physical properties of commercially available absorbents investigated in this work.

Table 2.6. Specifications of Te-VacS (<http://www.tecan.com>) used in Section 5.7.

Table 2.7. Composition of 1 x TEO buffer used in Section 2.6.5.

Table 4.1. Amino donors selected for study on the equilibrium yield of Ery tansamination by CV2025 ω -TAm.

- Table 4.2.** Isotherms expression for single component solutions.
- Table 4.3.** The mathematical relationships fitted to the adsorption isotherm data for adsorption of AP (in a mixed solution with Ery) and AP alone.
- Table 4.4.** The mathematical relationships fitted to the adsorption isotherm data for adsorption of Ery (in a mixed solution with AP) and Ery alone.
- Table 4.5.** List of productivity of the investigated process options and number of fold increases as comparison to standard CV2025 ω -TAm reaction.
-

- Table 5.1.** Properties of the cloned ω -TAm library and expression levels.
- Table 5.2.** Summary of parameters investigated for CV2025 ω -TAm bioconversions using the second enzyme system on the automated platform.
- Table 5.3.** Activity and prices of the various ADHs used in Sections 5.6.1 and 5.6.2.
-

- Table 6.1.** Comparison of reaction conditions used for preparative scale verification of bioconversion kinetics optimised at the microscale.

NOMENCLATURE AND ABBREVIATIONS

ABT	(2S,3R)-2-amino-1,3,4-butanetriol
ADH	Alcohol dehydrogenase
ADH-TB	Alcohol dehydrogenase from <i>Thermoanaerobium brockii</i>
AP	Acetophenone
AQC	6-aminoquinolyl-N-hydroxysuccinimidyl carbamate
BSA	Bovine serum albumin
C	liquid phase concentration at equilibrium (g.l^{-1})
C_i	initial liquid phase concentration(g.l^{-1})
Cl	Chloride
CV20205	<i>Chromacterium Violaceum</i> 20205
<i>C. violaceum</i>	<i>Chromacterium Violaceum</i>
d_B	Width of baffle (mm)
DCW	Dry cell weight
d_i	Diameter of impeller (mm)
DiTi	Tecan disposable tip
DOT	Dissolved oxygen tension (%)
d_T	Diameter of vessel (mm)
ϵ	Extinction coefficient
<i>E. coli</i>	<i>Escherichia coli</i>
EDTA	Ethylenediaminetetraacetic acid
E-PLP	Transaminase –PLP complex
E-PMP	Transaminase –PMP complex
Ery	L-erythrulose
λ	Path length equal to 1 cm

g	Gram
g_{ads}^{-1}	Equilibrium solid phase concentration of the solute in solution
g_{dew}	Grams of dry cell weight
GDH	Glucose dehydrogenase
H_3PO_4	Phosphoric acid
HCl	Hydrogen chloride
HEPES	N-2-hydroxyethylpiperazine-N'-ethanesulphonic acid
His ₆ -tag	6x histidine- tagged
HPA	Hydroxypyruvate
HPLC	High pressure liquid chromatography
hr	hour
IMAC	Immobilized metal-ion affinity chromatography
IPA	Isopropylalcohol
IPTG	Isopropyl β -D-1-thiogalactopyranoside
ISPR	<i>In situ</i> product removal
K	Thermodynamic equilibrium constant
kDa	Kilo Dalton
kg	Kilogram
K _i	Inhibition concentration
L	Litre
l	Liquid phase
LB	Luria Bertani
LiHa	Tecan handling arm / liquid handler
M	Molar
<i>M</i>	mass of wetted adsorbent in the experiment (g)
m	meter
MBA	(S)- α -Methybenzylamine
mbar	milibar
MeOH	Methanol
Mg^{2+}	Magnesium ion
$MgCl_2$	Magnesium chloride
mg	Milligram
min	Minute

mL	Millilitre
mM	Millimolar
mm	Milimeter
mmol	Millimol
n	Nano
N	Nitrogen
NaCl	Sodium Chloride
NADP ⁺	Nicotinamide adenine dinucleotide phosphate
NADPH	Reduced form of nicotinamide adenine dinucleotide phosphate
NaOH	Sodium Hydroxide
NH ₃	Ammonia
NH ₄ OH	Ammonium Hydroxide
OD ₆₀₀	Optical density at 600 nm
PLP	Pyridoxal 5'phospahte
PMP	Pyridoxamine phosphate
PPG	Polypropylene glycol
PTFE	Polytetrafluoroethylene
<i>q</i>	Equilibrium solid phase concentration of the solute (gg _{ads} ⁻¹)
RO	Reverse osmosis
RoMa	Tecan manipulator arm
rpm	Revolutions per minute
SA	Static surface area
SDS-PAGE	Sodium dodecyl sulfate polyacrylamide gel electrophoresis
TAm	Transaminase
TAm BSU09260_1971	ω-Transaminase from <i>Bacillus subtilis</i>
TFA	Trifluoroacetic acid
Te-VacS	Tecan vacuum manifold
TLC	Thin Layer Chromatography
U	Units of enzyme activity (μmolmin ⁻¹)
μL	Microlitre
μm	Micrometer
μmol	Micromole
UV/Vis	Ultra violet / visible

V	Volume (L)
<i>V.fluvialis</i>	<i>Vibrio Fluvialis</i>
v/v	Volume by volume
V _w	Total well volume
W	Watt
Wt	Wilde type
w/v	Weight by volume
XAD 7	Synthetic polymeric resins
XAD 16	Synthetic polymeric resins
XAD 1180	Synthetic polymeric resins
ω-TAm	ω-transaminase
°C	Degree Celsius
ΔG	Gibbs free energy
2xTY	<i>E. coli</i> rich media

1. INTRODUCTION AND AIMS OF THE PROJECT

1.1. DEVELOPMENT OF CHIRAL PHARMACEUTICALS

In pharmacology, chirality is an important factor in drug efficacy. Therefore, attaining enantiomerically pure intermediates and products efficiently and economically is of immense importance in industry (Sanchez and Demain, 2011). Pharmaceuticals with an asymmetric carbon (chiral centre) are termed chiral drugs which often present as the racemate (mixture of equal amounts of left and right-handed enantiomers). In an achiral environment, two enantiomers in a racemate show identical physical and chemical properties but in a chiral environment (i.e. *in vivo*), they demonstrate different chemical, biochemical, and pharmacologic behaviours. In the past decades, single-enantiomer drugs have been thought to be preferable to racemates due to the lack of technologies for single-enantiomers synthesis. Nevertheless, after the recognition that two enantiomers of the same compound can have different pharmacological activities and the emergence of new technologies of asymmetric synthesis and chiral separation, it has made it possible for pharmaceutical companies to develop single-enantiomer drug (Shimazawa et al., 2008). Furthermore, it is now an obligatory by the regulatory bodies that characterisation of the single optical isomers of a chiral drug compound is carried out before licensing a drug for the marketplace (FDA, 1992).

Subsequently, many single-enantiomers drugs have been approved and marketed with the worldwide market share of these drugs increased from 27 % in 1996 to 39 % in 2002 (Shimazawa et al., 2008). For example, Verapamil is a drug where the (*S*)-enantiomer is used to alleviate high blood pressure, whilst the (*R*)-enantiomer is used

to inhibit the resistance of cancer cells to chemotherapy agents (Wainer, 1993). Other examples are (S)-Ibuprofen and (S)-Ketoprofen which are the chiral switch drugs of the popular racemates (Figure 1.1). These drugs are the most numerous classes of non-steroidal anti-inflammatory drugs that are widely used for the treatment of inflammatory diseases, such as rheumatoid arthritis, as both analgesics and antipyretics. However, the racemates are responsible for many adverse reactions such as reactions affecting a range of organs, including the gastrointestinal tract, kidney, bone marrow, and liver systems. Therefore, with the combination of the stereospecificity of action with the configurationally inversion reaction have provided drug companies a rationale for the use of the (S)-enantiomers of these drugs in therapy, as this reduces the total dose and reduces the toxicity that is associated with the (R)-enantiomer (Leffingwell, 2003; Kelley et al., 1992).

Figure 1.2 further shows the importance of chiral drugs. Of the top five selling cardiovascular drugs, four are sold as single enantiomers (Lipitor®, Zocor®, Pravacol® and Vasotec®) while the fifth (Norvasc®) is a racemate which potentially may be important as the single (R)-(+)-enantiomer (Leffingwell, 2003; Zhang et al., 2002). An overall look at the 20 year period from 1983–2002 of worldwide approved drugs, according to chirality (Figure 1.3) indicates that single-enantiomers surpassed achirals whereas racemates represented the minority category at 23 % of worldwide approved drugs (Caner et al., 2004).

All these examples provide an insight into a number of chiral chemicals with significant pharmacological activity. A single enantiomer formulation would have higher potency and thus require lower dosages, subsequently reducing the potential side effects of the drug (Stinson, 1994). Similarly, in the agro-chemical industry, single enantiomer compounds may reduce application volumes thus reducing cost and lessening the environmental impact (Breuer et al., 2004).

(S)-Ibuprofen

(S)-Ketoprofen

Figure 1.1. The chemical structures of (S)-ibuprofen and (S)-ketoprofen drugs. Image reproduced from Leffingwell (2003).

Figure 1.2. Top 5 cardiovascular drugs in 2002. Sources: Nat. Rev. Drug Disc. 2(4), 344 (2003); Chem. & Eng. News 81(18), 48 (2003). Image reproduced from Leffingwell (2003).

Figure 1.3. Distribution of worldwide-approved drugs according to chirality in the period 1983–2002. *Including diastereomeric mixtures. Image reproduced from Caner et al. (2004).

It is estimated that pharmaceutical companies spend approximately \$ 0.8 to 1.3 billion US for drug discovery per new compound (Schmidt and Blaser, 2003), which consequently putting an enormous economic pressure. The technology harnessed, to both develop and manufacture a drug, therefore, needs to be cost effective, rapid and sustainable. Additionally the competition from the drug candidates of other companies requires the timely development of a drug to minimise the time to market. Nevertheless, the emphasis of either time or cost depends on the phase of development of a candidate drug (Yazbeck et al., 2004).

Primarily, during the discovery phase of a candidate compound, when small amounts of material, i.e 10 mg – 100 g are required, it is the time taken to produce material for further investigation and characterisation of pharmacological properties that are vital. Later on, when process development is being carried out, and production at the kilogram and potentially the ton-scale, is required, process cost and sustainability become the defining parameters. A cost effective process requires conversion at the highest possible yield with the minimum of side products utilising materials that are

affordable and available from reliable sources. The cost of goods is impacted by the value of process reagents. This includes both the starting materials and reagents used in each processing step, thus the number of processing steps can significantly increase overall costs. Productivity includes the output for time spent in the factory, which defines how many processing cycles can be completed in a given time, as well as the overall process yield. Overall product yield is also impacted on by the number of processing steps since yield losses will be incurred at each stage. The process developed is further limited by the sustainability of supply of materials, the availability of suitable facilities for operating the process, and in an age where the environmental issues are an important factor, the production and disposal of waste streams must be accounted for. Additionally, intellectual property issues may prevent the use of certain technologies in a commercial process.

The synthesis of optically pure products is often multi-step, employing complex chemistry and producing low product yields. The increase in complexity and subsequent cost of the production of homochiral compounds, versus racemates, has led to the development of several 'toolboxes' for asymmetric synthesis (Yazbeck et al., 2004). The approaches include asymmetric chemocatalysis, use of a precursor from a chiral pool, crystallisation of diastereomeric salts, biocatalysis, and chromatographic separation. The use of asymmetric chemocatalysis is an attractive option, particularly for hydrogenation reactions, although the scope of this technique may be limited by the commercial availability of catalyst, patent restrictions and the rarity of broad spectrum catalysts. Resolutions of racemic mixtures may be carried out by direct crystallisation, diastereomeric crystallisation, chromatography or enzyme kinetic resolution. These techniques, however, usually result in at least a 50 % yield loss, but higher yields may be possible by the introduction of a re-racemisation step, of the unwanted isomer, into the process (Park et al., 2002). Crystallisation faces limitations due to the lack of development of efficient high throughput screening methods. However, the generation of homochiral salts does result in ease of downstream processing. Chromatography faces high costs due to large waste streams and high cost of resins and scalability. Another approach to the synthesis of complex chiral compounds is the use of chiral synthons at the beginning of the synthesis. These are relatively simple enantiomerically pure starting compounds which provide the desired chirality in the reactions that follow. The selection of a

chiral precursor from an existing chiral pool of compounds may be limited by the chemicals available, with the majority of commercial chiral molecules (being both cost effective as a precursor molecule and available at suitable quantities) being amino acids and simple carbohydrates.

Additionally, the trend for new chiral pharmaceutical reagents is constantly developing due to the fact that the human body functions using chiral catalysis (Pollard and Woodley, 2006). Nature itself has demonstrated biological catalysts to have a role in the production of chiral molecules. For example, simple carbohydrates can serve as chiral starting materials for the synthesis of more complex molecules (Draths et al., 1992) which can be carried out by plants and microbes where the simple carbohydrate *D*-glucose is used as a starting material for the synthesis of amino acids and related metabolites. Biocatalysts may perform a synthetic or resolution role depending upon the reaction and was further described in the following Section 1.2.

1.2. BIOCATALYSIS

1.2.1. Industrial Biocatalysis

The increasing size and complexity of the molecules of chiral pharmaceutical reagents normally results in multiple chiral centres (Pollard and Woodley, 2006). Therefore, the major reason of using biocatalysis for a synthesis step is to exploit the region and stereoselectivity properties of biocatalyst to obtain high purity compounds whilst avoiding the need for difficult synthesis. Biocatalysis have turned out to be competitive compared with classic chemical as well as chemocatalytic synthetic approaches (Drauz et al., 2012). Some of remarkable advantages of biocatalysis in over chemocatalysis are biodegradability, sustainably produced, non-toxic, highly specific catalysts and mild reaction conditions (Lin et al., 2011). Figure 1.4 shows an aldol reaction for the asymmetric preparation of β -hydroxy α -amino acids that demonstrated an advantage of biocatalysis with the possibility of using substrates without the need for protecting groups due to the high selectivity of enzymes for specific functional groups. Whereas in the biocatalytic step, glycine can be used

directly as a donor, in a chemocatalytic reaction totally protected glycine is required. Therefore, biocatalysis offers a straightforward access, requiring only one synthetic step compared to five steps in the chemical approach (Drauz et al., 2012). Nevertheless the effective application of biocatalytic processes in the chemical industry depends mainly on cost competitiveness with the existing, and well established chemical processes (Sanchez and Demain, 2011).

Figure 1.4. (a) Multistep chemical and (b) protecting group-free biocatalytic strategies in an aldo reaction. Image reproduced from Drauz et al. (2012).

Furthermore, the principal driving forces for present and future research and development in industrial biocatalysis are including (Ghisalba et al., 2010):

- The continued demand for chiral building blocks and enantiomerically pure compounds, in general.
- A growing interest in areas of synthesis where biocatalysts offer clear advantages over purely chemical strategies (further described in the next Section 1.2.2).

- The multi functionality of the products, calling for sophisticated and laborious protection group strategies, has immense potential for selective and direct biocatalytic synthetic methodologies.
- International efforts to promote sustainable development and environmentally friendly technologies.

A significant increase in the use of biocatalysts for chemical synthesis has been observed within recent years (Sanchez and Demain, 2011). Despite a comparatively lower start, the implementation of biocatalysis processes at an industrial scale which is reflected by products commercialized at a scale over 100 kg on an annual basis, is almost doubling every decade and the market for enzymes has increased in an almost exponential manner from the 1960s to 2000 (Fernandes, 2010). Processes including biocatalytic steps are extensively reviewed (Pollard and Woodley, 2006; Breuer et al., 2004; Panke et al., 2004; Patel, 2001; Schmid et al., 2001; Schoemaker et al., 2003)

Some examples of the successful application of biocatalysis in industry are the use of acylases in the production of β -lactam antibiotics (De Vroom, 1999), the production of acrylamide from acetonitrile employing nitrile hydratase (Nagasawa and Yamada, 1990) and the industrial scale synthesis of chiral cyanohydrin (*S*)-*meta*-phenoxybenzaldehyde, an intermediate in the synthesis of pyrethroid insecticide using recombinant (*S*)-hydroxynitrilase lyase (Griengl et al., 1998). Further examples of complex drug compounds and the biocatalytic steps involved in their process developments are shown in Figure 1.5. These examples show the extensive influence of biocatalysis on the development of important pharmaceutically active compounds.

Alongside the increasing number of large-scale processes, is the development of process technology to overcome some of the limitations of processes involving biological systems thus enhancing the viability of a biocatalytic step. This technology includes the use of continuous reaction and separation bioreactors (De Roode et al, 2001), the use of packed bed reactors (Jeong et al., 2000) which can improve volumetric productivity as well as alleviate product inhibition, microscale high throughput techniques (Section 1.5) and many possible strategies for improving bioconversion performances (Section 1.4.10).

Figure 1.5. Complex drug compounds with multiple chiral centres and the biocatalytic step(s) associated with the development of each synthetic route. Image reproduced from Pollard and Woodley (2006).

1.2.2. Biocatalysis Processes

Bioconversion is becoming essential to the fine chemical industry in that their customers demand single isomer intermediates (Sanchez and Demain, 2011; Rogers, 1999). In many cases, biocatalysis has replaced chemical catalysis because of (Sanchez and Demain, 2011; Tao and Xu, 2009; Buchholz et al., 2005):

- Higher enantioselectivity and higher regioselectivity in aqueous solution.
- Do not require protection and deprotection of functional groups.
- Better stability.
- Operates under milder conditions, i.e avoidance of high and low temperatures, under mild pH values.
- Greater efficiency.
- Low energy consumption.
- Fewer by-products.
- Non-toxic when correctly used.
- Can be reused (immobilized).
- Can be degraded biologically.
- Can be produced in unlimited quantities.

Figure 1.6 shows comparisons of the traditional chemical and the new enzyme processes for the hydrolysis of penicillin G. (Buchholz et al., 2005). The chemical synthesis procedure used for the production was environmentally problematic solvents and toxic compounds, leading to toxic wastes that are difficult to recycle and therefore is not a sustainable process. In contrast, the enzyme process is more sustainable and leads to a considerable reduction in waste which in turn reduces the processing costs. Also, in this process the product yield could also be increased to > 95 %.

Figure 1.6. Comparison of the chemical and the enzymatic processes for the hydrolysis of penicillin G. The product, 6-aminopenicillinanic acid (6-APA), is used for the synthesis of semisynthetic penicillins with side chains other than phenylacetic acid. In the enzyme process, the by-product phenylacetic acid can be recycled in the production of penicillin by fermentation. Image reproduced from Buchholz et al. (2005).

Furthermore, although biocatalytic processes are now widely used in industry, there remain fundamental barriers to their widespread use which include (Lye and Woodley, 1999):

- Cheap and stable enzyme catalyst must become more easily available.
- Systematic design methods are needed to speed up the development process sequences. The design must also enable rational choices to be made between chemical and biocatalytic routes to the same end product.
- The low productivities that are often observed with biocatalytic systems, relative to the chemical equivalent must be enhanced in order to develop more economic processes.

Enzyme processes, as with all catalysed chemical processes can be divided into two categories (Buchholz et al., 2005):

1. *Equilibrium-controlled processes*: the desired product concentration or property has a maximum at the end-point of the process, the chemical equilibrium is independent of the properties of the enzyme, but is dependent upon on pH and temperature.

2. *Kinetically controlled processes*: the desired product concentration or property reaches a maximum, the concentration or properties of which depend on the properties of the enzyme, pH, and temperature. The process must be stopped when the maximum is reached.

As displayed in Figure 1.7, in both cases the time to reach the maximum product concentration or property depends on the properties and amount of enzyme used, and of the catalysed process (i.e endo- or exothermal, pH- and temperature dependence of equilibrium constants, solubility and stability of substrates, products) and therefore must be deliberated in the rational design of enzyme processes. Furthermore, other differences to consider are substrate concentrations and the formation of undesired by-products in un-catalysed bimolecular reactions (Buchholz et al., 2005).

Figure 1.7. Time-dependence (progress curves) of equilibrium- (solid line) and kinetically (broken line) controlled processes catalyzed by enzymes. The suitable end-points of these processes are those where the maximum product concentration or property is achieved – that is, A for the kinetically and B for the equilibrium controlled process. Such processes are illustrated with the hydrolysis of lactose in milk or whey, where mainly protein and fats are precipitated in the milk by addition of a ‘coagulating’ enzyme. The enzyme β -glucosidase that catalyzes the hydrolysis of lactose also catalyzes the kinetically controlled synthesis of tri- and tetra-saccharides. When lactose is consumed, these oligosaccharides are hydrolyzed. This also illustrates the formation of undesired by-products in enzyme-catalyzed processes. The oligosaccharides are by-products in the equilibrium controlled hydrolysis of lactose. On the other hand, in the kinetically controlled synthesis of the oligosaccharide that can be used as prebiotics, by-product formation is due to the hydrolysis to monosaccharides. The formation of the by-products must be minimized by selecting suitable process conditions and biocatalysts. Image reproduced from Buchholz et al. (2005).

The catalyst part of the biological system can thereby consist of whole cells, cellular extracts, or an isolated enzyme. For economic reasons, the whole cell biocatalysis is often primarily be considered over the use of cellular extract, isolated enzymes or permeabilized cells to perform biotransformations. This is possible when the following criteria are met: (i) no diffusion limitations for substrate(s) and/or product(s) and (ii) no side or follow-up reactions due to the presence of other cellular enzymes (Ghisalba et al., 2010). The further factors that can influence the decision of using each biological system for various bioconversions have been extensively reviewed (Sanchez and Demain, 2011; Chartrain et al., 2004). Biotechnological processes use one or more enzymes with or without co-factors or co-substrates as biocatalysts as illustrated and described in Figure 1.8.

Figure 1.8. Classification of biocatalytic processes with enzymes as biocatalysts. I and II must be performed with enzymes in living cells, III can be performed with enzymes in dead cells or as IV with isolated enzymes. Image reproduced from Buchholz et al. (2005).

Biocatalysis reactions can be operated under various process conditions (Ghisalba et al., 2010):

- Batch or fed-batch application of whole cells in free or immobilized form in an aqueous environment.
- Continuous application of whole cells in immobilized form in an aqueous environment.
- Application of whole cells in two-liquid phase, multiphase systems, or in micelles.
- Use of acetone-dried or permeabilized cells.
- Batch or fed-batch application of free crude or purified enzymes in aqueous or organic environment.
- Use of polyethyleneglycol (PEG)-modified enzymes in organic solvents.
- Continuous application of immobilized enzymes.
- Use of enzyme membrane reactors, the method of choice for systems with co-factor recycling or reactions with expensive enzymes.

1.3. CHIRAL AMINES

Chiral amines exist in more than one form, called enantiomers, and often only one of them has pharmacologic properties and is suitable for production in optically active drugs. Enantiomerically pure chiral amines are of increasing commercial value and widely used in the fine chemical and pharmaceutical areas in view of their application such as a resolving agent (Nieuwenhuijzen et al., 2002), chiral auxiliaries / chiral bases (Henderson et al., 2000), and pharmaceutical intermediates to produce various drug molecules (Berger et al., 2001). Some examples of chiral amines used in commercial molecules include L-tert-leucine (Kempf et al., 1991) in an HIV protease inhibitor used in AIDS therapy (Figure 1.9 (A)), *S*-(+)-clopidogrel (Gawronski, 2006) which targets thrombin to provide treatment for thrombosis (Figure 1.9 (B)) (Bajusz, et al, 1990) and *L*-6-hydroxynorleucine (Patel, 2001) which is an intermediate for antihypertensive Omapatrilat (Figure 1.9 (C)).

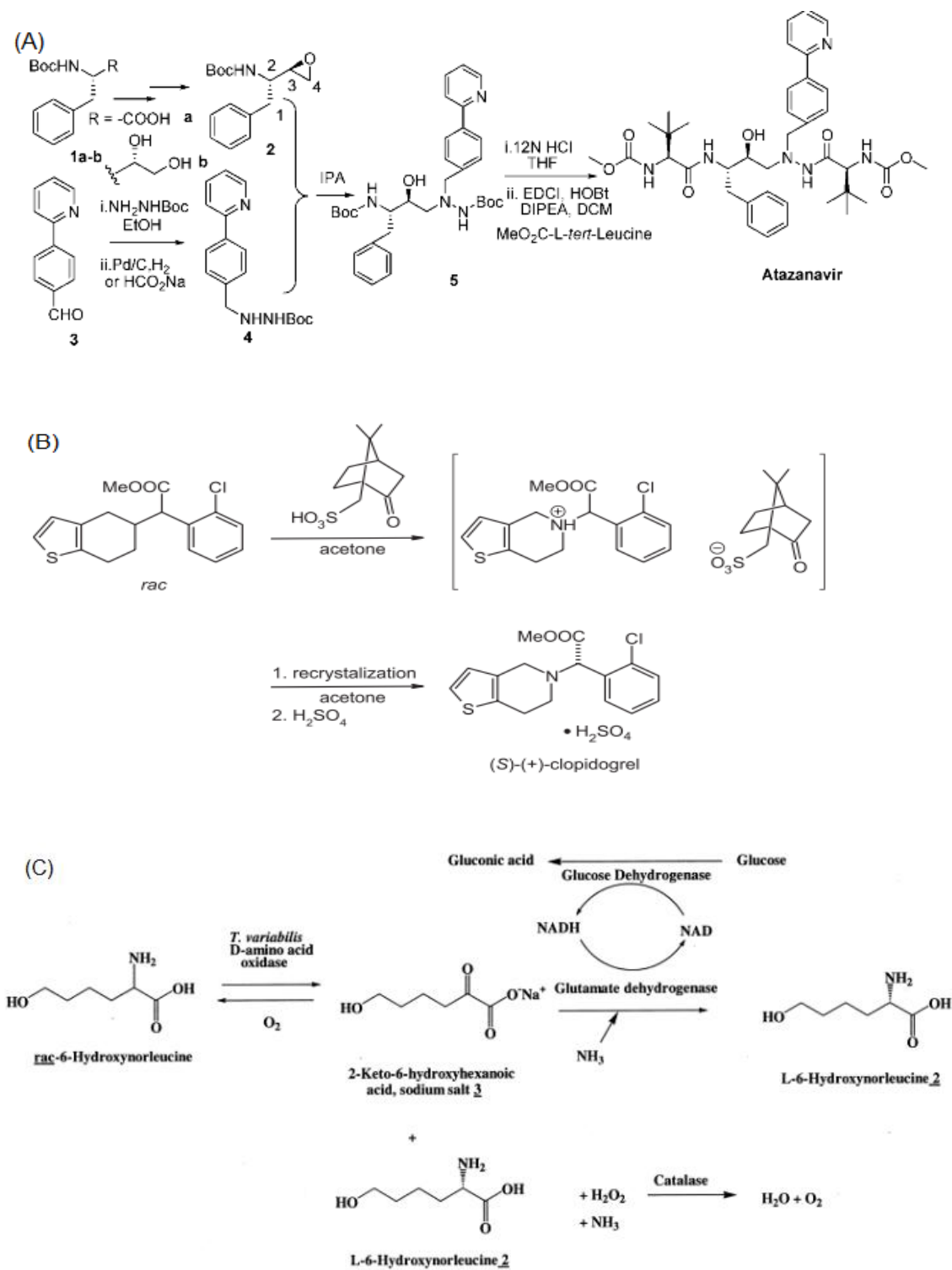


Figure 1.9. Examples of peptidomimetic drugs. (A) *L*-*tert*-leucine used in peptidomimetic HIV protease inhibitor (B) *S*-(+)-clopidogrel used in a drug for thrombosis therapy (C) *L*-6-hydroxynorleucine used as an intermediate in the synthesis of Omapatrilat, an antihypertensive drug.

Chiral amines can be produced by either chemical or biocatalytic synthetic routes (Breuer et al., 2004). The current methods used to prepare these compounds are mostly based upon the resolution of racemates either by recrystallization of diastereomeric salts (Jacques et al., 1980), or by enzyme-catalysed kinetic resolution of racemic substrates. In chemical kinetic resolution, two enantiomers show different reaction rates in a chemical reaction, thereby creating an excess of the less reactive enantiomer. However, taking the reaction to 100 % completion will again produce equal amounts of both enantiomers.. Meanwhile, the enzymatic kinetic resolution only converts one enantiomer depending on the stereoselectivity of the enzyme, and thus a 50 : 50 mixture of converted enantiomer product is obtained and the unreacted enantiomer remains intact. Biocatalytic kinetic resolutions using hydrolytic enzymes such as protease, lipase, esterase and transaminase have been studied extensively for preparing optically pure enantiomers (Shin and Kim, 1998; Gutman et al., 1992; Jackson et al., 1995; Tsai and Wei, 1994). Examples of both chemical and enzymatic kinetic resolution mechanisms are shown in Figures 1.10 and 1.11.

Figure 1.10. Kinetic resolution in the esterification reaction of racemic mandelic acid with optically active (-)-menthol to a pair of diastereomeric esters. The (R)-enantiomer of mandelic acid displays the higher reaction rate and with incomplete conversion, the reaction mixture becomes enriched in (S)-mandelic acid. Full hydrolysis of the incomplete esterification mixture gives an excess of (S)-mandelic acid. Taking the reaction to 100 % completion will again produce equal amounts of both esters. Image reproduced from Marckwald and McKenzie (1899).

Figure 1.11. Reaction scheme of the kinetic resolution via ω -TAm starting with racemic (rac) amines is limited by 50% maximum yield. For example, due to (S)-stereoselectivity of the ω -TAm, only (S)-amine is converted into ketone. Image reproduced from Koszelewski et al. (2010).

However, it is extremely difficult to produce the required enantiomer of many chiral amines by the standard chemical techniques (Nugent and El-Shazly, 2010) whilst the kinetic resolution method is also viewed as un-economic and non-competitive due to its disadvantage of producing only 50 % maximum of the desired enantiomer. Therefore, these approaches have been surpassed by other methods and attentions are recently turning towards enzyme-catalysed asymmetric synthesis approach with the use of ω -TAm (Figure 1.12) to generate chiral amines has received increasing attention (Koszelewski et al., 2010; Koszelewski et al., 2008; Shin and Kim, 1997) due to its emphasized characteristics as detailed in Section 1.2. For instance, out of 38 major asymmetric synthetic processes of the chemical industry, 22 use biocatalysis (Blaser and Schmidt, 2003).

Figure 1.12. Reaction scheme of the asymmetric synthesis of prochiral ketones via ω -TAm with theoretically a 100 % yield if the equilibrium can be shifted appropriately. Image reproduced from Koszelewski et al. (2010).

1.4. TRANSAMINASES (TAmS)

1.4.1. Introduction to TAm

Recently, TAmS (also known as aminotransferases) have received increased interest due to their great potential for the production of natural and non-natural amino acids as well as chiral amines, which are in demand by the pharmaceutical industry (Christen and Metzler, 1985; Sheldon, 1996; Shin and Kim, 1997; Stirling, 1992; Shin and Kim, 2001). Optically active amines and amino acids are required for the preparation of a broad range of biologically active compounds showing various pharmacological properties (Sutin et al., 2007; Dominik et al., 2008) such as building blocks in the synthesis of neurological, immunological, anti-hypertensive and anti-infective drugs. For example, biocatalytic transamination of L- Erythrulose (Ery) for synthesis of chirally pure 2-amino-1,3,4-butanetriol (ABT) is established to illustrate the importance of this compound as a chiral synthon for use as building blocks in the synthesis of protease inhibitors (Kwon and Ko, 2002), such as in the synthesis of NelfinavirTM (Figure 1.13), an HIV-protease inhibitor (Kaldor et al., 1997) Furthermore, it is estimated that 70 % of drugs involve an amino group reaction during their synthesis. In most cases, the pharmacological activities of these compounds are related to the configuration of the stereogenic center such as, between (S) and (R)-enantiomers.

Figure 1.13. Structure of the protease inhibitor drug NelfinavirTM. Highlighted section shows the use of ABT at the core of the molecule. Image reproduced from Ingram et al. (2007).

Compared to other enzymes such as amino acid dehydrogenase and amine dehydrogenases, and chemical methods for production of amino acids and chiral amines, the TAm have some superior features such as relaxed substrate specificity, rapid reaction rates and no requirement for external cofactor regeneration (Kaulmann et al., 2007). TAm can be divided into four subgroups, with groups I, III, and IV comprised of α -aminotransferases, whilst group II consists of ω -TAm. ω -TAm enzymes have the potential to access a range of substrates not accepted by α -aminotransferases.

Enantioenriched amines and amino acids can be produced via two methods (Section 1.5.4), which are asymmetric synthesis (Shin and Kim, 1999) using a chiral ketone (i.e amination of the ketone) and kinetic resolution (Shin and Kim, 1997) of racemic amine (i.e deamination of the amine). The strict enantioselectivity of ω -TAm is beneficial to achieving the high yield of unreacted (R)-enantiomer by kinetic resolution and to obtaining highly enantiopure (S)-enantiomer by asymmetric synthesis (Shin and Kim, 1999; 2001). In the asymmetric synthesis of chiral amines with ω -TAm, the choice of amino donor is of considerable importance. For instance, it is impractical to use some chiral amines as an amino donor in synthesizing other chiral amines due to their high cost, despite their high reactivity.

1.4.2. Classification of TAm

TAm can be divided into four subgroups based on their amino-acid sequence (Mehta et al., 1993, Sayer et al., 2007). All TAm known to date use the same co-enzyme to catalyze the same type of reaction and, as catalysts, are distinguished only by their substrate specificities. Their structural differences reflect their substrate specificities (Mehta et al., 1993). Subgroup I appears to be the most versatile, which their members accepting alanine, dicarboxylic and aromatic amino acids as substrates. In subgroup II, the substrates possess as a unique feature a distal amino group that undergoes the transamination reaction, and its functional homogeneity is reflected by a high degree of sequence similarity among its members. Subgroup III has two members, while their amino acids substrates are of different chirality but both share the same oxo acids substrate. Finally, subgroup IV also consisting only two members,

that acts on structurally and biosynthetically related substrates. Subgroup II, regarded as collectively ω -TAm, contains ornithine (EC 2.6.1.13), 4-aminobutyrate (EC 2.6.1.19), acetylornithine (EC 2.6.1.11), diaminopelargonate (EC 2.6.1.62) and ω -amino acid:pyruvate TAm (EC 2.6.1.18).

Since diamine-ketoglutaric TAm or 'amine TAm' (Kim, 1964; Samsonova et al., 2003) were reported capable of utilizing a substrate without a carboxylic acid group several other ω -TAm were also founded to show catalytic activity towards primary amines and aliphatic amines without carboxyl group (Yohana et al., 1987; Shin and Kim, 1999; Shin et al., 2003; Sayer et al., 2007, Kaulmann et al., 2007). Protein sequence of these characterized enzymes are not yet available, but they belong to ω -amino acid:pyruvate TAm that prefer pyruvate, as the amine acceptor rather than α -ketoglutarate (Kaulmann et al., 2007).

1.4.3. Structure of ω -TAm

Figure 1.14 shows the ribbon structure of the homodimeric ω -TAm from *Vibrio Fluvialis*, where each subunit had a molecular weight of 50 kDA. An active site model of the ω -TAm has been constructed (Figure 1.15) (Shin and Kim, 2002). This resulted in a two-binding site model, which contained two pockets, one large and one smaller, the latter one presenting a strong repulsion for a carboxylate, playing a vital role in the substrate specificity and stereoselectivity. The large pocket showed a dual recognition mode for both hydrophobic and carboxyl groups, and corresponded to a carboxylate trap, while the small pocket played the role of a side chain recognition site (Shin and Kim, 2002).

1.4.4. ω -TAm for Investigation

Transaminases are ubiquitously present in microorganisms and higher organisms and play an important role in amino-acid metabolism (Christen and Metzler, 1985). To date, general properties of ω -TAm were extensively studied using three different microorganisms, *Vibrio fluvialis* JS17, *Klebsiella pneumoniae* JS2F, and *Bacillus thuringiensis* JS64 (Shin and Kim, 2001).



Figure 1.14. Ribbon structure of homodimeric ω -TAM from *V. fluvialis* JS17. Figure created from the PDB structure file 1qgd using PyMOL Molecular Graphics System (DeLano, 2002) on World Wide Web <http://www.pymol.org>.



Figure 1.15. Two-Binding Site Model of ω -TAM from *V. fluvialis* showing (a) binding of the amino donor and (b) the binding of the amino acceptor. L and S denote large and small binding pockets respectively. Image reproduced from Shin and Kim (2002).

The ω -TAm from these three enzymes showed high enantioselectivity for certain enantiomers of chiral amines such as (S)- α -methylbenzylamine (Shin and Kim, 1998; Shin and Kim, 2001; Sayer et al., 2007) and demonstrated the highest amino acceptor reactivity for pyruvate (Shin and Kim, 2001). Among these strains, *Vibrio fluvialis* JS17, was found to be one of the most promising strains for both kinetic resolution and asymmetric synthesis. This makes ω -TAm from *Vibrio fluvialis* JS17 and other related enzymes suitable and good candidates as biocatalyst for the production of chiral amino alcohols.

However, since the *Vibrio fluvialis* JS17 strain was isolated from soil as reported by Shin and Kim (2001), it is not publicly available. Kaulmann et al. (2007) have searched for a new strain, which is *Vibrio fluvialis*-like amine transaminase family. By using BLASTP search, they have successfully recruited a novel ω -TAm from *Chromobacterium violaceum* DSM30191 (CV2025 ω -TAm). The gene from *C. violaceum* strain was cloned into the expression vector pET29a and expressed in *Escherichia coli* BL21 (Kaulmann et al., 2007). The ω -amino acid:pyruvate transaminases from *C. violaceum* shows 38 % sequence similarity to the ω -TAm from *Vibrio fluvialis* JS17 and also favour the transamination reaction in the forward direction. The CV2025 ω -TAm was thus extensively used here to achieve the research aim and objectives (Section 1.5). Also, a library of novel ω -TAMS from various strains (Table 2.3) (made available by the Institute of Structural and Molecular Biology, University College London) was studied as described in Chapters 5 and 6.

1.4.5. ω -TAm Bioconversions

Since it was discovered over 60 years ago, few processes using this enzyme have been commercialized due to the low equilibrium constant of the transaminases reaction that result in a low yield of product conversion. Figure 1.16 shows the general reaction scheme of a TAm reaction. However, the unfavourable equilibrium position is not a problem for transamination using ω -TAm, for example, the reaction between chiral amines and pyruvate (Shin and Kim, 1998). The conversion of (S)- α -methylbenzylamine (MBA) and pyruvate to acetophenone (AP) and L-alanine (Figure 1.17) using ω -TAm from *V. fluvialis* is almost quantitative since the equilibrium

entirely favours product formation in the forward direction, which is towards L-alanine (Shin and Kim, 1998; Kaulmann et al., 2007).

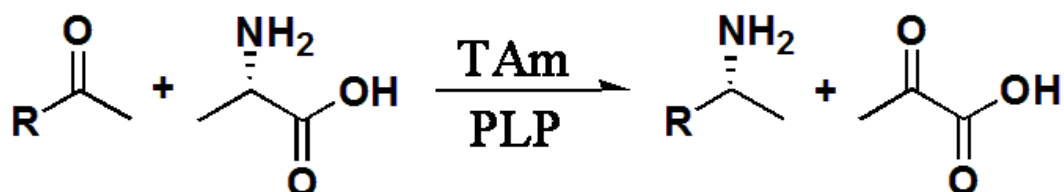


Figure 1.16. General reaction scheme of a TAM reaction where an amino group is transferred to a carbonyl group.

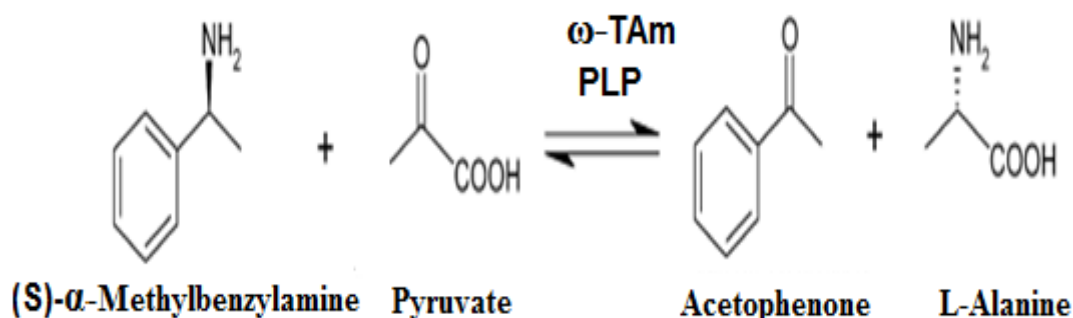


Figure 1.17. Reaction scheme of the ω -transamination (ω -TAM) bioconversion between (S)- α -methylbenzylamine (MBA) and pyruvate to acetophenone (AP) and L-Alanine in the presence of co-factor pyridoxal 5'-phosphate (PLP).

Investigation into stability of the purified TAM showed loss in enzyme activity over a long fermentation period (i.e 70 hours), and this suggests this enzyme is more stable in the environment of the lysate form (Ingram et al., 2007). Proteins in lysate are often subject to attack by endogenous proteases. However, by using E.coli BL21 gold (DE23) strain, lacking both the La and OmpT protease, reduces such degradation (Studier and Moffatt, 1986; Ingram et al., 2007). The lower instability of transaminase as observed by Ingram and co-workers (2007) may be due to the loss of the tetrameric conformation that is comprised of two loosely associated dimmers during purification.

In addition, it would be also appealing to compare the reactions using recombinant whole cells expressing ω -TAm with lysed cells, since whole cell biocatalyst represent the cheapest and often most efficient solution in industrial single and multi-step bioconversions. Moreover, immobilization techniques of the cells or enzymes can furthermore be used to improve the stability while adding the benefit of allowing the catalyst to be recycled for multiple batches.

Immobilization of enzymes can provide several advantages compared to free enzymes, including easy recovery and reuse of enzyme, improved operational and storage stability of the enzyme, the possibility for continuous operation in packed bed reactors, and minimizing protein contamination in the product (Sheldon, 2007). Immobilization of whole cell ω -TAm by entrapment in calcium alginate beads has been applied for the kinetic resolution of chiral amines in a packed bed reactor (Shin et al., 2001).

1.4.6. Reaction Mechanism of ω -TAm

ω -TAm is a well-characterized pyridoxal 5'-phosphate (PLP) dependent enzyme. As shown in schematic Figure 1.18, ω -TAm catalyses the enzymatic amino transfer by ping-pong bi-bi mechanism (Christen and Metzler, 1985). The mechanisms by which ω -TAm enzymes act can be divided into two half-reactions (Figure 1.19).

In the first half-reaction, the amino acid (amino donor) donates its amino group to the PLP form of the enzyme (E-PLP) to produce enzyme bound pyridoxamine 5'-phosphate (E-PMP), and the respective keto product is released. During the second-half reaction, the keto acid (amino acceptor) accepts the amino group from E-PMP to produce the corresponding amino acid and regenerates E-PLP, thus completes the transaminase cycle (Christen and Metzler, 1985). The fully regenerated ω -TAm's co-factor within the same two substrates reaction, hence avoid co-factor regeneration problems in oxidation / reduction reaction mechanisms of ω -TAm (Hwang et al., 2005; Pannuri et al., 2003).

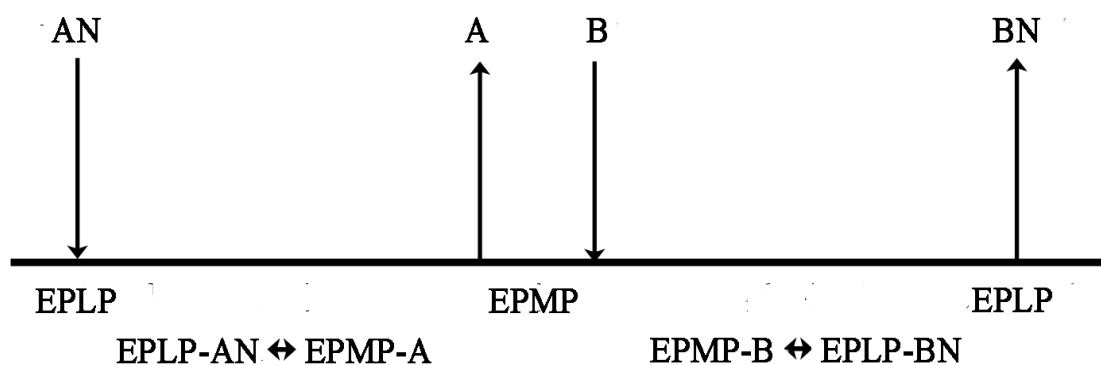


Figure 1.18. Schematic representation of the ping pong bi-bi ordered reaction mechanism used of ω -TAm.

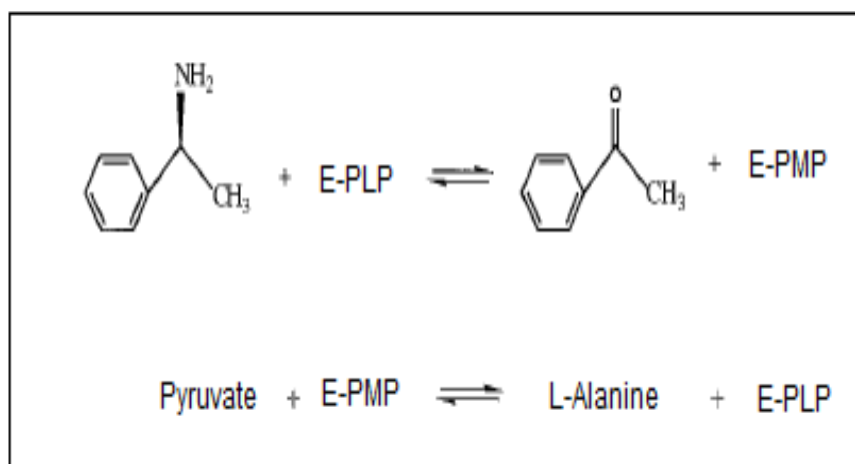


Figure 1.19. Schematic diagram of ω -transamination. E-PLP and E-PMP represent a complex between ω -transaminase and pyridoxal 5-phosphate and a complex between ω -transamination and pyridoxamine phosphate respectively.

1.4.7. Range of Potential of Amino Donors and Amino Acceptors

The substrate spectrum for *C. Violaceum* CV2025 ω -TAm as published by Kaulmann et al. (2007) was mainly obtained with a cell extract. As with the *Vibrio fluvialis* enzyme, CV2025 ω -TAm showed high activities towards amino donors of aromatic (S)-amines such as (S)- α -MBA and (S)-aminoindane with little or no reactivity towards (R)- α -MBA (Kaulmann et al., 2007). The high selectivity for (S)-amines

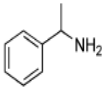
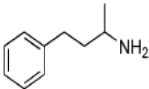
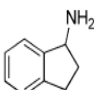
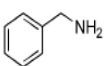
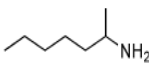
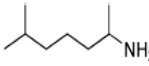
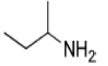
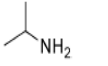
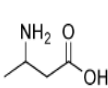
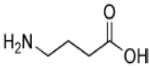
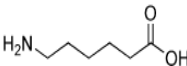
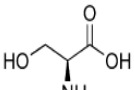
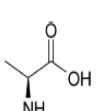
could lead to a useful asymmetric strategy for the preparation of enantiopure amines and amino alcohols (Shin et al., 2001; Yun et al., 2003; Yun et al., 2005; Kaulmann et al., 2007). In comparison to *Vibrio fluvialis* enzyme, CV2025 ω -TAm showed slightly lower reactivity for reactions with (*S*)-enantiomers and the reasons are remains to be elucidated.

Besides (*S*)- α -MBA and (*S*)-aminoindane, 1-methyl-3-phenylpropylamine and benzylamine were also can be considered as efficient candidates as an amino donor for transamination reaction by CV2025 ω -TAm (Table 1.1). Aminodiols (2-amino-1-phenylpropane-1,3-diol and 3-amino-1,2-propanediols), aliphatic amines and amino acid tested were also tested as amino donor but no significant activities were detected except for 1-methyl and 1,5-dimethylhexylamine (amines) and L-alanine (α -amino acids) which are in agreement with data obtained for *Vibrio fluvialis* enzyme (Kaulmann et al., 2007).

As for amino acceptor candidates, besides keto acids, such as pyruvate and hydroxyruvate (HPA), several aliphatic and aromatic aldehydes showed significant reactivity (Table 1.2). Distinctly from *Vibrio fluvialis* enzyme (Shin and Kim, 2001), higher conversions were observed for hydroxypyruvate (HPA) and glyoxylate (aliphatic aldehyde) for CV2025 ω -TAm reactions. Among the amine acceptors tested, only pyruvate, glyoxylate and benzylaldehyde allowed conversion of ≥ 90 % (Kaulmann et al., 2007). The incomplete transamination might be due to chemical equilibrium, acceptor reactivity and poor substrate/ products solubility and inhibitions effects.

The low molecular weight aldehydes such as propanal and butanal showed good amino acceptor reactivity as pyruvate (Shin and Kim, 1997; Stirling, 1992) and due to their low costs such aldehydes are favoured over relatively expensive pyruvate. However, when considering both reactivity and enzyme stability, pyruvate offered a better option (Shin and Kim, 2001).

Table 1.1. Specificity of CV2025 ω -transaminase towards various amino donors. Image reproduced from Kaulmann et al. (2007).

Specificity of CV2025 ω -TA towards various amino donors		Relative initial rates (%)	
		CV2025 TA ^a	<i>V. fluvialis</i> TA ^b
Amines			
(±)- α -Methylbenzylamine (MBA)		100 (69.4)	100 (112.0)
(±)-1-Methyl-3-phenylpropylamine		148.6	54.2 (61.4)
(±)-1-Aminoindane		183.0 (157.9)	156.5 (161.7)
Benzylamine		133.9	115.6
(±)-2-Aminoheptane		19.4	42.9
(±)-2-Amino-6-methylheptane		35.2	24.4
(±)- <i>sec</i> -Butylamine		<4 ^c	6.8
Isopropylamine		<4 ^c	3.6
Amino acids and derivatives			
(±)-3-Aminobutyric acid		4.7	7.0
γ -Aminobutyric acid		7.2	<1
6-Aminohexanoic acid		10.3	<1
L- α -Ser		9.0	6.4
L- α -Ala ^d		165.0	10.0

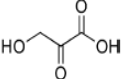
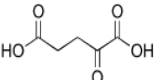
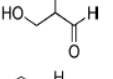
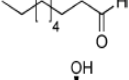
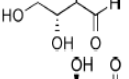
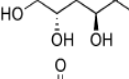
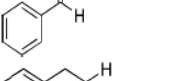
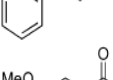
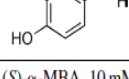
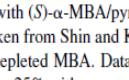
^a Reaction conditions: 10 mM pyruvate and either 20 mM racemic donor, 10 mM enantiomer or 10 mM achiral donor, 0.4–0.8 U/ml CV2025 TA, 37 °C, pH 7.0. Values in parentheses represent relative reactivities of 10 mM (*S*)-enantiomers in comparison to the respective 20 mM racemic mixtures. For arylc donors, initial rates were determined from donor depletion, for aliphatic donors from pyruvate depletion.

^b Relative initial rates determined by Shin and Kim [26]. Note that initial rates have been determined with half the substrate concentrations and from 10 min reactions.

^c The detection limit for pyruvate depletion was ca. 4%. Other tested substrates with relative reactivities of less than 4% were: 2-aminoisobutyric acid, β -Ala, taurine, L- α -Asp, (±)-3-amino-1,2-propanediol; of less than 4% (detection limit for arylc amino donor depletion): (*R*)- α -MBA, L- α -Phe, (±)-3-amino-3-phenyl propionic acid, anthranilic acid, (1*S*,2*S*)-APP, (1*R*,2*R*)-APP. L- α -Ala was not tested with pyruvate as the acceptor.

^d The reactivity of L- α -Ala was measured by using glyoxylate as an amino acceptor and compared with that of (*S*)- α -MBA with glyoxylate. For comparison: the relative initial rate for the L- α -Ala/glyoxylate reaction with *V. fluvialis* TA as determined by Shin et al. [19].

Table 1.2. Specificity of CV2025 ω -transaminase towards various amino acceptors. Image reproduced from Kaulmann et al. (2007).

Specificity of CV2025 ω -TA towards ketoacids and aldehyde acceptors		CV2025 TA ^a		<i>V. fluvialis</i> TA ^b
		Conversion at equilibrium (%) ^c	Relative initial rate (%)	Relative initial rate (%)
Keto acids				
Pyruvate		95–100	100	100
HPA		65	144.1	29.2
α -Ketoglutarate		<5	<5	0.3
Aldehydes				
Glyoxylate		95–100	176.2	60.2
Glycolaldehyde		47–57	106.6	n.d.
(\pm)-Glyceraldehyde		40	116.1	n.d.
Propanal		60–70	132.3	36.4
Butanal		74–78	122.9	113.5
Hexanal		8–14	81.3	106.2
Nonanal		8–10	78.2	0.9
D-Erythrose		14–22	60.6	n.d.
D-Fructose		n.d.	<5	n.d.
Benzaldehyde		90	91.2	72.8
Phenylacetaldehyde		68	107.0	68.5
(<i>E</i>)-Cinnamaldehyde		>60 ^d	79.7	31.5
Vanillin		>60 ^d	61.7	n.d.

^a Reaction conditions: 10 mM (*S*)- α -MBA, 10 mM acceptor, 0.4–0.8 U/ml CV2025 TA, 37 °C, pH 7.0. Initial rates were calculated from MBA depletion in 3 min and related to the rate obtained with (*S*)- α -MBA/pyruvate. The detection limit was 5%.

^b Relative initial rates were taken from Shin and Kim [26].

^c Based on concentration of depleted MBA. Data were obtained from three independent experiments and generally varied by no more than 6% from the mean (exception: data variation of up to 25% with nonanal). The reactions were monitored until equilibrium was reached (mostly after 2–3 h).

^d The reactions were not run to equilibrium.

1.4.8. Asymmetric Synthesis and Kinetic Resolution

ω -TAm catalyzed production of targeted chiral amine compounds are either by direct asymmetric synthesis from pro-chiral ketones or kinetic resolution of racemic amines. The choice of reaction methods between asymmetric synthesis from prochiral compounds and kinetic resolution from racemic compounds depends on the enantioselectivity of the enzyme and the economics of the reaction process. The strict enantioselectivity of the enzyme is beneficial to achieve high yield of either unreacted (R)-enantiomer by kinetic resolution or (S)-enantiomer by asymmetric synthesis (Shin et al., 2001; Shin and Kim, 1999). As described earlier in Section 1.4.8, the kinetic resolution method is, however, always hampered by a maximum of 50 % theoretical yield. ω -TAm which has sufficiently high enantioselectivity, could lead to a useful asymmetric synthesis method permitting the production of high enantiopure homochiral amines.

Asymmetric synthesis has been one of the central themes in biotransformation (Klibanov, 1990; Shin and Kim, 1999) as well as in modern organic chemistry (Chan, 1993; Sonawane et al., 1992; Shin and Kim, 1999). The asymmetric synthesis of chiral amines with ω -TAm may offer many potential advantages over kinetic resolution. These advantages include: the lack of need for reductive amination to prepare racemic amines from ketone precursors, chiral precursors are usually less expensive than racemic mixtures (Sheldon, 1996; Shin and Kim, 1999) and two fold higher theoretical yield (Shin and Kim, 1999). However, the challenges of using this method are to shift the equilibrium to the product side, especially when using amino acid as an amino donor, stereoselectivity of the enzyme has to be perfect, which is not always the case for ω -transaminase (Dominik et al., 2008), and much more severe product inhibition than the kinetic resolution method (Shin and Kim, 1998; Shin and Kim, 1999).

1.4.9. ω -TAm Bioconversion Process Challenges

Despite many advantages, such as broad substrate specificity (Section 1.4.7), high turnover rate, and high stability (Taylor et al., 1998), the industrial use of ω -TAm has

been limited, mainly due to the low equilibrium constant of the bioconversion reaction. Also, severe product inhibition will prevent from using high concentrations of amine substrate (Shin and Kim, 1998). As described earlier in Section 1.4.8, the best approach to the pure chiral amine would be asymmetric synthesis, if possible (Shin and Kim, 1998), however, proved to be difficult due to these limitations. Therefore, recent work has started focusing on overcoming tackle these issues for a higher reaction yield.

1.4.9.1. ω -TAm Thermodynamic Equilibrium

The low equilibrium constant of the ω -TAm reaction is the main problem that inhibits high bioconversion. The transamination reaction (Section 1.3.1) is reversible, and the optimum bioconversion rate is determined by the initial concentrations and the thermodynamic equilibrium constant (K) of the reaction (Tufvesson et al., 2011). Meanwhile, K is determined by the change in Gibbs free energy (ΔG) for the reaction given by the difference in ΔG between the products and the reactants. For instance, the amine transfer from an amino acid to an alpha keto acid to form another amino acid, the change in ΔG is small and in turn the equilibrium constant of the reaction is around one (Tufvesson et al., 2011; Taylor et al., 1998). The equilibrium constant of the reaction determines how low a concentration of product or co-product is required to achieve the desired yields. Therefore, the knowledge of the reaction equilibrium constant and / or ΔG (Jankowski et al., 2008) is important in determining of the process strategy needed to meet the requirements in terms of yield and product concentration (Tufvesson et al., 2011; Seo et al., 2011).

Kaulmann et al. (2007) reported on transamination of a range of amino acceptors of keto acids and aldehydes with MBA, and the results showed only a few acceptors allowed conversion of more than 70 % (Table 1.2) after the equilibrium was reached. These observations were due to the equilibrium being strongly in favor of the MBA (amine donor). The kinetic study for ω -TAm from *Bacillus thuringiensis* JS64 demonstrated by kinetic resolution of α -methylbenzylamine, reported a K of about 10^{-3} (Shin and Kim, 1998). When 2-propyl amine was used as the amine donor, the equilibrium becomes more favorable, but still the equilibrium lies strongly in favor of the reactants (Truppo et al., 2009).

1.4.9.2. Substrate and Product Inhibitions

Inhibition by substrate and / or product is another significant problem that needs to be overcome for an efficient industrial transamination process. Substrate inhibition is a common phenomenon in enzyme chemistry, which is virtually always observed with a fast reacting substrate enantiomer for enzyme processing a defined stereoselectivity (Shin and Kim, 2002; Wang et al., 1999; Kaiser, 1980). Accurate understanding of substrate inhibition is critical to determine the optimal substrate concentration to be used for the reaction.

Substrate inhibition of ω -TAm result from the formation of abortive dead-end complexes, such as between the amino donor and E-PMP and / or amino acceptor and E-PLP (Shin and Kim, 1998), which restrain them from undergoing further reaction and inhibits the formation of the right Michaelis complexes. This phenomenon is due to the presumably similar active site structures and recognition mechanisms of both E-PLP and E-PMP, thus each enzyme form can facilitate non-productive binding.

For instance, it was reported that substrate inhibition as observed when either keto acid (i.e pyruvate) or other reactive aldehyde (i.e. butyraldehyde) was used in the ω -TAm bioconversions (Shin and Kim, 2002). They also found that (R)-enantiomers of amines severely inhibit the enzyme activity even though the (R)-amines are nearly non-reactive due to high-enantioselectivity of ω -transaminase. The high propensity for this non-productive binding indicates that binding pockets of ω -transaminase have not evolved to precisely control enantioselectivity and substrate preference during the binding step (Shin and Kim, 2002). The substrate inhibition problem can be overcome by controlling the substrate concentration in the medium (Shin and Kim, 2002).

Meanwhile, product inhibition phenomena (Shin and Kim, 1996) result from the right formation of Michaelis complex between product and transaminase enzyme. This is due to the reversibility of enzyme reaction, which product can bind to the enzyme and thus reduces the chances of substrate binding to the enzyme active site.

1.4.10. Possible Strategies for Improving Reaction Performances

Systematic design methods are hence necessary to overcome the thermodynamic equilibrium and inhibition limitations to enhance productivity of the ω -TAm biocatalytic process prior industrial application. Recently, a number of methods have been demonstrated to (at least) partly overcome these challenges, such as:

1.4.10.1. *In situ* product removal (ISPR) methods

In situ product removal (ISPR) methods can be used to address both thermodynamic and inhibition limitations by selectively removing the product from the reaction solution as soon as it is formed which can also further benefit subsequent downstream processing (Lye and Woodley, 1999; Jauregi and Varley, 1998; Jauregi et al., 1997). Besides, ISPR method is also used to increase the productivity or yield of biocatalytic processes by minimizing product losses owing to degradation or un-controlled release and reducing the total number of downstream-processing steps (Lye and Woodley, 1999).

The best strategy for ISPR will depend on the properties of the product amine as well as other components in the reaction mixture. In general, a strategy is considered favorable when it produces a huge driving force for separating the product from the other components (Tufvesson et al., 2011). The physico-chemical properties that are most commonly exploited for ISPR are volatility, solubility, charge, hydrophobicity, and molecular size (Tufvesson et al., 2011; Lye and Woodley, 1999). One of the example of an effective ISPR application is the removal of an enzyme that inhibit L-erythrulose from the reaction medium of transketolase catalysed condensation of glycoaldehyde with hydroxypyruvate (Figure 1.20) using an immobilized phenylboronate resin (Affigel 60) (Lye and Woodley, 1999).

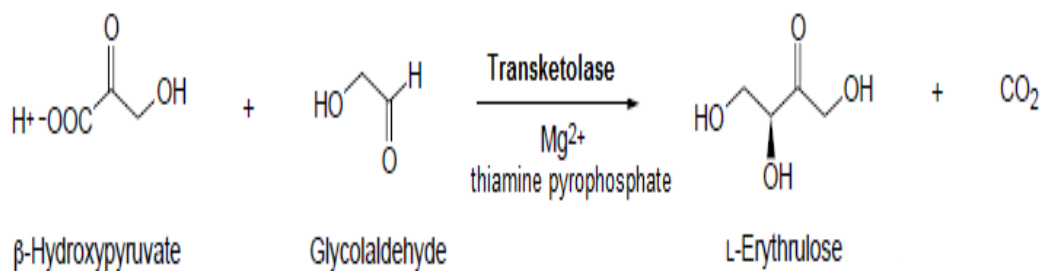


Figure 1.20. Transketolase catalysed condensation of glycolaldehyde with β -hydroxypyruvate to yield L-erythrulose with the evolution of carbon dioxide.

Industrial examples of research into ISPR techniques have shown some impressive results, and most of the cases involve the implementation to overcome inhibitory or toxic effects of the product on the biocatalyst. The stereoselective reduction of 3,4-methylene dioxyphenyl acetone to S-3,4-methylene-dioxyphenyl isopropanol by a whole cell *Zygosaccharomyces rouxii* biocatalyst with XAD-7 resin application for simultaneous in situ substrate supply has been demonstrated up to a scale of 300 L with the final product increased from 6 g.L⁻¹ to 40 g.L⁻¹ (Vicenzi et al., 1997). Likewise, XAD-2 was used for ISPR substrate supply of geraniol that inhibits *Ceratocystic variolorum* biocatalyst at 20 L scale and managed to increased production of monoterpenes from 0.04 g.L⁻¹ to 1.9 g.L⁻¹ (Schindler, 1982). Both of these examples were operated in batch mode operation of ISPR techniques.

An example of an industrial continuous ISPR process has been described for the conversion of niacin to 6-hydroxynicotinic acid by whole cells of *Achromabacter xylosoxidans* to overcome the magnesium salt of the product which is insoluble at neutral pH (Kulla, 1991). The continuous ISPR process allowed a productivity of 1.5 g.L⁻¹.hr⁻¹ to be obtained. These examples have clearly highlighting the role of the application of ISPR techniques in improving the yield and productivity of biocatalysts processes, and these three impressive industrial ISPR examples are summarised in Table 1.3 (Lye and Woodley, 1999).

Table 1.3. Examples of industrial *in situ* product removal research. Image reproduced from Lye and Woodley (1999).

	Stereoselective reduction (Vicenzi et al., 1997)	Monoterpene synthesis (Schindler, 1982)	6-Hydroxynicotinic-acid synthesis Kulla, 1991
ISPR rationale	Toxicity	Inhibition	Inhibition
ISPR method	Amberlite XAD-7	Amberlite XAD-2	Continuous precipitation
Biocatalyst	<i>Zygosaccharomyces rouxii</i>	<i>Ceratocystis variispora</i>	<i>Achromobacter xylosoxidans</i>
Scale	300 l	20 l	Not stated
Benefit	6.7× increase in product concentration	48× increase in product concentration	Increased volumetric productivity
Abbreviation: ISPR, <i>in situ</i> product removal.			

A biphasic extractive system was verified as one of the keys to the success of enzymatic resolution reaction at high substrate concentration (Shin and Kim, 1997). Furthermore, the two-liquid-phase system (Wubbolts et al., 1996; Van Sonsbeek et al., 1993; Shin and Kim, 1999) has proved versatile in biotransformation, permitting high concentrations of substrate of low solubility to be used in aqueous media, the shifting of equilibrium positions, and the removal of product inhibition (Shin and Kim, 1999).

The possible drawbacks of this system are phase and/or solvent toxicity to enzyme and mass transfer limitations attributable to a restricted interfacial area. A biphasic reaction system (Figure 1.21) was successfully introduced to keep the concentration of inhibitory products low at the reaction site (i.e aqueous phase) despite the difficulty in constructing a continuous process, and a serious problem of interfacial enzyme inactivation in emulsion state (Shin et al., 2001) in kinetic resolution with ω -transaminase (Shin and Kim, 1999; Shin and Kim, 1998). Also, in order to overcome the problems encountered in the two-liquid-phase system, an enzyme membrane reactor (EMR) with a membrane contractor can be used to facilitate emulsion-free extraction (Shin and Kim, 2001).

Furthermore, evaporation of a volatile product (or by-product) may also be an option for shifting the equilibrium towards the product and overcoming inhibition. Yun et al. (2004) have previously reported a great achievement with reduced pressure method

that significantly enhance the yield of ω -TAm bioconversion of (*R,S*) *sec*-butylamine by greatly remove an inhibitory product, 2-butanone. For volatile amines, distillation could also be a possible route for product recovery in kinetic synthesis. For example (*R*)-*sec*-butylamine (boiling point 63 °C) was recovered by distillation of the product mixture under basic conditions (Hanson et al., 2008). Also, it was later reported, a small enhancement in yield by sweeping the reactor with nitrogen gas to remove the acetone formed (Savile et al., 2010).

Nevertheless, there are limitations with all ISPR strategies which are commonly related to the selectivity of separation and the relative concentrations of the reaction components, including the solvent. For instance, in using resin adsorption it was observed that the ketones or amines have similar distribution behaviour and, therefore, will co-extract into the solvent or resin unless another driving forces are in place such as ionization (Tufvesson et al., 2011).

Figure 1.21. Reaction scheme of ω -transamination in biphasic system. Image reproduced from Shin and Kim (1997).

1.4.10.2. Alternative Amino Donor

Low equilibrium constant is a common problem in ω -TAM bioconversion, however, depending on substrate combinations, some of them have equilibrium constants that are high enough not to limit the reaction (Shin and Kim, 1997; 1998) such as ω -amino acid: pyruvate ω -TAM shown catalytic activity toward aliphatic amines not bearing a carboxyl group (Yohana et al., 1987; Christen and Metzler, 1985). Therefore, the simplest and most straightforward approach is the screening of ω -TAM for amine donor specificity in search for a combination with suitable amine acceptors bearing high equilibrium constant toward the desired product.

1.4.10.3. Addition of Excess Substrate

Another simple option for shifting the equilibrium towards a high yield of the product would in principle be to use an excess of either amine donor or amine acceptor. This strategy was applied by Savile et al. (2010) for the production of Sitagliptin at high substrate concentrations using an approximately 10-fold excess of 2-propylamine. However, the use of this strategy is limited to those cases when the equilibrium is only slightly unfavourable (Tufvesson et al., 2011).

1.4.10.4. Auto-Degradation of By-product

Another convenient approach is the use of self-degrading by-product or products. For instances, the spontaneously cyclized of the amino-keto acid formed when using ornithine or lysine as amine donor has thus favoured the reaction in the direction of the amine (Ager et al., 2001; Li et al., 2002). The similar approach was used recently to shift the equilibrium of the transaminase reaction (Truppo et al., 2010).

1.4.10.5. Enzymatic Cascade / Second Enzyme Reactions

The transamination reaction can be coupled to other enzymatic steps that convert the by-product into a non-reactive compound or back to the original substrate hence increase yield of the desired product. Recently, a multitude of different coupling reactions have been proposed and reported (Truppo and Turner, 2010; Koszelewski et al., 2008; Koszelewski et al., 2009; Yun et al., 2003). Nevertheless, for the greatest

feasibility, the interactions and compatibility of the enzymes and associated reagents first need to be considered.

1.5. MICROSCALE HIGH-THROUGHPUT EXPERIMENTATION

1.5.1. Conventional Microwell Plate Platform

The need to improve the efficiency of biocatalyst process development is a constant challenge as efforts to continue to reduce the overall timeline of pharmaceuticals from design to market and reduce overall development costs (Pollard and Woodley, 2006). The development of industrial biocatalytic bioconversion is usually a slow process compared with the traditional chemical routes (Pollard and Woodley, 2006; Yazbeck et al., 2004). This is due to the necessity to screen a large set of biocatalyst libraries in order to identify the appropriate enzymes, followed by a large amount of data that need to be collected at each stage of the process development (Lye et al., 2003; Fernandes, 2010). Therefore, the need to develop new methods that could handle large quantities of biocatalysis experiments is become crucial.

Parallel experimentation on miniaturised platforms is gaining increasing attention mainly for shortening bioprocess development, and offers a cost-effective method of process optimization (Micheletti and Lye, 2006). Additional key advantages of microscale techniques include (Lye et al., 2002; Lye et al., 2003):

- Rapid evaluation of large enzyme libraries.
- Reduction in the quantity of materials including expensive enzymes and substrates required for process development.
- Rapid generation of early data for process design and model establishment predictive of larger scale operations.
- Early identification of the optimum reaction conditions and reactor configurations.
- Promotion of a rapid and efficient translation from discovery to pilot plant scale.
- Capacity to automate the complete bioprocess as will be discussed further in the following Section 1.5.2.

A majority of the microscale bioprocess studies have been developed on miniaturized reactors mostly using multi-well plates (Fernandes, 2010). The microwell systems are commercially available in different geometries and sizes with scales ranging from 20 to 2000 μL (Micheletti and Lye, 2006; Doig et al., 2002). Figure 1.22 shows the dimensions of 3 standard size microwell bioreactors.

Figure 1.22. Diagram representation of individual microwell formats: (a) 96-deep square well format; (b) 24-round well format; (c) 96-round well format. V_w represents the total well volume; SA represents the static surface area available for gas-liquid mass transfer. Image reproduced from Lye et al. (2003).

Although the use of microscale techniques has been comprehensively used during the past decade for screening purposes, it is only recently that studies on fundamental engineering aspects have been performed, including mass and heat transfer phenomena and scaling up techniques (Zhang et al., 2008; Marques et al., 2009; Barrett et al., 2010).

Of special interest is the liquid mixing in such small reactors, which behave differently from larger scale processes in terms of the importance of diffusion and

convection (Matosevic et al., 2008). Orbital shaking of microwell plates has been found to be the most efficient way to promote mixing, and several studies have been conducted to determine the critical speed to assure an uniform mixing (Micheletti et al., 2006). These studies have led to a better understanding of the reaction conditions and engineering principles of the microscale tools, and will provide excellent guidance toward successful scale translation (Zhang et al., 2008; Islam et al., 2008).

Recent studies have also focused on the quantification of enzyme kinetics using microscale tools (Lye et al., 2002). Doig et al. (2002) have performed a microscale study of a whole cell cyclohexanone monooxygenase performing the oxidation of bicyclic ketones to synthesize chiral lactones. They were able to characterize the oxygen mass transfer behaviour under different reaction conditions and microwell geometries, as well as accurately determined the substrate inhibition parameters. Furthermore, the use of microscale techniques integrated with analytical tools such as HPLC (high-performance liquid chromatography) for the reliable determination of kinetic parameters has been established using cellular extracts, pure and immobilized enzymes (Chen et al., 2008; Matosevic et al., 2011).

Due to the high level of parallelization and reduced requirements of materials involved, intensive screening of biocatalysts and process variables has, therefore, become more feasible whilst the reproducibility of bioconversion processes have been substantially improved (Fernandes, 2010). Therefore, microscale bioprocessing techniques have emerged as an ideal tool that can be used to study and evaluate the different components in the process development, characterization and ultimately implementation of bioconversion processes to production scale.

1.5.2. Automation Microscale Platform

The benefits of miniaturization of bioprocessing will further arise from the adoption of automated operation of whole bioprocess sequences that facilitate the parallel evaluation of whole bioprocess performance at the earliest product development. The established microwell formats can be easily adopted with ready automation processes as numbers of commercially available laboratory robotic platforms are recently started to receive a great attention.

The applications of microtitre plate with integration of automation robots of bioprocess development will greatly help to reduce the labour requirement, increases the operational and analytical accuracy and minimizes the number of expensive large-scale trials required which in turn reduce the total cost to market of new biopharmaceuticals (Zhang et al., 2008). Recently, the use of automated shaken microtitre plates have been become widely explored for studies of wide range bioprocess operations that include complex bioprocess developments such as stem cell expansion, mammalian cell culture, bacterial fermentation, biotransformation and downstream processing. The factors influence the industrial uptake of microscale bioprocess technologies is summarizes in Figure 1.23.

Automated microscale approaches have been studied expansively for the rapid and quantitative collection of bioprocess design data (Lye et al., 2003; Micheletti and Lye, 2006). Of special interest is a study reported on the robotic application that linked fermentation, induction and bioconversion steps using a Packard Multiprobe II robot for investigation of trade-offs between recombinant production and specific cyclohexance monooxygenase (CHMO) activity and bioconversion (Ferreira-Torres et al., 2005) and the same approach was later had been repeated for a tranketolase (TK)-expressing *E.coli* biocalyst using a Tecan robotic platform (Micheletti et al., 2006).

Furthermore, a commercial robotic liquid handling workstation (Freedom EVO) was successfully modified for parallel microscale chromatography application to accelerates automated high-throughput separations by microscale biochromatography (Britsch et al., 2008). The robot also helps to overcome sample preparation and separation bottlenecks in numerous applications where multiple samples are to be processed or analysed. The applications include, screening of cell culture supernatants for recombinant monoclonal antibodies, rapid two-dimensional parameter optimization in the development of individual process chromatography steps, and a variety of new diagnostic applications for medical purposes (Britsch et al., 2008).

Jackson et al. (2006) have reported an automated microscale Normal Flow Filtration (NFF) technique that is able to quantitatively evaluate the influence of upstream processing conditions on the microfiltration behaviour of *E. coli* fermentation broths based on the use of a Tecan VacS two-position vacuum filtration manifold with Tecan

Genesis Freedom liquid handling robot. The technique used in this work alongside microwell fermentation studies allows the integrated parallel quantification and optimisation of upstream and downstream operations. Chen et al. (2008), recently published work where a full kinetic model was established using automated microscale tools, evaluating key parameters such as substrate and product inhibition.

Figure 1.23. Capabilities framework for the industrial adoption of high-throughput technologies. This illustration is based on the implementation of high-throughput screening programmes in the pharmaceutical sector. Arrows represent the progression of microwell and microfluidic systems, respectively. Image reproduced from Micheletti and Lye (2006).

1.6. AIM AND OBJECTIVES OF THE PROJECT

Recently bioconversion processes have received increased interest as replacements for conventional chemical syntheses, especially those for chiral and environmentally unfriendly syntheses (Section 1.2). The advantage of biocatalysis lies (Section 1.2.2) in the ability to operate at near neutral pH, ambient temperatures, pressures and in an aqueous environment. More importantly, biocatalysts are highly reaction specific, enantiomer-specific and regio-specific (Illanes, 2008). However, the widespread use of biocatalysis in industry requires conversions to achieve higher space-time yields than is currently possible (Pollard and Woodley, 2006). As described in Section 1.4.9, an issue generic to many types of bioconversions is the need to overcome unfavourable reaction equilibrium.

ω -TAMs converts a carbonyl group to an amino group, and is an industrially relevant example of a biocatalyst featuring unfavourable equilibrium positions which are a problem in a range of asymmetric syntheses (Section 1.4). ω -TAMs have received increased interest due to their great potential for the production of natural and non-natural amino acids as well as other chiral amines, which are in demand by the pharmaceutical industry (Christen and Metzler, 1985; Sheldon, 1996; Shin and Kim, 1997; Stirling, 1992; Shin and Kim, 2001). Optically active amines are required for the preparation of a broad range of biologically active compounds (Section 1.1) showing various pharmacological properties (Sutin, 2007; Koszelewski et al., 2008) such as building blocks in the synthesis of neurological, immunological, anti-hypertensive and anti-infective drugs. The challenges for industry are (i) how to select a suitable transaminase for a particular bioconversion, (ii) need to be able to explore early bioprocess solutions to overcoming equilibrium control of reaction and increase product yield, (iii) need to evaluate both substrates and products for inhibitory effects (iv) need to rapidly identify cheap and ready sources of amine donors for each TAM/substrate combination and (v) how to evaluate different process options for increasing space-time yields quickly and cost effectively.

The **aim** of this research is, therefore, to create and demonstrate microscale process methodologies for overcoming the major factors limiting bioconversion production rate and yield. For ω -TAMs there are typically low equilibrium constants and product

inhibition as described in Section 1.4.9. In particular, generic solutions for shifting the reaction equilibrium towards product formation for ω -TAm bioconversions will be highlighted with the application of high-throughput microscale methods that are predictive of larger scale operating conditions. In order to achieve this aim, the primary **objectives** of the project are summarized below.

- The first objective is to develop techniques for the evaluation of the basic kinetic properties and parameters of the ω -TAm enzyme at the micro-scale (< 1mL). ω -TAm activity was initially studied with MBA and pyruvate as model substrates known to have rapid reaction rates and high yields. The validated methods obtained from microwell scale were then used for further investigation of mechanisms to overcome the reaction equilibrium problem. The results of this work are presented and discussed in Chapter 3.
- The second objective was then to establish novel microscale methods to enable evaluation of different process solutions to overcome product inhibition and equilibrium control of reactions and hence increase product formation. Four approaches were demonstrated for the CV2025 ω -TAm asymmetric synthesis of chiral amines. The first option examined ω -TAm bioconversions with different types of amino donors as alternatives to MBA. The second option couples ω -TAm with alcohol dehydrogenase (ADH) and glucose dehydrogenase (GDH) for removing the inhibitory AP by conversion to non-inhibitory (R)-1-Phenylethanol. The third and fourth approaches are based on physical *in situ* product removal (ISPR) methods of applying reduced pressure conditions for evaporation of the volatile AP and utilizing synthetic polymeric resins for adsorption of AP to eliminate it from the reaction system. The results of this work are presented and discussed in Chapter 4.
- The third objective was to integrate the methods established in Chapter 4 into an efficient automated microscale process sequence. The research here was mainly focussed on comparison of both conventional and automated microscale processes techniques and the potential benefits of increased processing speed and reduced experimental costs attained with the automation

platform. The automated microscale process sequences were also applied to the evaluation of ω -TAm libraries. The results of this work are presented and discussed in Chapter 5.

- The fourth objective was to illustrate successful scale-up of selected ω -TAm reactions identified in Chapter 5. The scale-up of CV2025 ω -TAm bioconversions with optimised second enzyme reaction conditions and using a novel BSU09260_1971 ω -TAm from *Bacillus subtilis* capable of using L- α -Serine as amino donor were performed at μ L and preparative scales to demonstrate the capacity of the microscale automation tools to speed up bioprocess design and optimisation and evaluation of a broad range of biocatalyst and process options. The results of this work are presented and discussed in Chapter 6.
- Finally, in Chapter 7, the generic outcomes of this work are highlighted and suggestions for future work are presented.

2. MATERIALS AND METHODS

2.1. MATERIALS

2.1.1. Reagents and Suppliers

Nutrient broth and nutrient agar were obtained from Fisher Scientific (Leicestershire, UK). All other reagents were obtained from Sigma-Aldrich (Gillingham, UK) unless otherwise stated and were of the highest purity available. Reverse osmosis (RO) water was used in all experimental work.

2.1.2. Media Preparation

E. coli BL21 fermentations for expression of CV2025 ω -TAm obtained from plasmids pQR800 and pQR801 were performed using LB-glycerol (Luria-Bertani media) medium, the contents of which are described in Table 2.1. *E. coli* fermentations for expression of ω -transaminases obtained from plasmids pQR426, pQR813, pQR956, pQR960, pQR978, pQR985, pQR1010, pQR1014, pQR1017, pQR1019 were performed using 2xTY (*E. coli* rich media) medium the contents of which are described in Table 2.2.

The different components of both media were weighed out and dissolved in RO water to a final volume of 1 L. The pH of the media was adjusted to pH 7 with a solution of 1 M NaOH when necessary. The medium were then autoclaved at 121 °C for 15 min.

Table 2.1. Composition of the LB-glycerol medium used in *E. coli* fermentations for expression of CV2025 ω -transaminases obtained from plasmids pQR800 and pQR801.

Component	Concentration (g.L ⁻¹)
Yeast extract	5.0
Tryptone	10.0
NaCl	10.0
Glycerol	10.0

Table 2.2. Composition of the 2xTY medium used in *E. coli* fermentations for expressions of ω -transaminases obtained from plasmids pQR426, pQR813, pQR956, pQR960, pQR978, pQR985, pQR1010, pQR1014, pQR1017, pQR1019.

Component	Concentration (g.L ⁻¹)
Yeast extract	10.0
Tryptone	16.0
NaCl	5.0

2.1.3. Agar Plate Preparation

LB agar and 2xTY agar were prepared by adding 15 g.L⁻¹ of agar to LB-glycerol medium and 2xTY medium as described in Tables 2.1 and 2.2, respectively. The agars prepared were then autoclaved at 121 °C for 15 min. Once cooled down to a temperature between 40 - 50 °C, 30 mL of media were poured into each standard size Petri dish (Fisher Scientific, UK) under aseptic conditions. The agars were then allowed to solidify before use.

2.1.4. Antibiotic Solution

The antibiotic kanamycin was dissolved in RO water to a concentration of 150 g.L⁻¹. The solution was then sterilized by passing it slowly through a 0.2 μ m filter (Fisher Scientific, UK) and aseptically transferred into previously sterilized 1.5 mL

Eppendorf tubes and stored at -20 °C. The antibiotic was added to all LB glycerol medium, 2xTY medium, LB agar and 2xTY agar before the start of any culture.

2.1.5. Glycerol Stocks

To prepare master stock cultures, a single colony was picked from the plate containing the desired enzyme (Section 2.2.1). This was then inoculated into a sterile 250 mL shake flask containing 25 mL of culture medium with the corresponding antibiotic. When the culture reached an OD of 0.5 at 600 nm (Section 2.6.3), 400 μ L aliquots of cell broth were mixed aseptically in sterilized 1.5 mL Eppendorf tubes with 200 μ L of a 50 % (v/v) filter sterilized glycerol solution. The aliquots were then frozen and stored at -80 °C and were used throughout the rest of this project.

2.1.6. Transaminase plasmids

ω -TAm from plasmids pQR800 and pQR801 (with an N-Terminal His6-tag) contained the complete CV2025 ω -TAm gene and were constructed in previous work (Kaulmann et al., 2007). The other ten novel transaminases used in this work came from different microorganisms as listed in Table 2.3. The genes were selected after an exhaustive bioinformatics analysis. Using as a query pQR801 sequence, sequences were collected and aligned. A phylogenetic tree was constructed using MEGA 5.0 and sequences closely related to pQR801 were selected. The selected sequences were pulled out and producing microorganisms were identified. Microorganisms were obtained either from Professor John Ward (Institute of Structural and Molecular Biology, UCL) personal collection or from DSMZ (Germany). The genomic DNA were then purified. The primers were designed containing the NdeI and Xho I restriction sites. TAmS were amplified by PCR and ligated into pET29a vector (Merk, USA), which contained inducible T7 promoter, the Lac repressor and codes for resistance to kanamycin. All TAmS constructed were fully sequenced to check they were in the right orientation and to verify that there were no mutations were included during amplification. The *E.coli* BL21 BL21gold (DE3) transformed with each plasmid constructed were kindly provided by Professor John Ward.

Table 2.3. List of ω -TAm novel library.

Microorganism	Construct Gene ID	Plasmid
<i>Chromobacterium violaceum DSM30191</i>	CV2025	pQR801
<i>Pseudomonas putida KT 2440</i>	PP2799	pQR811
<i>Pseudomonas aeruginosa PAO2</i>	PAO0221	pQR813
<i>Bacillus licheniformis</i>	BLi00474	pQR985
<i>Klebsiella pneumoniae</i>	KPN_03745	pQR1011
<i>Bacillus subtilis</i>	BSU09260_1971	pQR960
<i>Deinococcus geothermalis</i>	Dgeo_1177	pQR978
<i>Kineococcus radiotolerans</i>	Krad_4078	pQR956
<i>Micrococcus luteus</i>	Mlut_00920	pQR1014
<i>Rhodospirillum rubrum</i>	Rru_A1254	pQR1017
<i>Rhodobacter sphaeroides</i>	Rsph17025_2835	pQR1019

2.2. FERMENTATIONS

2.2.1. Shake Flask Fermentations Using LB Media

Glycerol stocks of *E.coli* BL21 contained plasmids of each of the ω -TAMs were grown in LB agar plate in the presence of kanamycin ($150 \mu\text{g}\cdot\text{mL}^{-1}$). Using a single colony from the agar plate, an overnight culture of the cell was then inoculated in a 200 mL shake flask (20 mL working volume) containing LB glycerol broth as described in Table 2.1 again with the addition of a similar concentration of kanamycin. Growth was performed at 37°C with orbital shaking at 250 rpm using an SI 50 orbital shaker (Stuart Scientific, Redhill, UK). The total volume of this culture was then used to inoculate a 2 L shake flask (200 mL working volume). When the OD_{600} reached a value of 1.8 - 2.0, *Isopropyl β -D-1-thiogalactopyranoside* (IPTG) was added to a final concentration of 0.2 mM. After 5 hours of induction, the cells were harvested, and 2 mM co-factor, pyridoxal-5-phosphate (PLP) was added prior to storage at -20°C following removal of the broth by centrifugation (Hettich Universal

320 Benchtop Centrifuge, GMI Inc, USA), or immediate use for whole cell bioconversions (Section 2.3.1).

2.2.2. Shake Flask Fermentations Using 2xTY Media

Cells grown in 2xTY media were cultured as described in Section 2.2.1, except they were first cultured at 37 °C but following IPTG induction (when OD₆₀₀ reached a value of 1.8 - 2.0) the temperature was lowered to 30 °C prior to harvest after a further 5 hours.

2.2.3. 7.5 L New Brunswick Fed-batch Fermentation

Batch fermentation was carried out in a 7.5 L fermentor (BioFlo 110, New Brunswick, Hertfordshire, UK) with a working volume of 5.0 L. The fermentor had an aspect ratio of 1.79:1 and was comprised of two six-bladed dual Rushton-type impellers ($d_i = 59$ mm, $d_i/d_t = 0.25$) and four equally spaced baffles. The temperature was monitored by a thermocouple and automatically controlled at 37 °C via cold water circulation in the external jacket of the fermentor or a heating jacket. The pH was measured using an Ingold gel filled pH probe (Ingold Messtechnik, Urdorf, Switzerland), and was controlled with the addition of 85 % v/v H₃PO₄ (acid) and 28 % v/v NH₄OH (base). DOT was monitored using a polarographic oxygen electrode (Ingold Messtechnik, Urdorf, Switzerland) and was set to be maintained at 80 % through a cascade control of the impeller speed. Ingoing air was sterilized by passage through a 0.2 µm membrane filter and dispersed in the vessel at the base of the lower turbine with a ring sparger at a constant of flow rate was 5 L.min⁻¹ (1 vvm).

The vessel was filled with 4.5 L of LB glycerol media, and all the probe calibrations and pre-sterilization procedures were performed following the manufacturer instructions. The fermentor was then sterilized as a complete unit in an autoclave at 121 °C for 20 min, and after the media was cooled down, the corresponding antibiotic (Section 2.1.4) and sterilized antifoam PPG, was added to a final concentration of 0.2 g.L⁻¹. The fermentor was then inoculated aseptically with five 100 mL shake flasks cultures previously grown overnight as described in Section 2.2.1. The fermentor was

initially contained LB glycerol media of 3 g.L⁻¹ of glycerol. After the glycerol was consumed, and thus the glycerol becoming limiting, the culture was supplemented with two shots addition of pre-sterilized 5 g.L⁻¹ of glycerol at two time intervals. Data was logged by on-line measurements of DOT, pH, temperature and impeller speed using the BioCommand software (BioFlo 110, New Brunswick, Hertfordshire, UK) as well as by taking regular OD₆₀₀ measurements as described in Section 2.6.2.

2.3. BIOCATALYST PREPARATION

2.3.1. Whole Cell and Lysate Forms

Fresh *E.coli* BL21 cells containing the required ω -transaminase used for whole cell bioconversions were usually obtained as described in Sections 2.2.1 and 2.2.2. When a cell-free lysate was needed, upon thawing, the cell pellet was resuspended in 50 mM HEPES buffer (pH 7.5) with additional 2 mM PLP and were sonicated with a Soniprep 150 sonicator (MSE, Sanyo, Japan) using 10 seconds on / off at 10 μ m amplitude for 10 cycles. Cells were placed on ice to stop overheating during the sonication. The sonicated lysate was then centrifuged at 5000 rpm in Falcon tubes for 5 min (Hettich Universal 320 Benchtop Centrifuge, GMI Inc, USA) to remove cell debris. The resulting supernatant was then filtered through a 0.2 μ m filter (ParadiscTM 25 AS, Whatman, UK) to obtain clarified extract. The clarified supernatant was finally aliquoted into 1.5 mL Eppendorf tubes to be stored at -20 °C. Prior to the initiation of a bioconversion, the frozen lysates (300 μ L) were thawed in a water bath at 30 °C for typically 10 min and then immediately incubated with co-factors PLP.

2.3.2. Purified Enzymes (His₆-tag Purification)

The transaminases expressed from all plasmids except pQR800 have an N-terminal His₆-tag to facilitate rapid single-step purification using His-Select Nickel Affinity Gel which is an immobilized metal-ion affinity chromatography (IMAC) product. The His-Select Nickel Affinity Gel was stored in 30 % (v/v) ethanol and removed just prior to use. The affinity gel was thoroughly resuspended with gentle inversion, and

an appropriate aliquot was removed for use (3 - 4 mL affinity gel was used for 5 mL of clarified recombinant protein prepared as described in Section 2.3.1). The affinity gel was then poured into a spin column (Spin Column Pierce Zeba empty, Thermo Scientific Pierce, Fisher Scientific UK Ltd, Loughborough, UK). The composition of all buffers used for the enzyme purification procedure is shown in Table 2.4, the pH of all buffers was 7.5 and all steps were performed at room temperature. All separations steps were performed by using spin protocol, which an additional gravity force was added by spinning the column in a centrifuge for 2 min at 1000 rpm.

The affinity gel was first washed with 1 - 2 volumes of deionized water to remove the ethanol. After equilibration with 1 column volume of equilibration buffer, the purification was commenced by loading the lysate solution. The spin column was then left for 15 - 30 min on an orbital shaker (~175 rpm) to gently mix the affinity gel and the lysate solution. Following removal of the supernatant, the affinity gel was washed with 3 - 4 column volumes of washing buffer. The affinity gel suspension was then again mixed gently on an orbital shaker for 4 min prior removing the supernatant. Elution was carried by gently mixing the affinity gel with a volume of 2.5 - 5 mL of elution buffer for 30 - 60 min on an orbital shaker prior to collection of the supernatant of histidine containing protein.

Table 2.4. His₆-tag enzyme purification buffers used for affinity purification (Section 2.3.2).

Buffer	Components
Equilibration	50 mM HEPES buffer (pH 7.5), 0.4 mM PLP, 0.5 M NaCl, 15 mM Imidazole.
Wash	50 mM HEPES buffer (pH 7.5), 0.4 mM PLP, 0.3 M NaCl, 20 mM Imidazole.
Elution	50 mM HEPES buffer (pH 7.5), 0.4 mM PLP, 0.3 M NaCl, 250 mM Imidazole.

The affinity gel was cleaned after each run. The affinity gel was washed with 2 column volumes of deionized water followed by a cleaning step which was performed by passing through 5 column volumes of 6.0 M guanidine HCl (Fisher Fisher

Scientific UK Ltd, Loughborough, UK), pH 7.5. The guanidine HCl solution was then removed by washing with 2 - 3 column volumes of deionized water. The affinity gel was then re-equilibrated with 2 - 3 column volumes of equilibration buffer for immediate use or was washed with 1 - 2 column volumes of 30 % (v/v) ethanol and finally resuspended in 30 % (v/v) ethanol and stored at 2 - 8 °C.

Following recovery of a fraction of his-tagged protein, in order to remove free EDTA and EDTA-nickel complexes from the elution buffer, the enzyme solution was desalted using a PD-10 desalting column (GE Healthcare UK Ltd, Buckinghamshire, UK) containing 8.3 mL of SephadexTM G-25 medium with a size exclusion limit of 5000 M_r. The column storage solution was removed just prior use. All the separation steps were performed under gravity. The column was first equilibrated with 25 mL of 50 mM HEPES buffer containing 4 mM PLP. A Labmate PD-10 Buffer Reservoir (GE Healthcare UK Ltd, Buckinghamshire, UK) was employed for ease of use as it allows loading of the total 25 mL buffer in one go. 2.5 mL of protein solution containing supernatant was then loaded into the column, and the flow-through discarded once the solution had completely entered the packed bed. For sample volumes less than 2.5 mL, 50 mM HEPES buffer was added to adjust the volume to 2.5 mL. Elution was carried out with 3.5 mL 50 mM HEPES buffer containing 4 mM PLP added to the column. The eluate of purified enzyme was analysed by SDS-PAGE as described in Section 2.6.5. The purified enzyme solution was stored in the fridge at 4 °C for a period of up to 2 weeks before use.

2.3.3. Alcohol Dehydrogenase (ADH)

Commercially available alcohol dehydrogenases from *Lactobacillus kefir* (0.44 U.mg⁻¹ protein where 1 U corresponds to the amount of enzyme which reduces 1 µmol acetophenone to phenylethanol per minute at pH 7.0 and 25 °C) and *Thermoanaerobium brockii* (0.5 U.mg⁻¹, 1 U will oxidize 1.0 µmol of 2-propanol to acetone per minute at pH 7.8 at 40 °C in the presence of NADP⁺) were dissolved in HEPES buffer (pH 7.5) with concentrations depending on the required reaction concentrations (i.e 0.5 M, 1.0 M and 1.5 M) as discussed in Sections 4.5 and 5.6. Magnesium ions (Mg²⁺) form an essential part of the active enzyme which prevents enzyme deactivation (Hummel, 1990) and so 10 mM MgCl₂ was added to each

solution to help stabilize the enzyme activity. The enzyme solutions were either used immediately in bioconversion reactions, or stored in the fridge at 4 °C and used within 24 hours. Meanwhile, the ADHs in powder form were stored at -20 °C for up to 12 months.

2.3.4. Glucose Dehydrogenase (GDH)

Commercially available Glucose dehydrogenase from *Pseudomonas sp.* (260 U.mg⁻¹, where 1 U corresponds to the amount of enzyme which will oxidizes 1 μmol β-D-glucose to D-glucono-δ-lactone per minute at pH 8.0 and 37 °C) was dissolved in HEPES buffer (pH 7.5) with concentrations depending on the reaction concentrations (i.e 0.5 M, 1.0 M and 1.5 M) as discussed in Sections 4.5 and 5.6. The enzyme solutions were either used immediately in bioconversion reactions or stored in the fridge at 4 °C and used within 24 hours. Meanwhile, the GDH in powder form was stored at -20 °C for up to 12 months.

2.4. SYNTHESIS OF PRODUCT AND DERIVATIZING REAGENT

2.4.1. Chemical Synthesis of ABT Product Standard

The chemical synthesis of ABT was performed as described by Ingram et al. (2007). Briefly *L*-erythrulose (4 g, 33 mmol), was suspended in acetone:dimethoxypropane 9:1 v/v (30 mL) and *p*-toluenesulfonic acid (catalyst) was added. The mixture was stirred at room temperature under N₂ for 3 hours during which time the reaction mixture became homogeneous. The reaction was monitored by TLC (Thin layer chromatography) using a 2:1 v/v, ethyl acetate: hexane running solvent.

Sodium acetate (0.5 g) was then added, and the reaction solution was stirred for a further hour before the mixture was filtered and concentrated to dryness. The residue was purified by flash chromatography on silica gel (ethyl acetate/hexane 1:2 v/v) to yield the desired 3,4-*O*-isopropylidene acetal.

To an aliquot of the produced acetal (487 mg, 3.02 mmol) in methanol (10 mL) was added benzylamine (660 μ L, 6.04 mmol) and then sodium cyanoborohydride (570 mg, 9.06 mmol). The pH was adjusted to pH 6.0 using acetic acid and the reaction was stirred at room temperature for 6 hours. The reaction was monitored by TLC (1:1, ethyl acetate:hexane). The mixture was concentrated under vacuum, and the residue partitioned between dichloromethane (100 mL) and sodium hydrogen carbonate (aq, sat) (100 mL) with vigorous stirring.

Solid sodium carbonate was added to the suspension in small portions to ensure that the final pH of the aqueous layer was 9. The layers were then separated, the aqueous phase was extracted with further dichloromethane (two times 100 mL) and the organic phases combined and concentrated to dryness. The residue was purified by flash chromatography on silica gel (ethyl acetate/hexane 1:1 v/v then neat ethyl acetate) to yield the desired amine as a 1:1 mixture of diastereomers.

To a solution of the previously produced amine (200 mg, 0.80 mmol) in MeOH (5 mL) was added 1 M HCl (aq) drop wise to give a mixture that gave a dark red colour to moist litmus paper. The reaction was stirred at room temperature and was monitored by TLC (1:1 v/v, ethyl acetate: hexane). After 2 hours, the reaction was completed, and the mixture concentrated to dryness to yield the crude amine as the hydrochloride salt. This residue was re-dissolved in MeOH (5 mL) and hydrogenated (balloon pressure) in the presence of palladium on carbon (10 % wt/wt, 100 mg) at room temperature overnight. The catalyst was removed by filtration, and the solvent was removed under vacuum to yield 2-amino-1,3,4-butanetriol (ABT) as a 1:1 mixture of *threo* and *erythro* diastereomers.

2.4.2. Enzymatic Synthesis of ABT

The enzymatic synthesis of ABT was performed in a 100 mL scale bioconversion with 200 mM ERY, 0.2 mM PLP and 30 % v/v of CV2025 ω -TAm lysate (final enzyme concentration of 0.3 g.L⁻¹). To this mixture, a solution of 300 mM isopropylamine (pH 7.5) was added in a fed batch mode using a P-1 peristaltic pump (Pharmacia Fine Chemicals, Uppsala, Sweden) with a flow rate of 2.1 mL.hr⁻¹ for 48

hours until the total volume of the reaction was approximately 200 mL. The temperature of the CV2025 ω -TAm catalyzed reaction was maintained at 30 °C using a circulating water bath (Grant Instruments, Cambridge, UK), and the pH was kept at 7.5 by the automatic addition of 1 M NaOH using a 718 STAT Titrino pH controller (Metrohm Ion Analysis, Switzerland).

After the bioconversion, the enzyme was spun down (5000 rpm, at 4 °C for 15 min), and the mixture was additionally filtered through a 0.2 μ m sterile filter (ParadiscTM 25 AS, Whatman plc. Kent, UK). 50 g of Amberlite IRA-410 resin (Sigma-Aldrich, Gillingham, UK) was added to the reaction mixture for 1 hour, and the resin was then removed by filtration. The remaining aqueous mixture was then passed through 80 g of an Isolute SCX-2 ion exchange column (Biotage, Uppsala, Sweden), and the column was washed with 400 mL of methanol. The column was then eluted with 500 mL 4 M NH₃ and the eluent was evaporated to yield 2-amino-1,3,4-butanetriol (ABT).

2.4.3. Synthesis of Derivatizing Reagent

The derivatizing agent 6-aminoquinolyl-*N*-hydroxysuccinimidyl carbamate (AQC) was synthesized ‘in house’ according to a previously published protocol (Cohen and Michaud, 1993). Di (*N*-succinimidyl) carbamate (3 g, 6 mmol), was refluxed in 25 mL of dry acetonitrile. Dropwise addition of a 6-aminoquinoline (1.5 g, 5 mmol) solution in dry acetonitrile was carried out over 45 min. Following a further 30 min reflux, concentration was carried out to half the original volume. The solution was stored at –4 °C overnight. The crystals were then filtered off and stored in *vacuo* until used for derivatization step as described in Section 2.6.6.

2.5. BIOCONVERSION REACTIONS

2.5.1. Microscale Experimental Platform

Microscale bioconversions were performed either in a glass 96-well, flat-bottomed microtiter plate with individual wells having a diameter of 7.6 mm and height of 12 mm (Radleys Discovery Technologies, Essex, UK) or in 2 mL flat bottom standard glass vials (Chromacol, UK) of dimension of 12 x 32 mm with 8 mm screw neck.

The microplate was covered with a thermoplastic elastomer cap (Figure 2.1) designed to work with automated equipment (Micronic, Lelystad, Netherlands) while glass vials were well-sealed with 11 mm snap caps, PTFE / silicone (Chromacol,UK).

Figure 2.1. Cap for 96-microwell plate used for ω -TAm bioconversions. (A) Diagram of thermoplastic elastomer cap (B) Cap specifications (<http://www.micronic.com/products/98/tpe-capcluster-96>).

All the bioconversions were performed using 300 μ L total volume at 30 $^{\circ}$ C unless noted otherwise, and orbital shaking was provided at 300 rpm with a Thermomixer Comfort shaker (shaking diameter of 6 mm, Eppendorf, Cambridge, UK). Reactions were carried out in 50 mM HEPES buffer pH 7.5 unless noted otherwise, and the concentration of ω -TAm co-factor pyridoxal-5-phosphate (PLP) was 0.2 mM in all cases. Biocatalyst, either as a whole cell suspension, lysate or purified together with the co-factor solutions were always added first to the reaction vessel. They were then left to incubate for 20 min at 30 $^{\circ}$ C, prior to initiation of the reaction by the addition of the substrate solutions.

Aliquots of 20 μ L were taken at various time intervals, and quenched with 180 or 380 μ L of a 0.1 % (v/v) trifluoroacetic acid (TFA) solution. They were then centrifuged

for 5 min at 5000 rpm and transferred into an HPLC vials for further analysis. The specific activities were determined as the amount of Ery, AP and ABT formed per unit of time normalized by the amount of enzyme used in the reaction. The specific activity was based on the measured mass of the ω -TAm present in each bioconversion. For whole cell experiments, this was calculated based on 50 % of the dry cell weight being protein (Watson, 1972), combined with data on the percentage of total protein that was determined to be ω -TAm by SDS-PAGE analysis described in Section 2.6.5.

2.5.2. Preparative Scale Bioconversions

Bioconversions at preparative scale (volumes of 30 mL) were performed in a 50 mL titration vessel with a thermostated jacket (Metrohm Ion Analysis, Switzerland) (Figure 2.2). Temperature was maintained at 30 °C using a circulating water bath (Grant Instruments, Cambridge, UK), mixing was achieved using a magnetic stirrer at 300 rpm, and the pH was maintained at pH 7.5 by automated addition of 1 M NaOH using a 902 STAT Titrino pH controller (Metrohm Ion Analysis, Switzerland) with Tiamo 2.2 Workplace software. Sampling procedures were performed in the same way as in Section 2.5.1.

2.5.3. Second Enzyme Reaction

Bioconversions involving a second enzyme reaction were performed similarly as in Section 2.5.1. Reactions were carried out in HEPES buffer of various concentrations as discussed in Sections 4.5 and 5.6., pH 7.5. 0.5 g.L⁻¹ CV2025 ω -TAm lysate with 0.2 mM PLP co-factor solutions added first and left incubated for 20 min at 30 °C, prior to initiation of the reaction by the addition of 1.5 g.L⁻¹ ADH, 0.025 g.L⁻¹ GDH, 1 mM NADPH, 50 mM MBA, 50 or 70 mM Ery and 70 mM glucose unless otherwise stated. All enzymes, co-factors and substrates concentrations were as specified, unless noted otherwise. Again, sampling procedures were performed in the same way as in Section 2.5.1. The pH of the reaction solutions were measured using pH indicator papers (Universalindikator pH indicator pH 1 - 14, Merck Chemical Ltd., UK) at the end of each reaction period.

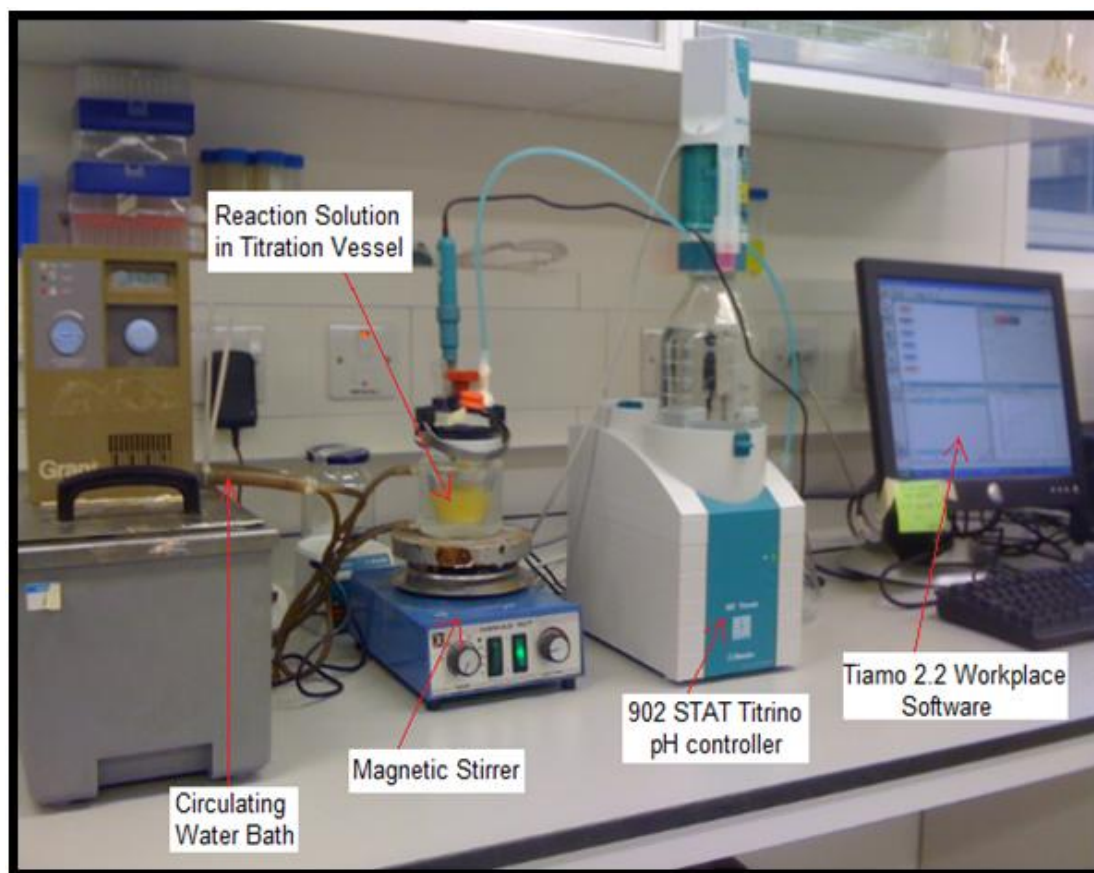


Figure 2.2. Preparative scale worktable layout used for ω -TAm bioconversions with second enzyme system (Section 6.3) and L- α -serine alternative amino donors (Section 6.4). The units operation involves the utilization of the reaction solution titration vessel placed on a magnetic stirrer for mixing purpose and connected to 902 STAT titrino pH controller and circulating water bath for pH and temperature control respectively. The 902 STAT titrino pH controller was controlled online by Tiamo 2.2 Workplace Software.

2.5.4. Reduced Pressure Reaction

Reduced pressure reactions carried out at 5 torr were performed using the same 300 μ L total reaction volume with 50 mM MBA, 50 or 70 mM Ery, 1 $\text{g}\cdot\text{L}^{-1}$ CV2025 ω -TAm, 0.2 mM PLP and 50 mM HEPES buffer (pH 7.5) at 30 $^{\circ}\text{C}$. For applying the 5 torr reduced pressure conditions, a glass 96-microwell plate was placed in an automation compatibility 96-well vacuum manifold (Supelco, Sigma-Aldrich, Gillingham, UK) which was connected to the vacuum/ pressure pump (Millipore, Durham, UK) and placed in incubator (Gallenkamp Economy Size 2 Fan Incubator, Severn Sales, Bristol, UK) for temperature control as shown in Figure 2.3. Sampling procedures were performed in the same way as in Section 2.5.1. The rate of water

evaporation was determined at this reduced pressure by measuring the weight loss over time. The evaporation study was carried out under similar conditions as the bioconversion reaction described.

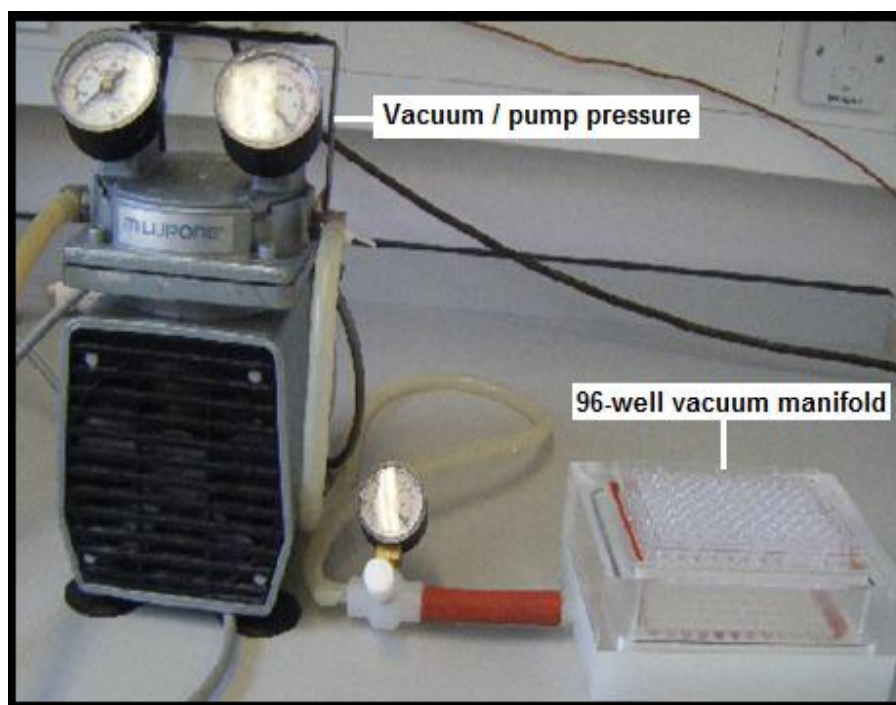


Figure 2.3. Diagram of system used for bioconversion at reduced pressure.

2.5.5. ISPR Resin Adsorption Isotherms and Bioconversions

Prior to adsorption and bioconversion experiments the commercial adsorbents (Table 2.5) used in this work as shown in Table 2.5 were conditioned as per the manufacturer's guidelines. In order to first wet the particles dry adsorbent was transferred to a 250 mL beaker and methanol was added to fully cover the adsorbent bed. The adsorbent was stirred gently and then left to stand for 30 min. The methanol was then decanted off and RO water was added, again completely covering the adsorbent bed. The adsorbent was stirred again and left to stand for a further 30 min. The wash water was decanted off, and fresh RO water added. The adsorbent was left to stand in this condition until use. Before use, the adsorbent slurry was filtered, washed with several bed volumes of RO water and filtered again until the adsorbent was dry to touch. Wetted adsorbents were used throughout this research.

Table 2.5. The chemical and physical properties of commercially available adsorbents investigated in this work.

Adsorbent	Chemical nature	Mesh size	Surface area (m ² .g ⁻¹)	Wet density (g.mL ⁻¹)	Pore volume (mL.g ⁻¹)
XAD 7	Acrylic ester	20 - 60	450	1.05	1.14
XAD 1180	polyaromatic	20 - 60	600	1.01	1.68
XAD 16	polyaromatic	20 - 60	800	1.02	1.82

Adsorption isotherms of each adsorbent were determined by weighing different amounts of adsorbent into a 96-microwell plate. The adsorbent in each well was then contacted with 300 μ L of each substrate and product solution which were prepared in 50 mM HEPES buffer, pH 7.5. The well-closed microwell plate was agitated at 500 rpm at 30 °C. In order to determine when equilibrium had been reached, several wells were prepared to contain equal amounts of adsorbent. Each well was sampled every 30 min and analyzed by HPLC as stated in Section 2.6.6. Equation 2.1 was used to calculate q , the equilibrium solid phase concentration (g.g_{ads}⁻¹) of the solute in each sample. C_i and C are respectively the initial liquid phase concentration and the liquid phase concentration at equilibrium (g.l⁻¹). V is the volume of the liquid phase (l) and M is the mass of wetted adsorbent in the experiment (g).

$$q = \frac{(C_i - C)V}{M} \quad \text{Equation 2.1}$$

Bioconversions involving ISPR resin adsorption were performed as described in Section 2.5.1 but with the additional of wetted adsorbent resins at various mass loading (30 mg ,60 mg, 100 mg, 200 mg, 1000 mg) and were shaken at 500 rpm. In order to obtain kinetic profiles, reactions were conducted using a sacrificial well procedure, where for each reaction several identical reaction wells were prepared and the entire content of a single well was used for sampling at each time interval. At every sampling point, a portion of the reaction solution was quenched as described in Section 2.5.1 and kept for HPLC analysis. Any solution left in the well was discarded (filtered with 0.2 μ m filter (Pall, MI, USA)), and the well was refilled with isopropyl alcohol (IPA) to desorb bound compounds. The adsorbent in isopropylalcohol

solution was left shaking on a thermomixer shaker for an hour prior to sampling for determination of concentrations of absorbed compounds onto resins by HPLC as described in Section 2.6.6.

2.5.6. Automated Microscale Bioconversion Processes

A Tecan platform (Tecan Genesis, Tecan UK Ltd, Berkshire, UK), equipped with an eight channel pipette arm and a Roma arm for plate manipulation was used for automated microscale process studies as shown in Figure 2.4. This was controlled using Gemini software. Disposable tips (200 μL and 1000 μL MBP[®]-BioRobotix[™] Tips, VWR International Ltd., Magna Park, UK) was used for reagent addition.



Figure 2.4. Tecan Genesis robotic platform. General views from (A) left side (B) right side.

The accuracy and precision of pipetting was checked before each experiment for the low viscosity liquids, and the dispense volumes used in this work and the error was less than 5 % in all cases (Chen et al., 2008; Micheletti et al., 2006). All the experiments were carried out in glass 96-well microtiter plates with reaction conditions as previously described in Sections 2.5.1, 2.5.3 and 2.5.4 unless otherwise stated. The microwell plate was covered with 5 layers of pre-cut pierceable films for robotics (X-Pierce™, Excel Scientific Inc., Sigma, UK). Reaction temperature and shaking were likewise controlled by the Thermomixer Comfort shaker placed in a Class II robotic containment cabinet. The reduced pressure reaction which was performed using a Tecan vacuum separator (Te-VacS™, Tecan UK Ltd, Berkshire, UK), was conducted at room temperature (23 °C). Te-VacS™ specification details are displays in Table 2.6.

Table 2.6. Specifications of Te-VacS (<http://www.tecan.com>) used in Section 5.7.

Compatibility	Genesis Series and Freedom EVO®
Integration onto Tecan platforms	Vacuum block can be accessed by robotic manipulator and liquid handling arms
Software control	Gemini™, FACTS™, Freedom EVOware®
Performance characteristics	
Capacity per Unit Te-VacS	Two 96-well plates/cartridges
Vacuum	Max. pressure difference 700 mbar Max. effective flow rate 22 l/min
Waste container control	Liquid level sensor
Dimensions (L x W x H)	
Vacuum block	255 mm x 155 mm x 50 mm
Waste bottle	160 mm x 160 mm x 530 mm
Te-VacS tower for Te-VacS	300 mm x 700 mm x 340 mm
Weight	
Vacuum block	3.3 kg
Waste bottle	2 kg
Te-VacS tower	12 kg
Supply ratings	24V DC max. 192 W

For the bioconversion reactions 20 μL aliquots were taken at various time intervals and quenched with 380 μL of a 0.1 % (v/v) trifluoroacetic acid (TFA) solution. They were then sampled into another 96-deep well storage plate with capacity 2.2 mL (Anachem Ltd., Bedfordshire, UK). The plate was then centrifuged using Tecan automated centrifuge (*Tecan UK Ltd*, Berkshire, UK) integrated with the robotic platform for 10 min at 5000 rpm, and transferred into HPLC vials for further analysis. All HPLC analyses were conducted manually (off-line) as described in Section 2.6.6. The Tecan scripts for automated microscale processes can be found in Appendix IV.

2.6. ANALYTICAL METHODS

2.6.1. Dry Cell Weight (DCW) Measurement

1.5 mL aliquots of cell suspension were added to pre-dried and pre-weighed 2.2 mL Eppendorf tubes which were then centrifuged at 13,000 rpm for 5 minutes (Eppendorf AG, Germany). The supernatant was discarded, and the tubes were left to dry at 90 °C for 24 hours until they reached a constant weight. The biomass concentration in $\text{g}_{\text{dcw}}\cdot\text{L}^{-1}$ of the culture could then be calculated. All analyses were performed in triplicate.

2.6.2. Optical Density Measurements for Biomass Quantification

Optical density measurements were performed at a wavelength of 600 nm (OD_{600}) using an Ultraspec 4000 variable wavelength spectrophotometer (Pharmacia Biotech, USA). A small aliquot of *E. coli* BL21 culture medium was taken from the appropriate culture and diluted with RO water when needed so that the optical density measurement was between 0.1 - 0.8 absorbance units. A calibration curve relating the OD_{600} measurement (Section 2.6.1) from a serial dilution of broth sample to the corresponding $\text{g}_{\text{dcw}}\cdot\text{L}^{-1}$ measurement was constructed and is shown in Appendix I. The calibration relationship determined was that 1 unit of (OD_{600}) was equal to 0.4 $\text{g}_{\text{dcw}}\cdot\text{L}^{-1}$.

2.6.3. Bradford Assay Total Protein Quantification

Protein concentrations of the lysates were obtained using the Bradford assay (Bradford, 1976) following the instructions of a commercial protein assay kit (Bio-Rad Laboratories Inc., Hemel Hempstead, UK). The method is based on the proportional binding of the dye Coomassie blue to proteins. Within the linear range of the assay ($\sim 5 - 25 \mu\text{g.mL}^{-1}$), the more protein present, the more Coomassie binds. Furthermore, the assay is colorimetric, as the protein concentration increases, the color of the test sample becomes darker. The protein concentration was calibrated against the most widely used protein, bovine serum albumin (BSA) standard curve which was generated for each assay (Appendix II). Absorbance measurements at 595 nm were carried out on an ATI Unicam UV/VIS spectrophotometer (Spectronic, Leeds, United Kingdom).

2.6.4. Purified Enzyme Quantification by UV Absorbance.

The quantification of pure enzyme concentration was performed by UV absorbance at 280 nm using an ATI Unicam UV/VIS spectrophotometer (Spectronic, Leeds, UK). Readings were blanked with the appropriate buffer solution. Absorbance measurements were converted to protein concentration using the Beer-Lambert law:

$$A = \epsilon\lambda c \quad \text{Equation 2.2}$$

Where A was the absorbance at 280 nm, ϵ is the extinction coefficient previously determined as $78,000 \text{ M.cm}^{-1}$ for ω -TAM (Matosevic, 2009), λ was the path length equal to 1 cm, and c was the protein concentration in mol.L^{-1} .

2.6.5. SDS-PAGE Electrophoresis

SDS-PAGE for protein analysis was carried out on a Mini-Protean II system (Bio-Rad Laboratories Inc., Hemel Hempstead, UK) using 8 % (w/v) Tris-Glycine commercial gels (1.5 mm, 10 well, Invitrogen, Paisley, UK). TEO buffer was used as SDS PAGE sample buffer and the contents of which are described in Table 2.7. The different components were measured out and dissolved in RO water to 1 L. The prepared 1x

TEO buffer pH was 8.4 - 8.5 at 25 °C and was diluted 20 times for use in SDS-page analysis.

Table 2.7. Composition of 1 x TEO buffer used in Section 2.6.5.

Component	Concentration (g. L⁻¹)
Tricine (free acid)	143.4
Tris (free base)	145.4
Sodium dodecyl sulphate (SDS)	20.0
Sodium meta-bisulphate	5.2

Clarified lysate or pure enzyme solutions were mixed (1:1) with Lamelli 2x concentrated protein sample buffer (Sigma-Aldrich, UK) and heated to 99 °C in a PCR machine (Techne LTD, Cambridge, UK) for 10 min. Samples were subsequently loaded onto the gel using 20 µL per well. A range of 15 to 20 µg of total protein was applied per lane to avoid saturation of the bands. 5µL of EZ-Run Prestained Rec Protein Ladder (Thermo Fisher Scientific Inc, UK) was always loaded in the first lane of the gel as protein molecular weight marker.

The gel was stained with 50 mL of Coomassie Blue staining solution containing 0.1 % (w/v) Coomassie Blue R-250, 40 % (v/v) methanol and 10 % (v/v) acetic acid and it was microwaved for 1 min and left on orbital shaker (Luckham 4RT Rocking Table, Genetic Research Instrumentation Ltd., Essex, UK) for 15 - 30 min. After washing the Coomassie Blue solution, the gel was de-stained overnight on orbital shaker with a solution 10 % acetic acid and 40 % (v/v) methanol. All gels were visualized and quantified (where appropriate) on a Gel-Doc-it bioimaging system with Labworks 4.5 software (Bioimaging systems, Cambridge) (Hierro et al., 2007). The software automatically detected and edited the splayed lanes, faint bands and tight doublets, and quantitate with a standard calibration curve from known amounts or individual lane lane loading using 1D Gel Analysis Tool. The software was also quickly measured the band instensities from uniform areas with accurate background subtraction for expression analysis using Area Density Analysis Tool.

2.6.6. HPLC Methods

A Dionex (Camberly, UK) microbore HPLC system controlled by **Chromeleon** client 6.80 software was employed for all RP-HPLC analysis. This system is comprised of a P680 gradient pump, ASI-100 automated sampler injector, STH 585 column oven and UVD170U UV detector.

MBA, AP and (R)-1-phenylethanol were analyzed using an ACE 5 C18 reverse phase column (150 mm x 4.6 mm, 5 μ m particle size, Advance Chromatography Technologies, Aberdeen, UK). A gradient was run from 15 % acetonitrile/ 85 % 0.1 % (v/v) TFA to 72 % acetonitrile/ 28 % TFA over 8 min, followed by a re-equilibrium step for 2 min (oven temperature, 30 °C, flow rate 1 mL.min⁻¹). Detection was performed by UV absorption at 210 nm (MBA) and 250 nm (AP). The retention times (in min) under these conditions were MBA, 3.4 min, AP, 7.28 min and (R)-1-phenylethanol 6.45 min.

Ery and pyruvate were analysed with an Aminex HPX-87H Ion exchange column (300 mm x 7.8 mm, Biorad, Hemel Hempstead, UK). 0.1 % (v/v) TFA was used as mobile phase for isocratic elution with an oven temperature of 65 °C and a flow rate of 0.6 mL.min⁻¹. Detection was via electrochemical detection using a standard triple protection, after raising the pH to 11 - 12 by post column addition of 0.5 N NaOH (final flow rate of 1.2 mL.min⁻¹). The retention times of Ery and pyruvate are 11.63 min and 10.43 min respectively.

2-amino-1,3,4-butanetriol (ABT) and L- α -serine were analyzed using an ACE 5 C18 reverse phase column with UV detection at 254 nm and oven temperature of 37 °C. Mobile phases used were A = 140 mM sodium acetate, pH 5.05 and B = 100 % acetonitrile. A gradient was run from 85 % A to 100 % A over 10 min, flow rate 0.5 mL.min⁻¹, followed by a column wash phase and re-equilibrium step at 1 mL.min⁻¹. Samples for analysis were first derivatized using AQC as the derivatizing agent. This derivatizing agent was synthesized "in house" as previously described in Section 2.4.3. Samples were mixed with borate buffer and briefly vortexed. A clean tip was used to reconstitute AQC reagent, which was first prepared prior to use by mixing

AQC reagent powder with dried acetonitrile as reagent diluent and heated at 55 °C until the powder dissolves. The solution was then immediately vortexed (WhirliMixer™, Fisons Scientific Equipment, Leicestershire, UK) for a few seconds and incubated at room temperature for 1 min prior to transfer to HPLC vial. The retention times of derivatized ABT and L- α -Serine were 8.9 min and 7.3 min respectively. Example chromatograms for each method and calibration curves for each of the above analysed compounds can be found in Appendix III.

2.6.7. Mass Spectrometry

Chemical ionisation (CI) mass spectrometry (Section 6.5) analyses were performed on a Thermo Finnigan MAT900xp. Methane was used as carrier gas. Operating conditions: capillary temperature 300°C, capillary voltage 9V, spray voltage 4.5 kV, sheath gas 80, auxiliary gas 30, and sweep gas 0 arbitrary units. Results are shown in Appendix V.

3. MICROSCALE QUANTIFICATION OF ω -TRANSAMINASE KINETICS

3.1. INTRODUCTION

As described in Section 1.4.4, the ω -TAm from *C. violaceum* DSM30191 (CV2025 ω -TAm) is a *Vibrio fluvialis*-like amine transaminase that shows high enantioselectivity for chiral amines, such as *S*- α -methylbenzylamine, and demonstrated the highest activity with pyruvate as amine acceptor (Kaulmann et al., 2007). While the CV2025 ω -TAm has been comprehensively studied with respect to substrate spectrum and its potential for ketodiol conversion (Kaulmann et al., 2007), there are little kinetic data in the literature on its use for industrial bioconversions. Only the recent work of Rios et al. (2011), has begun to characterise the bioconversion kinetics, but with an emphasis on establishing two-step bioconversions rather than optimisation of the CV2025 ω -TAm reaction yield.

To date most of the conventional, laboratory scale studies on the CV2025 ω -TAm have employed sealed glass vials of around 2 mL total volume and 1 mL working volume (Ingram et al., 2006). Conversion of these methods into microplate formats is worth further investigation as these would enable a further reduction in scale and the introduction of parallel operation. Adoption of microplate formats also facilitates the ready automation of ω -TAm experiments (Lye et al., 2003) and take advantage of the large commercial investment in laboratory robotics. The ability to relate bioconversion kinetics from conventional scales to the microscale would then

facilitate high throughput investigation and improve understanding of the key engineering parameters of ω -TAm bioconversion to aid efficient bioprocess design.

The choice of a particular type of reaction to study between asymmetric synthesis from prochiral compounds and kinetic resolution from racemic compounds depends on the enantioselectivity of the enzyme and the economics of the reaction process (Section 1.4.8). ω -TAm which have sufficiently high enantioselectivity could lead to a useful asymmetric synthesis permitting the production of highly enantiopure chiral amines. The asymmetric synthesis of chiral amines with ω -TAm may also offer many potential advantages over kinetic resolution as described in Section 1.4.8.

An accurate understanding of enzyme kinetic properties is a prerequisite for the effective optimisation of ω -TAm catalysed bioconversions. Here, the CV2025 ω -TAm catalysed bioconversion between MBA and pyruvate (Figure 3.1) was selected as an initial model reaction for study with the CV2025 ω -TAm. This is known to have a fast reaction rate with these substrates (Section 1.4.5) and is easily quantified by HPLC, (Section 2.6.6.) therefore, making it a good model for microscale evaluation of CV2025 ω -TAm reaction conditions, parameters and behaviours.

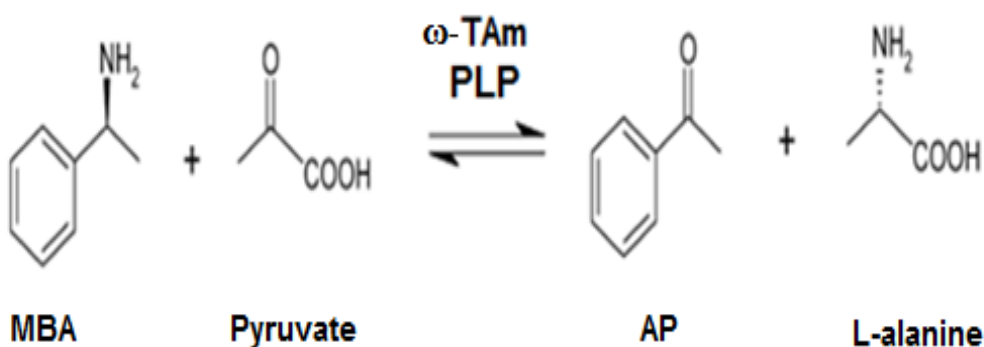


Figure 3.1. Reaction yield scheme of the CV2025 ω -TAm catalyzed transamination between (S)- α -methylbenzylamine (MBA) and pyruvate to acetophenone (AP) and L-Alanine in the presence of co-factor, pyridoxal-5-phosphate (PLP).

3.2. AIM AND OBJECTIVES

The aim of this Chapter was to develop microwell experimental methods for evaluation of the basic kinetic properties of the CV2025 ω -TAM from *C. violaceum* DSM30191 at the microlitre scale (< 1 mL). The preliminary approach will involve investigations of a model reaction of MBA and pyruvate each at a relatively low substrate concentration of 50 mM each. Validated microwell scale methods for quantitative data generation could enable further investigation of enzyme mechanisms with different substrates under optimum reaction conditions to help overcome the low ω -TAM reaction yields. The key objectives of this Chapter are thus:

- To initially increase CV2025 ω -TAM production in *E. coli* by optimisation of fermentation conditions for enzyme expression and to scale-up production of the biocatalyst from shake flask to 7.5 L stirred bioreactor scales.
- Use of the published model of ω -TAM bioconversions to establish base-line bioconversion kinetics for conventional lab scale reactions.
- To establish equivalent microscale experimental methods in 96-microwell plate formats for CV2025 ω -TAM bioconversions at the 300 μ L scale and to compare these with the standard laboratory scale bioconversion kinetics.
- To identify a suitable reaction system with readily analyzed substrates that displays typical, equilibrium controlled bioconversion kinetics that might be further developed or enhanced by microscale process design for overcoming unfavorable reaction equilibrium

3.3. ω -TRANSAMINASE PRODUCTION AND LYSATE PREPARATION

3.3.1. CV2025 ω -TAM Production at Shake Flask and 7.5 L Bioreactor Scales

The growth and production studies of *E.coli* BL21 (DE3) Gold cells with plasmid pQR801 for expressing the CV2025 ω -TAM were accomplished in shake flask and

bioreactor scale fermentations. The shake flask fermentation was performed in a 2 L shake flask with a working volume of 200 mL. The fermentation procedure was detailed in Section 2.2.1 while the media used (LB-glycerol) was defined in Table 2.1. The shake flask scale fermentation was shown to reach typical final biomass concentration of $1.4 \text{ g}_{\text{dcw}} \text{ L}^{-1}$. As observed in the growth curves (Figure 3.2), cells grew exponentially and the induction of CV2025 ω -TAm expression was achieved by the addition of 1 mM IPTG when an $\text{OD}_{600\text{nm}}$ of ~ 0.6 was reached. The cell growth reached a plateau once the stationary phase was reached after a period of approximately 7 hours. The fermentation was stopped and harvested 3 hours later.

In order to increase the total volume of fermentation and the overall amount of CV2025 ω -TAm produced, the fermentation was scaled up to a 7.5 L stirred tank fermenter with a working volume of 5 L which was operated in a fed-batch mode (Section 2.2.3). Fed-batch is the most common mode of fermentation operation in industry because it allows for control of the environment conditions and particularly maintenance of the glucose concentration at defined levels (Lemuth et al., 2008). Parameters like DOT, pH, temperature and impeller speed were logged throughout the fermentation.

As shown in Figure 3.2, cells grew exponentially during the initial batch phase with a specific growth rate of 0.365 hr^{-1} . Cell growth reached a plateau after 4 hours indicating limitation of a key nutrient. At this point feeding was started with pre-sterilized medium containing $5 \text{ g}\cdot\text{L}^{-1}$ glycerol to promote further cell growth and hence a higher final cell density (Section 2.2.3). The detection of a sharp rise in the DOT profile at approximately 4 hours was also an indication of reduced oxygen consumption suggesting glycerol limitation in the growth medium.

Following feed addition cells resumed growth almost instantaneously as indicated by both the increase in biomass dcw (Figure 3.2) and the reciprocal decrease DOT level (Figure 3.3). 1.0 mM IPTG was added to induce CV2025 ω -TAm synthesis after 7 hours of fermentation when the OD_{600} of the broth reached 6.0 ($3.4 \text{ g}_{\text{dcw}}\cdot\text{L}^{-1}$). 0.2 mM PLP was also added to the broth at this point in order to study the effects of co-factor on CV2025 ω -TAm expression and catalytic activity. Cell growth continued after

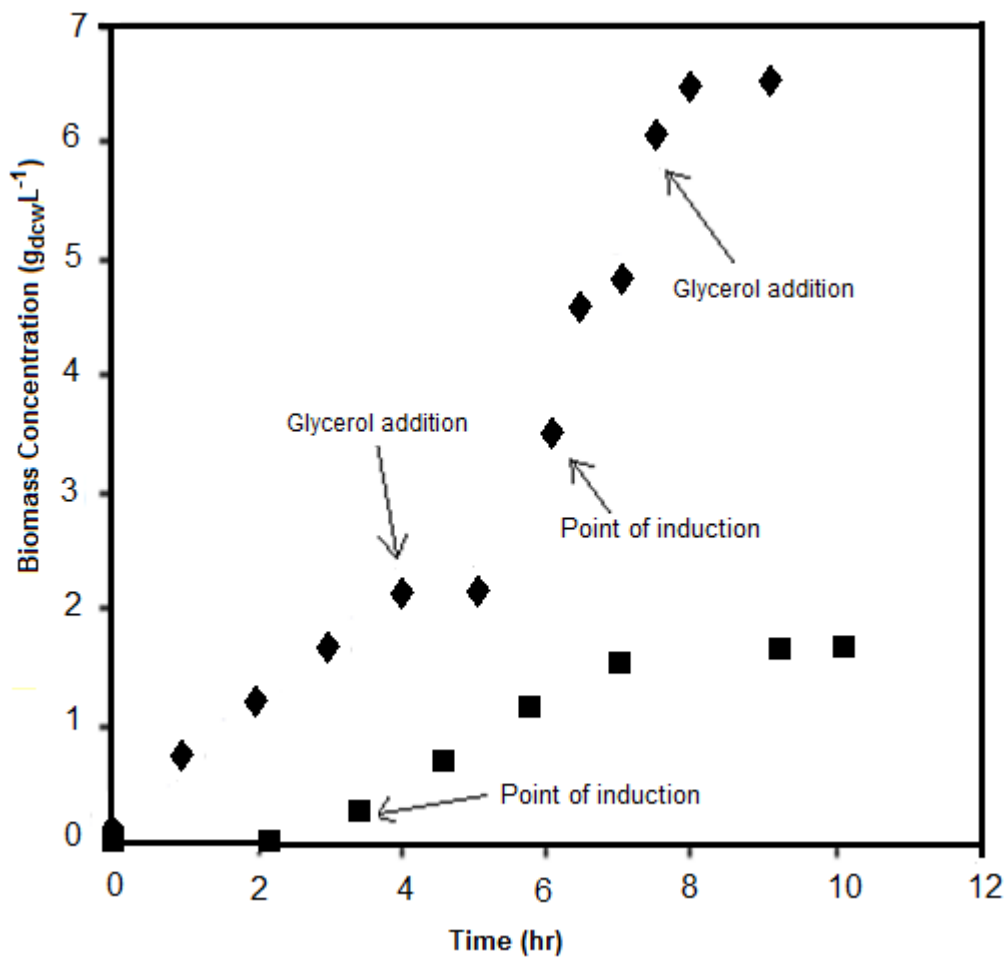


Figure 3.2. Growth kinetic profiles for *E.coli* BL21 (DE3) Gold cells containing plasmid pQR801 in a 2 L shake flask (■) and a 7.5 L bioreactor (◆) cell cultivation scales with the fed-batch operation. The temperature for both scales was set at 37 °C. Cell cultivation conditions for the 7.5 L bioreactor were pH 7.5, 800 rpm and air flow of 1.4 L min⁻¹. Cell cultivation carried out as described in Sections 2.2.1 (Shake flask scale) and 2.2.3 (bioreactor scale).

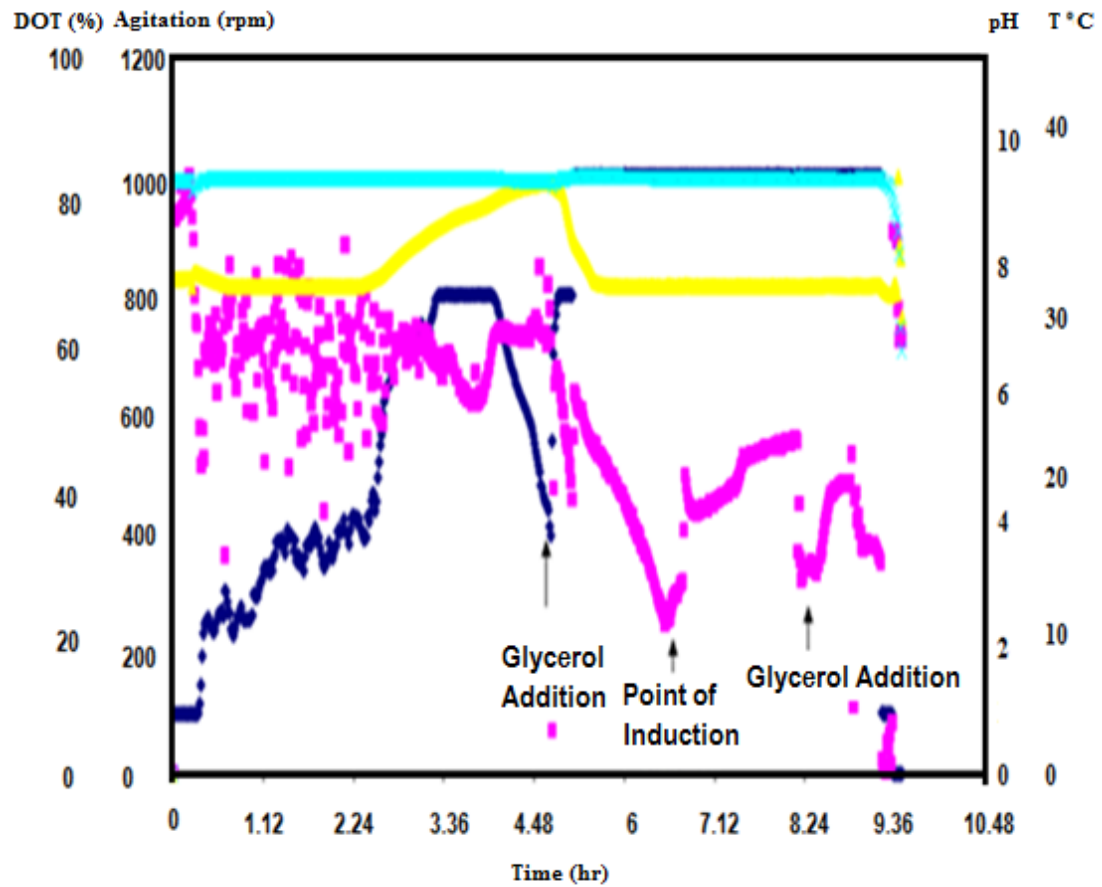


Figure 3.3. Online measurement of pH (\blacktriangle), temperature (\times), DOT(\blacksquare) and agitation rate (\blacklozenge) for the 7.5 L fed-batch bioreactor fed-batch fermentation shown in Figure 3.2. Operating conditions and experimental procedure as described in Section 2.2.3.

feeding at a growth rate of 0.240 hr^{-1} . As observed in the initial batch culture phase, the cell growth reached a stationary phase plateau after a further 4 hours, and hence a second batch of feed addition glycerol was supplied. The fermentation was continued for an hour and then stopped as decreases in agitation speed (which was controlled in a cascade manner by stirrer speed) as well as DOT level were observed.

The maximum biomass concentration obtained in the first 7.5 L fermenter run was $6.9 \text{ g}_{\text{dcw}}\cdot\text{L}^{-1}$ which was about 6-fold higher than the corresponding shake flask culture described earlier. As expected, the improvement of cell growth rate was due to the improvement of oxygen transfer rates and better controlled environmental conditions in the stirred bioreactor. Above all, the fed-batch mode used for the addition of nutrient feeding as cell experienced nutrients shortage have proof to greatly enhance the growth rate. The effect of PLP addition on CV2025 ω -TAm catalytic activity is further discussed in Section 3.3.3.

3.3.2. Characterization of CV2025 ω -TAm Synthesis

At the end of the cultures, cells were lysed and total intracellular proteins were analysed using the Bradford assay (Section 2.6.3). Using a BSA standard curve (Appendix II), the total protein concentrations measured at the end of the shake flask and 7.5 L bioreactor cultures were $2.6 \text{ g}\cdot\text{L}^{-1}$ and $5.2 \text{ g}\cdot\text{L}^{-1}$ respectively indicating a 2-fold increase in the stirred bioreactor.

SDS-PAGE analysis of the soluble intracellular protein showed that the recombinant CV2025 ω -TAm migrated as a single band of approximately 47.5 kDa (Kaulmann et al., 2007). The CV2025 ω -TAm was seen to be expressed at a high level (Figure 3.4) making up some 40 % w/w ($1.04 \text{ g}\cdot\text{L}^{-1}$) and 43 % w/w ($2.22 \text{ g}\cdot\text{L}^{-1}$) of the protein in the clarified soluble fraction for the shake flask and 7.5 L bioreactor cultures respectively. All the bioconversion reactions with CV2025 ω -TAm in this research were carried out either using lysates from shake flask or 7.5 L bioreactor fermentations unless otherwise stated.

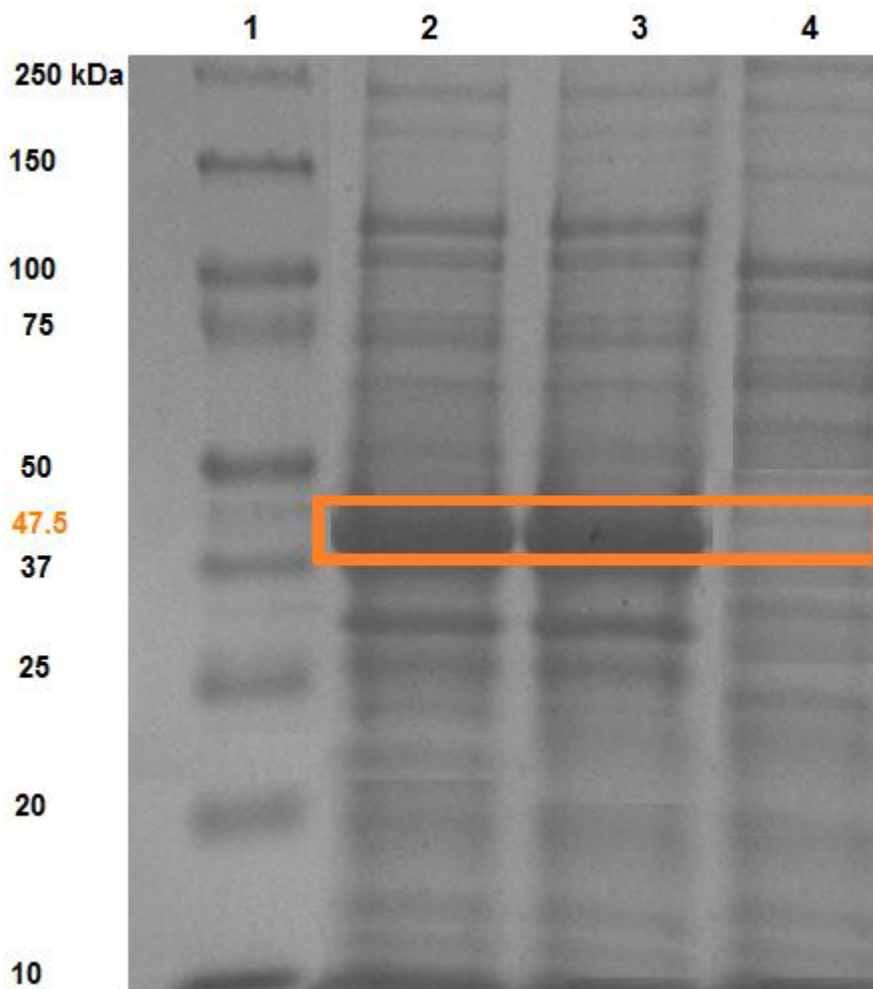


Figure 3.4. SDS-PAGE gels showing intracellular expression of CV2025 ω -TAm in cellular extracts of *E. coli* BL21 (DE3)-Gold cells. Lane 1 is protein marker, Lane 2 is protein expression from shake flask culture, Lane 3 is protein expression from 7.5 L bioreactor culture and Lane 4 is protein expression from uninduced plasmid of *E. coli* BL21 (DE3)-Gold cells. Molecular weight of CV2025 ω -TAm is 47.5 kDa and for both culture scales it appears highlighted in the box.

3.3.3. Influence of Pyridoxal 5' Phosphate (PLP) Addition

Like other classes of transaminases (Section 1.4.2), ω -TAm requires PLP as a firmly bound prosthetic group. The addition of low concentrations of PLP to the enzyme solution enhances formation of E-PLP, resulting in enhancement of enzyme stability (Shin et al., 2003). Enzyme stability in the reaction mixture is a very important factor affecting bioconversion yield and productivity (Ingram et al., 2007; Shin et al., 2003). This is especially true in bioconversions lasting over 24 hours, which can be the case for the CV2025 ω -TAm with the majority of amino donors and amino acceptors (Smith et al., 2010; Ingram et al., 2007).

The effect of PLP on enzyme stability was studied by comparison of CV2025 ω -TAm bioconversion kinetics using lysates produced from either the 7.5 L bioreactor or the shake flasks. CV2025 ω -TAm obtained from shake flask culture was added with 0.2 mM PLP during centrifugation step in cell free lysate preparations (Section 2.3.1) and was incubated with the same concentration of PLP in bioconversion reactions prior to substrate addition (Section 2.5.1).

In contrast, CV2025 ω -TAm produced from the bioreactor was synthesised in the presence of 0.2 mM PLP added from the start of the fermentation process (Section 3.3.1). After harvesting, the process was followed by cell free lysate preparation (Section 2.3.1) in which PLP was again added prior to sonication and in centrifugation steps, and finally the lysate was incubated with PLP in the bioconversion reaction (Section 2.5.1).

Figure 3.5 shows the experimental progress curves for the CV2025 ω -TAm catalysed bioconversion of 50 mM MBA and 50 mM pyruvate using biocatalyst produced in both the shake flasks and the 7.5 L fermenter with concentrations of 0.6 g.L⁻¹ and 0.3 g.L⁻¹ CV2025 ω -TAm respectively. Good agreement was found between the experimental data, where the conversion was only much faster using the shake flask biocatalyst as expected due to its 2 times higher concentration of CV2025 ω -TAm (Section 3.3.2). Nevertheless, the specific initial rates of bioconversions with CV2025 ω -TAm obtained from the fermenter were marginally higher than the shake flask scales which were 2.88 and 2.1 $\mu\text{mol}\cdot\text{min}^{-1}\cdot\text{mg}^{-1}$ respectively. The bioconversions

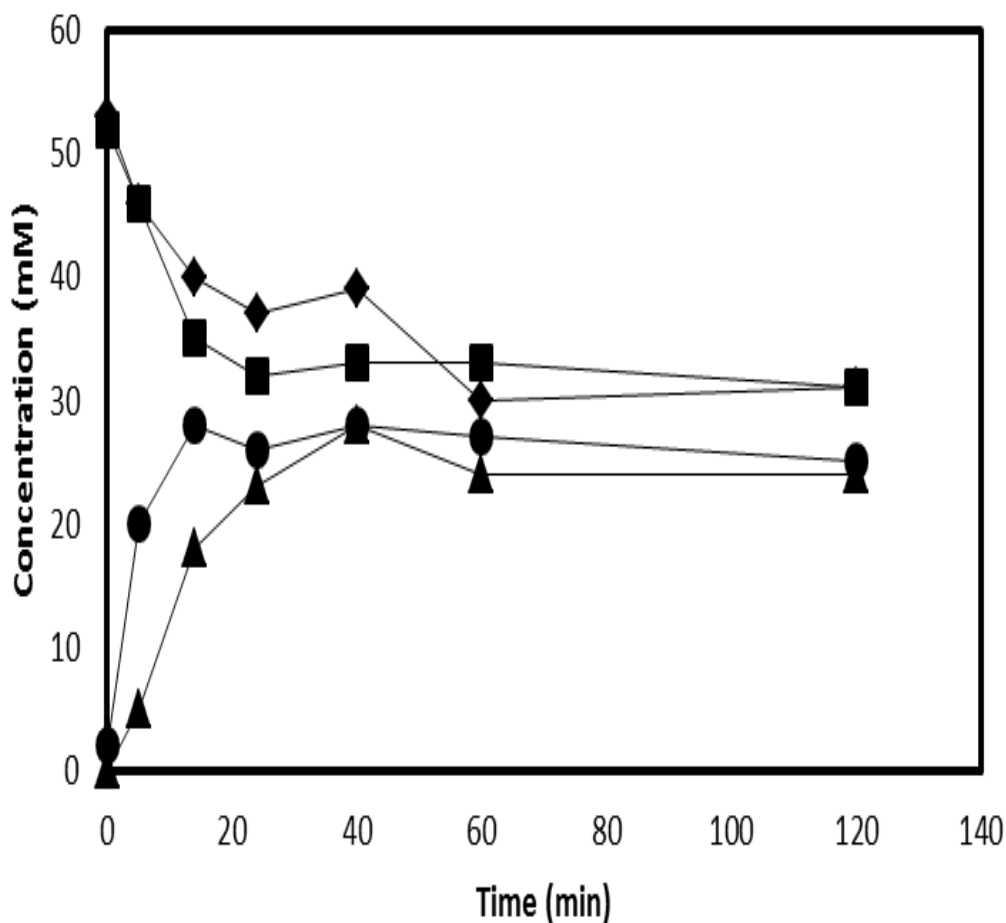


Figure 3.5. Bioconversion kinetics of CV2025 ω -TAM clarified lysates obtained from 2 L shake flask (where 0.3 mM PLP was added only during centrifugation step) and 7.5 L bioreactor fermentation (where 0.3 mM PLP was added during the fermentation process and during cell free lysate preparation) (Section 3.3.1): MBA consumption (■) and AP production (●) for 2 L shake flask cell culture and MBA consumption (◆) and AP production (▲) for 7.5 L bioreactor cell culture. Reaction conditions: 0.6 g.L⁻¹ CV2025 ω -TAM for 2 L shake flask culture and 0.3 g.L⁻¹ CV2025 ω -TAM for 7.5 L bioreactor cells culture; 0.2 mM PLP; [MBA] and [pyruvate] were 50 mM each; 30 °C; pH 7.5; 300 rpm in 50 mM HEPES buffer; total volume of 300 μ L in glass vials. Bioconversions performed as described in Section 2.5.1.

from both scales shown a comparable optimum conversion of approximately 60 % (mol.mol⁻¹) reached at 16 min for biocatalyst from shake flask scale and 40 min for biocatalyst from bioreactor scale. This observation indicates the extra addition of PLP to the fermentation process and lysate preparation steps significantly improves the CV2025 ω-TAm catalytic activity. Therefore, the CV2025 ω-TAm concentration of 0.3 g.L⁻¹ was chosen as a standard parameter for investigating the CV2025 ω-TAm bioconversions further throughout the study.

3.3.4. Stability of Stored and Fresh Cells Lysate

CV2025 ω-TAm bioconversions using fresh lysate and stored lysate frozen at -80 °C were performed to examine their effect on enzyme stability. Hence, both types of clarified lysates were used to catalyse the bioconversion of 50 mM MBA and 50 mM pyruvate. As shown in Figure 3.6, the frozen lysate was stable for at least 6 months as the reaction kinetics showed no significant difference to those using freshly prepared CV2025 ω-TAm lysate. The stored lysate used here was obtained from the 7.5 L bioreactor fermentation (Section 3.3.1). Accordingly, the addition of an excess PLP during the fermentation (Section 3.3.3) may be one of the factors responsible for ensuring the long-term stability of CV2025 ω-TAm activity during storage.

As a consequent of these results, either fresh or stored lysate were used throughout this study interchangeably. In general, the storage stability can vary from a few weeks to more than a year and is dependent on the nature of the protein and the storage conditions used. Freeze-thaw cycles are known to compromise protein stability. Repeated freeze-thaw cycles will cause protein damage due to ice crystal formation during freezing that can lead to protein denaturation and also cause a loss of phosphate groups (Cao et al., 2003). Therefore, the lysates prepared here for frozen storage were initially dispensed and prepared in single-use aliquots so that repeated freeze-thaw cycles were avoided.

The same practice was applied in preparing frozen stock solutions of substrates, products and others compounds used in this research. In these cases, the compounds were prepared in the desired type and concentration of buffer and were adjusted to the

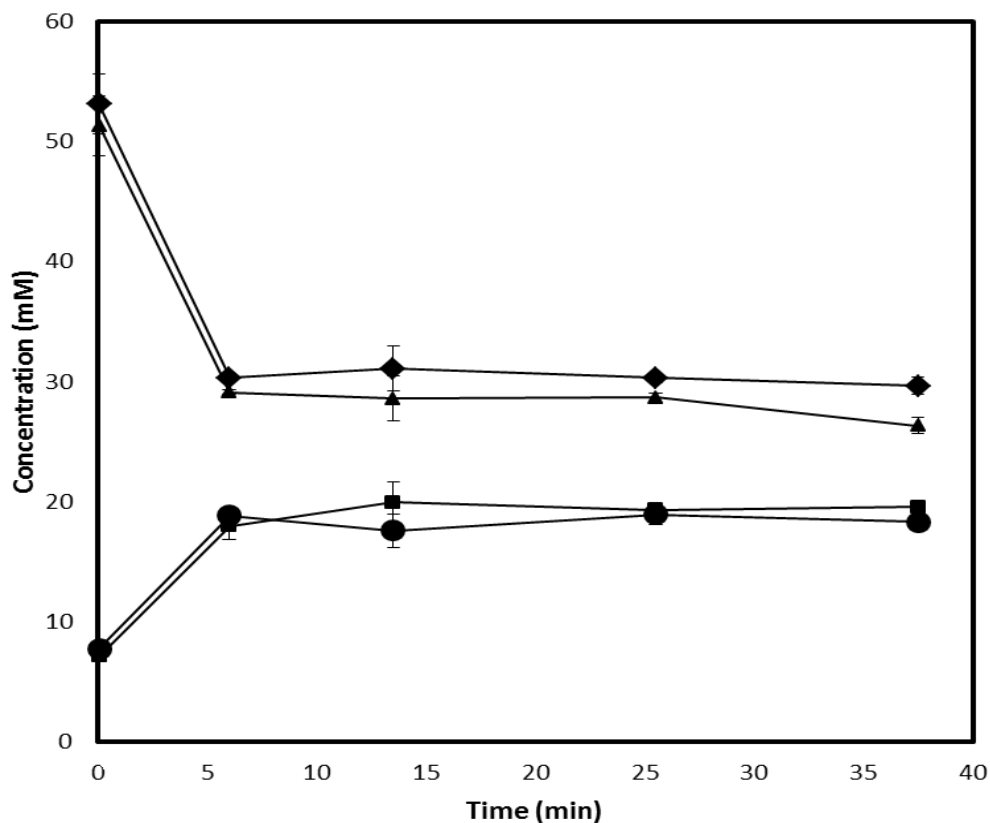


Figure 3.6. Bioconversion kinetics using either fresh or stored clarified CV2025 ω -TAm lysates (6 months at $-80\text{ }^{\circ}\text{C}$): MBA consumption (\blacklozenge) and AP production (\blacksquare) for fresh clarified lysate and MBA consumption (\blacktriangle) and AP production (\bullet) for stored clarified lysate. Reaction conditions: $0.3\text{ g}\cdot\text{L}^{-1}$ CV2025 ω -TAm; 0.2 mM PLP; [MBA] and [pyruvate] were 50 mM ; $30\text{ }^{\circ}\text{C}$; pH 7.5; 300 rpm in 50 mM HEPES buffer; total volume of $300\text{ }\mu\text{L}$ in glass vials. Stored lysate obtained from 7.5 L bioreactor fermentation (Section 3.3.1) and bioconversions performed as described in Section 2.5.1. Error bars represent one standard deviation about the mean ($n=3$).

desired pH prior to storage at -20 °C. Control experiments showed that freezing of these stock solutions for up to 6 months had no significant impact on the CV2025 ω -TAm bioconversion kinetics.

3.4. IDENTIFICATION OF LEAD ω -TRANSAMINASE AND INITIAL BIOCONVERSION CONDITIONS

3.4.1. Activity of His-tagged (PQR801) and non His-tagged (PQR800) CV2025 ω -TAm

Labelling of recombinant proteins with polypeptide fusion partners or affinity tags is a useful method to facilitate subsequent protein purification and detection. Poly-histidine tags (His-tags) are among the most commonly used affinity tags (Heijbel, 2003). Plasmid pQR801 expressing the CV2025 ω -TAm enzyme was therefore constructed with a His₆-tag at the enzyme's N-terminus to facilitate rapid single-step purification using His-Select Nickel Affinity Gel, an immobilized metal-ion affinity chromatography (IMAC) product. The use of IMAC to rapidly purify His-tagged proteins is widely used as a tool for simple and inexpensive production of large quantities of pure industrial enzymes (Benevides et al., 2003; Bastida, et al., 1998; Crowe et al., 1994; Porath et al., 1975).

CV2025 ω -TAm clarified lysates obtained from two different plasmids pQR800 (non His-tagged protein) and pQR801 (His-tagged protein) were used in a comparative study to check that there were no detrimental effects of adding the His-tag on CV2025 ω -TAm activity and stability. As shown in Figure 3.7, both enzyme preparations showed similar bioconversion kinetics with 50 mM MBA and 50 mM pyruvate as substrates. The non His-tagged CV2025 ω -TAm showed marginally higher AP production rates while the MBA consumption rates were similar. The slightly higher AP production measured for the non His-tagged enzyme (CV2025 ω -TAm with plasmid pQR800) is most probably due to experimental errors caused by the way in which reaction samples were treated particularly regarding AP evaporation during sample storage and HPLC analysis. Overall, the results suggest that the poly-His tag fusion did not affect the activity and stability of the CV2025 ω -TAm and so enzymes

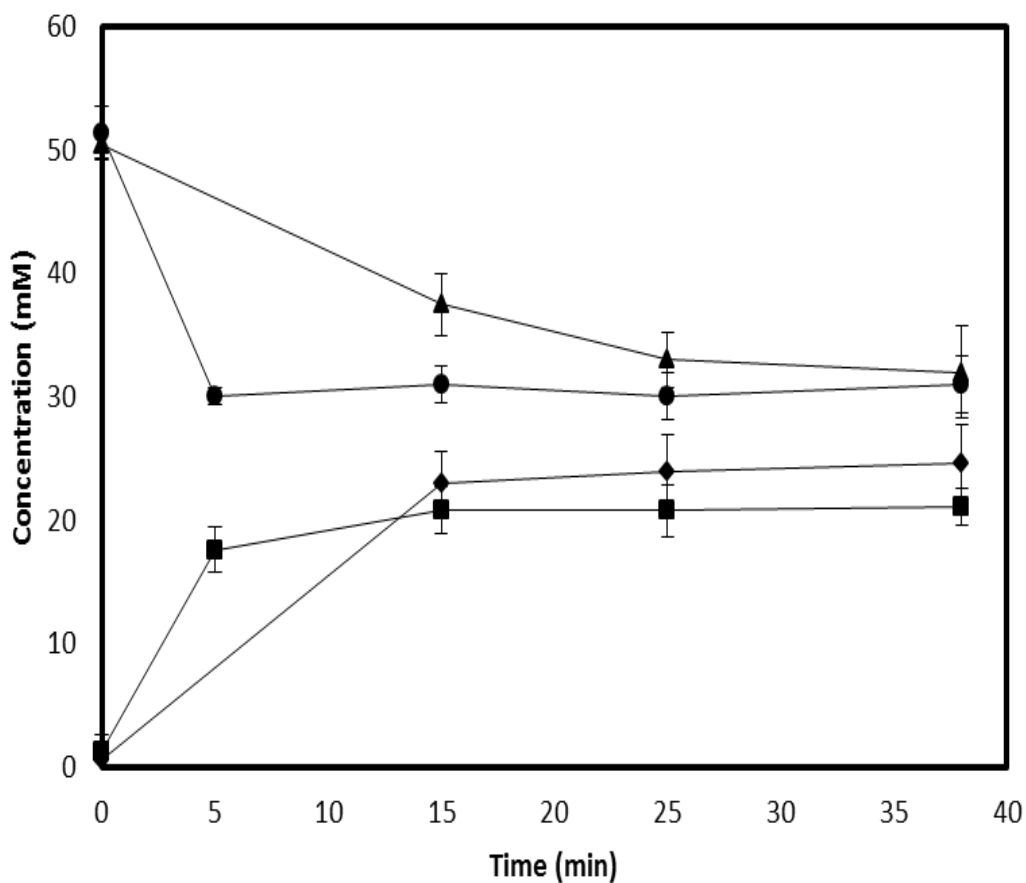


Figure 3.7. Bioconversion kinetics of CV2025 ω -TAm clarified lysates prepared using plasmids pQR 800 (non His-tagged) and pQR801 (His-tagged): MBA consumption (▲) and AP production (◆) for non His-tagged lysate and MBA consumption (●) and AP production (■) for His-tagged lysate. Reaction conditions: 0.3 g.L^{-1} CV2025 ω -TAm; 0.2 mM PLP; [MBA] and [pyruvate] were 50 mM ; $30 \text{ }^\circ\text{C}$; pH 7.5; 300 rpm in 50 mM HEPES buffer; total volume of $300 \text{ }\mu\text{L}$ in glass vials. Bioconversions performed as described in Section 2.5.1. Error bars represent one standard deviation about the mean ($n=3$).

preparations used during the remainder of this research were prepared from His-tagged plasmids.

3.4.2. Activity Determination at Laboratory and Microwell Scales

Previous laboratory studies on CV2025 ω -TAm bioconversions were performed using conventional 2 mL, flat bottom, snap-cap vials (Section 2.5.1). These come with a wide selection of sealing caps appropriate for an excellent seal preventing evaporation. The vials are Class 1 hydrolytic extraction neutral borosilicate glass to give assurance of sample stability and low extraction of compounds in liquid samples making them appropriate when dealing with compounds such as MBA which is known to degrade plastic vials. In developing an equivalent high-throughput microscale approach, microwell plate formats will be employed. These are typically manufactured in a range of well densities (6 – 1536 wells) and materials. The advantages include the available range of microtitre plates and associated equipment such as multi-channel pipettes, laboratory robotic platforms, microplate readers and HPLC autosamplers.

Consequently, a comparative study to translate the conventional CV2025 ω -TAm bioconversion method into an effective 96-microwell plate format was performed. Choices of plate type, material and options for sealing individual wells were among the major factors for consideration. The material used for sealing individual wells within the plate can have a significant effect on the overall performance of the reaction system. Without an effective seal, loss of volatile components such as AP, from the reaction mixture will impact on reaction kinetics, equilibrium and analysis. As mentioned in Section 2.5.1, a glass, 96-microwell plate was used which shows the good compatibility with most type of solvents and resistance to chemical attack. Wells were sealed using a thermo plastic elastomer cap to prevent evaporation.

The CV2025 ω -TAm is more stable as a lysate instead of purified enzyme hence this form of the biocatalyst was used (Ingram et al., 2007). Similarly to the previous extensive studied ω -TAm from *Vibrio fluvialis* (Shin and Kim, 2001), substrate inhibition of the CV2025 ω -TAm by MBA and pyruvate was not observed below 100 mM. Reaction solutions containing 50 mM each of MBA and pyruvate were thus used

to examine bioconversion kinetics in the microwell format and standard vials. Again, both reactions were performed as previously described in Section 2.5.1.

In experiments with both formats containers were sealed throughout the reaction and the covers were only peeled off at each sampling point. Overall CV2025 ω -TAm bioconversions performed using either conventional standard glass vials or 96-well plates showed suitably comparable results. The initial rates determined in both reaction formats were maximised up to 30 to 40 min of reaction (Figure 3.8). After approximately 60 % ($\text{mol}\cdot\text{mol}^{-1}$) conversion, the product concentrations peaked and then decreased slightly in the last 3 time points. This is most probably because some AP had evaporated out of the system during sample preparation and analysis.

In previous work, it was found that the bioconversion of 50 mM MBA and 50 mM pyruvate catalysed by the ω -TAm from *Bacillus thuringiensis* JS64 gave almost quantitative bioconversion since the equilibrium completely favours product formation in the forward direction producing L-alanine (Shin and Kim, 1998; Kaulmann et al., 2007). This was not the case using the CV2025 ω -TAm. The product inhibition exerted by AP could be the major cause for the incomplete conversion attained (Shin and Kim, 1998). This assumption is confirmed later in Section 4.3 and methods to remove AP during the reaction so as to increase yield are explored in Chapters 4 and 5.

3.4.3. Influence of pH

The effect of pH on CV2025 ω -TAm activity in both clarified lysate and whole cell forms were investigated as shown in Figure 3.9. The optimum pH for activity of the CV2025 ω -TAm lysate appears to be about pH 7.5. This is in agreement with the previous work using CV2025 ω -TAm for the synthesis of (2S, 3S)-2-aminopentane-1, 3-diol from (3)-1,3-dihydroxypentane-2-one and isopropylamine substrates (Smith et al., 2010). In contrast, for the whole cell CV2025 ω -TAm, the enzyme activity remained almost unaffected at all pH values tested apart from at pH 8 where a significantly lower activity was measured. This is because the internal environment of the cell is still much closer to neutral and is usually fairly insensitive to the external environment (Guo et al., 2009b).

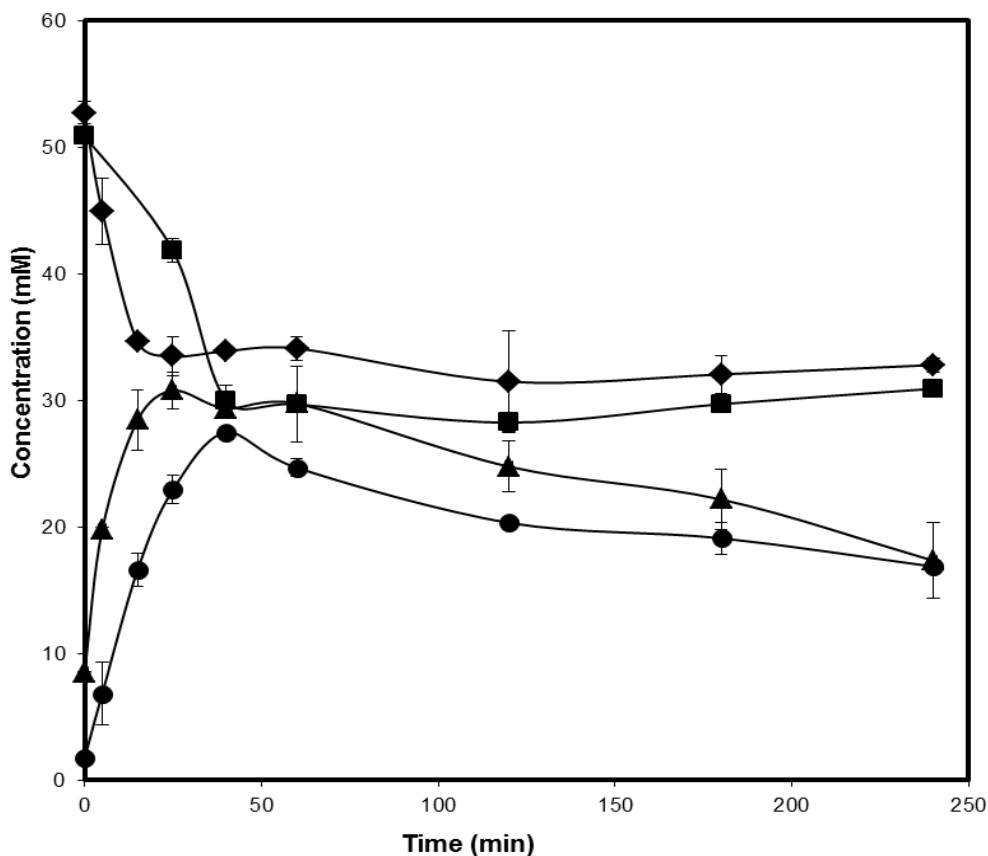


Figure 3.8. Bioconversion kinetics for CV2025 ω -TAM clarified lysate performed in glass vials and 96-well glass microplate formats: MBA consumption (◆) and AP production (▲) for vial format and MBA consumption (■) and AP production (●) for 96-microwell plate format. Reaction conditions: 0.3 g.L⁻¹ CV2025 ω -TAM; 0.2 mM PLP; [MBA] and [pyruvate] were 50 mM; 30 °C; pH 7.5; 300 rpm in 50 mM HEPES buffer; total volume of 300 μ L, CV2025 ω -TAM obtained from 7.5 L bioreactor fermentation (Section 3.3.1) and bioconversions performed as described in Section 2.5.1. Error bars represent one standard deviation about the mean (n=3).

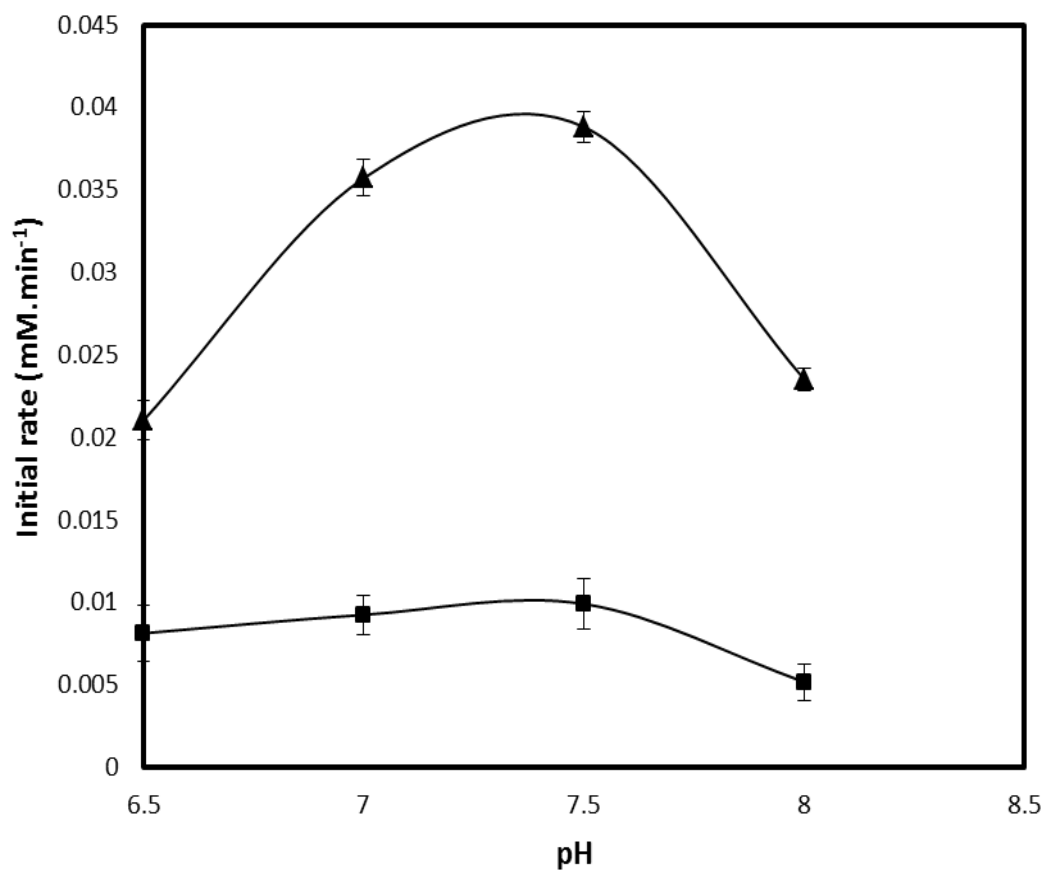


Figure 3.9. Effect of pH on the initial rate of AP production by clarified CV2025 ω -TAm lysate (▲) and whole cells (■) of *E. coli* with plasmid pQR801 expressing CV2025 ω -TAm. Reaction conditions: [MBA] and [pyruvate] were 50 mM; 30 °C; 300 rpm in 50 mM HEPES buffer; total volume of 300 μ L in 96-glass microwell plate. Bioconversions performed as described in Section 2.5.1. Error bars represent one standard deviation about the mean (n=3).

3.5. L-ERYTHRULOSE (ERY) BIOCONVERSION KINETICS

3.5.1. Kinetic Profile of CV2025 ω -TAm Bioconversion

In the previous sections pyruvate was used as substrate in order to develop the microscale experimental methods to be used throughout this thesis. However, most industrially relevant substrates tend to show poor equilibrium conversions (Tufvesson et al., 2011; Buchholz et al., 2005). Since the major aim of this thesis is to explore microscale methods to increase ω -TAm bioconversion yields, a new reaction model was chosen for investigation.

The particular bioconversion investigated will use Ery as amino acceptor (Figure 3.10). Among various amino acceptors tested in a previous study (Kaulmann et al., 2007), Ery shows a low conversion yield of just 14 - 22 % at reaction equilibrium (Table 1.2 (Chapter 1.4.7)).

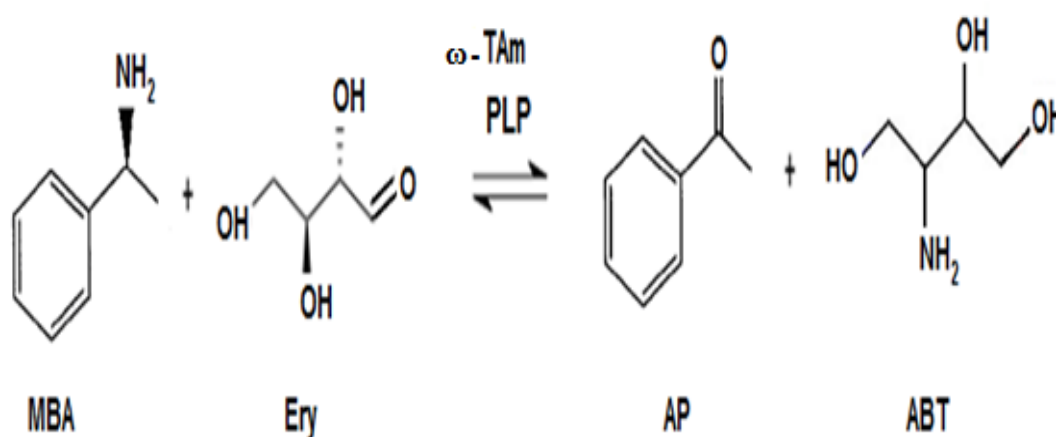


Figure 3.10. Reaction yield scheme of the CV2025 ω -TAm catalyzed transamination between (S)- α -methylbenzylamine (MBA) and L-erythrulose (Ery) to acetophenone (AP) and 2-amino-1,3,4-butanetriol (ABT) in the presence of co-factor pyridoxal-5-phosphate (PLP).

As discussed in Section 3.4.2, experiments will be performed in a 96-well glass microtitre plate covered with a thermo plastic elastomer cap for closed environment conditions. In addition, based on all the previous studies, the reaction conditions selected for this preliminary reaction evaluation were 30 °C, pH 7.5 in 50 mM HEPES

buffer using a clarified CV2025 ω -TAm lysate produced from plasmid pQR801 (His-tagged). The biocatalyst was produced in a single 7.5 L fermentation (Section 3.3.1) so as to provide a continuous and stable source of CV2025 ω -TAm for use in all subsequent studies.

The CV2025 ω -TAm bioconversion was conducted as detailed in Section 2.5.1. A complete kinetic profile comprising depletion of both substrates and formation of both products were plotted here for more precise analysis of the actual data attained (Figure 3.11). In order to quantify the ABT product a derivitization method using AQC reagent (Section 2.4.3) was used prior to HPLC analysis (Section 2.6.6).

As shown in Figure 3.11, after 15 hours, the final reaction yield was only 26 % ($\text{mol}\cdot\text{mol}^{-1}$). This is about half that obtained in the previous reactions with pyruvate as amino acceptor. The low conversion observed here underlines the unfavourable equilibrium seen with many ω -TAm substrates which may also be influenced by strong by-product (AP) inhibition (Section 1.4.9). This reaction therefore provides a useful and relevant model system by which to investigate methods for increasing the bioconversion yield.

3.5.2. Influence of Biocatalyst Form: Clarified Lysate and Whole Cells

The kinetics of the Ery bioconversion using the CV2025 ω -TAm were further studied to evaluate both isolated enzyme and whole cell forms of the biocatalyst. Whole cell biocatalysts are easier to prepare, but in developing whole-cell biocatalytic processes, it is becoming important to consider the effects of medium, process conditions, substrates, and products, on cell physiology, enzyme activity, and cofactor regeneration (Held et al., 2000).

As shown in Figure 3.12 the whole cell CV2025 ω -TAm biocatalyst showed a better performance than the clarified lysates for bioconversion of 50 mM MBA and 50 mM Ery. Typical reactions kinetic profiles of CV2025 ω -TAm bioconversions in the case of whole cell and clarified lysate forms are preceded with optimum product yield of 40 % ($\text{mol}\cdot\text{mol}^{-1}$) and 26 % ($\text{mol}\cdot\text{mol}^{-1}$) respectively.

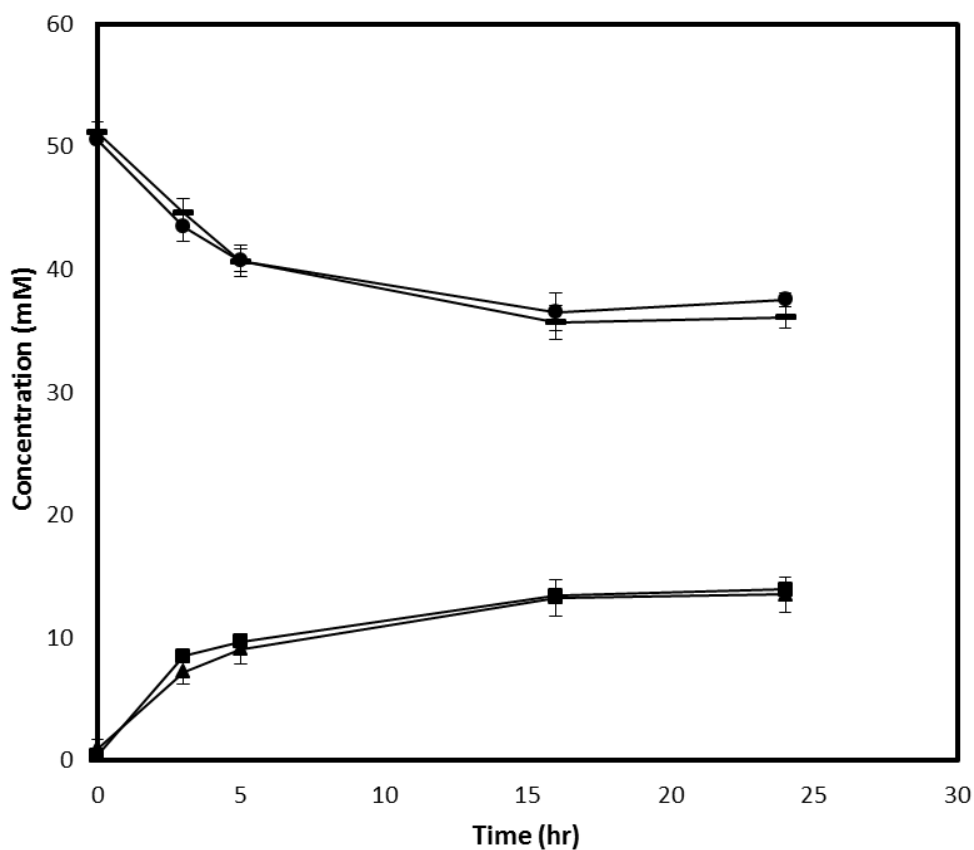


Figure 3.11. Bioconversion kinetics using CV2025 ω -TAm clarified lysate with Ery as amino acceptor: MBA consumption (●); Ery consumption (-); ABT production (▲) and AP production (■). Reaction conditions: $0.3 \text{ g}\cdot\text{L}^{-1}$ CV2025 ω -TAm; 0.2 mM PLP; [MBA] and [Ery] were 50 mM ; $30 \text{ }^\circ\text{C}$; pH 7.5; 300 rpm in 50 mM HEPES buffer; total volume of $300 \text{ }\mu\text{L}$ in 96-glass microwell plate. Biocatalyst obtained from 7.5 L bioreactor fermentation (Section 3.3.1) and bioconversions performed as described in Section 2.5.1. Error bars represent one standard deviation about the mean ($n=3$).

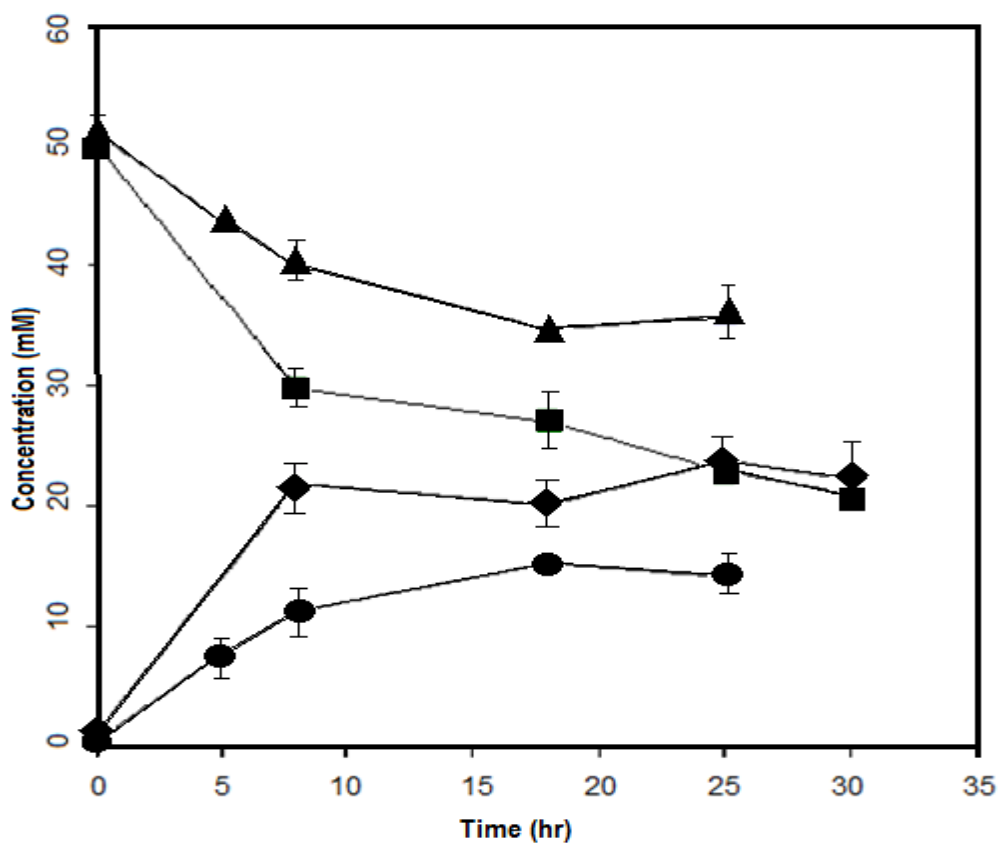


Figure 3.12. Bioconversion kinetics of CV2025 ω -TAM in whole cell and clarified lysate forms: Ery consumption (\blacktriangle) and ABT production (\bullet) for clarified lysate and Ery consumption (\blacksquare) and ABT production (\blacklozenge) for 96-microwell plate format. Reaction conditions: $0.3 \text{ g}\cdot\text{L}^{-1}$ CV2025 ω -TAM; 0.2 mM PLP; [MBA] and [Ery] were 50 mM ; $30 \text{ }^\circ\text{C}$; pH 7.5; 300 rpm in 50 mM HEPES buffer; total volume of $300 \text{ }\mu\text{L}$ in 96-glass microwell plate. Bioconversions performed as described in Section 2.5.1. Error bars represent one standard deviation about the mean ($n=3$).

Previous ω -transaminases bioconversions studies also reported the same outcome 40 % (mol.mol^{-1}) and 26 % (mol.mol^{-1}) respectively. Previous ω -transaminases bioconversions studies also reported the same outcome attributed to an increase in stability of the enzyme inside the cell (Shin and Kim, 1997), metabolism consumption of inhibitory compounds (Shin and Kim, 1999) and the effect of the cell membrane in partitioning inhibitory components between the inside and outside of the cell (Yun et al., 2004).

The high cell yield, the low production costs (i.e cheap biomass), and the processes are usually robust would appear to favour the application of whole cell biocatalyst industrially. However, the organisms have to be cultivated, side reactions are common, and purification steps involve cell removal and product extraction from a possibly complex medium (Sanchez and Demain, 2011). Further, in developing high throughput rapid screening processes, the whole cell versus clarified lysate form might appear inconsequential as the processes are more complicated and hence time consuming. Thus, CV2025 ω -TAM in clarified lysate form has more potential of achieving true preparative relevance for this project enables quicker, simpler and rapid microscale technique processes for identification of ω -TAM catalytic activity and its subsequent improvement.

3.6. SUMMARY

The work performed in this initial chapter demonstrated the utility of microscale reaction formats for the quantitative study of CV2025 ω -TAM bioconversion kinetics. This now provides a basis for studies in subsequent chapters of the thesis.

For biocatalyst production, fed-batch fermentation is advantageous for providing a large and constant source of biocatalyst (Section 3.3.1). In comparison to shake flask culture, CV2025 ω -TAM expressed in bioreactor with the fed-batch supply of PLP (Section 3.3.2) was benefited as it helped tremendously to increase CV2025 ω -TAM catalytic activity (Section 3.3.3). Moreover, the CV2025 ω -TAM expressed from his-tagged labelled plasmid (pQR801) shown an equivalent activity to non his-tagged

CV2025 ω -TAm (pQR800) (Section 3.4.1). CV2025 ω -TAm bioconversions of MBA with Ery as amino acceptor (Section 3.5.1) showed more typical unfavourable equilibrium control than with pyruvate as verified by its relatively lesser reaction yield observed. Beside chemical equilibrium, the incomplete transamination might also be due to acceptor reactivity, poor substrate / product solubility and inhibition effects.

In summary, the validated method and technique of the reaction in the conventional vial format was successfully mimicked into 96-glass microwell plate format. The comparable CV2025 ω -TAm bioconversion reactions presented by both formats (Section 3.4.2) suggest that the microwell plate format can be developed as a promising method for further exploring ω -TAm biocatalysts potentials in manual conventional method as well as automation platform.

4. MICROSCALE PROCESS OPTIONS TO INCREASE ω -TAm BIOCONVERSION YIELDS

4.1. INTRODUCTION

Biocatalytic processes (Section 1.2) are becoming increasingly competitive with conventional organic syntheses and have been used in industry for preparing optically pure amine enantiomers (Section 1.3) showing various pharmacological properties (Sutin, 2007; Koszelewski et al., 2008). Enantioenriched amines can be produced by either asymmetric synthesis (Shin and Kim, 1999) using an achiral ketone (i.e. amination of the ketone) or via kinetic resolution of a racemic amine (i.e. stereoselective deamination of the unwanted isomer) (Shin and Kim, 1997).

The direct asymmetric synthesis of chiral amines using an ω -transaminase potentially offers significant advantages over chemical syntheses or kinetic resolution (Section 1.4.8). Nevertheless, certain challenges must be addressed (Section 1.4.9). These relate to the speed of biocatalytic process development (relative to chemical processes) and the need to (i) shift the reaction equilibrium to product formation and (ii) overcome issues of product inhibition (Shin and Kim, 1997; Shin and Kim, 1999). These challenges currently hinder attainment of high substrate conversion yields and the attainment of high product concentrations (Shin and Kim, 1998).

A number of recent publications have begun to address the issues of shifting the equilibrium towards product formation for ω -TAm catalysed bioconversions (Truppo

and Turner, 2010; Truppo et al., 2009; Hohne et al., 2008; Yun et al., 2003). Examples include the use of a second enzyme system and auto degradation of bi-product (Section 1.4.10). While benefits have been reported in each case the implementation of such methods requires considerable further experimentation to optimise bioconversion conditions. Figure 4.1 summarises some of the potential process options available to overcome low yielding, equilibrium-controlled ω -TAm reactions or those with inhibitory substrates or products. The focus in this chapter will be the creation of novel microscale experimental methods to enable the rapid and parallel evaluation of the different process options. Such approaches would provide the data necessary for early stage process design and economic evaluation.

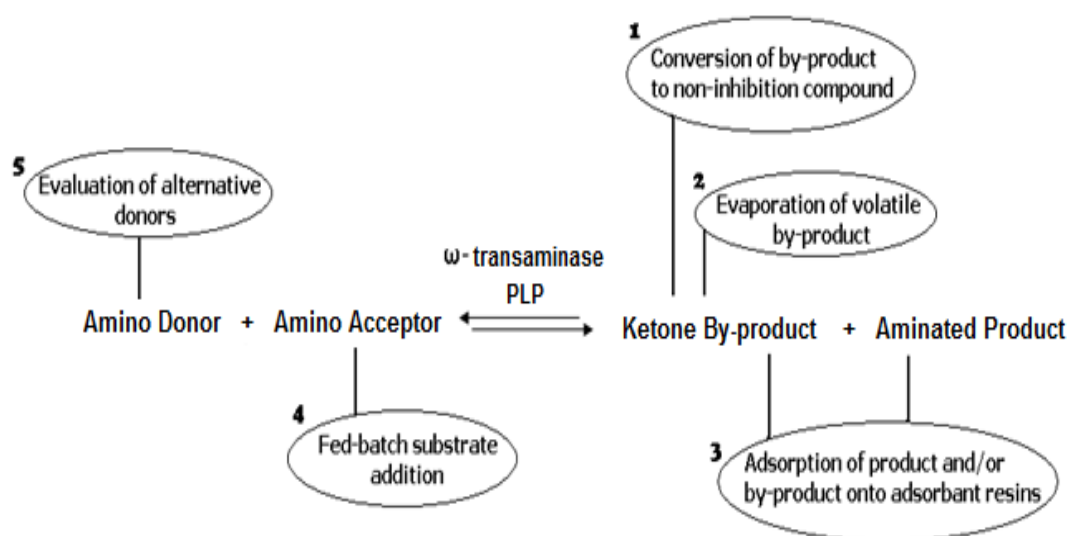


Figure 4.1. Overview of potential process options to increase the yield of equilibrium-controlled ω -TAm bioconversions.

4.2. AIM AND OBJECTIVES

The aim of this chapter is to establish a series of novel microscale methods to enable experimental evaluation of the different process options identified in Figure 4.1. The feasibility of these approaches will be investigated for the CV2025 ω -TAm catalyzed asymmetric synthesis of chiral amines using Ery as substrate and MBA as the initial amine donor. The methods to be established here will enable selective removal of

inhibitory by-products and evaluation of different amine donors. The key objectives of this chapter are thus:

- To confirm by-product inhibition to the CV2025 ω -TAM bioconversion by AP.
- To identify alternative amino donors and establish microscale methods to evaluate their impact of overall bioconversions yields.
- To develop micorscale methods for enzymatic *in-situ* product removal of inhibitory by-products such as AP, in this case by applying a second enzyme, ADH to catalyze AP reduction into (R)-1-phenylethanol and hence shift the reaction towards product formation.
- To develop microscale physical *in-situ* product removal methods for volatile products or by-products by promoting evaporation under reduced pressure.
- To develop microscale physical *in-situ* product removal methods based on the introduction of adsorbent resins for selective binding of unwanted by-product overcoming inhibitory of equilibrium limitations.

4.3. STANDARD CV2025 ω -TAM BIOCONVERSION KINETICS AND YIELD

In order to illustrate the problem of low yielding, equilibrium-controlled reactions initial experiments with CV2025 ω -TAM were performed at equilmolar substrate concentrations as described in Section 3.5.1. In this case, only 26 % ($\text{mol}\cdot\text{mol}^{-1}$) conversions were achieved when 50 mM of each substrate MBA and Ery were used.

The inhibition of CV2025 ω -TAM by the amine by-product (AP) is believed to be one of the reasons why the conversion does not progress to completion as shown in Figure 4.3. This inhibition study was performed by exogenously adding increasing amounts

of AP into the reaction mixture before the biotransformation reaction proceed. Product inhibition (Section 1.4.9) results from the formation of a Michaelis complex between AP and the ω -transaminase enzyme. This is due to the reversibility of enzyme reaction, where product can bind to the enzyme and thus reduces the chances of substrate binding to the enzyme active site. In similar experiments with exogenous addition of increasing amounts of MBA or Ery, inhibitory effects on reaction kinetics were not observed at concentrations below 100mM (Rios et al., 2011) and so these can be considered negligible relative to AP by-product inhibition.

To increase the product yield, four approaches were subsequently evaluated: evaluation of alternative amino donors, use of a second enzyme system, and physical ISPR methods via reaction under reduced pressure and the use of adsorbent resins. These are illustrated in Figure 4.2. The aim is to selectively remove AP from the reaction system, thereby overcoming the inhibition effects and also shifting the reaction equilibrium to the right increasing the final yield of the desired product, ABT. These method approaches will each be developed to operate at 300 μ L scale in 96-glass microwell scale as described earlier in Chapter 3. The conversion yield (26% ($\text{mol}\cdot\text{mol}^{-1}$)) attained from equimolar bioconversion of MBA and Ery at 50 mM will be considered the baseline against which potential improvements in bioconversion yield can be evaluated.

4.4. EVALUATION OF ALTERNATIVE AMINO DONORS

Kaulmann and co-workers (2007) have previously reported on the specificities of CV2025 ω -TAm towards various amino donors (Section 1.4.7). Their study was based on relative initial rates using 10 mM Pyruvate as amino acceptor (Table 1.1) instead of Ery. Their work nevertheless provides insight into the selection of potential alternative amino donors for use with ERY.

Five amino donors were investigated, as an alternative to MBA as used in the standard CV2025 ω -TAm bioconversion. The main aim was to identify amino donors leading to reduced by-product inhibition. Furthermore, in industrial asymmetric synthesis the choice of amino donor is important as this will impact on the overall process cost

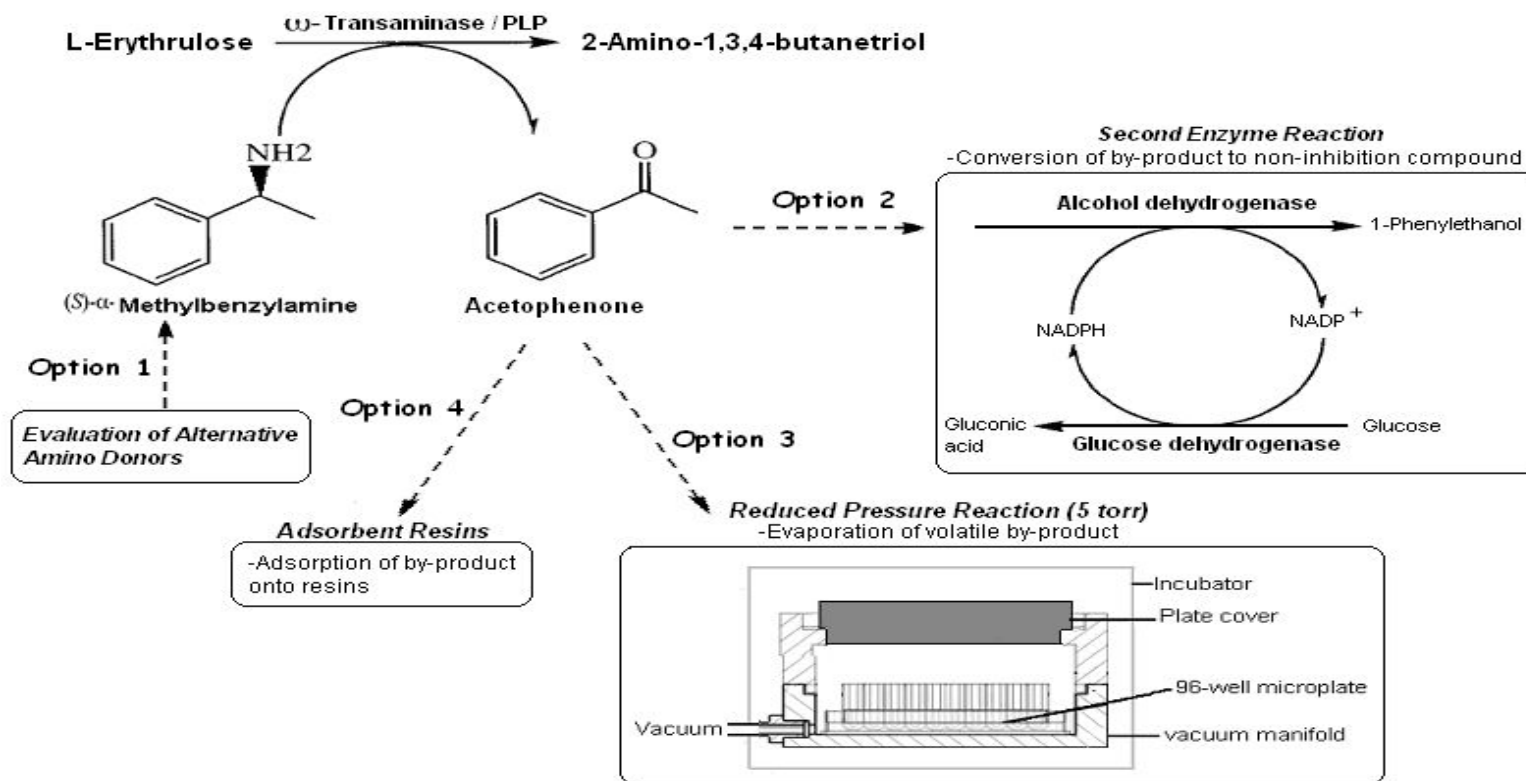


Figure 4.2. Process options investigated in this work at microwell scale to overcome thermodynamic and equilibrium limitations of the CV2025 ω-TAm bioconversion.

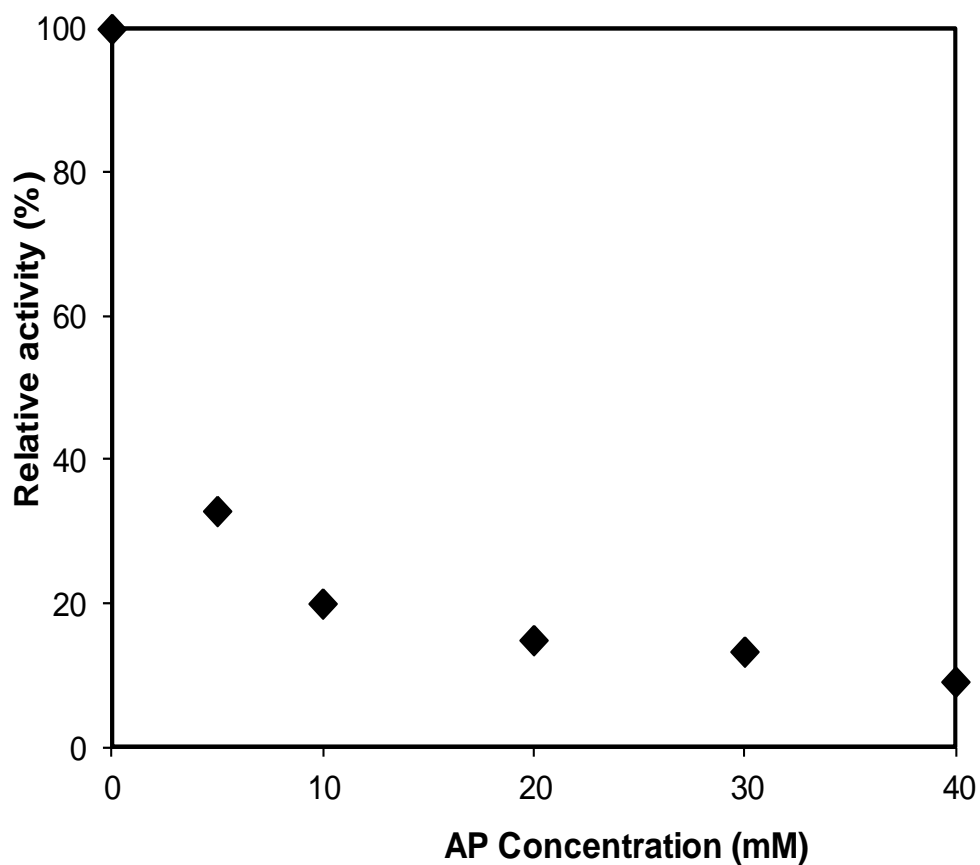
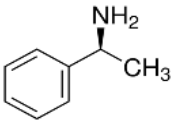
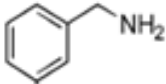
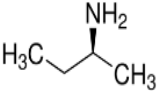
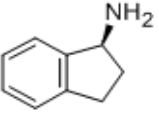
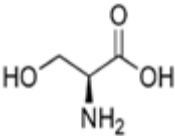


Figure 4.3. Quantification of product inhibition effects by AP. Reactions were carried out with equimolar MBA and Ery at 50 mM by the addition of specified concentration of AP (0, 10, 20, 30, 40 mM) prior to start of the CV2025 ω -TAm bioconversion. Reaction conditions: 0.3 g.L⁻¹ CV2025 ω -TAm in lysate form; 0.2 mM PLP; 30 °C; pH 7.5; 300 rpm in 50 mM HEPES buffer; total volume of 300 μ L in 96-glass microwell plate. Bioconversions performed as described in Section 2.5.1.

(Shin and Kim, 1999). Table 4.1 summarises the properties of the alternative amino donors selected. These were investigated for the transamination of Ery at equimolar concentrations of 50 mM of each substrate. As depicted in Figure 4.4 the results from CV2025 ω -TAm bioconversions with Ery as the amino acceptor, showed higher conversion yields towards all tested alternative compounds with the exception the aromatic amino donor Benzylamine.

Table 4.1. Amino donors selected for study on the equilibrium yield of Ery transamination by CV2025 ω -TAm.

Amino donor		Chemical Formula	Chemical Structure
Amines	<i>S</i> -(+)- α -methylbenzylamine (MBA)	$C_8H_{11}N$	
	Isopropylamine	$(CH_3)_2CH_2NH_2$	
	Benzylamine	$C_6H_5CH_2NH_2$	
	<i>S</i> -(+)- <i>sec</i> -butylamine	$C_2H_5CH(NH_2)CH_3$	
	<i>S</i> -(+)-1-aminoindan	$C_9H_{11}N$	
Amino acid	L- α -serine	$C_3H_7NO_3$	

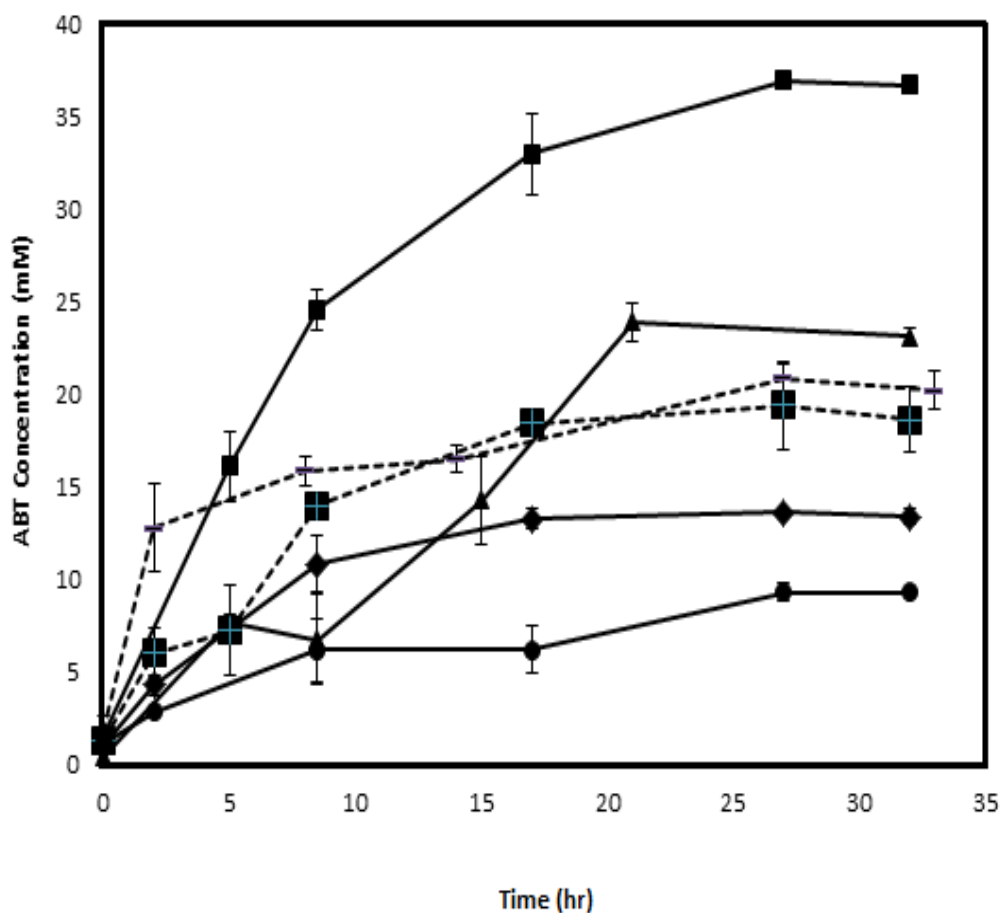


Figure 4.4. Effect of alternative amino donors on ABT product formation kinetics for the profile of CV2025 ω -TAM clarified lysate bioconversions of Ery with alternative amino donors (Section 4.4) which were: MBA (◆); isopropylamine (■); benzylamine (●); S-(+)-sec-butylamine (- - -); S-(+)-1-aminoindane (◻) and L- α -serine (▲). Reaction conditions: 0.3 g.L⁻¹ CV2025 ω -TAM in lysate form; 0.2 mM PLP; [amino donor] and [Ery] were 50 mM; 30 °C; pH 7.5; 300 rpm in 50 mM HEPES buffer; total volume of 300 μ L in 96-glass microwell plate. Bioconversions performed as described in Section 2.5.1. Error bars represent one standard deviation about the mean (n=3).

When MBA was substituted with the much cheaper, more volatile, and more water-soluble substrate, isopropylamine, a nearly 3-fold increase in final bioconversion yield was attained. This is most probably because the by-product in this case (acetone) is less inhibitory and more volatile than AP. Nevertheless the reaction required a longer time, more or less double the period of the standard reaction, to reach completion. It is anticipated that a similar reaction yield can be obtained in a shorter period by using a more concentrated CV2025 ω -TAm lysate. Different substrate ratios, for instance an increased concentration of amino donor, could also be expected to promote higher reaction rates (Smith et al., 2010; Rios et al., 2011). Additionally isopropylamine and its by-product, acetone, could be more easily removed downstream owing to their high volatilities compared to aromatic amine donors (Smith et al., 2010).

A final product concentration of 20 mM ABT was detected when another aliphatic amine, *S*-(+)-1-*sec*-butylamine was used as an alternative amino donor. This represents a 14 % ($\text{mol}\cdot\text{mol}^{-1}$) increase in the reaction yield compared to the standard reaction. This result however contradicts the earlier works based on initial rates, which indicated a lower rate than with MBA as amino donor (Kaulmann et al., 2007; Shin et al., 2003).

MBA was next substituted with two other aromatic amino donors; *S*-(+)-1-aminoindan and benzylamine. CV2025 ω -TAm bioconversion with *S*-(+)-1-aminoindane showed nearly an equal conversion yield to the reaction with *S*-(+)-1-*sec*-butylamine. These observations once again confirm the good reactivity of CV2025 ω -TAm towards a broad range of (*S*)-amines that could be potentially useful (Section 1.4.7) for the production of enantiopure amines and amino alcohols (Kaulmann et al., 2007; Yun et al., 2005; Yun et al., 2003; Shin et al., 2001; Shin and Kim, 1999). Using benzylamine as amine donor for transamination of Ery yielded a yield of approximately 8 % ($\text{mol}\cdot\text{mol}^{-1}$) considerably lower than with MBA.

Finally, using L- α -Serine, a naturally occurring amino acid, an increased reaction yield of 46 % ($\text{mol}\cdot\text{mol}^{-1}$) was obtained. The use of amino acids as an amine donor is noteworthy considering their availability at relatively low cost and the strategies available for their selective extraction (Kaulmann et al., 2007). Therefore, the transamination of Ery could be further examined with other amino acids and their

derivatives such as L- α -alanine, 6-aminohexanoic acid and γ -aminobutyric acid which were previously tested (Kaulmann et al., 2007) and gave promising results based on initial reaction rates.

In summary, of the five alternative amine donors tested, four of them showed good conversion with Ery to ABT. Some proved to be very effective being both cheaper than MBA (isopropylamine and L- α -Serine) and giving significantly enhanced reaction yields. These positive results suggest screening of alternative amino donors is likely to be a simple, quick and reliable option for helping to optimise ω -TAm bioconversion yields.

4.5. SECOND ENZYME SYSTEM

For *in-situ* removal of the inhibitory AP, one option is to reduce it to the chiral alcohol, (R)-1-phenylethanol by applying a second enzyme, ADH (Figure 4.2). Coupling ADH with ω -TAm has previously been shown to help alleviate reaction inhibition and also provide access to the synthesis of chiral alcohols (Yun et al., 2003). ADHs is biocatalysts that been previously used for the synthesis of optically pure compounds by reduction of prostereogenic ketones to the corresponding optically active alcohol (Yun et al., 2003; Koeller and Wong, 2001; Hummel, 1999). However, in this study the aim is to utilise ADH to establish an efficient micro-scale solution for in situ removal of an inhibitory by-product by conversion into a non-inhibitory compound and hence to shift the reaction equilibrium towards completion.

The commercially available ADH from *Lactobacillus kefir* selected for this study is a NADPH-dependent enzyme (Bradshaw et al., 1992). As this co-factor is expensive, an effective and economically viable co-factor regeneration system also needs to be implemented. In general, there are two methods to recycle the co-factor, which are a coupled-enzyme process or a coupled-substrate approach (Faber, 2004; Peters, 1998).

In the coupled-substrate process, a second substrate (i.e 2-propanol, isopropanol) is added to the reaction system and is oxidised by the same enzyme for NADPH regeneration. However, the maximum conversion of this option is usually limited by

the thermodynamics of the system as there is competition between substrate, product, co-substrate and co-product. There is also the potential for inhibition or deactivation of ω -TAm by the newly added. For instance, the previous study by Yun et al. (2003) examining the use of 2-propanal coupled to the ADH revealed a critical decrease in both activity and stability of the ω -TAm JS17 from *Vibrio fluvialis*.

In the coupled-enzyme process, an independent enzyme such as glucose dehydrogenase (Truppo and Turner, 2010; Koszelewski et al., 2009; Yun et al., 2003), formate dehydrogenase (Rissom et al., 1999) or glucose-6-phosphate dehydrogenase (Hummel, 1990) is also added into the reaction medium. In this work, glucose dehydrogenase from *Pseudomonas sp.* (GDH) has been selected to couple with ADH in order to recycle the co-factor NADPH. This enzyme was chosen as it has high specific activity (Yun et al., 2003), a favourable equilibrium for NADPH (Hummel, 1999), no inhibitory effect of the glucose co-substrate on ω -TAm activity (Yun et al., 2003) and is also commercially available.

A further consideration when implementing the NADPH recycling system is that good control of pH is needed because the gluconolactone product formed from glucose (Figure 4.2) is spontaneously hydrolysed to gluconic acid causing a decrease in pH. As shown previously, the optimum pH for CV2025 ω -TAm activity in lysate form is about pH 7.5 with activity decreasing rapidly at lower pH values (Section 3.4.3).

As presented in Figure 4.5, when the second enzyme bioconversion was carried out in 50 mM HEPES buffer (pH 7.5), the reaction reached completion after 5 hours based on production of (R)-1-phenylethanol (which also attributed to the conversion of AP) by ADH, which was 13 mM and at the level where AP become inhibitory to the CV2025 ω -TAm (Figure 4.3). This is equivalent to the optimum AP conversion achieved in the standard CV2025 ω -TAm bioconversion at 16 hours (Figure 4.5). However, the pH of the second enzyme bioconversion solution measured at this time had declined to 4.5 where the activity of the CV2025 ω -TAm was likely to decrease or deactivate thus prevented the reaction to progressing any further. Nevertheless, the comparable resulted in a yield of CV2025 ω -TAm bioconversion with the second enzyme system assimilation was accomplished at 3 times earlier (at 6 hours) than the standard CV2025 ω -TAm reaction (at 16 hours). This confirms the second enzyme

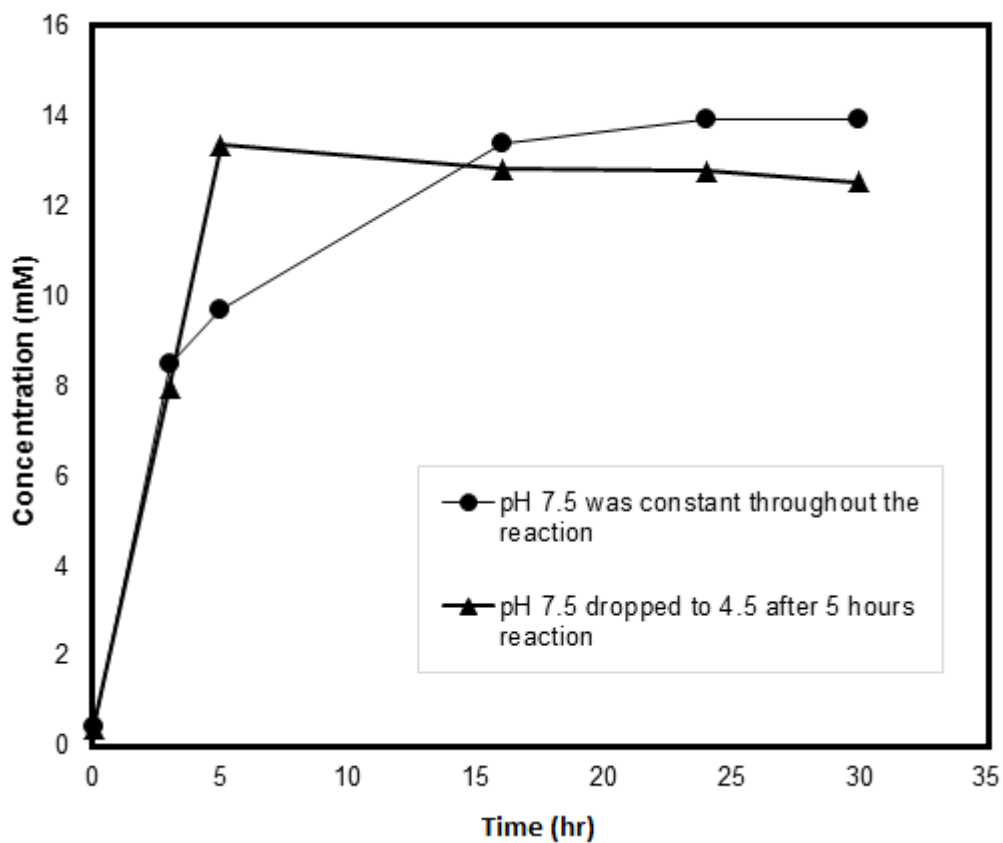


Figure 4.5. Influence of second enzyme system on CV2025 ω -TAm bioconversion kinetics: (R)-1-Phenylethanol production from the preliminary study with second enzyme system (Section 4.5) (\blacktriangle) and AP production from standard CV2025 ω -TAm reaction (Section 4.3) (\bullet). Reaction conditions: 0.3 g.L^{-1} CV2025 ω -TAm in lysate form; 0.2 mM PLP; [MBA] and [Ery] were 50 mM ; 1 mM NADPH; 70 mM glucose; ADH (1.2 g.L^{-1}); GDH (0.02 g.L^{-1}); $30 \text{ }^\circ\text{C}$; pH 7.5; 300 rpm in 50 mM HEPES buffer; total volume of $300 \text{ }\mu\text{L}$ in 96-glass microwell plate. Bioconversions performed as described in Section 2.5.3.

system behaved as anticipated, but points to the need to more tightly control pH in the reactions.

For preparative scale bioconversions and above pH-stat devices can easily be used for control of pH and maintenance of the optimum value during bioconversions (Truppo et al., 2010). However, such an approach is not yet possible for the high throughput, microwell scale methods being developed here. In order to achieve effective pH control, in this case higher buffer concentrations will be investigated realising that if enhancements in bioconversion yield are seen during high throughput studies the optimum reaction conditions can later be verified by a pH stat study at a larger scale. Consequently, second enzyme bioconversions were operated with stronger buffer solutions of 0.5 M, 1.0 M and 1.5 M HEPES (pH 7.5). All the substrates, co-factors and substituted ADH and GDH enzymes (Section 2.3.3 and 2.3.4) apart from CV2025 ω -TAM were hence prepared in these targeted HEPES concentrations and were adjusted to pH 7.5 when necessary (Section 2.5.3).

Figure 4.6 displays the measured CV2025 ω -TAM bioconversion kinetics using the second enzyme system at the various HEPES buffer concentrations. The reaction with the lowest HEPES concentration of 0.5 M proceeded to only 50 % ($\text{mol}\cdot\text{mol}^{-1}$) conversion and the pH value at the end of reaction was decreased to 7.0. Meanwhile, an ABT production of 36 mM, corresponding to 72 % ($\text{mol}\cdot\text{mol}^{-1}$) reaction conversion, was obtained in 1.0 M HEPES where the final pH value was 7.2. Finally for the reaction with the highest HEPES concentration of 1.5 M the product yield increased to 43 mM ABT (86 % ($\text{mol}\cdot\text{mol}^{-1}$)) and the pH only decreased to 7.4. In this case, the time needed to achieve this maximum yield was also quicker by 8 hours in comparison to the reactions at lower HEPES concentrations.

As the substrate inhibition exerted by amino acceptor (Ery) was nearly negligible (Rios et al., 2011), the effect of using higher initial concentrations of Ery to drive the equilibrium further towards completion was also examined. This would also increase conversion of amino donor (i.e MBA) as well as increasing the final product concentration (i.e ABT). When the reaction in 1.5 M HEPES was repeated with 70 mM Ery, there was almost complete conversion of 50 mM MBA and a final product concentration of 49 mM ABT was obtained in 20 hours as also shown in Figure 4.6.

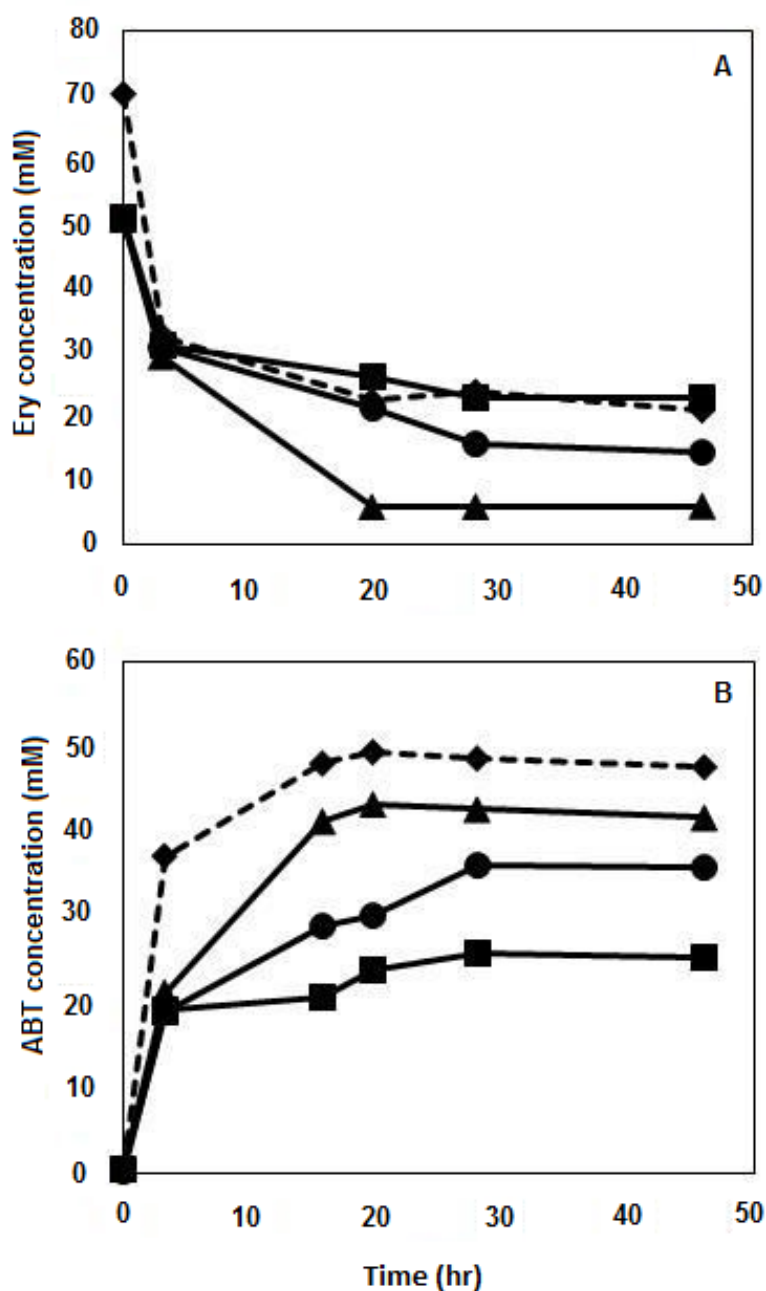


Figure 4.6. CV2025 ω -TAM bioconversion kinetics using the second enzyme system at increased buffer concentrations: (A) Ery consumption and (B) ABT production. The reaction mixture contained 50 mM MBA, 50 mM Ery in different HEPES (pH 7.5) concentrations of 0.5 M (■) 1.0 M (●) or 1.5 M (▲) and 70 mM Ery in 1.5 M HEPES (◆). Reaction conditions: 0.3 g.L⁻¹ CV2025 ω -TAM; 0.2 mM PLP; [MBA] and [Ery] were 50 mM; 1 mM NADPH; 70 mM glucose; ADH (1.2 g.L⁻¹); GDH (0.02 g.L⁻¹); 30 °C; pH 7.5; 300 rpm in various concentrations HEPES buffer; total volume of 300 μ L in 96-glass microwell plate. Bioconversions performed as described in Section 2.5.3.

The 40 % (mol.mol⁻¹) excess of Ery added at the start of the reaction helped further increase the initial reaction rate to nearly 2-fold over that when the substrates were initially present at equal molar ratio.

4.6. PHYSICAL ISPR METHOD: OPERATION AT REDUCED PRESSURE

Other potential methods for overcoming unfavourable thermodynamic equilibria and ketone product inhibition are by operating the bioconversion at reduced pressure or higher temperatures in order to encourage evaporation of unwanted compounds (Yun et al., 2004). These options, however, are only applicable when the unwanted compound (i.e by-product) is more volatile than the other substrates and the target product. This is the case here for the AP by-product (Yun et al., 2004). The option of studies at higher temperatures is not explored as this may lead to decreased ω -TAm activity and denaturation (unless interest's thermophiles enzyme is used).

Various options for operation of parallel experiments at reduced pressure were therefore studied to develop parallelization reactions application at microscale format. 300 μ L scale reactions were performed in an un-covered 96-glass microwell plate integrated with a commercially available 96-well vacuum manifold as depicted in Figure 4.2. The 96-well vacuum manifold requires a different vacuum source that was originally designed for 96-well filter plates and solid phase extraction (SPE). Instead of operating in normal SPE mode, in the reduced pressure system, the reaction plate was placed inside the vacuum manifold whilst a fresh cleaned plate was placed at the top to serve as the cover and to provide a closed environment system. Considering the total bioconversion volume, a very mild vacuum was initially used of 5 torr (~6.67 mbar) controlled by a vacuum / pressure pump was applied to this novel reaction system to avoid rapid evaporation of the reaction solution (i.e water).

In micro-scale bioprocesses, it is very important to determine the evaporation rate of reaction media (i.e water) for accurate quantification of substrate and product concentrations. Here, the average rate of evaporation across a plate was determined based on gravimetric analysis. In short, evaporation experiments were carried out in a microwell plate containing 300 μ L RO water comprising 50 mM HEPES buffer. At

each sampling point, the weight of water left inside the well was measured. Likewise, bioconversion kinetics were subsequently measured at a constant evaporation rate and for operation at 5 torr pressure and 30 °C. As shown in Figure 4.7, the water evaporation kinetics followed the first-order rate law and was constant at $6.8 \mu\text{L}\cdot\text{hr}^{-1}$ during the course of the bioconversions.

The evaporation rates of ABT, MBA and Ery were determined by carrying out a control reaction using 300 μL 50 mM HEPES buffer containing 50 mM of each compound at pH 7.5. In the same way as described in Section 2.5.4, these control reactions were carried out at 5 torr vacuum pressure in a 96-microwell plate placed in the vacuum manifold. Solutions were sampled at specific times and analysed by HPLC (Section 2.6.6). The AP evaporation rate was carried out likewise, but with 40 mM AP as that is its maximum water solubility.

The ABT, MBA and Ery did not show any selective evaporation and their concentrations increased equally during this control reaction. After correction for the amount of water evaporated (Figure 4.7) the concentrations were the same as the starting conditions and so any substrate evaporation effects are considered (data not shown). In contrast, the evaporation rate of AP was quantified to be $1.22 \text{ mM}\cdot\text{hr}^{-1}$.

For operation under reduced pressure condition, the evaporation behaviour of ionisable compounds involved will change according to the reaction pH since this affects their ionization states. The CV2025 ω -TAM bioconversion reaction performed here was carried out at pH 7.5 which is close to neutral pH, therefore the ionisable compounds MBA, Ery and ABT evaporation rates were less affected by pH at the reduced pressure environment. The AP however is not an ionisable compound therefore its evaporation rate does not change regardless the pH.

Nevertheless, it might be important to determine the evaporation rates of ionisable compounds involved if the optimum reaction under normal atmospheric pressure is far from neutral pH. This is because, losing of substrates and / or targeted product are expected as reaction progress relative to their strong evaporation rates under the reduced pressure condition.

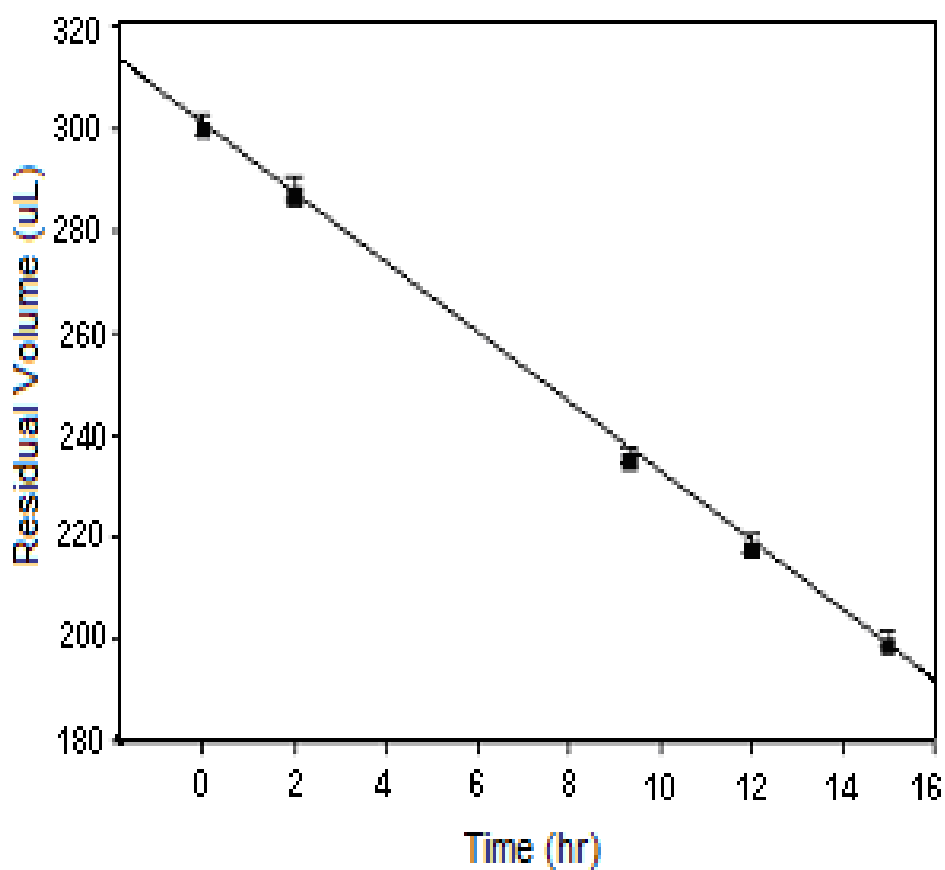


Figure 4.7. Average water evaporation kinetics across a 300 μL plate operated at 30 $^{\circ}\text{C}$ under reduced pressure and 5 torr pressure. The water evaporation constant is $6.8 \mu\text{L}\cdot\text{hr}^{-1}$. Experiment conditions: 5 torr vacuum pressure; 30 $^{\circ}\text{C}$; RO water contained 50 mM HEPES buffer (pH 7.5); total volume of 300 μL in 96-glass microwell plate placed in 96-well vacuum manifold connected to vacuum / pressure pump for pressure source. Reaction performed as described in Section 2.5.4. Error bars represent one standard deviation about the mean ($n=6$).

And when this is the case, we might expect the optimal pH of the reaction will be no longer equivalent to the reaction conducted at atmospheric pressure. In understanding the evaporation behaviour of an ionisable compound at different pH under reduced pressure, Yun and co-workers (2004) have derived mathematical equations that allow prediction of the evaporation rate constants (Figure 4.8).

Kinetic profiles of the CV2025 ω -TAM reaction carried out at 5 torr applied pressure are shown in Figure 4.9. As water evaporation will likely affect the outcome of reactions over long time periods a high CV2025 ω -TAM concentration (i.e. 1.0 g.L⁻¹) was used to ensure the reaction could reach equilibrium 24 hours or less where the maximum level of water evaporation would be 50 % (vol.vol⁻¹). When equivalent concentrations (i.e. 50 mM) of both substrates were used, the optimum ABT yield was 28 mM in 12 hours. This is equivalent to a 30 % (mol.mol⁻¹) increase over the yield of the standard CV2025 ω -TAM reactions (Figure 4.9).

When the initial Ery concentration was increased to 70 mM, as previously observed with the second enzyme reaction system (Section 4.5), the product concentration increased slightly further to 33 mM ABT, some 40 % (mol.mol⁻¹) higher than the standard CV2025 ω -TAM bioconversion (Section 3.5.1).

By comparison with results from the second enzyme system (Section 4.5), it can be concluded that the relatively small increases in conversion at reduced pressure are most probably due to the fact that only a proportion of the inhibitory AP is being evaporated. While more AP could be removed by operation at lower pressures, this would lead to further problems with water evaporation. While the microscale methods for operation at reduced pressure has been shown to work, the benefits of physical *in-situ* product removal by evaporation will only be found in cases where the by-products are considerably more volatile than the AP studied here.

4.7. PHYSICAL ISPR METHOD: APPLICATION OF ADSORBENT RESINS

The fourth approach to alleviate the problems of product inhibition and an unfavourable equilibrium constant problem is *in situ* product removal using adsorbent

$$\frac{[\text{BA}][\text{H}^+]}{[\text{BAH}^+]} = 10^{-\text{pKa}} \quad (1)$$

$$[\text{BA}]_{\text{total}} = [\text{BA}] + [\text{BAH}^+] \quad (2)$$

$$\frac{d[\text{BA}]_{\text{total}}}{dt} = -k_{\text{overall,e}} [\text{BA}]_{\text{total}} \quad (3)$$

$$\frac{d[\text{BA}]}{dt} = -k_e [\text{BA}] \quad (4)$$

$$\frac{1}{K_{\text{overall,e}}} = \frac{1}{k_e} + \frac{1}{k_e} 10^{\text{pKa} - \text{pH}} \quad (5)$$

Figure 4.8. Mathematical equations for prediction of evaporation rate constant. The ratio of protonated to deprotonated form is governed by the pH of solvating media as Equations (1) and (2), where $[\text{BA}]_{\text{total}}$, $[\text{BA}]$ and $[\text{BAH}^+]$ are the concentrations of ionised amine, deprotonated ionised amine and protonated ionised amine respectively. To accurately predict the evaporation rate constant of the ionised amine, the overall evaporation rate constant ($k_{\text{overall,e}}$) and evaporation rate constant (k_e) of free amine are defined as in Equations (3) and (4) respectively. Combining Equations (1) - (4) yields Equation (5). While ($k_{\text{overall,e}}$) is sensitive to pH, the (k_e) of non-ionised amine form is constant. The linear regression between $1/K_{\text{overall,e}}$ and $10^{-\text{pH}}$ gives the values of pKa and k_e of the ionised amine, and consequently yields the calculation of $K_{\text{overall,e}}$ at a given pH. (Yun et al., 2004).

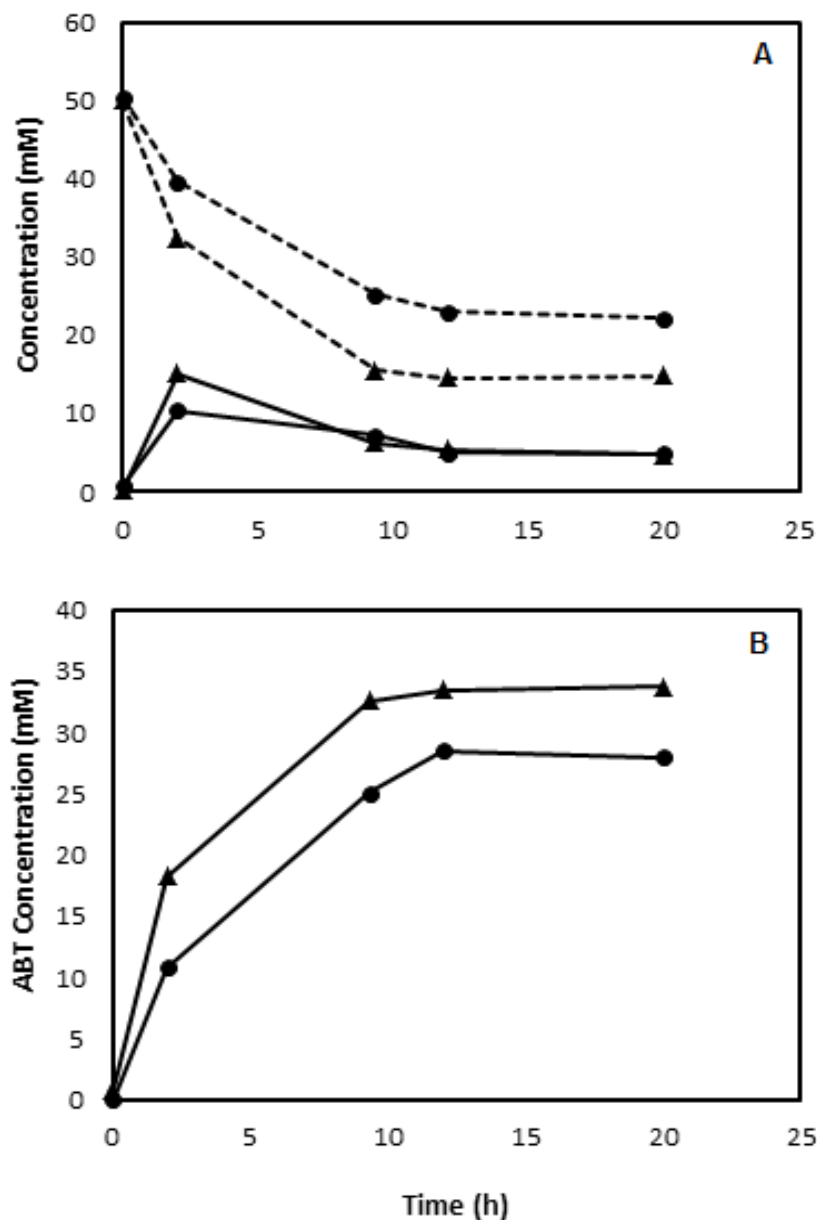


Figure 4.9. CV2025 ω -TAM bioconversion kinetics for operation at reduced pressure: (A) MBA (---) consumptions and AP (—) productions; (B) ABT productions (values plotted are corrected for evaporation). The reaction mixture (300 μ L) contained 50 mM MBA; Ery of either 50 mM (●) or 70 mM (▲); 1 g.L⁻¹ CV2025 ω -TAM in lysate form; 0.2 mM PLP and 50 mM HEPES buffer. Reaction conditions: 30 °C; pH 7.5; 5 torr vacuum pressure; total volume of 300 μ L in 96-glass microwell plate placed in 96-well vacuum manifold connected to vacuum / pressure pump for pressure source. Bioconversions performed as described in Section 2.5.4.

resins to selectively binding the unwanted by-product (Lye and Woodley, 1999). Three commercially available hydrophobic polymeric resins called Amberlite™ XAD 7, XAD 1180 and XAD 16 were investigated. Further details on the resins are listed in Table 2.5. These were chosen particularly because they have been previously shown to absorb AP from the reaction solution (Yang et al., 2008; Nakamura et al., 2000). To desorb bound products from the resins isopropyl alcohol was used.

4.7.1. Equilibrium Adsorption Isotherms

Adsorption isotherm studies were initially conducted to measure the capacity and selectivity of each resin towards the various solutes present in the bioconversions. The adsorption capacity depends on the properties of the adsorbant and adsorbate, temperature, solution pH and amount of impurities presence (Yang et al., 2003). Nevertheless, the molecular basis of adsorption is poorly understood, and it is not currently possible to predict performance based solely on chemical and physical properties alone. Experimental adsorption isotherms are therefore used to obtain information on the equilibrium adsorption relationships. The experimental isotherms data were correlated to three well-known isotherm models namely Langmuir, Freundlich and Linear (Du et al., 2008; Yang et al., 2003). The mathematical relationships for each data set is shown in Table 4.2. The adsorption isotherm experiments were carried out as described in Section 2.5.5.

For ISPR application with the CV2025 ω -TAm bioconversion studied here, it is desirable that the adsorbent should have high capacity and affinity for the by-product AP whilst demonstrating minimal binding of the substrates MBA and Ery. Based on initial adsorption equilibrium experiments the ability of all the adsorbents to bind AP was considerably greater than Ery (Figures 4.10, 4.11, 4.12) and MBA (results for MBA showed similar binding affinity as seen for Ery). Meanwhile, the initial experiment on the binding of ABT showed less than 2 % (mol.mol^{-1}) was adsorbed by resins. Of the tested resins, XAD-16 demonstrated the highest adsorption capacity for AP with XAD 7 and XAD 1180 showing marginally less binding. These results confirm the adsorption ability of these resins for AP as previously reported by Yang et al. (2008) and also show that AP will out compete Ery for binding sites on the resin. This is confirmed by the binding constants calculated for each component in Table 4.3

and 4.4. Theoretically, the use of these resins in the bioconversion should be able to bind any produced AP driving the reaction towards completion.

Table 4.2. Isotherms expression for single component solutions.

Model name	Model Equation
Langmuir	$q = (q_{max} KC) \cdot (K + C)^{-1}$
Freundlich	$q = k \cdot C^{(\frac{1}{b})}$
Linear	$q_{max} = k \cdot C + b$

Where,

$C = \text{concentration (g.L}^{-1}\text{)}$

$K = \text{equilibrium constant}$

$B = \text{constant for each adsorbent}$

$q_{max} = \text{saturation concentration of the adsorbent phase at equilibrium (g)}$

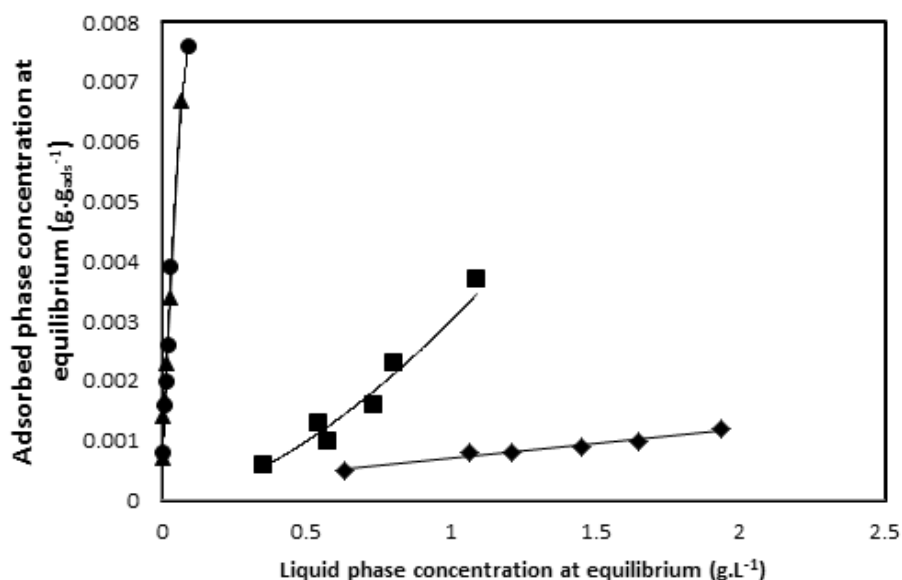


Figure 4.10. Equilibrium adsorption isotherms on XAD 7 resin: AP as sole solute (●); AP in the presence of equimolar Ery (▲); Ery as sole solute (■); Ery in the presence of equimolar AP (◆) prepared in 50 mM HEPES buffer (Section 4.7.1). Experiment conditions: 30 °C; pH 7.5; 50 mM HEPES buffer; 500 rpm; total volume of 300 μL in 96-glass microwell plate. Experiments performed as described in Section 2.5.5. The solid lines represent mathematical relationships fitted to the data as presented in Tables 4.3 and 4.4.

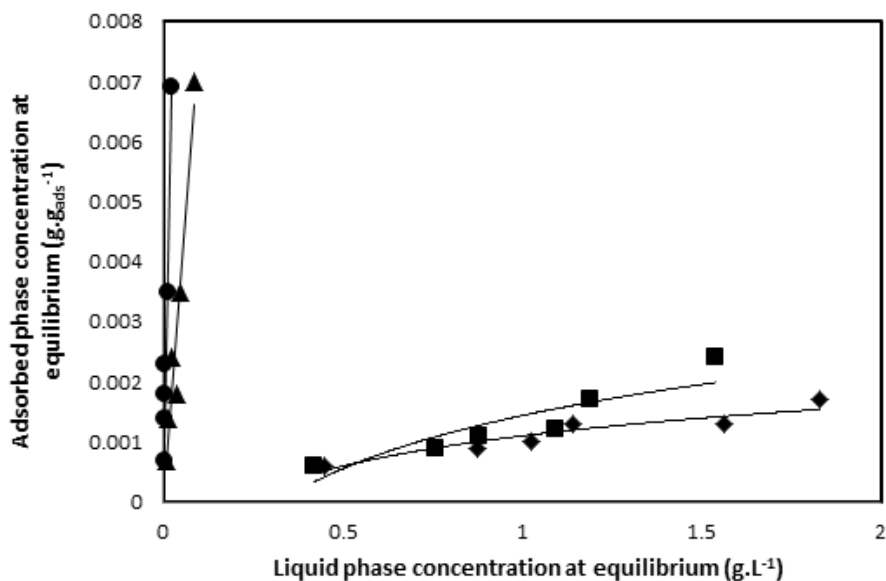


Figure 4.11. Equilibrium adsorption isotherms on XAD 1180 resin: AP as sole solute (●); AP in the presence of equimolar Ery (▲); Ery as sole solute (■); Ery in the presence of equimolar AP (◆) prepared in 50 mM HEPES buffer (Section 4.7.1). Experiment conditions: 30 °C; pH 7.5; 50 mM HEPES buffer; 500 rpm; total volume of 300 μ L in 96-glass microwell plate. Experiments performed as described in Section 2.5.5. The solid lines represent mathematical relationships fitted to the data as presented in Tables 4.3 and 4.4.

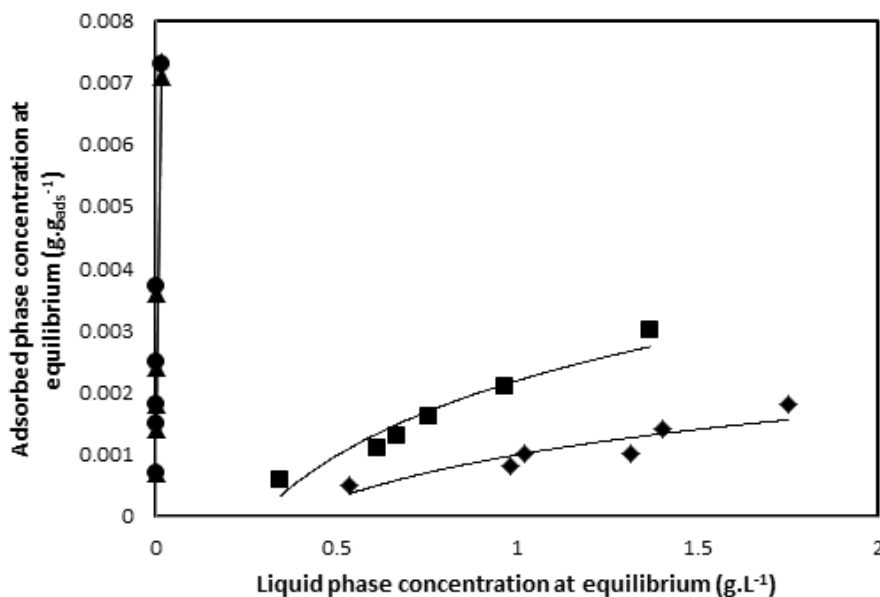


Figure 4.12. Equilibrium adsorption isotherms on XAD 16 resin: AP as sole solute (●); AP in the presence of equimolar Ery (▲); Ery as sole solute (■); Ery in the presence of equimolar AP (◆) prepared in 50 mM HEPES buffer (Section 4.7.1). Experiment conditions: 30 °C; pH 7.5; 50 mM HEPES buffer; 500 rpm; total volume of 300 μ L in 96-glass microwell plate. Experiments performed as described in Section 2.5.5. The solid lines represent mathematical relationships fitted to the data as presented in Tables 4.3 and 4.4.

Table 4.3. The mathematical relationships fitted to the adsorption isotherm data for adsorption of AP (in a mixed solution with Ery) and AP alone. y represents the adsorbed phase concentration at equilibrium (g_{ads}^{-1}) and C represents the liquid phase concentration at equilibrium ($g.L^{-1}$). Each mathematical relationship is visualized as a solid line in Figures 4.10, 4.11, and 4.12.

Adsorbent	Fitted adsorption isotherm			
	AP (mixed with Ery)	R^2	AP	R^2
XAD 7	$y = 0.043C^{0.69}$	0.997	$y = \frac{0.0258C}{0.102 + C}$	0.997
XAD 1180	$y = 7.45 \times 10^{-2}C + 1.22 \times 10^{-4}$	0.932	$y = 0.28C + 5.58 \times 10^{-4}$	0.985
XAD 16	$y = 0.31C + 1.39 \times 10^{-3}$	0.835	$y = \frac{0.012C}{9.97 \times 10^{-3} + C}$	0.990

Table 4.4. The mathematical relationships fitted to the adsorption isotherm data for adsorption of Ery (in a mixed solution with AP) and Ery alone. y represents the adsorbed phase concentration at equilibrium (g_{ads}^{-1}) and C represents the liquid phase concentration at equilibrium ($g.L^{-1}$). The best fitting isotherms equation is indicating by the solid line in Figures 4.10, 4.11 and 4.12.

Adsorbent	Fitted adsorption isotherm			
	Ery (mixed with AP)	R^2	Ery	R^2
XAD 7	$y = 2.19 \times 10^{-4}C - 4.83 \times 10^{-4}$	0.983	$y = 3.17 \times 10^{-3}C^{1.75}$	0.970
XAD 1180	$y = 1.04 \times 10^{-3}C^{0.73}$	0.920	$y = 1.31 \times 10^{-3}C$	0.956
XAD 16	$y = 9.16 \times 10^{-4}C^{1.16}$	0.923	$y = 2.4 \times 10^{-3}C - 2.85 \times 10^{-4}$	0.990

4.7.2. CV2025 ω -TAm Bioconversions with ISPR by Adsorptive Resins

Bioconversion reactions were carried out at 300 μ L scale using equimolar MBA and Ery at 50 mM. ISPR adsorbent resins as described in Section 2.5.5. In order to obtain a complete reaction profile for the total amount of compound absorbed from the resin, a ‘sacrifice well’ approach was used. At each interval time, all the liquid in the well was carefully aspirated off and isopropyl alcohol immediately added and then left shaken for 5 hours to ensure all solute was fully desorbed. Full details of the reaction procedure are described in Section 2.5.5. Besides isopropyl alcohol, nearly any water-miscible organic solvent can be used to desorb the absorbed absorbate from resins AmberliteTM XADs (Vicenzi et al., 1997).

The preliminary bioconversion reactions with CV2025 ω -TAm in clarified lysate in the presence of 20 % (w.w⁻¹) adsorbent resins were found to only proceeded to between 5 % to 10 % (mol.mol⁻¹) conversions (data not shown). These are far less than the standard lysate reaction which achieved 26 % (mol.mol⁻¹) conversion (Section 3.5.1). The reason for this is unclear since the concentration of total protein in the supernatant remained constant. One possibility then is that there is selective binding of the PLP co-factor but this was not explored further.

Consequently experiments were also performed using whole cell CV2025 ω -TAm biocatalyst as previously described in Section 3.5.2. The whole cell biocatalyst has a typical size of 0.2 - 0.5 microns which should be larger than the pore size of the resin particles which are approximately 0.03 microns or less (Table 2.5). Figure 4.13 presents the bioconversions with the ISPR resins method mediated by whole cell ω -TAm biocatalyst. The CV2025 ω -TAm bioconversions accompanied by use of 20 % (w/w) of the adsorbents XAD 7 and XAD 16 accomplished 50 % (mol.mol⁻¹) conversion whilst a marginally lower conversion of 46 % (mol.mol⁻¹) was attained with XAD 1180. These yields are equivalent to 12 % and 8 % (mol.mol⁻¹) improvements over the standard CV2025 ω -TAm whole cell bioconversion without the resin adsorption.

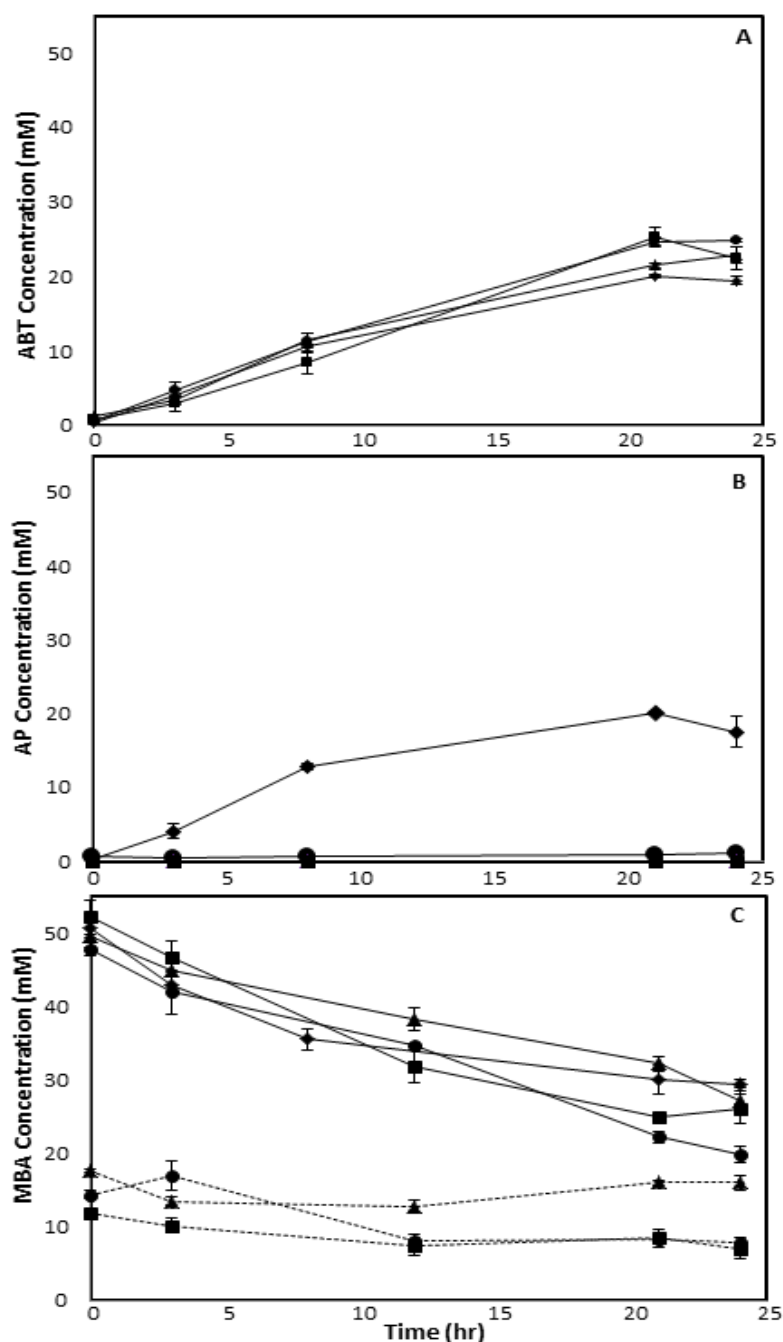


Figure 4.13. Influence of ISPR adsorbent resin selection on CV2025 ω -Tam bioconversion kinetic profiles performed with three ISPR adsorption resins (XAD 7 (●); XAD 1180 (▲); XAD 16 (■) system (Section 4.7.2) and CV2025 ω -Tam whole cell standard reaction (◆) (Section 3.5.2). (A) ABT production (total concentrations in both aqueous and resins phases); (B) AP production (in the aqueous phase); (C) MBA productions: (---) MBA total concentrations in aqueous and resins phases; (- - -) MBA concentrations in resins phase only. Reaction conditions: 0.3 g.L⁻¹ CV2025 ω -Tam in whole cell form; 0.2 mM PLP; [MBA] and [Ery] were 50 mM, 60 mg (wetted) adsorption resin; 30°C; pH 7.5; 500 rpm in 50 mM HEPES buffer; total volume of 300 μ L in 96-glass microwell plate. Bioconversions performed as described in Section 2.5.5. Error bars represent one standard deviation about the mean (n=3).

AP was totally removed from the aqueous reaction solution owing to the presence of the resins. This showed that all resins behaved as anticipated based on the single and multiple component studies described in Section 4.7.1. As soon as the solute phase equilibrium reached, MBA was being adsorbed onto each adsorbent in the concentrations of 13 mM (XAD 7), 11 mM (XAD 16) and 17 mM (XAD 1180) (Figure 4.13c). Thus, theoretically 37 mM, 39 mM, 33 mM MBA respectively were left in aqueous solutions. Likewise, about the same amount of Ery was being absorbed onto each adsorbent resin leaving about 40 mM (XAD 7), 42 mM (XAD 16) and 38 mM (XAD 1180) of Ery in the aqueous solutions during the reaction courses (Data not shown). As shown in Figure 4.13c, the concentrations of MBA adsorbed onto resins were almost from the start of the reactions were nearly remained persistent till the termination courses. This indicated the binding affinities of all resins towards MBA were very strong. However, about 20 to 30 % ($\text{mol}\cdot\text{mol}^{-1}$) of MBA were still left detected in the aqueous solutions at the end of reaction courses.

Further bioconversions were performed at various resins mass loading. The study indicated the reactions with 20 % ($\text{w}\cdot\text{w}^{-1}$) resins (as described above) were the best overall. Reactions attempted with 33.3 % and 66.7 % ($\text{w}\cdot\text{w}^{-1}$) loaded resins failed to increase the reactions conversion higher than the standard bioconversion (data not shown). The equilibrium between adsorbent and the aqueous phase at certain concentration may pose an inhibition effect to enzyme (Rudroff et al., 2006). Besides, most of the remarkable ISPR resin applications were reported with simple and straightforward bioconversion mechanism of biocatalyst catalysed single substrate to alleviate inhibitions of substrate / product and cell toxicity (Guo et al., 2009a; Yang et al., 2008; Rudroff et al., 2006; Nakamura et al., 2000).

Despite the initially promising behaviour seen in the single and two-component studies, it is clear that the potential benefits to the bioconversion reaction are less easy to predict. Further complications include protein adsorption onto the resin and the potential for lysis of whole cells due to shaking in the presence of 20 % ($\text{w}\cdot\text{w}^{-1}$) resin.

4.8. SUMMARY

The aim of this chapter was to establish a series of novel microscale methods to enable experimental evaluation of the different process options for overcoming low equilibrium constant as well as selectively removing an inhibitory product (AP) in the micro-scale processing technique. The experimental studies performed have shown the benefit (or otherwise) of each of the four systems developed.

The benefits seen with each method for CV2025 ω -TAM bioconversions carried out at equimolar substrate concentration are summarized in Table 4.5. In comparison, the second enzyme reaction (Section 4.5), a system applying ADH *Bacillus kefir* as a second enzyme and coupling with GDH *Pseudomonas sp.* for co-factor NADPH regeneration has the highest product yield than the other three investigated options. The excellent result of 86 % (mol.mol⁻¹) conversions obtained from second enzyme system with 1.5 M HEPES buffer shown that CV2025 ω -TAM is very stable in a very strong buffer solution. The evaluation of alternative amino donors (Section 4.4) however still represents the simplest and fastest option meanwhile reduced pressure system (Section 4.6), is an efficient method for overcoming inhibition or suppresses the unfavourable equilibrium constant cause by a compound having high volatilities property. The ISPR resin adsorptions method (Section 4.7) only applicable for whole-cell biocatalyst utilisation. The highest optimum yield of 12 % (mol.mol⁻¹) attained from this method is still low and thus should be further examined for significant yield improvement. Employing second enzyme and reduced pressure systems with a higher ratio of amino acceptor to amino donor had also further increased the reactions conversion to 98 % (mol.mol⁻¹) for second enzyme system and 66 % (mol.mol⁻¹) for reduced pressure system.

In more general terms, the best method for increasing bioconversion yield will depend on the particular enzyme and reactants being studied. In this case, the methods developed here are generic and can be applied to any bioconversion having established.

Table 4.5. List of productivity of the investigated process options and number of fold increases as a comparison to standard CV2025 ω -TAm reaction.

Option	Optimum ABT product concentration (equimolar substrates reaction)	Fold increase in yield
Evaluation of alternative amino donors (bioconversion by CV2025 ω -TAm in <i>lysate</i> form)	36 mM (Isopropylamine as the amino donor)	2.8
Second enzyme system (bioconversion by CV2025 ω -TAm in <i>lysate</i> form)	43 mM	3.3
Reduced pressure (bioconversion by CV2025 ω -TAm in <i>lysate</i> form)	28 mM	2.2
Adsorbent resins (bioconversion by CV2025 ω -TAm in <i>whole cells</i> form)	25 mM	1.3

5. AUTOMATION AND PARALLEL OPERATION OF MICROSCALE PROCESS OPTIONS

5.1. INTRODUCTION

The rapid kinetic evaluation of novel biocatalysts such as TAM is important given their potential for diverse industrial application. Nevertheless, TAM biocatalysts are known to have low conversion yields due to the reversible equilibrium between products and substrates (Shin and Kim, 1996; Christen and Metzler, 1985). In this work, the microscale methods developed in Chapter 4 are systematically applied in order to increase the product yield of an ω -TAM bioconversion known to be equilibrium-controlled (Section 4.3).

In general one of the main criticisms of biocatalytic systems is that they are relatively slow to implement (Pedro, 2010; Lye et al., 2003). Therefore, the automation of the approaches developed in Chapter 4 holds the possibility to efficiently examine the activity of a large number of biocatalysts acting on a wide range of substrates. In addition, this would also allow options to decrease production costs to be explored through a variety of improvements leading to potentially high space-time yields using biological and engineering principles (Ghisalba et al., 2010).

Over the past decade, the drive to identify new drug compounds had led to intensive development of high throughput screening techniques. As described in Section 1.5.2 much of the automation technology is based on microwell formats to reduce sample

volume and enable the application of laboratory robotics to increase throughput (Lye et al., 2003). A range of innovative methods is now being used to accelerate process development in both academia and industry, with automated approaches playing an increasing role over the conventional manual platform as well as larger scale trials approaches. The advantages of such automated microscale methods include the following: higher sample throughput and potentially increased assay precision, reduced cost of bioprocess development and speed up the development process of bioconversion system (Lye et al., 2009).

5.2. AIM AND OBJECTIVES

The aim of this chapter is to integrate the microscale methods established in Chapter 4, for overcoming low yield, equilibrium controlled ω -TAm bioconversions, into an integrated and automated microscale process sequence. The research here was mainly focussed on comparison of both conventional and automated microscale processes techniques and the potential benefits of increased processing speed and reduced experimental costs. The key objectives of this chapter are thus:

- To characterize a novel ω -TAm library for parallel evaluation with a view to identifying a better ω -TAm than currently used CV2025 ω -TAm in term of catalytic activity, selectivity and stability.
- To establish automated microscale process sequences to facilitate rapid process characterization and evaluation of the ω -TAm library to identify those capable of giving industrially relevant space-time yields at pilot scale. They will be tested on the standard reaction of MBA and Ery at 50 mM and also with a range of alternative amino donor substrates on the established automated microscale platform.
- To demonstrate the benefits of the automated microwell method to further evaluate performance of the second enzyme reaction. The method is developed to enable rapid evaluation and optimization of broaden range of reaction

parameters and conditions for increase production yield and significantly reduce the production cost prior scaling up productions.

- To establish microscale automated approaches of reduced pressure system using integrated robot system and equipment of a vacuum manifold (Te-VacS) for advance modification and implementation for efficient parallel investigation of the *in-situ* product removal process option.

5.3. CHARACTERISATION OF ω -TRANSAMINASE LIBRARY

5.3.1. Parallel *E.coli* BL21 (DE3) Gold Batch Growth Kinetics

A focussed library of ten different ω -TAm enzymes each expressed in the same *E.coli* host was evaluated in this work. This diverse library of enzyme sources was established with the intent to evaluate it for better catalytic activity, selectivity and stability. The initial production of the ω -TAm library was carried out in 2 L shake flasks with a working volume of 200 mL as previously described in Section 2.2.2. Each fermentation was carried out in duplicate.

Instead of LB media, the library was grown using another complex medium 2xTY (Ferreira Vaz et al., 2011). This is also commonly used for *E.coli* growth and was used here for higher biomass production and evaluate the influence of the culture medium on the expression of ω -TAm. 0.2 mM PLP additions were supplied to the fermentation and lysate preparation steps to enhance the ω -TAm stability and boost its catalytic activity as discussed earlier in Section 3.3.3. The composition of the media used (2xTY) was defined in Table 2.2. As observed in the growth curves (Figure 5.1), the cell growth kinetics were similar and reached a stationary phase after a fermentation period of approximately 7 hours. This is similar to that observed when the CV2025 ω -TAm was grown with LB medium (Section 3.3.1).

Most of the *E.coli* cultures carrying the alternative ω -TAm plasmids grown using the 2xTY medium obtained higher growth cells density than previously obtained with *E.coli* expressing the CV2025 ω -TAm with LB medium. The only exceptions were

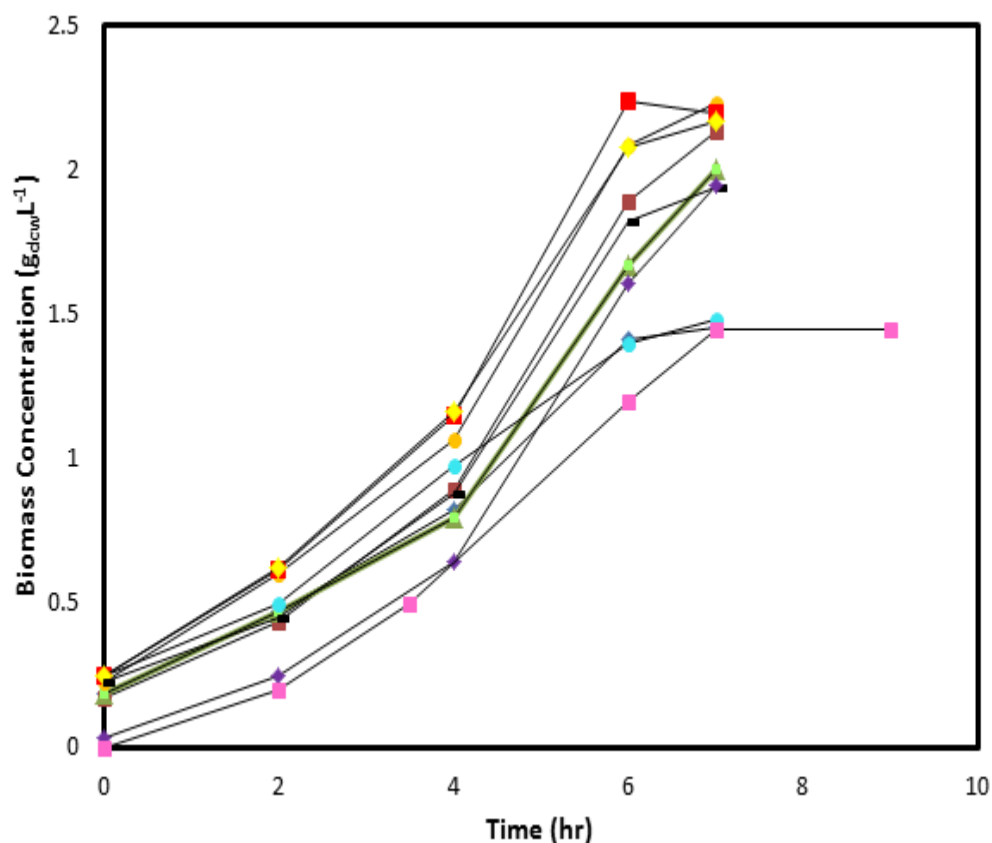


Figure 5.1. Batch growth kinetics for *E. coli* BL21 (DE3) Gold strains each expressing different ω -TAM plasmids cultured in 2xTY media: pQR1017 (◆); pQR956 (■); pQR1019 (▲); pQR985 (■); pQR960 (●); pQR811 (●); pQR813 (■); pQR1011 (◆); pQR1014 (-); pQR978 (◆). The CV2025 ω -TAM expressed from pQR801 (■) was grown using LB media as previously discussed in Section 3.3.1. The fermentations temperature of the novel ω -TAM strains were set at 37 °C initially but after IPTG induction (OD_{600} reached a value of 1.8 - 2.0) the temperature was then lowered to 30 °C prior harvested the next 5 hours. Cell cultivation was performed in 2L shake flask using pH 7.5 and 250 rpm. The cultivation procedure details were as described in Section 2.2.2.

the *E.coli* with Rru_A1254 ω -TAM (pQR1017) and BSU09260_1971 ω -TAM (pQR960). Both these recombinant *E.coli* strains only reached a final biomass concentration of $1.4 \text{ g}_{\text{dcw}}\text{L}^{-1}$ similar to the *E.coli* with CV2025. The increased biomass density obtained with the new medium may also be due to the difference in fermentation temperature. As mentioned in Section 2.2.2, instead of applying a constant temperature of $37 \text{ }^{\circ}\text{C}$, the temperature was lowered to $30 \text{ }^{\circ}\text{C}$ once induced with IPTG. As shown in Figure 5.1, the shake flask scale fermentations of the *E.coli* with the rest of alternative ω -TAMs were grown to final biomass concentrations between 2 to $2.2 \text{ g}_{\text{dcw}}\text{L}^{-1}$. ω -TAM biocatalysts were used either in lysate (Section 2.3.1) or purified form (Section 2.3.2) as specified for each particular reaction.

5.3.2. Quantification of ω -TAM and Host Cell Protein Production

The concentrations of proteins produced by the ω -TAM library strains were analysed by the Bradford assay using absorbance measurements, A_{595} (Section 2.6.3). The total protein concentrations of shake flask were again determined using a BSA standard curve (Appendix II) and were as detailed in Table 5.1.

SDS-PAGE assays were subsequently conducted using equal concentrations of total protein loaded onto the gel based on the Bradford assay measurements. The unpurified recombinant ω -TAMs migrated on the SDS-PAGE as a single band of in the size range between 46 to 51 kDa as displayed in Figure 5.2.

Despite the higher growth cells density, most of new ω -TAMs were expressed at a high level approximately comparable to the CV2025 ω -TAM at 1.0 g.L^{-1} with the exception to BLi00474 ω -TAM, Krad_4078 ω -TAM and Rru_A1254 ω -TAM which made up to only 0.19 , 0.32 and 0.36 g.L^{-1} of the ω -TAM from the clarified soluble fraction respectively. In addition, despite growing to the same cell density (Figure 5.1) as the other strains, the BLi00474 ω -TAM from *Bacillus licheniformis* only had a low total protein expression of 2.35 g.L^{-1} hence the very low ω -TAM concentration.

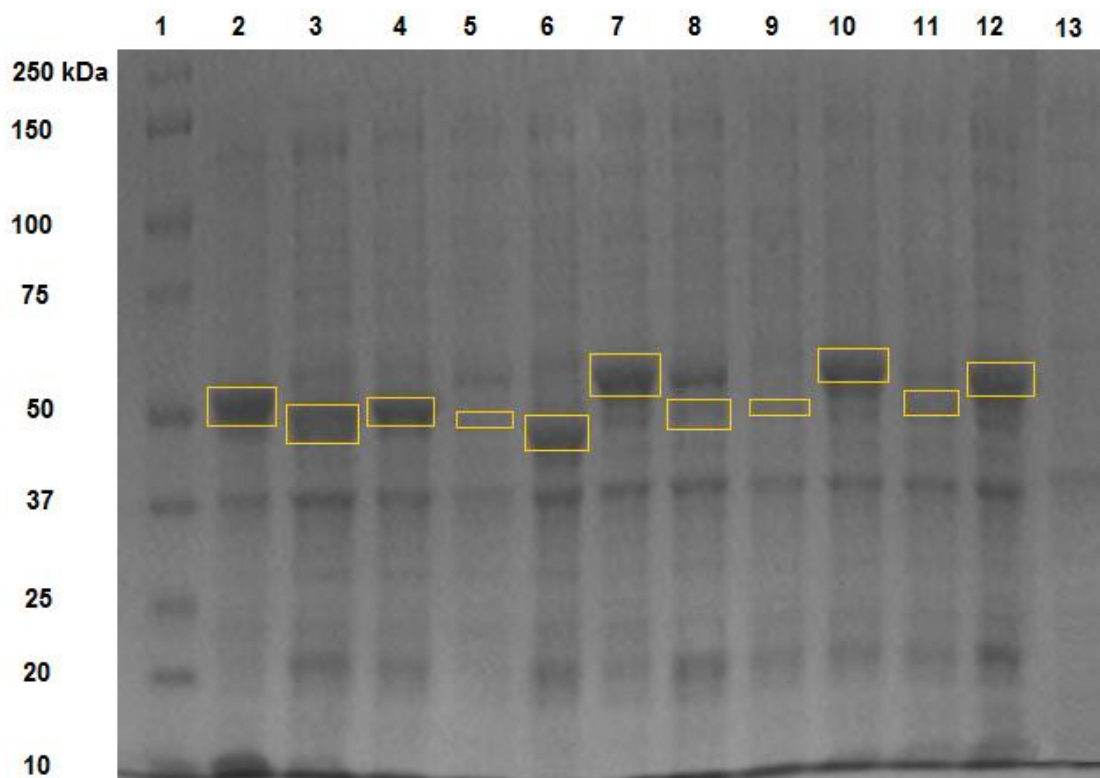


Figure 5.2. SDS-PAGE analysis showing expression of the library of novel ω -TAm enzymes compared to the CV2025 ω -TAm (pQR801). Results are from clarified cellular extracts produced from the fermentations showing in Figure 5.1: Lane 1 is protein marker; lane 2 is pQR801 lane 23 is pQR811; lane 4 is pQR813; lane 5 is pQR985; lane 6 is pQR1011; lane 7 is pQR960; lane 8 is pQR978; lane 9 is pQR956; lane 10 is pQR1014; lane 11 is pQR1017; lane 12 is pQR1019; and lane 13 is a null strain of *E.coli* BL21 (DE3). Molecular weights of ω -TAm varied between 46 to 51 kDa as specified in Table 5.1. The ω -TAm expressions are highlighted in the box.

Table 5.1. Properties of the cloned ω -TAM library and expression levels. The construct gene ID is the external link to National Center for Biotechnology Information (NCBI)'s record for the gene or the organism-specific ID relevant to the clone. The total protein concentrations were analysed by Bradford assay (Section 2.6.3) and ω -TAM concentrations were calculated from SDS-PAGE gel (Figure 5.2).

Microorganism	Construct Gene ID	Plasmid	Molecular Weight (kDa)	Total protein concentration (g.L ⁻¹)	ω -TAM concentration (g.L ⁻¹)
<i>Chromobacterium violaceum DSM30191</i>	CV2025	pQR801	47.5	7.5	1.0
<i>Pseudomonas putida KT 2440</i>	PP2799	pQR811	49.7	6.9	1.2
<i>Pseudomonas aeruginosa PAO2</i>	PAO0221	pQR813	51.1	8.5	1.6
<i>Bacillus licheniformis</i>	BLi00474	pQR985	50.3	2.4	0.2
<i>Klebsiella pneumoniae</i>	KPN_03745	pQR1011	50.1	7.4	1.0
<i>Bacillus subtilis</i>	BSU09260_1971	pQR960	49.9	4.5	0.6
<i>Deinococcus geothermalis</i>	Dgeo_1177	pQR978	46.7	7.4	0.7
<i>Kineococcus radiotolerans</i>	Krad_4078	pQR956	50.9	5.9	0.3
<i>Micrococcus luteus</i>	Mlut_00920	pQR1014	50.2	7.0	1.2
<i>Rhodospirillum rubrum</i>	Rru_A1254	pQR1017	50.4	5.2	0.4
<i>Rhodobacter sphaeroides</i>	Rsph17025_2835	pQR1019	50.1	6.3	1.4

5.4. BIOCONVERSION AUTOMATION PLATFORM DESIGN AND DEVELOPMENT

5.4.1. Overview of the Tecan Platform

The commercially available Tecan Genesis (<http://www.tecan.com>) laboratory robotic platforms (Figure 2.4) enable integration with associated equipments such as spectrophotometric plate readers, centrifuges, HPLC autosamplers and vacuum manifolds. The Tecan robot used here features 8 separate pipetting tips mounted on a single liquid handling arm (LiHa). The LiHa system has liquid level sensing on each tip. The system is based on measurement of electrical resistance which enable tracking of the liquid level during aspiration and dispense, to prevent air uptake and can be used to ensure minimal tip contamination. Additionally the LiHa system also comes with variable liquid handling parameters (liquid classes such as water, Gemini predefined liquid, and custom define liquid for any reagent intended to use which specifies speeds, air gaps and detection modes) to increase accuracy and precision. The LiHa system is able to move in XYZ directions over the entire platform, the pipetting head can spread between 9 and 20 mm to cope with different microwell plates or other laboratory vessel used such as reagent troughs, vials and Eppendorf tubes. The pipette tips can either be disposable (DiTi) or fixed. DiTi are available in a variety of sizes for ranges of volumes capacity and are also offered with and without filter. Meanwhile, the fixed tips require sufficient wash steps present between aspirate of different reagents.

With the Tecan platform, the contents of wells were mixed by specifying the number of mix cycles of simultaneous aspirate and dispense steps using an appropriate volume of liquid. The pipette calibration was done by measuring the weight of water dispensed in pre-weighed Eppendorfs tubes assuming a density of 998 kg.m^{-3} . The pipetting precision used in the study was usually allowed between 0 to 5 % (v/v). The system was also equipped with a gripper tool known as a robotic manipulator arm (RoMa). Likewise, robotic arm also can move in XYZ axes with rotation angle 270° over the entire platform. The gripper spaces range 58 to 140 mm and comprise gripper force of up to 10 N. These features make the robot a very convenient platform to transport the equipment such as microplates from one rack / carrier to another rack /

carrier as well as to the integrated equipment. All the equipment racks and carriers such as microwell plate carrier, vials rack and Eppendorfs rack can be custom programmed into the Gemini software provided that it does not exceed the travel heights of the pipette tips (110 mm) and the RoMa. Moreover, when aseptic operation is needed, the entire workstation can be sterilized with Ultraviolet (UV) light and then operated within the available Class-2 robotic safety cabinet.

5.4.2. Preliminary Bioconversion Automation Platform Evaluation

To obtain a precise and uniform distribution of the materials in robotic platform designed, the required methods and integrate necessary associated equipment are to be primarily developed. Similarly to the established manually microwell scale bioconversions (Chapter 3), there are several significant challenges and constraints that emerged in order to transform it into an efficient automation platform. This includes solutions to evaporation and correct choice of pipette tips. Most importantly, it also need to first compare the data from manual experiments to those obtained using the automation platform.

The microwell plates used for bioconversions were the same as those used in the manual process i.e glass 96-well, flat-bottomed microtiter plate (Section 2.5.1). Again, the issue of plate cover that provide well closed system in order to prevent compounds and water evaporation was the first to be resolved. This was a major challenge as in manual platform, we can easily apply the cover which easily peels off at each sample time interval, but in automation we need to choose the best plate cover that compatible with the LiHa.

The glass 96-well reaction plate was placed on the Thermomixer Comfort shaker for temperature and shaking control. Another plate was needed for sampling the reaction at each time interval which was placed in an adjacent plate carrier available with the Tecan platform. The plates were initially sealed with Thermo plastic elastomer cap that was previously used in manual platform (Section 2.5.1). Unfortunately, the cap did not perform well with either fixed tips or disposable tips. This issue was resolved by replacing the seal with pre-cut pierceable films from Excel Scientific that support automation and robotic applications. Instead of 1 adhesive layer the plates were sealed

with 5 layers of films for a better assurance to prevent samples evaporation and contamination. Disposable tips were used to perform liquid aspirating and dispensing by penetrated through the pre-cut over each well. The pre-cut hairline "X" pattern created four flaps that bend easily when pushed by disposable tips, and returned to their original position after each pipetting for continued protection.

The RoMa was used to move plates to the integrated centrifuge (Section 2.5.6) controlled by Gemini software and placed underneath the Tecan workstation for samples clarification. The clarified samples were then dispensed into HPLC vials placed on the HPLC rack. Here, they were first derivatized using AQC reagent as described in Section 2.6.6. Finally, each vial was manually capped and transferred for off-line HPLC analysis of substrate and product concentrations (Section 2.6.6.) The use of automation has accelerated the sample preparation for analysis while offered significant time savings by reducing preparation time by an order of magnitude compared with manual preparation. Figure 5.3 shows the layout of the deck of the entire platform.

The sensitivity of the automated method established was determined by comparing the original method with that modified conditions to allow the design of an efficient automated platform. As shown in Figure 5.4, the result obtained using the automated platform was comparable to those obtained by manual determination (Chapter 3). Moreover, the comparable AP concentrations measured from both automated and manual platforms highlighted the credibility of the established platform in ensuring well closed system protecting evaporation whilst maintained its overall efficiency and effectiveness.

5.5. PARALLEL EVALUATION OF ALTERNATIVE AMINO DONORS

As described in Section 4.4, the simplest and most easily implemented option for overcoming low yielding equilibrium controlled reaction was the evaluation of alternative amino donors. Using the manual approach it was possible to address five alternative co-substrates (isopropylamine, benzylamine, s-(+)-sec-butylamine, s-(+)-1-aminoindane and L- α -serine) to MBA solely with the CV2025 ω -TAm expressed from plasmid pQR801.

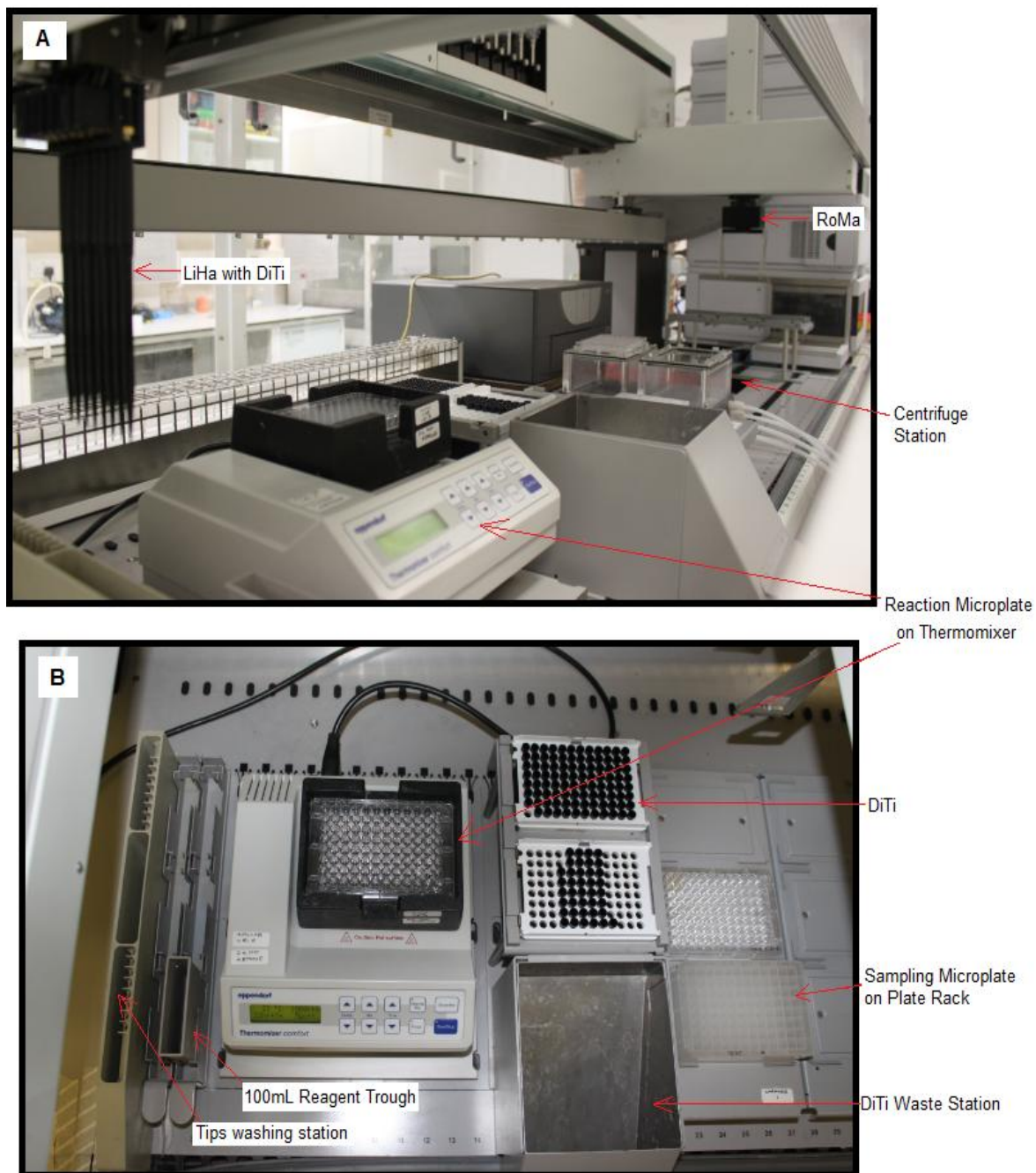


Figure 5.3. Detail of the robotic platform used for ω -TAM bioconversions with alternative amino donors (Section 5.5) and second enzyme system (Section 5.6). (A) Platform side view and (B) platform top view. Both images show the worktable layout of integrated equipment involved on the Tecan Genesis robot. Abbreviations: RoMa is robotic manipulator arm; LiHa is liquid handling arm / liquid handler; DiTi is disposable pipette tips.

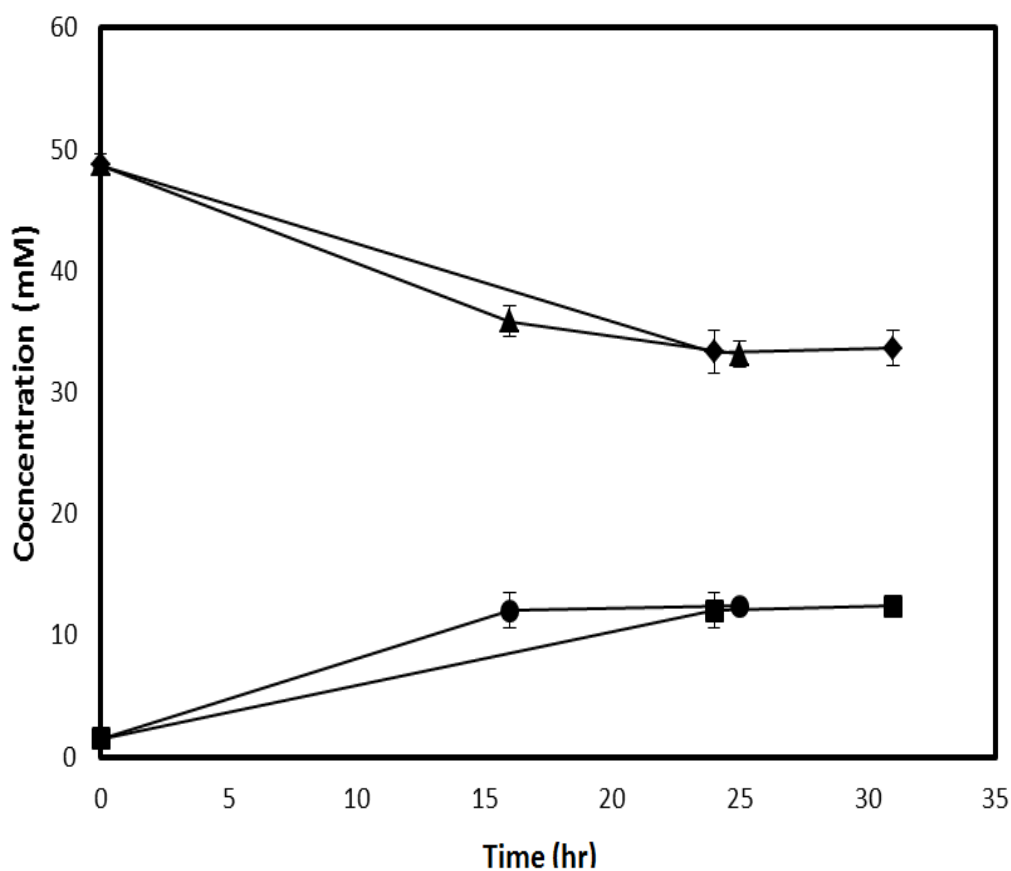


Figure 5.4. Comparison of automated and manual microwell methods for bioconversion kinetics of CV2025 ω -TAm (pQR801). Automated experiments performed using 96-microwell plate covered with 5 layers pre-cut pierceable films (Section 5.4) and manual experiments performed using 96-microwell plate covered with thermo plastic elastomer cap (Section 3.5): MBA consumption (\blacklozenge) and AP production (\blacksquare) for the automation experiments and MBA consumption (\blacktriangle) and AP production (\bullet) for the manual experiments. Reaction conditions: 0.3 g.L^{-1} CV2025 ω -TAm; 0.2 mM PLP; [MBA] and [Ery] were 50 mM ; $30 \text{ }^\circ\text{C}$; pH 7.5; 300 rpm in 50 mM HEPES buffer; total volume of $300 \text{ }\mu\text{L}$. Bioconversions performed as described in Sections 2.5.6 (automated experiments) and 2.5.1 (manual experiments). Error bars represent one standard deviation about the mean ($n=3$).

The further development of this approach into an automated methodology now facilitates a wider range of parallel experimentation involving six amino donors to be evaluated with each of the enzymes in the novel ω -TAM library (Section 5.3). In this way, it is possible to simultaneously characterise each enzyme's substrate range and the potential benefits for better ketodiol conversion with a range of amino donors. The individual reactions were again performed using equimolar concentrations of amino donor and Ery (amino acceptor) at 50 mM. All reactions were performed at equivalent ω -TAMs concentrations of 0.3 g.L⁻¹. The unit operations performed here on the automated platform were similar to those defined in Section 5.4.2 and mainly corresponded to the disposable tips utilization approach.

The effectiveness of the automated approach was first established by the excellent agreement seen between the automated (Figure 5.5) and manual (Figure 4.4) experimental result for the standard bioconversion (50 mM MBA and 50 mM Ery) using CV2025 ω -TAM. In this case, the final conversion yields of the automated and manual processes were 12 mM and 13 mM ABT respectively. As shown in Figure 5.5, under these standard reaction conditions, none of the novel ω -TAMs evaluated achieved greater performance than the CV2025 ω -TAM (pQR801). Only the PA00221 ω -TAMs (pQR813) and PP2799 ω -TAMs (pQR811) showed reasonable conversion about 16 % (mol.mol⁻¹) lower than CV2025 ω -TAMs. Meanwhile, the remaining TAMs achieved 50 % (mol.mol⁻¹) or less of the conversion reached by CV2025 ω -TAMs (Graph A of Figure 5.5).

When MBA was replaced with the aliphatic amine compounds isopropylamine and sec-butylamine of the ten novel ω -TAMs tested, only two showed significant activity towards isopropylamine whereas lower reactivity were detected from the remaining eight TAMs tested. The PA00221 ω -TAM (pQR813) and PP2799 ω -TAM (pQR811) accomplished conversions of 20 mM and 16 mM of ABT respectively which were still much lower than with the CV2025 ω -TAM (pQR801) which was 35 mM. When sec-butylamine was used as an alternative amino donor, none of the novel ω -TAMs reached an improved reaction conversion over CV2025 ω -TAM (pQR801). Bioconversion using sec-butylamine with PA00221 ω -TAM (pQR813) produced a similar conversion to CV2025 ω -TAM (pQR801) which were 14 mM and 15 mM ABT respectively. However, with this amine donor it would be feasible to increase the

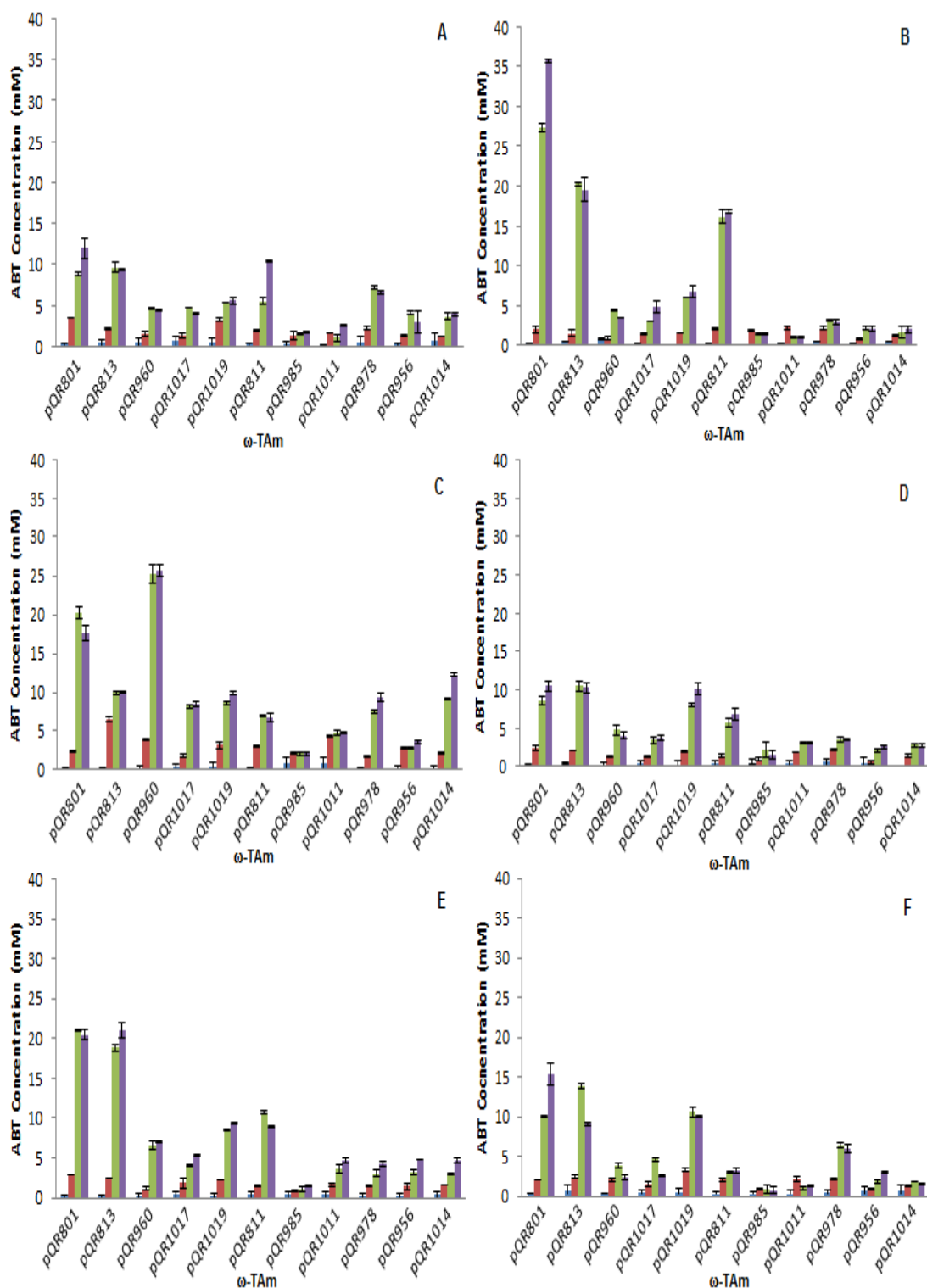


Figure 5.5. Summary of measured bioconversion kinetics of the ω -TAM library on the microscale automation platform (Section 5.5) using alternative amino donors: (A) MBA; (B) isopropylamine; (C) L- α -serine; (D) benzylamine; (E) s- (+)-1-aminoindane; (F) s-(+)-1-sec-butylamine. The reactions were sampled at 0 hr (■); 6 hr (■); 20 hr (■) and 30 hr (■). Reaction conditions: 0.3 g.L⁻¹ ω -TAM; 0.2 mM PLP; [Amino Donor] and [Ery] were 50 mM; 30 °C; pH 7.5; 300 rpm in 50 mM HEPES buffer; total volume of 300 μ L in 96-glass microwell plate covered with 5 layers pre-cut pierceable films (Section5.4). Bioconversions performed as described in Sections 2.5.1 and 2.5.6. Error bars represent one standard deviation about the mean (n=3).

product yield by applying reduced pressure operation (Sections 4.6 and 5.7) to encourage evaporation of its resulting volatile ketone product, 2-butanone. The performances of all the ω -TAMs evaluated with these alternative amino donors are detailed in Graphs B (isopropylamine) and F (sec-butylamine) of Figure 5.5.

MBA was next substituted with the aromatic amino donors, benzylamine and S-1-aminoindane. It was formerly reported that ω -TAM from *Vibrio fluvaris* (Shin and Kim, 2001) and CV2025 (Kaulmann et al., 2007) showed high activities towards amino donor of aromatic (S)-amines such as MBA and (S)-aminoindane. Nonetheless, only PA00221 ω -TAM (pQR813) and Rsph17025_2835 ω -TAM (pQR1019) using benzylamine and PA00221 ω -TAM (pQR813) using s-1-aminoindane showed equivalent activities to the CV2025 ω -TAM. Their resulted product formations were 12 mM and 21 mM respectively. Yet again, as shown in Graphs D (benzylamine) and E (s-1-aminoindane) of Figure 5.5, the remaining ω -TAMs displayed low conversions of 5 mM ABT or less.

In the case of BSU09260_1971 ω -TAM (pQR960), enzyme was identified that had a better catalytic activity than CV2025 (pQR801) when an amino acid, L- α -serine was used as amino donor. As presented in Graph C (Figure 5.5) BSU09260_1971 ω -TAM (pQR960) catalysed the conversion of 50 mM L- α -serine and 50 mM Ery yielded 25 mM ABT equivalent to a 23 % ($\text{mol}\cdot\text{mol}^{-1}$) higher conversion than CV2025 ω -TAM.

L- α -Serine is a compound naturally occurring in *E.coli* cells and is also available commercially at a considerably cheap price than many other amino donors tested. Therefore, this novel ω -TAM bioconversion was selected for subsequent scale-up studies (Section 6.4). Comparable data obtain at a larger scale will help confirm the novel ω -TAM biocatalytic activity for the transamination of Ery using the relatively cheap donor, L- α -serine. The identification of this reaction also indirectly proves the effectiveness of these microscale studies as a rapid tool for quantitative evaluation of various biocatalysts and reaction conditions.

Overall the results indicate the relatively narrow substrate range of most ω -TAMs apart from PP2799 ω -TAM (pQR811), PAO0221 ω -TAM (pQR813) and Rsph17025_2835 ω -TAM (pQR1019) which each showed relatively good activity

with a variety of amine donors. These ω -TAMs have significantly broader substrate specificities towards different amino donors than the CV2025 ω -TAM (pQR801). The asymmetric synthesis of the tested amino donors with all novel ω -TAMs were no greater than 25 mM, which yet again signifying the extremely unfavourable thermodynamic equilibrium and products and / or substrates inhibitions. In general, most ω -TAMs showed better and considerably higher reactivities towards aromatic amines than aliphatic amines and amino acids as witnessed in the previous reported work (Hwang and Kim, 2004).

5.6. OPTIMIZATION OF SECOND ENZYME REACTION CONDITION

5.6.1. Parallel CV2025 ω -TAM Bioconversions with Second Enzyme Reaction Using Alcohol Dehydrogenase (ADH) from *Lactobacillus Kefir*

As presented in Section 4.5, the utilization of ADH, an NADP⁺ dependent enzyme, coupled with GDH for efficient NADPH co-factor regeneration is one potential option for *in-situ* AP removal. This led to a 3.3-fold increase in bioconversion yield, but under the conditions used is likely to be uneconomic due to the expense of the additional enzymes and co-factors involved. Obtaining enantiomerically pure intermediates and products efficiently and economically is of immense importance in the pharmaceutical and chemical industries (Sanchez and Demain, 2011). Hence, the work presented here aims to use the microscale process platform to evaluate the most economically feasible conditions. In practice, this will involve the study of reduced concentrations of enzymes at varying ratios and reduced reactant / co-factor concentrations. In addition, 1.5 M HEPES was used for all reactions performed here to ensure pH was well kept at about its optimum value as noted earlier in Section 4.5. The unit operations performed on the automated platform were as defined in Section 5.4.2 and mainly corresponded to the disposable tips utilization approach. Table 5.2 summarizes the variable parameters used for further investigation.

The automated process conditions allowed for the evaluation of a much wider range of enzyme and reactant concentrations than the manual process. When the initial glucose concentration was maintained at a concentration of 70 mM, equal to the previous manual process, the concentration of ADH used could be decreased from 1.2

g.L⁻¹ down to 0.03 g.L⁻¹ while still obtained the same production producing 40 mM ABT at 21 hours (Figure 5.6 (A-1)). In terms of AP conversion into (R)-1-phenylethanol by the second enzyme ADH coupled with GDH, it was observed that the AP produced was almost totally consumed (2 mM or less left in the reaction solution) when the ADH concentration reduced to 0.03 g.L⁻¹ or less (Figure 5.6 (A-2)). Further reduction of the ADH concentration to only 0.003 g.L⁻¹ significantly reduced the bioconversion yield by more than 20 % (mol.mol⁻¹) while the concentration of AP left in the reaction was 8 mM (above the inhibitory concentration). When the same ADH concentration was used with reduction of the GDH concentration from 0.02 g.L⁻¹ to 0.002 g.L⁻¹, the reaction conversion further declined to 28 mM ABT, whereas only approximately half AP was succeeded to diminish from the reaction solution (Figure 5.6 (A-1 and A-2)).

Table 5.2. Summary of parameters investigated for CV2025 ω-TAm bioconversions using the second enzyme system on the automated platform.

	Enzyme concentrations	
	ADH (g.L ⁻¹)	GDH (g.L ⁻¹)
Glucose (mM) 70, 50, 25	1.2	0.02
	0.3	0.02
	0.03	0.02
	0.003	0.02
	0.003	0.002

It was also possible to achieve comparable ABT production when the glucose concentration was reduced to 50 mM. However, a consequence of this was that AP reduction by the second enzyme reaction was reduced, with 8 mM AP being left in solution (a concentration close to the inhibitory level (Section 4.3)) whereas only 2 mM or less was left in solution at the higher 70 mM glucose concentration (Figure 5.6 (B-2)).

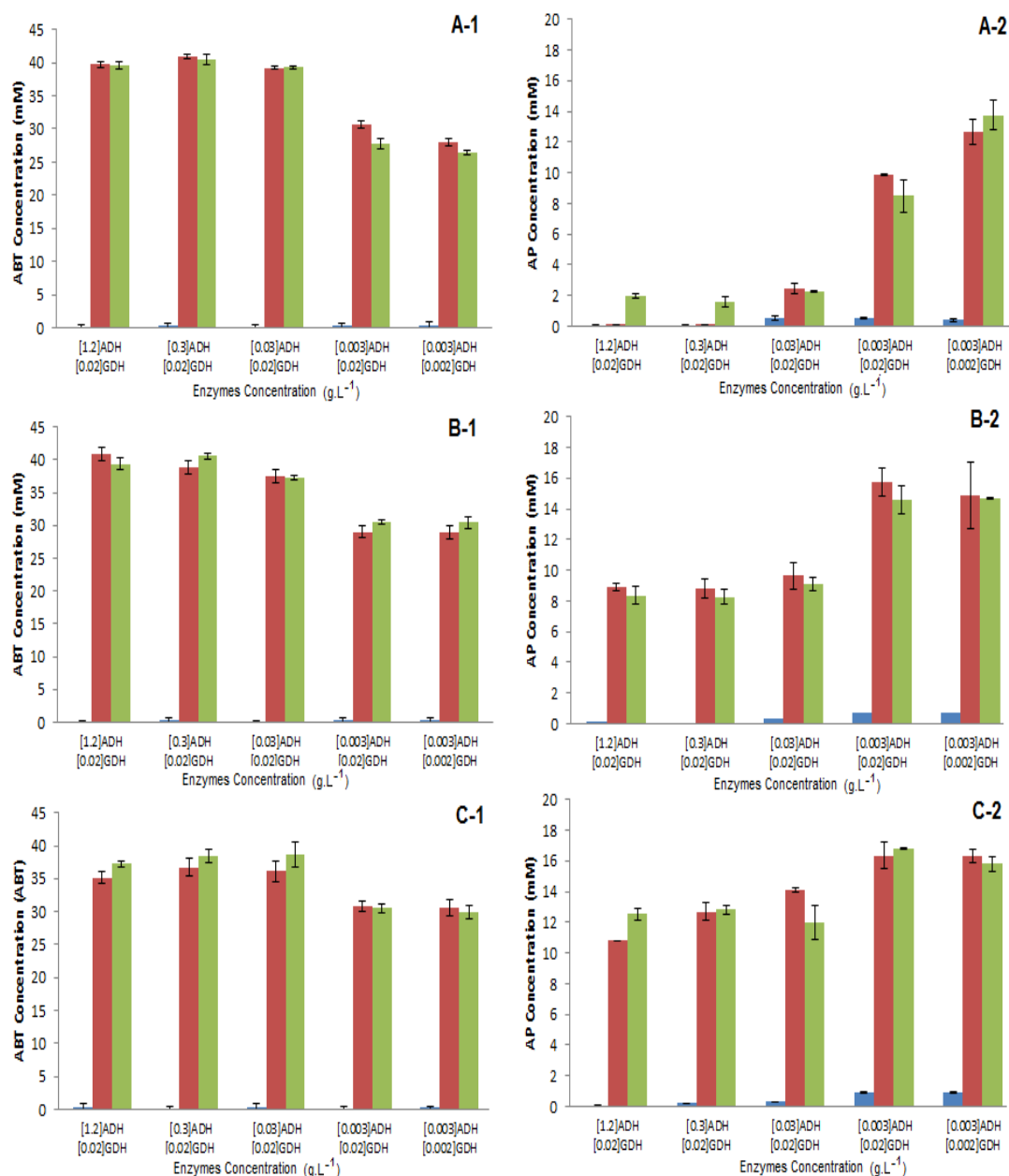


Figure 5.6. Bioconversion kinetics of CV2025 ω -TAm (pQR801) using the second enzyme system with various ratios of ADH, GDH and glucose (as described in Table 5.2). Experiments performed using ADH from *Lactobacillus kefir* on the microscale automation platform (Section 5.6.1): (A-1) ABT productions and (A-2) AP consumption of reaction using 70 mM Glucose; (B-1) ABT productions and (B-2) AP consumption of reaction using 50 mM Glucose and (C-1) ABT productions and (C-2) AP consumption of reaction using 25 mM Glucose. The reactions were sampled at 0 hr (■); 21 hr (■) and 25 hr (■). Reaction conditions: 0.3 g.L⁻¹; CV2025 ω -TAm; 0.2 mM PLP; [MBA] and [Ery] were 50 mM, 1 mM NADPH; 30 °C; pH 7.5; 300 rpm in 1500 mM HEPES buffer; total volume of 300 μ L in 96-glass microwell plate covered with 5 layers pre-cut pierceable films (Section 5.4). The concentrations of ADH and GDH used in the reactions are as mentioned in the Enzyme Concentration (g.L⁻¹) of each graph. Bioconversions performed as described in Sections 2.5.3 and 2.5.6. Error bars represent one standard deviation about the mean (n=3).

At the lowest glucose concentration (25 mM) evaluated, similar ABT production was observed for all the combination of ADH and GDH concentrations tested. As expected, as the glucose concentration was reduced beyond that of the starting substrate it reduced the rate of second enzyme reaction as displayed by increased in AP concentrations in the solutions (Figure 5.6 (C-2)). Theoretically, for every 1 mM glucose will convert 1 mM AP. Equally, for the first 3 reactions of ADH concentrations 1.2, 0.3 and 0.03 g.L⁻¹, of about 40 mM ABT produced and as predicted about 15 mM or more AP was left unconverted in the reactions. Furthermore at this glucose concentration, we have it just enough to convert an amount of AP produced to lowered it down to below its inhibition concentration (K_i). Complete reactions observations were depicted in Figure 5.6.

Confirmation that glucose was the limiting factor was obtained from a control reaction carried out at very low glucose of 5 mM is shown in Figure 5.7. It was observed at glucose limitation, the CV2025 ω-TAm bioconversion reaction conversion decreased to 25 mM from 40 mM of ABT as previously reached with excess glucose concentration under identical reaction conditions and parameters.

5.6.2. Parallel CV2025 ω-TAm Bioconversions with a Second Enzyme Reaction Using Alcohol Dehydrogenase (ADH) from *Thermoanaerobium Brockii*

An alternative ADH from *Thermoanaerobium brockii* (ADH-TB) was also used to catalyse the second enzyme reaction in order to provide an activity and cost comparison to the previously studied ADH from *Lactobacillus kefir*. Again, the experimental design involved the use of the automated platform to simultaneously explore and minimise the various enzyme and glucose concentrations.

As presented in Figure 5.8, the CV2025 ω-TAm bioconversion reactions with application of the second enzyme reaction using ADH-TB and 70 mM glucose displayed an optimum conversion of 40 mM ABT as previously obtained using ADH from *Lactobacillus kefir* (Section 5.6.1). Nevertheless, the conversion rate observed was 4-fold slower with ADH-TB than earlier observed with the ADH *Lactobacillus kefir*. Furthermore, 20 % (mol.mol⁻¹) of AP was detected as being unconverted to (R)-

1-phenylethanol while the earlier bioconversions using ADH from *Lactobacillus kefir* showed complete depletion of AP from the reaction solution (Figure 5.6 (A-2)). Also, alongside the decreased rate of the ADH-TB only approximately 60 % ($\text{mol}\cdot\text{mol}^{-1}$) corresponding 30 mM ABT conversion (Figure 5.8 (A-1)) was achieved with 10 mM AP was quantified left in the reaction solution (Figure 5.8 (A-2)).

Comparable results were found when glucose was present at initial concentrations of 50 mM and 25 mM in the second enzyme reactions with ADH-TB (Figure 5.8 (B-1 and C-1)). For both sets of reaction conditions, no yield improvement was accomplished as ADH-TB and GDH concentrations were decreased.

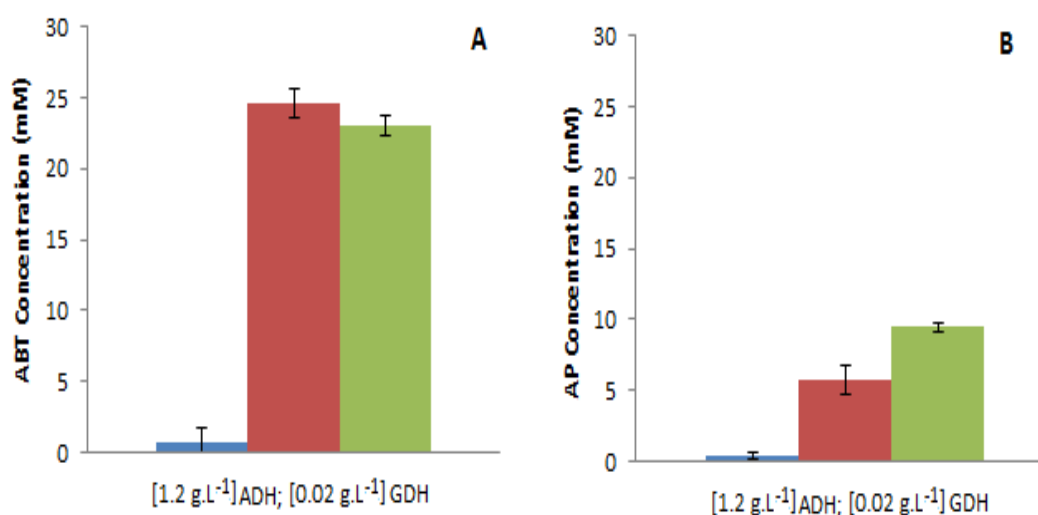


Figure 5.7. Bioconversion kinetics of CV2025 ω -TAm (pQR801) using the second enzyme reaction with ADH from *Lactobacillus kefir* and Glucose limitation on the microscale automation platform (Section 5.6.1): (A) ABT productions and (B) AP consumption. The reactions were sampled at 0 hr (■); 20 hr (■) and 25 hr (■). Reaction conditions: 0.3 g.L⁻¹ CV2025 ω -TAm; 1.2 g.L⁻¹ ADH; 0.02 g.L⁻¹ GDH; 0.2 mM PLP; [MBA] and [Ery] were 50 mM, 5 mM Glucose; 1 mM NADPH; 30 °C; pH 7.5; 300 rpm in 1500 mM HEPES buffer; total volume of 300 μ L in 96-glass microwell plate covered with 5 layers pre-cut pierceable films (Section 5.4). Bioconversions performed as described in Sections 2.5.3 and 2.5.6. Error bars represent one standard deviation about the mean (n=3).

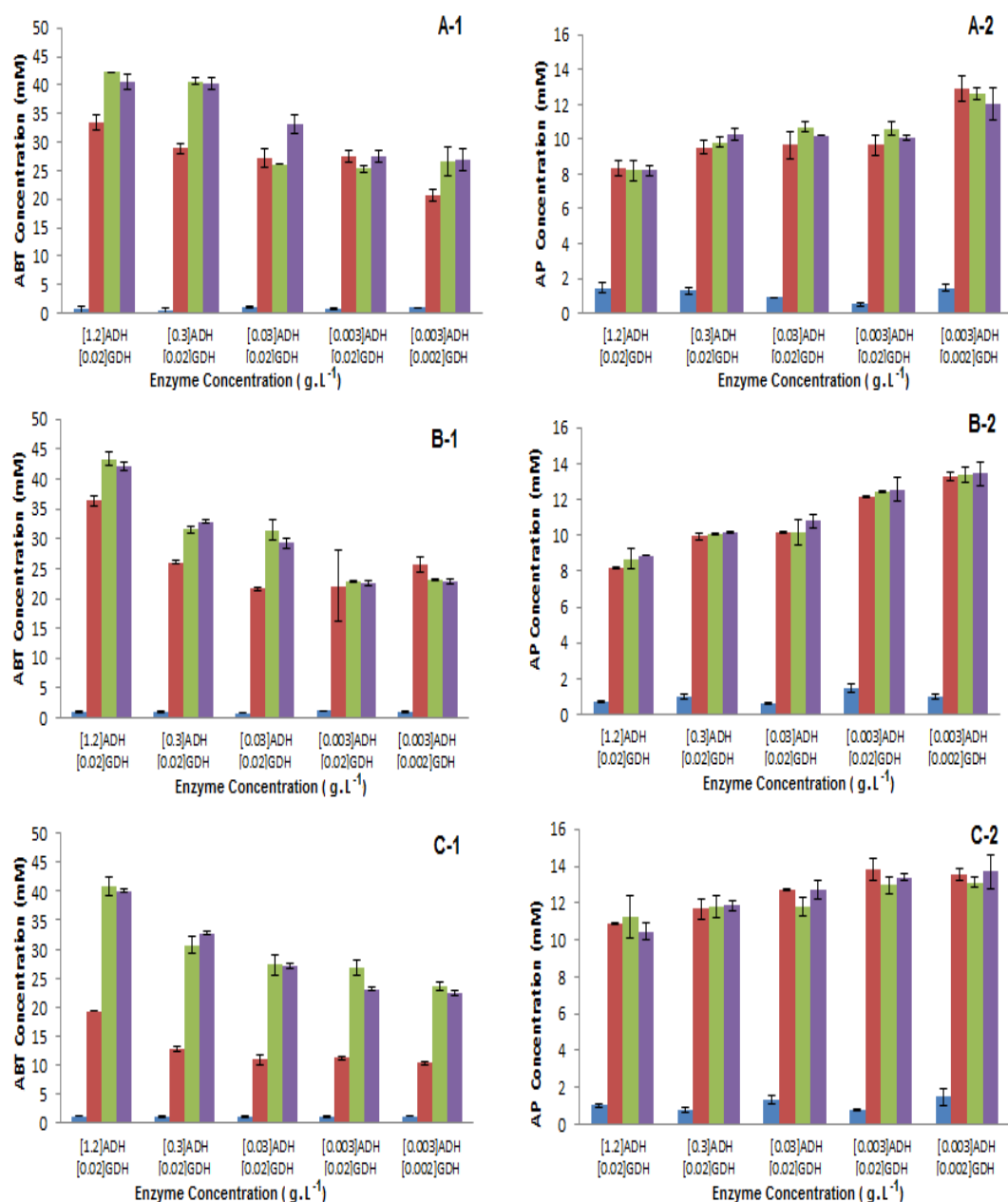


Figure 5.8. Bioconversion kinetics of CV2025 ω -TAM (pQR801) using second enzyme reaction with various ratios of ADH, GDH and glucose (as described in Table 5.2). Experiments performed using ADH from *Thermoanaerobium brockii* on the microscale automation platform (Section 5.6.2): (A-1) ABT productions and (A-2) AP consumption of reaction using 70 mM Glucose; (B-1) ABT productions and (B-2) AP consumption of reaction using 50 mM Glucose and (C-1) ABT productions and (C-2) AP consumption of reaction using 25 mM Glucose. The reactions were sampled at 0 hr (■); 6 hr (■); 20 hr (■) and 25 hr (■). Reaction conditions: 0.3 g.L⁻¹ CV2025 ω -TAM; 0.2 mM PLP; [MBA] and [Ery] were 50 mM; 1 mM NADPH; 30 °C; pH 7.5; 300 rpm in 1500 mM HEPES buffer; total volume of 300 μ L in 96-glass microwell plate covered with 5 layers pre-cut pierceable films (Section 5.4). The concentrations of ADH and GDH used in the reactions are as mentioned in the Enzyme Concentration (g.L⁻¹) of each graph. Bioconversions performed as described in Sections 2.5.3 and 2.5.6. Error bars represent one standard deviation about the mean (n=3)

Overall, the low product yield and the greater AP accumulation in the CV2025 ω -TAm bioconversions when using ADH-*TB* as the second enzyme indicated a relatively slow reaction rate. This once again implies that the glucose excess amount plays a substantial role in driving the second enzyme reaction faster. Consequently, it will promote the reduction of interconversion (i.e AP to MBA) rate of the CV2025 ω -TAm reaction whilst hinder the accumulation of AP concentration to reach K_i . This indeed verifies another possible candidate that accepted AP, however under the conditions applied, the AP reduction rate was substantially slower.

Further, the practical use of the ADH-*TB* was also previously observed to be limited to substrates with bulky side chains such as AP despite its recognition for thermal stability and broad substrates range (Hummel, 1990).

5.6.3. Economic Considerations of Second Enzyme Reactions

Use of the automated microscale methods to study the second enzyme system has provided a better understanding of how changes in a reaction variable will affect the overall CV2025 ω -TAm bioconversion rate and yield. As presented in Sections 5.6.1 and 5.6.2, ADH from *Lactobacillus kefir* showed a better biocatalytic performance than ADH-*TB*. Although the concentration of the ADH from *Lactobacillus kefir* could be reduced to low levels (i.e 0.03 g.L⁻¹), the dual enzyme reaction nevertheless performs efficiently under high substrate concentrations. In addition, the second enzyme reaction catalysed by ADH *Lactobacillus kefir* can perform reasonably well at glucose concentrations as low as 25 mM. However, the possibility of using lower glucose concentrations for bioconversions with ADH-*TB* was ruled out since 70 mM seem to be the most favourable concentration. This again proves the ADH *Lactobacillus kefir* performance which is most likely due to its good catalytic activity and stability (Table 5.3).

In general, the main reason to choose a biocatalytic process is the cost advantage over other available process options including chemical synthesis (Ghisalba et al., 2010). If the cost issue is addressed particularly on a price per mg basis of ADH enzyme from both studied strains, ADH from *Lactobacillus kefir* is again shown to be the best enzyme as the market price is 4 times cheaper than ADH-*TB* (Table 5.3). Glucose as

the co-substrate, however, is considerable cheaper at £0.13 per gram and will have less impact on process economics. Therefore, it is best to use at least an equal concentration of glucose to the first reaction substrate concentration (i.e 50 mM) to promote higher recycling of co-factor NADPH and consequently drive the second enzyme reaction rate even faster or to completion.

In summary, the automated evaluation of second enzyme reaction conditions has made this a more attractive process option since it was possible to explore a higher number of variables simultaneously. These identified significant opportunities for reducing the cost of operating the second enzyme system.

Table 5.3. Activity and prices of the various ADHs used in Sections 5.6.1 and 5.6.2.

Enzyme	Activity (units mg ⁻¹)	Market Price £ (per mg)
ADH <i>Lactobacillus kefir</i>	0.4 (1 unit will reduce 1 µmol AP per min at pH 7 and 25 °C to phenylethanol)	1.16
ADH <i>Thermoanaerobium brokii</i>	3.82 (1 unit will oxidize 1 µmol of 2-propanol to acetone per min at pH 7.8 and 40 °C in the presence of NADP ⁺)	4.12

5.7. PARALLEL EVALUATION OF REDUCED PRESSURE REACTION

5.7.1. The Design of Reduced Pressure System Automation Platform

The microscale technique designed for reduced pressure reactions in Section 4.6 used a customised vacuum manifold (Te-VacS) that could be located on the deck of the Tecan robotic workstation. Indeed, the vacuum manifold used in Section 4.6, the Te-VacS module was originally designed for integration with a Tecan platform and its operation could be controlled by the Gemini software. The Te-VacS module provides two separate vacuum blocks positions connected to a high performance vacuum pump

and its specification details are displayed in Table 2.6 (Section 2.5.6). The combined use of the Te-VacS and the integrated robotic manipulator RoMa allows full automation of this biocatalytic process option in a 96-well format similar to the procedure already performed manually.

The reduced pressure was applied by specifying the vacuum time and the applied pressure intended for each reaction studied. The Te-VacS vacuum block was configured to host the glass 96-microwell plate for this reduced pressure operation. Once the enzyme and substrates were dispensed using disposable tips into the reaction plate, this was placed inside the vacuum block. The automated sequence then continues with the RoMa placing another plate on the top of Te-VacS which acted as lid. The reaction begins once the vacuum is applied. Given the closed nature of the vacuum block the vacuum was released at defined time intervals to allow reaction sampling. Once again the RoMa arm was used to remove the plate lid to allow the disposable tips to aspirate the sample solution. Once this was done the RoMa arm placed the plate lid back on the vacuum block, and the pressure was again applied to continue the reaction. The sample solution was clarified by centrifugation and sample aliquots were derivatized in HPLC vials as described in Section 5.4.2. Figure 5.9 illustrates the layout of the Tecan platform set up for reduced pressure bioconversions.

5.7.2. Parallel CV2025 ω -TAm Bioconversions at Reduced Pressure

The work presented here aims to establish the feasibility of the automated vacuum manifold for performing reduced pressure bioconversions with robotic integration. Again considering the total volume of the reaction, it was intended to apply mild pressure to encourage the evaporation of AP as reaction progress (Section 4.6). It was found that the minimum pressure that can be effectively applied to the system was 30 mbar (~22.5 torr). This pressure was about 4 times higher than what have been applied in manual system using vacuum/ pressure pump. Unlike the manual process, the Tecan workstation did not have independent temperature control. Because it was not possible to control the temperature on the automated platform at 30 °C, reactions were compared with / without the applied vacuum at ambient temperature, 23 °C.

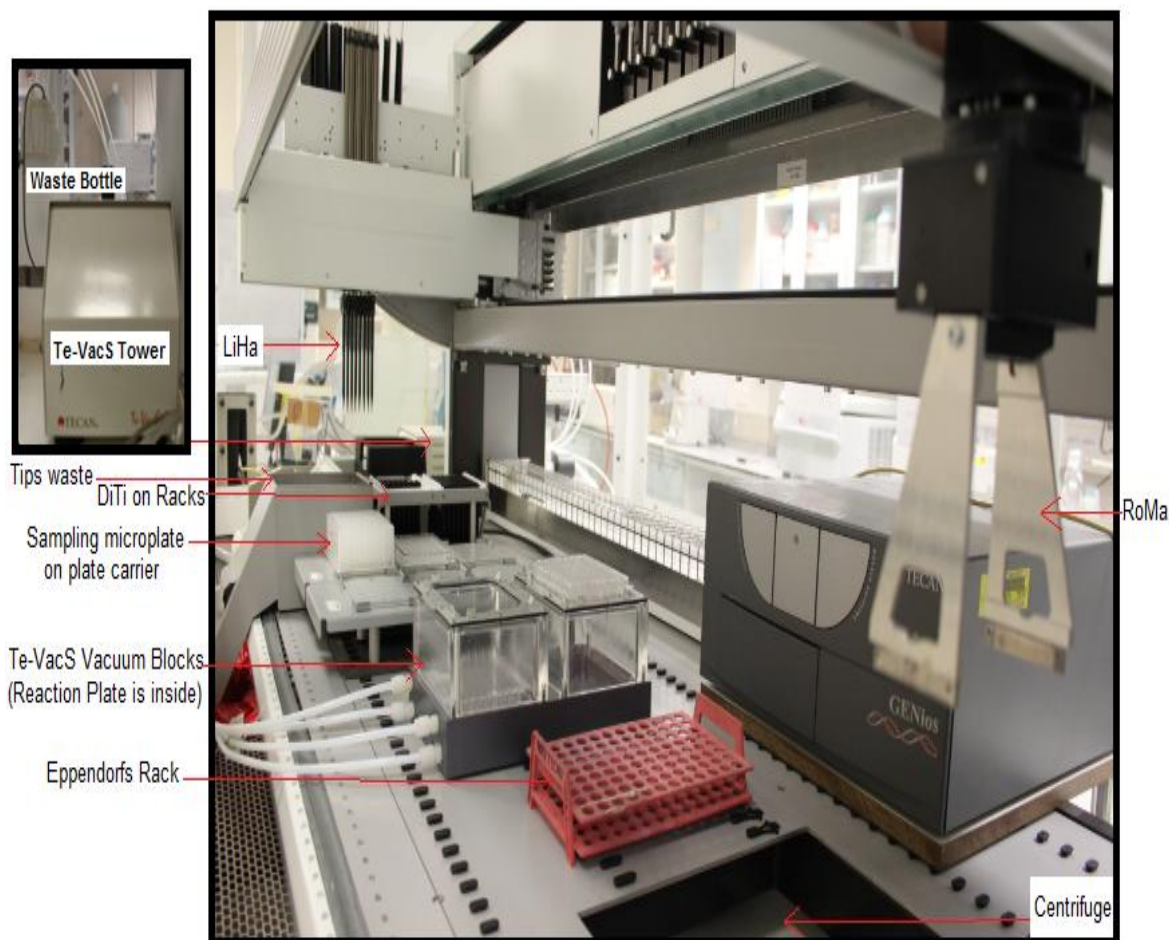


Figure 5.9. Detail of the robotic platform used for CV2025 ω -TAM standard bioconversions with reduced pressure system using a Te-VacS vacuum separator (Section 5.7). The image shows the worktable layout of the integrated equipment involved on the Tecan Genesis robot. Abbreviations: RoMa is robotic manipulator arm; LiHa is liquid handling arm / liquid handler; DiTi is disposable pipette tips.

Before preceded with the reaction, yet again the evaporation rate of the reaction medium was first determined in order to facilitate accurate measurement of product and substrate concentrations. Again the water evaporation rate was measured based on gravimetric analysis. The water evaporation rate was found to be constant at $1.25 \mu\text{L}\cdot\text{hr}^{-1}$ (Figure 5.10) during the course of bioconversion. This was about 5 times slower than observed in the manual process (Figure 4.7) most likely due to the lower operating temperature. The quantification of all compound concentrations for reduced pressure reactions were subsequently corrected for evaporative losses. Again, CV2025 ω -TAm in clarified lysate form was used to catalyse MBA and Ery bioconversions at equimolar concentrations of 50 mM.

The CV2025 ω -TAm reaction under reduced pressure option was monitored only for a 19 hour period as the reaction was expected to be completed faster than previous studies. This was due to the use of 3 times the concentration of CV2025 ω -TAm (i.e. $1.0 \text{ g}\cdot\text{L}^{-1}$) in the clarified lysate form to accelerate the reaction rate to ensure the reaction could reach equilibrium 24 hours or less where the maximum level of evaporation would be 10 % ($\text{vol}\cdot\text{vol}^{-1}$). The reaction profiles for automated reduced pressure reactions are shown in Figure 5.11. These can be compared to a control reaction at normal atmospheric pressure at room temperature.

The substrate consumption rates and product yields are plotted together in Figure 5.11. The optimum product yield of CV2025 ω -TAm under reduced pressure method was 19 mM ABT in 16 hours. When it is compared to the standard reaction conducted at the same room temperature ($23 \text{ }^\circ\text{C}$ instead of $30 \text{ }^\circ\text{C}$), the reduced pressure condition applied has proven to facilitate an improved production yield by approximately 2.3-fold. Moreover, the system also have successfully shown its substantial effect on the ability and purpose to encourage more than 80 % ($\text{mol}\cdot\text{mol}^{-1}$) AP evaporation during the course of reaction which was in an excellent agreement to the manual platform (Section 4.6).

Despite the technical limitation of temperature control, we have demonstrated the capability of reduced pressure option on a robotic platform to be effective for the study of reduced pressure bioconversion in order to remove inhibitory and volatile

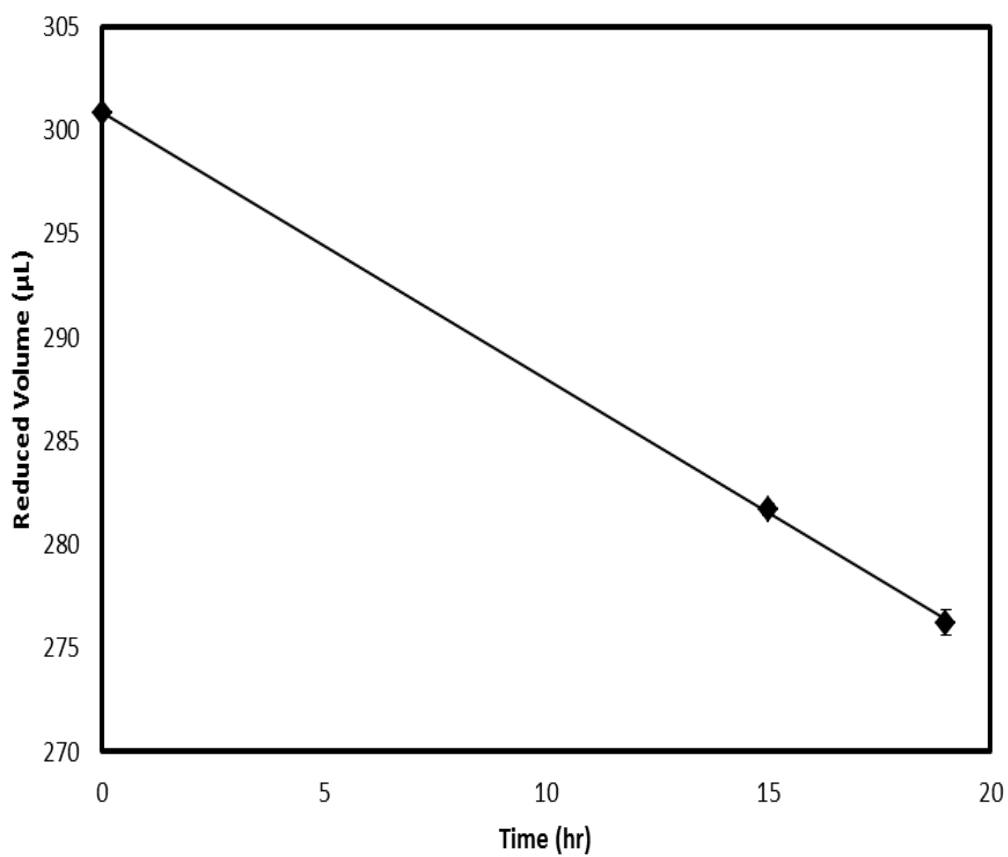


Figure 5.10. Microwell evaporation kinetics of water at 23 °C in the automated reduced pressure system (Section 5.7). Experiments performed at 30 mbar from 96-glass microwell plates. The water evaporation rate was constant at $1.25 \mu\text{L}\cdot\text{hr}^{-1}$. Error bars represent one standard deviation about the mean (n=3).

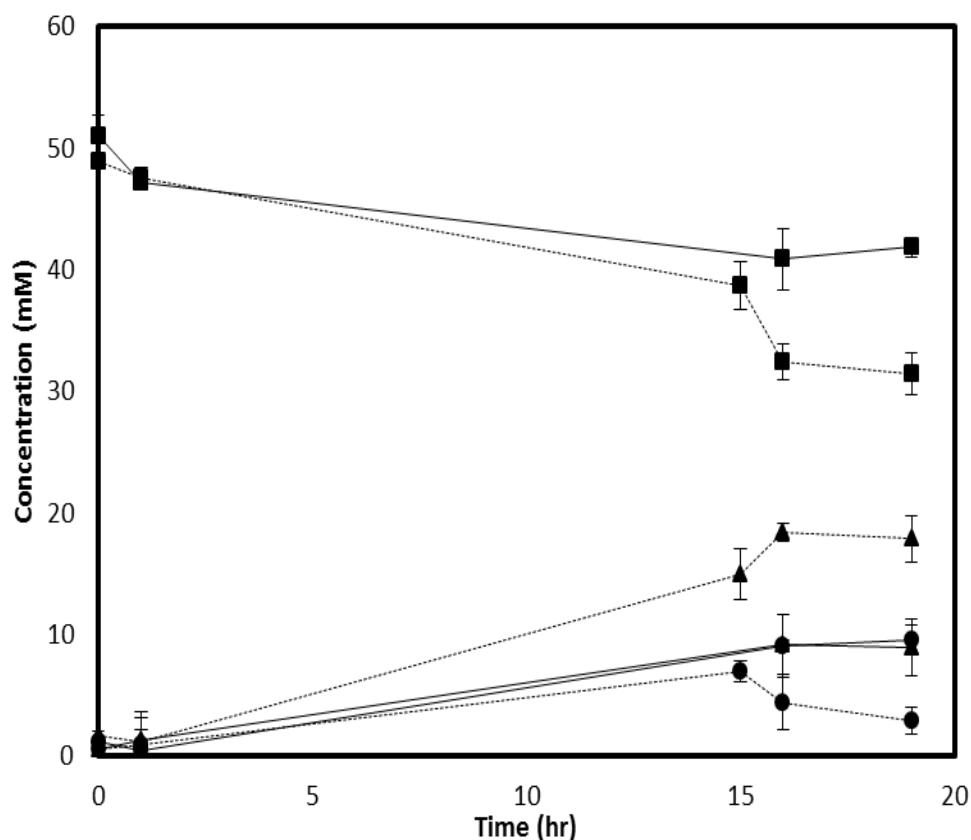


Figure 5.11. Bioconversion kinetics of CV2025 ω -TAM (pQR801) performed at reduced pressure on microscale automated platform and manual method. Experiments performed using 96-microwell plate covered with 5 layers pre-cut pierceable films (Section 5.7) and manual experiments using 96-glass microwell plate covered with thermo plastic elastomer cap performed at room temperature (23 °C): MBA consumption (- ■ -), ABT(- ▲ -) and AP productions (- - ● -) for the CV2025 ω -TAM bioconversions under the reduced pressure automation format and MBA consumption (■), ABT (▲) and AP(●) productions for the CV2025 ω -TAM bioconversions at 23 °C with manual experiments. Reaction conditions of both platforms: 1.0 g.L⁻¹ CV2025 ω -TAM; 0.2 mM PLP; [MBA] and [Ery] were 50 mM; 23 °C; pH 7.5; 300 rpm in 50 mM HEPES buffer; total volume of 300 μ L in 96-glass microwell plate. Bioconversions performed as described in Sections 2.5.4 and 2.5.6. The data plotted for reduced pressure reactions were corrected for water evaporation rate (Figure 5.10). Error bars represent one standard deviation about the mean (n=3).

side products. In addition, the automation reaction system also developed as a fast and reliable as verified from the data achieved. One of the major features of the system is its flexibility, allowing examination of hundreds of samples using 2 parallel 96-well micro-plates reactions to be conducted on the couple vacuum blocks come with adaptation of the system online setup for intended applied pressure. In short, the automation platform successfully plays its role as one of the simplest and most cost effective routes to improved reaction yields of bioconversions encompassed unfavourable thermodynamic equilibrium with reduce bioprocess optimization times.

5.8. SUMMARY

In this chapter, the successful automation of the microscale bioprocess methods developed in Chapter 4 has been described. These have been applied to the detailed evaluation and optimisation of ω -TAM reaction conditions at the 96-well plate scale. The automated systems have facilitated a significant increase in parallel experimentation and the simultaneous evaluation of different process conditions and their optimization.

Automated evaluation of a library of novel ω -TAM and a range of alternative amino donors showed most had specific activities equal or poorer than the CV2025 ω -TAM (Section 5.5). Therefore, this work shows that the CV2025 ω -TAM is still one of the most promising biocatalyst for asymmetric synthesis of broad substrates specificity. However, the experiments did identify one novel ω -TAM from *Bacillus subtilis* that have a high catalytic activity for transamination of Ery using L- α -serine as amino donor which resulted in a 23 % (mol.mol⁻¹) improved conversion yield than CV2025.

The work here also demonstrated the utility of the automation platform for the rapid evaluation and optimisation of reaction conditions when using more complicated second enzyme reactions where multiple parameters must be evaluated simultaneously (Section 5.6). The optimised reaction could be performed at 40-fold reduction in the concentration of ADH from *Lactobacillus kefir* whilst maintaining comparable reaction conversion. This would lead to significant cost saving in terms of process economics. In contrast, evaluation of new ADH from *Thermoanaerobium*

brokii over a wide range of reaction conditions indicated little improvement over the first ADH studied.

Finally, automation of bioconversions performed at reduced pressure was also achieved in a fully automated, hands-free manner (Section 5.7). The automated reduced pressure showed advantages over normal pressure CV2025 ω -TAm bioconversion as confirmed by 2.3-fold production yield improvement.

Overall, this chapter has demonstrated automation of all the microscale unit operations developed in the previous chapter. Once again these have been shown to be able to increase the yield of equilibrium controlled CV2025 ω -TAm bioconversions by use of alternative amino donors or the in situ removal of inhibitory AP (Section 3.5). Automation of the unit operations has enabled parallel and more detailed evaluation of reaction conditions than was possible with the manual methods. This has led to identification of one ω -TAm / amino donor combination that has increased rates and yields compared to the CV2025 ω -TAm. It has also demonstrated how the microscale methods can be used to optimise and reduce the costs of bioconversions such as those using co-factor recycling systems. In the next chapter, the important findings of this chapter will be validated at preparative scale.

6. PREPARATIVE SCALE

VERIFICATION OF MICROSCALE

BIOCONVERSION KINETICS

6.1. INTRODUCTION

As discussed in Section 1.5 microscale bioprocessing techniques can be used for to reduce costs and timescales of biocatalytic process development (Lye et al., 2003). Automation of these techniques can further accelerate the collection of bioconversion design data and the optimisation of reactions conditions (Chapter 5). However, one of the challenges of conducting early stage process studies at the microscale is the need for effectively translating the micro-scale process information into conventional laboratory or pilot plant scales (Zhang et al., 2008; Doig et al., 2002; Micheletti et al., 2006; Smith et al., 2010).

Experiments performed during early stage bioprocess development need to provide insights into the most suitable strategies for further process optimization and scale-up in order to maximize the yield of product on substrate and catalyst (Smith et al., 2010; Liddell, 2009). These issues are addressed in this final chapter. With the increase in scale reactions, conditions can frequently differ especially for industrial applications. Examples of changes include: use of more concentrated solutions to improve space-time yield, differences in mixing methods (overhead versus magnetic versus shaking), use of solvents that are more amenable to larger scale production and reductions in enzyme loading in order to improve process economics (Wells, 2006).

6.2. AIM AND OBJECTIVES

The automation studies in the previous chapter helped identify microscale reaction conditions that enabled a 40-fold reduction in the concentration of ADH used for AP by-product removal (Section 5.6.1) and identification of novel ω -TAM from *Bacillus subtilis* that had a high catalytic activity for transamination of Ery using L- α -Serine as amino donor (Section 5.5). The aim of this chapter is to validate these important findings at preparative scale. Validation of the microscale results is important to the capacity for microscale automation tools to speed up biocatalytic process development and design. The key objectives of this chapter are thus:

- To scale-up the CV2025 ω -TAM bioconversion using the optimised second enzyme reaction conditions and investigate the implementation of pH-stat control at the preparative scale.
- To validate the novel bioconversion kinetics with BSU09260_1971 ω -TAM from *Bacillus subtilis*, using L- α -serine as amino donor.
- To confirm ABT product synthesis from the above bioconversions using Mass spectrometry and bioconversions of L- α -serine and Ery perform using a null strain of *E.coli* BL21 (DE3) in clarified lysate form.

6.3. VERIFICATION OF OPTIMISED SECOND ENZYME REACTION CONDITIONS

In the preceding work, microscale experimentation have been presented to explore the second enzyme reaction first using manual methods (Section 4.5) and subsequently to optimise reaction conditions using parallel, automated experimentation (Section 5.6). Despite the considerable reduction in enzyme requirements, the microscale methods relied on high buffer concentrations for microwell pH control given the stoichiometric production of gluconic acid. Here, the preparative scale up of the optimised bioconversion conditions is presented using a 902 STAT Titrino pH controller device application (Section 2.5.2). This is important

for comparison and evaluation of the effectiveness of microscale reactions and also reduction of the amount of salts needed during the process in order to further minimize the production cost.

The second enzyme reaction (Figure 4.2) was scaled-up from 300 μL parallel microwell studies to a 30 mL working volume laboratory scale stirred bioreactor. This represents a 100-fold increase in volume. The optimization conditions for this reaction were described in Section 5.6.1, and consisted of 0.03 g.L^{-1} ADH from *Bacillus kefir*, 0.02 g.L^{-1} GDH and 50 mM Glucose. Further details of the preparative scale reaction conditions are displayed in Table 6.1. The transamination reaction was likewise performed using equimolar concentrations of MBA and Ery at 50 mM each, and the CV2025 ω -TAm concentration was fixed at 0.3 g.L^{-1} in clarified lysate form (Section 2.3.1).

Results from the preparative scale process are depicted in Figure 6.1. The temperature was kept constant at 30 $^{\circ}\text{C}$ using a circulating water bath in contrast to an “under plate” heated platform used for the microscale experiments (Chapters 4 and 5). Instead of orbital shaking, the preparative scale bioreactor was mixed with a magnetic stirring bar in order to maintain adequate mixing and mass transfer rates. Changes in pH, temperature, and NaOH volume addition were monitored online using Tiamo 2.2 Workplace software (Section 2.5.2).

Initial experiments performed the reaction in pure water but, due to the absence of any buffering capacity in the solution, it was difficult to maintain the pH at an optimal value of pH 7.5 (Section 3.4.3). In particular, it was hard to stabilize the pH at a desired value due to rapid pH fluctuation as soon as the reaction was started and gluconic acid was formed by the second enzyme system (Figure 4.2). Subsequently the pH-STAT experiments began with 50 mM HEPES buffer present which significantly improved the stability of pH control. The pH of the preparative scale bioconversion was maintained at 7.5 by the automated addition of 1.0 M NaOH in replacement of 1500 mM HEPES buffer used in the microscale reactions (Section 5.6.1).

Table 6.1. Comparison of reaction conditions used for preparative scale verification of bioconversion kinetics optimised at the microscale. Verification involved scale-up of the selected second enzyme reaction conditions and use of an alternative amino donor previously optimised in automated, microscale experiments (Sections 5.6.1 and 5.5) and repeated here at preparative scale (Section 6.3 and 6.4).

Bioconversion scale	Microscale	Preparative scale
Temperature (°C)	30	30
Temperature control	Under plate heated platform	Circulating water bath
Mixing Speed (rpm)	300	300
Mixing device	Orbital Shaking platform (diameter= 6 mm)	Magnetic stirrer
Working reaction volume	300 µL	30 mL
Working volume and vessel	550 µL glass microplate	50 mL glass stirred bioreactor
pH	7.5	7.5
Buffer	1500 mM HEPES buffer (Second Enzyme Reaction) 50 mM HEPES buffer (Alternative Amino Donors Reaction)	50 mM HEPES buffer
pH controller	-	pH stat with 1.0 M NaOH (aq)

In comparison to the microscale results in Section 5.6.1, the preparative scale reaction achieved a final ABT concentration of 27 mM, which represents a 26 % ($\text{mol}\cdot\text{mol}^{-1}$) decrease in reaction yield over 21 hours (Figure 6.1). A similar difference was seen in the initial rates of conversion respectively. This suggests that the CV2025 ω -TAm biocatalyst lost its activity more quickly in lysate form in the 30 mL bioreactor. This may be due to the use of the magnetic stirrer bar providing more vigorous mixing or the impact of the concentrated alkali additions used for pH control at the larger scale. Moreover, the discrepancies were further observed when the reaction was prolonged for another few hours. At the microlitre scale, the final conversion was constant at its optimum for the next few hours, whereas about 20 % ($\text{mol}\cdot\text{mol}^{-1}$) of the product was lost over a further 3 to 5 hours.

In the preparative bioconversion, AP was almost completely removed from the reaction solution unlike what had been observed earlier in the microscale reaction, where approximately 20 % ($\text{mol}\cdot\text{mol}^{-1}$) AP was left unconverted to 1-PE and remained in solution. In the preparative scale bioconversion, the greater removal of AP is thought to be attributed to evaporation. Unlike the microscale format, where the reaction plate was covered with either thermo plastic elastomer cap (Chapters 3 and 4) or pre-cut pierceable films (Chapter 5), the glass vessel of the preparative scale (Figure 2.2) was not well covered and allowed further AP evaporation as the reaction progress. This was further exaggerated due to the high liquid surface area to volume ratio in the glass vessel.

Therefore, it can be concluded that the slightly difference in the final yield was mainly attributed to either the transamination reaction mechanism or the differences of reaction conditions between scales. Microscale, preparative and process scale bioreactors can present differences in fluid dynamics, solvent evaporation, shear stress, mass and heat transfer phenomena, and the methods used for pH control. These can cause significant and often unpredictable discrepancies in the bioconversion behaviour at the different scales (Doig et al., 2002; Micheletti et al., 2006; Nealon et al., 2006; Matosevic et al., 2008).

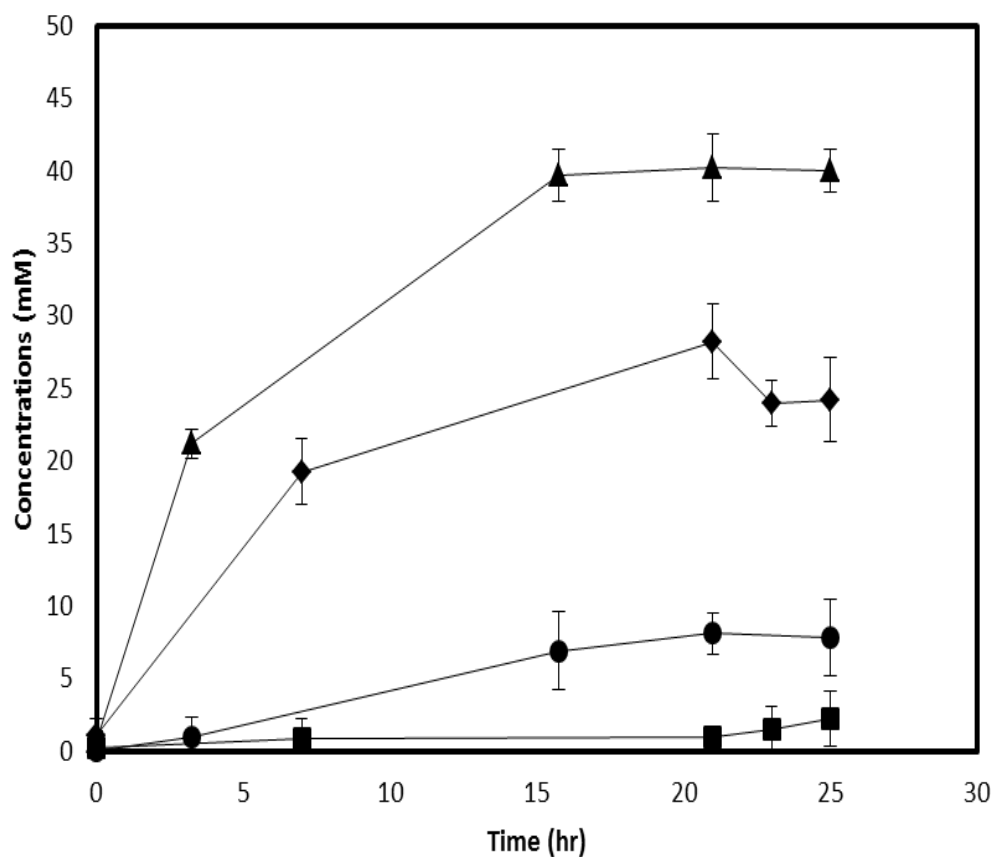


Figure 6.1. Comparison of preparative scale (Section 6.3) and automated microwell platform (Section 5.6.1) for bioconversion kinetics of CV2025 ω -TAM (pQR801) with second enzyme reaction using ADH from *Lactobacillus kefir*: ABT (\blacklozenge) AP (\blacksquare) productions of preparative scale and ABT (\blacktriangle) AP (\bullet) productions of automated microwell platform. Reaction conditions of preparative scale: 0.3 g.L⁻¹ CV2025 ω -TAM; 0.03 g.L⁻¹ ADH; 0.02 g.L⁻¹ GDH; 0.2 mM PLP; [MBA] and [Ery] were 50 mM; 50 mM Glucose; 1 mM NADPH; 30 °C; pH 7.5; 300 rpm in 50 mM HEPES buffer; total volume of 30 mL in the developed preparative scale bioreactor (Figure 2.2). Section Bioconversions performed as described in Sections 2.5.2. Reaction conditions of automated microwell platform as described in Figure 5.6. Error bars represent one standard deviation about the mean (n=3).

6.4. VERIFICATION OF THE USE OF ALTERNATIVE AMINO DONORS AND ω -TRANSAMINASES: L- α -SERINE AS AMINO DONOR

6.4.1. Transamination of Ery Using L- α -serine by BSU09260_1971 ω -TAm in Clarified Lysate Form

In Section 5.5, the automated microwell experiments allowed parallel evaluation of a library of novel ω -TAMs and led to the discovery that the BSU09260_1971 ω -TAM from *Bacillus subtilis* (pQR960) could catalyse Ery conversion using L- α -serine as amino donor and at a better rate than the more widely studied CV2025 ω -TAM. Here, the reaction kinetics will be verified at preparative scale, and the identity of the ABT product confirmed. The preparative scale reaction was performed using equimolar concentrations of L- α -serine and Ery of 50 mM (Figure 6.2). The BSU09260_1971 ω -TAM concentration was kept constant at 0.3 g.L⁻¹ in clarified lysate form. The preparative scale process reaction conditions and equipment setup are as depicted in Table 6.1 and Figure 2.2 (Section 2.5.2) respectively.

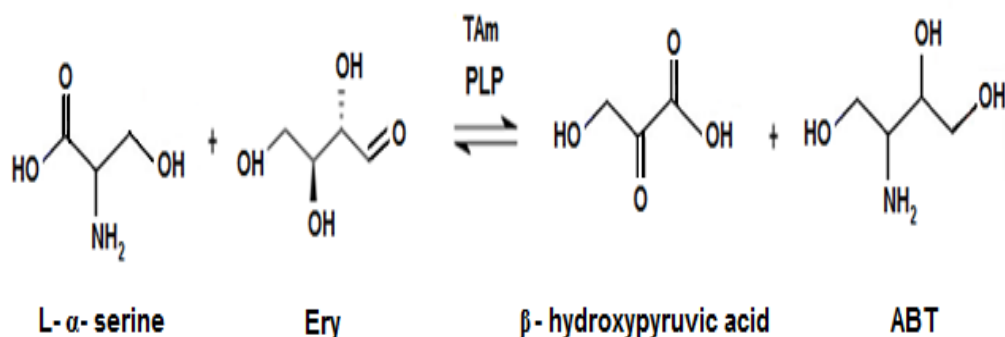


Figure 6.2. Reaction scheme of the BSU09260_1971 ω -TAM from *Bacillus subtilis* (pQR960) catalysed transamination between L- α -serine and L-erythrulose (Ery) to β -hydroxypyruvic acid and 2-amino-1,3,4-butanetriol (ABT) in the presence of co-factor pyridoxal-5-phosphate (PLP).

The BSU09260_1971 ω -TAM catalysed L- α -serine and Ery to by-product β -hydroxypyruvic acid and targeted product ABT showed similar reaction kinetics and conversions to the μ L scale format up to around 15 hours with optimum conversion of

42 % (mol.mol⁻¹) (Figure 6.3). At longer times, there was a rapid decrease in L- α -serine and ABT concentrations. However, the reaction rate in the bioreactor was relatively faster as the optimum yield was reached 6 hours earlier than the μ L scale reaction. This observation was consistent with the pH changes monitored online. The pH was maintained approximately constant over time at pH 7.5 as observed by the continuous addition of NaOH to the reaction solution. However, no addition of NaOH was observed 5 hours before it reached the optimum point. This indicates that the transamination rate was decelerating due, most likely, to decreases in the activity of the enzyme.

The degradation of the ABT product over prolonged reaction periods (> 5 hours) was again observed, as earlier detected in Section 6.3. Additionally a decrease of amino donor, L- α -serine was also observed. Prior the reaction termination, only about 6 mM of L- α -serine was quantified left in the reaction solution which may have led to the slightly lower ABT yield seen in the preparative scale bioconversion. The degradation of ABT and L- α -serine is again thought to be due to either NaOH concentration or competing reactions.

Serine is a non-essential amino acid that can be synthesized and degraded in cell metabolism for maintenance and utilization in several pathways of serine catabolism (Hama et al., 1988). Therefore, the serine consumption by side reactions using the clarified lysate is not unexpected. However, the disappearance of L- α -serine was greater than observed in the microscale reactions presented earlier in Chapters 4 and 5. Visual observations indicated that the reaction solution changed colour in the preparative scale bioconversion from an initial pale yellow, due to the presence of the co-factor PLP, into a bright yellow after 4 to 5 hours and finally a brownish colour at the termination point. This further suggests either non-specific side reactions using the lysate or degradation of the serine due to the NaOH used for pH control.

In practice, to overcome the side reactions of the L- α -serine, it is possible to perform the bioconversion with a higher concentration of amino acceptor instead of equimolar substrates. The CV2025 ω -TAm bioconversions of MBA and Ery as discussed in Chapter 4 shown that the 20 mM excess of amino acceptor did facilitate the acceleration of the initial reaction rate faster and consequently increased the reaction

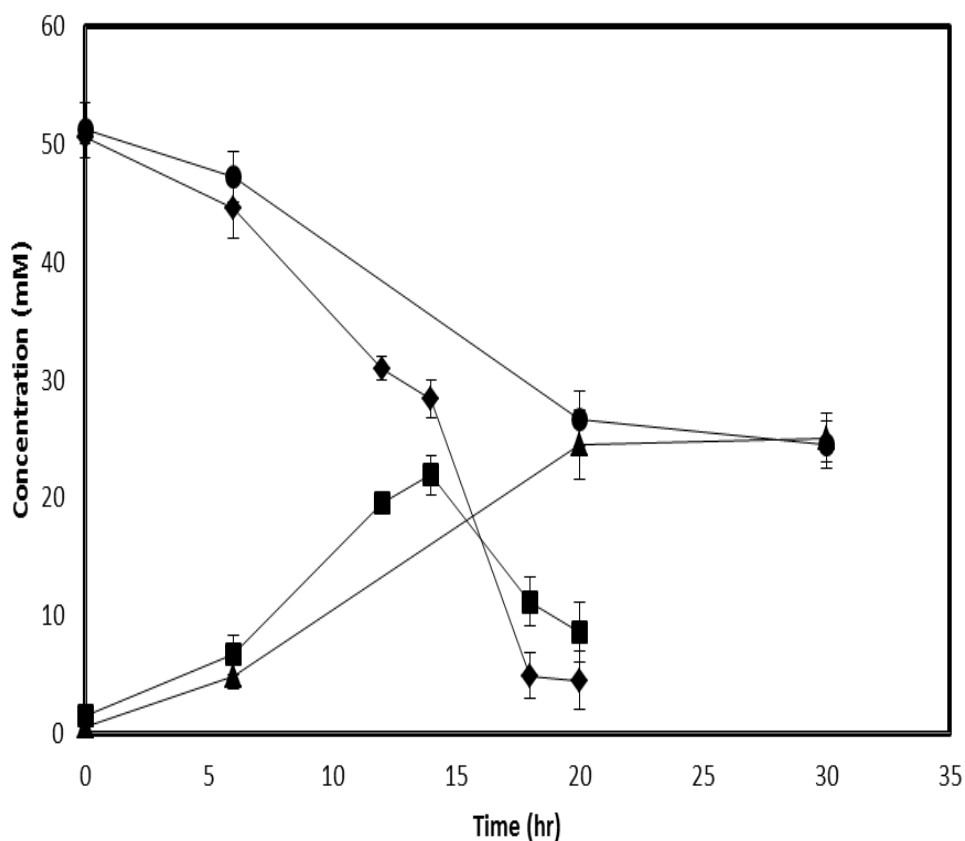


Figure 6.3. Comparison of preparative scale (Section 6.4.1) and automated microwell platform (Section 5.5) for bioconversion kinetics of BSU09260_1971 ω -TAM (pQR960) in clarified lysate form with *L*- α -serine as an alternative amino donor: *L*- α -serine consumptions (♦) ABT (■) productions for preparative scale and *L*- α -serine consumptions (●) ABT (▲) productions for automated microwell platform. Reaction conditions of preparative scale reactions: 0.3 g.L⁻¹ BSU09260_1971 ω -TAM clarified lysate; 0.2 mM PLP; [*L*- α -serine] and [Ery] were 50 mM; 30 °C; pH 7.5; 300 rpm in 50 mM HEPES buffer; total volume of 30 mL in the developed preparative scale bioreactor (Figure 2.2). Bioconversions performed as described in Sections 2.5.2. Reaction conditions of automated microwell platform as described in Figure 5.5. Error bars represent one standard deviation about the mean (n=3).

yield by additional of 20 % (mol.mol⁻¹). Previous reported work on the study of transamination also by CV2025 ω-TAm with varying substrate ratios of isopropylamine and 1,3-dihydroxypentan-2-one, also exposed an excess of 20 mM amine acceptor have driven the ω-TAm bioconversion yield give rise to an increase of 25 % (mol.mol⁻¹) targeted product (Smith et al., 2010).

6.4.2. Transamination of Ery Using L-α-serine by BSU09260_1971 ω-TAm in Purified Form

In order to prove that ABT synthesis from L-α-serine and Ery (Figure 6.3) was catalysed by the BSU09260_1971 ω-TAm from *Bacillus subtilis*, a preparative scale bioconversion was performed using purified enzyme. This would also enable a comparison of bioconversion kinetics between lysate and isolated enzyme forms. The BSU09260_1971 ω-TAm enzyme expressed from the pQR960 plasmid contains an N-terminal His-tag and hence was purified using a His- Select Nickel Affinity Gel as discussed in Section 2.3.2. Otherwise, bioconversion conditions and equipment setup were as previously depicted in Table 6.1 and Figure 2.2 (Section 2.5.2) respectively.

The concentrations of lysate and purified proteins were analysed by Bradford assay (Section 2.6.3). The total protein concentration of shake flask culture used in this study was 4.53 g.L⁻¹. The recombinant BSU09260_1971 ω-TAm migrated on an SDS-PAGE gel as a single band of approximately 50 kDa. The BSU09260_1971 ω-TAm was expressed at a significant level and ω-TAm concentrations in the lysate and purified preparations were 0.62 g.L⁻¹ and 0.5 g.L⁻¹ respectively as accessed by SDS-PAGE analysis (Figure 6.4).

As shown in Figure 6.5, the bioconversions with purified BSU09260_1971 ω-TAm revealed an almost 4-fold lower conversion rate than with the clarified lysate (Section 6.4.1). However, using the purified enzyme there is a stoichiometric relationship between L-α-serine utilisation and ABT formation as predicted by Figure 6.3. No additional decreases in substrate or product were observed during the course of reaction, owing to the elimination of unwanted side reactions by the use of purified enzyme.

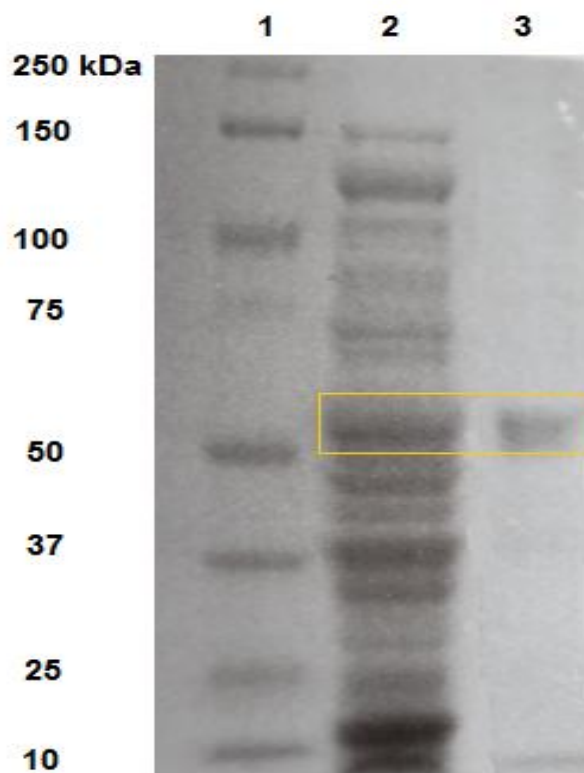


Figure 6.4. SDS-PAGE gel showing expression of the BSU09260_1971 ω -transaminase in cellular extracts of *E. coli* BL21 (DE3)-Gold cells. Lane 1 is the protein molecular weight marker, Lane 2 shows protein composition of lysate form, Lane 3 shows purified ω -TAm form. Molecular weight of BSU09260_1971 ω -TAm is approximately 50 kDa as highlighted in the box. Cells produced as described in Section 2.2.2 and ω -TAm purified as described in Section 2.3.2.

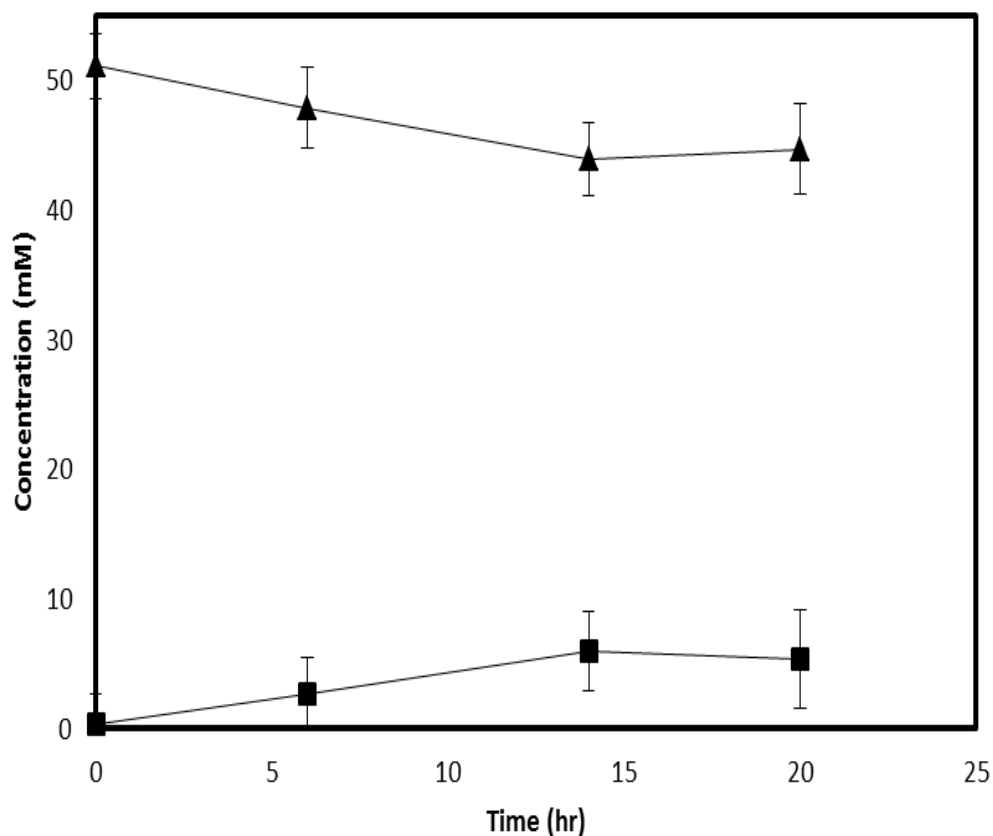


Figure 6.5. Preparative scale bioconversion kinetics of purified BSU09260_1971 ω -TAM (pQR960) using L- α -serine as amino donor: L- α -serine (▲) consumption and ABT (■) production. Reaction conditions: 0.3 g.L⁻¹ BSU09260_1971 ω -TAM in purified form; 0.2 mM PLP; [L- α -serine] and [Ery] were 50 mM; 30 °C; pH 7.5; 300 rpm in 50 mM HEPES buffer; total volume of 30 mL in the developed preparative scale bioreactor (Figure 2.2). Bioconversions performed as described in Sections 2.5.2. Error bars represent one standard deviation about the mean (n=3).

This confirms that one of the major factors for both substrate and product losses discussed in Sections 6.3 and 6.4.1, is due to the high susceptibility of the reagents to side reactions catalysed by other enzymes in the lysate. Furthermore, no colour changes were observed in the reaction solution with the purified enzyme which remained pale yellow throughout.

The low transamination rate of Ery using L- α -serine using purified BSU09260_1971 ω -TAm was most probably due to the low stability of the enzyme in purified form. Previous work with CV2025 ω -TAm reported a 50 % decrease of transamination rate over long reaction period of 70 hours that was mainly due to enzyme inactivation rather than unfavourable thermodynamic equilibrium (Ingram et al., 2007). To date few reports exist in the literature of ω -TAm used in purified form.

The structure of the closely related ω -amino acid pyruvate aminotransferase from *pseudomonas sp.* F-126 has been determined to be a tetramer comprised of two closely associated dimers (Watanabe et al., 1989). Ingram and co-workers (2007) also further suggested that the increased instability of purified β -alanine: pyruvate TAm from *pseudomonas aeruginosa* they used may probably due to the loss of the tetramic conformation during the purification step. Likewise, this could also be the same reason that has caused the instability and subsequently a remarkably low reactivity of the BSU09260_1971 ω -TAm.

6.5. CONFIRMATION OF ABT PRODUCT SYNTHESIS

The final objective of this work was to confirm the identity of the ABT product produced in the preparative scale bioconversions (Sections 6.3 and 6.4.1). ABT is not commercially available, therefore it was obtained by chemical and enzymatic syntheses as described in Sections 2.4.1 and 2.4.2. The ABT produced was derivatized by AQC reagent (Section 2.4.3) and then analysed by HPLC analysis (Section 2.6.6). The data obtained provided a calibration curve for ABT quantification from all bioconversions performed throughout the research. In order to confirm the identity of the ABT produced in the preparative scale bioconversions, it was purified and analysed by chemical ionization (CI) mass spectrometry (Section 2.6.7). The

fingerprints from the analysis can be found in Appendix V which confirms ABT synthesis.

In addition, bioconversions of L- α -serine and Ery at 50 mM were performed using a null strain of *E.coli* BL21 (DE3) in clarified lysate form as a control. The null strain was grown under sterile condition using LB media in shake flask scale as described in Section 2.2 without the addition of antibiotic kanamycin, IPTG or PLP. The bioconversion was performed as described in Section 2.5.2 using 0.3 g.L⁻¹ proteins in the clarified lysate form as quantified by Bradford assay (Section 2.6.3). HPLC analysis (Section 2.6.6) of the reaction samples obtained over extended time periods showed a detectable, but not quantifiable peak appearing at a retention time equivalent to ABT. This was most probably formed from naturally occurring transaminases present in *E.coli*. These results, therefore, confirm that the ABT synthesised in the reactions performed here was due to the activity of the heterologously expressed ω -transaminases.

6.6. SUMMARY

On the basis of the optimized process design information obtained at the microwell scale (Chapter 5), selected bioconversions were verified here at the preparative scale. This work involved a 100-fold increase in reaction scale.

The scale-up of CV2025 ω -TAm bioconversion using optimised conditions for use of the second enzyme system (Section 6.3) as a contrast to the microscale reaction (Section 5.6.1) shown 26 % (mol.mol⁻¹) declined in reaction conversion due to enzyme inactivation. Meanwhile, the transamination of Ery using L- α -serine by the novel BSU09260_1971 ω -TAm in lysate form (Section 6.4.1) was 21 mM ABT yield corresponding 42 % (mol.mol⁻¹) showed almost similar optimum yields and initial rates to the microscale reactions described in Section 5.5. The identity of the ABT product formed in the preparative scale bioconversions was confirmed by mass spectrometry and bioconversions of L- α -serine and Ery performed using a null strain of *E.coli* BL21 (DE3).

Overall these results show that optimised conditions from microscale experiments can be rapidly repeated at preparative scales. Small differences in the rates and yields measured can be attributed to changes in bioreactor design and reaction conditions, that will help guide further process optimisation and scale-up. The automated microwell scale platform developed here, therefore, provides a useful tool for the quantitative evaluation of larger numbers of biocatalyst and bioprocess options for enhancing the yields of equilibrium controlled bioconversions.

7. CONCLUSIONS AND FUTURE WORK

7.1. SUMMARY OF PROJECT ACHIEVEMENTS

In this thesis, a series of four microscale methodologies have been created to study process options for increasing the yield of equilibrium-controlled and product inhibited bioconversions with a particular emphasis on transaminase catalysed processes. The methods involved evaluation of alternative amino donors and selective removal of inhibitory by-products by either in-situ enzymatic conversion to non-inhibitory compounds, continuous evaporation of volatile by-products or adsorption of inhibitory by-products onto polymeric resins. These methods were created specifically for micro-scale and parallel operation (Chapters 3 and 4) and were capable of automation on a robotic system (Chapter 5) to facilitate parallel, high throughput evaluation and ultimately process design and optimization.

The first approach involving evaluation of alternative amino donors proved to be the simplest and most rapid to implement. Evaluation of a range of five alternative donors to the commonly used MBA, helped identify isopropylamine as a cheaper, less inhibitory donor of the CV2025 ω -TAm. For the transamination of Ery using isopropylamine, an almost 3-fold higher conversion yield than with the standard MBA was realised (Section 4.4). Automation of this approach allowed the simultaneous evaluation of a library of ten novel ω -TAm from various strains each with five alternative amino donors. The results of this worked showed that the CV2025 ω -TAm remains one of the most promising biocatalyst for optically pure amine synthesis (Figure 5.5). The results also led to the discovery of a novel ω -TAm from *Bacillus*

subtilis capable of the effective transamination of Ery using L- α -Serine as amino donor with a 23 % (mol.mol⁻¹) improvement on the conversion yield with CV2025 ω -TAm (Section 5.5).

The second approach involved a second enzyme system coupling *in-situ* the CV2025 ω -TAm bioconversion with ADH from *Lactococcus kefir* and GDH from *Pseudomonas sp.* for the rapid enzymatic conversion of the inhibitory AP by-product (Figure 4.2) to the non-inhibitory (R)-1-phenylethanol. These bioconversions showed the highest product yield of 86 % (mol.mol⁻¹), more than with any of the other CV2025 ω -TAm bioconversions using the alternative process options (Section 4.5). Despite the largest increase in conversion yield, the second enzyme method is regarded as the most complicated and expensive to implement due to the cost of the available coupling enzymes and the need to match their activities. These issues were later resolved by further optimization studies using the automated experimental approach that allowed reaction kinetics to be evaluated over a wide range of enzyme and reactant concentrations (Section 5.6). Equivalent product yields were reached with a 40-fold decrease in the concentration of ADH and a 20 mM decrease in glucose. The optimised method hence represents a more cost effective option, and it was rapidly established from the automated and parallel experimentation.

The third approach was the reduced pressure method that used a commercially available 96-well plate vacuum manifold and vacuum pump for established reduced pressure operating conditions. This is a simple and efficient approach for overcoming inhibition and suppresses the unfavourable equilibrium constant caused by compounds that are more volatile than others reactants and the desired product. This method demonstrated a 2.2-fold increase of yield of the standard CV2025 ω -TAm reaction (Section 4.6). This approach could also be automated using the vacuum manifold (Te-VacS) controlled by the Tecan Gemini software as detailed in Section 5.7. The current absence of temperature control on the automation platform meant that the same increases in yield could not be attained during automated operation, but the principle of the method was still successfully demonstrated.

The fourth approach involved ISPR using adsorbent resins to selectively bind the by-product AP to alleviate inhibition effects and shift the reaction equilibrium. Three

commercially available synthetic polymeric resins called Amberlite™ XADs (XAD 7, XAD 1180, XAD 16) were evaluated. This method however, was only shown to be applicable for whole-cell ω-TAm bioconversion since in lysate form, the enzyme and co-factor PLP were absorbed onto resins. Nevertheless a 1.3-fold higher yield was obtained than with the standard CV2025 ω-TAm whole cell bioconversion (Section 4.7).

Finally, the optimised microscale reaction conditions involving the second enzyme reaction and use of the BSU09260_1971 ω-TAm from *Bacillus subtilis* for the bioconversion of L-α-serine and Ery were each scaled-up 100-fold for preparative scale investigations in a pH-stat. Both systems performed similarly at the larger scale although differences in mixing and the use of concentrated NaOH for pH control led to decreases in the rates and yields observed. For example, with the second enzyme reaction (Section 6.3) employing a 40-fold decrease in ADH concentration a 26 % (mol.mol⁻¹) decline in the yield of conversion was measured compared to the microscale results (Section 5.6.1). Likewise, for the transamination of Ery using L-α-serine by the novel BSU09260_1971 ω-TAm in lysate form (Section 6.4.1) there was a decrease in reaction yield by just 10 % (mol.mol⁻¹). Nevertheless, these scale-up studies confirmed the utility of the microscale techniques for rapid identification of optimised process conditions applicable to at least preparative scale.

In general, the best process option will depend on particular reaction being studied and the economical advantage. If the cost issue is addressed particularly on the main additional cost of material involved for each process option, the use of alternative amino donors is likely to be the best in terms of ease and cost (i.e isopropylamine is available at only £ 0.02 per mL). The reduced pressure system is an efficient and low cost method but only applicable when having high volatilities by-product. Meanwhile, the ISPR adsorption resin application is also a cost effective process option (amberlite XAD resin is available at £0.02 per 100 mg) but in this case a further study is required for significant yield improvement. Despite have shown the best result, the second enzyme system is the most costly option due to the expensive additional enzymes (ADH is available at £ 1.16 per mg and GDH is £ 9.11 per mg) and co-factor (NADPH is available at £100 per mg) involved and thus will significantly have further economic impact at large scale.

Overall, this work has demonstrated the potential of different process options to shift unfavourable reaction equilibrium toward product formation and to overcome issues of product inhibition. The research described here shows that microscale methods can be used to rapidly and effectively explore these process options using minimum quantities of material. Such approaches can be integrated on commercially available automation platforms for high throughput evaluation of different biocatalyst-bioprocess options and the rapid optimisation of selected bioprocess conditions.

7.2. FUTURE WORK

Whilst the overall aim of this project was achieved, future work is required to expand these micro-scale methods to further increase reaction yields, and to enable better integration of these approaches with whole bioprocess studies and emerging high-throughput analytical techniques. A detailed list of future work recommendations is given below.

- For the second enzyme method, at least 80 % ($\text{mol}\cdot\text{mol}^{-1}$) conversion using a considerably reduced enzyme loading than was typically applied (Sections 4.5 and 5.6) have been able to reach. However, for further system optimisation particularly from an economic point of view, an alternative way is to construct a recombinant *E.coli*, having all three heterologous genes of ω -TAm (Kahulmann et al., 2007; Shin and Kim, 2001), alcohol dehydrogenase (Chen, et al., 2008) and glucose dehydrogenase (Galkin et al., 1997) expressed.
- Future studies are necessary to identify the crucial parameters that may affect the performance of the ISPR adsorbent resins in order to achieve higher bioconversion rates and yields. Studies could be performed with a wider range of adsorbent resins or new ones could be synthesised with the required binding selectivity.
- Automation of the ISPR experiments using adsorptive resins at 300 μL scale could be further developed. Full automation of the method is challenging

owing to unavailability of device for automatically weighing and transferring the small quantities of resin needed for study (Section 4.7). Development of such a device would be important in order to carry this aspect of the work forward.

- An excess of amino acceptor substrate has been proven in literature to accelerate the initial reaction rate and yield (Sections 4.5 and 4.6). Such an approach could be further exploited by fed batch operation which it should be possible to implement on the automation platform.
- The key parameters affecting scale up of the bioconversion to the preparative scale using the second enzyme method and alternative amino donor method were established in Sections 6.3 and 6.4. Future scale-up studies are necessary in order to get better quantitative agreement between the rates and yields achieved at the two different scales. Further scale-up to the >10L scale should also be investigated.
- As was found in Section 6.4.2, the ω -TAm loss its activity and stability in the purified form. Further studies should be performed in immobilization techniques to improve the stability of the enzyme, while adding the benefit of allowing the enzyme to be recycled and used in a continuous flow bioprocess.
- Finally, it would be beneficial to demonstrate ‘whole process’ automation linking sequences of individual unit operations including micro-well fermentation, induction, bioconversion, product recovery and analysis on a single robotic platform. These would enable the full potential of the high-throughput nature of this work to be explored, for example, for studies on the interaction between fermentation and bioconversion conditions and for evaluation of larger biocatalyst libraries.

8. REFERENCES

- Adamo, M.F.A., Aggarwal, V.K., Sage, M.A.** (2000). Epoxidation of alkenes by amine catalyst precursors: Implication of aminium ion and radical cation intermediates, *J Am Chem Soc.*, **122**, 8317-8318.
- Ager, D.J., Li, T., Pantaleone, D.P., Senkpeil R.F., Taylor, P.P., Fotheringham, I.G.** (2001). Novel biosynthetic routes to non-proteinogenic amino acids as chiral pharmaceutical intermediates, *J Mol Catal B Enzym*, **11**, 199–205.
- Anderlei, T., Zang, W., Papaspyrou m., B'uchs, J.** (2004). Online respiration activity measurement (OTR, CTR, RQ) in shake flasks, *Biochem. Eng. J.*, **17**, 187–194.
- Bajusz, S., Szell, E., Bagdy, D., Barabas, E., Horvath, G., Dioszegi, M., Fittler, Z., Szabo, G., Juhasz, A.** (1990). Highly Active and Selective Anticoagulants: D-Phe-Pro-Arg-H, a Free Tripeptide Aldehyde Prone to Spontaneous inactivation, and Its Stable N-Methyl Derivative, D-Me-Phe-Pro-Arg-H., *J Med Chem*, **33**, 1729-1735.
- Barrett, T. A., Wu, A., Zhang, H., Levy, M. S., and Lye, G. J.** (2010). Microwell engineering characterization for mammalian cell culture process development. *Biotechnology and bioengineering*, **105**, 260-75.
- Bastida, A., Sabuquillo, P., Armisén, P., Fernández-Lafuente, R., Huguet, J., and Guisán, J. M.** (1998). A single step purification, immobilization and hyperactivation of lipases via interfacial adsorption on strongly hydrophobic supports. *Biotechnol. Bioeng.* **58**, 486-493
- Benevides C. C. Pessela, Vian, A., Mateo, C., Fernández-Lafuente, R., García J. S., Guisán, J. M., and Carrascosa, A. V.** (2003). Overproduction of *Thermus* sp. Strain T2 β -Galactosidase in *Escherichia coli* and Preparation by Using Tailor-Made Metal Chelate Supports, *Appl. Environ. Microbiol.* vol. **69** no. **4**, 1967-1972.

- Berger, M., Albrecht, B., Breces, A., Neruda, W. & Woisetschläger, M.** (2001). *S(+)-4-(1-Phenyl-ethylamino)quinazolines as Inhibitors of Human Immunoglobulin E Synthesis: Potency is dictated by stereochemistry and atomic point charges at N-1*, *J. Med. Chem.*, **44**, 3031.
- Blaser, U. H., Schmidt, E., Eds.** (2003). *Asymmetric catalysis on industrial scale: challenges, approaches and solutions*, Wiley-VCH: Weinheim.
- Bradford, M. M.** (1976). A rapid and sensitive method for the quantitation of microgram quantities of protein utilizing the principle of protein-dye binding. *Analytical Biochemistry*, **72**, 248-54.
- Bradshaw, C.W., Hummel, W., Wong, C-H.** (1992) *Lactobacillus kefir ADH: a useful catalyst for synthesis*, *J. Org. Chem.*, **57**, 1532-1536.
- Brands, K. M. J., Payack, J. F., Rosen, J. D., Nelson, T. D., Candelario, A., Huffman, M. A., Zhao, M. M., Li, J., Craig, B., Song, Z. J., Tschaen, D. M., Hansen, K., Devine, P. N., Pye, P. J., Rossen, K., Dormer, P. G., Reamer, R. A., Welch, C. J., Mathre, D. J., Tsou, N., McNamara, J. M., Reider, P. J.** (2003). Efficient synthesis of NK1 receptor antagonist Aprepitant using a crystallisation-induced diastereoselective transformation. *J. Am. Chem. Soc.*, **125**, 2129–2135.
- Breuer, M., Ditrich, K., Habicher, T., Hauer, B., Kessler, M., Stürmer, R., Zelinsky, T.** (2004). Industrial methods for the production of optically active intermediates. *Angew Chem Int Ed*, **43**, 788–824.
- Britsch, L., Schroeder, T., Friedle, J.** (2008). Automated, High-Throughput Chromatographic Separation of Biological Compounds, *American Biotechnology Laboratory*, Volume **26**, Number 6.
- Buchholz, K., Kasche, V., Bornscheuer, U. T.** (2005). *Biocatalysts and Enzyme Technology*, WILEY-VCH Verlag GmbH & Co. KGaA, Weinheim (Introduction to Enzyme Technology).
- Buckland, B.C., Drew, S. W., Connors, N. C., Chartrain, M. M., Lee, C., Salmon, P. M., Gbewonyo, K., Zhou, W., Gailliot, P., Singhvi, R., Olewinski Jr., R. C., Sun, W-J., Reddy, J., Zhang, J., Jackey, B. A., Taylor, C., Goklen, K. E., Junker, B., Greasham, R. L.** (1999). Microbial conversion of indene to indandiol a key intermediate in the synthesis of Crixivan. *Metab. Eng.*, **1**, 63–74.

- Caner, H., Groner, E., Levy, L.** (2004). Trends in the development of chiral drugs, *Drug Discovery Today*, Volume 9, Issue 3, 105-110.
- Cao, E., Chen, Y., Cui, Z., Foster P. R.** (2003). Effect of freezing and thawing rates on denaturation of proteins in aqueous solutions, *Biotechnology and Bioengineering*, Volume 82, Issue 6, pages 684–690.
- Chan, A. C. S.** (1993). A new route to important chiral drugs, *Chemtech*, 23, 46-51.
- Chartrain, M., Starr, M.** (2004). Fungal bioconversions: applications to the manufacture of pharmaceuticals. In *Handbook of Industrial Mycology*; An, Z., Ed., Maecel Dekker: New York, 563-595.
- Chen, B. H., Hibbert, E. G., Dalby, P. A., Woodley. J. W.** (2008). A new approach to bioconversion reaction kinetic parameter identification, *AIChE Journal*, Wiley Online Library, 54, 2155–2163.
- Christen, P., Metzler, D.E.** (1985). *Transaminases*. New York, NY: Wiley.
- Crowe, J., Döbeli, H., Gentz, R., Hochuli, E., Stuber, D., Henco, K.** (1994). 6xHis-Ni-NTA chromatography as a superior technique in recombinant protein expression/purification. *Methods Mol. Biol.*, 31, 371-387.
- Cohen, S.,A., Michaud, D.P.** (1993). Synthesis of a fluorescent derivatizing reagent, 6-aminoquinolyl-N-hydroxysuccinimidyl carbamate, and its application for the analysis of hydrolysate amino acids via high performance liquid chromatography, *Anal Biochem*, 211, 279-287.
- Daniel, R., Griffin, Yang, F., Carta, G., Gainer, J. L.** (1998). Asymmetric reduction of acetophenones with-Calcium-Alginate-Entrapped Baker's Yeast in organic solvent, *Biotechnol. Prog.*, 14, 588-593.
- DeSantis,G., Wong, K., B., Farwell, Chatman, K., Zhu, Z., G.,Tomlinson, Huang, H., Tan, X., Bibbs, L., Chen, P., Kretz, K., Burk, M. J.** (2003). Creation of a productive, highly enantioselective nitrilase through gene site saturation mutagenesis (GSSM). *J. Am. Chem. Soc.*, 125, 11476–11477.
- De Vroom, E.** (1999). The Central Role of Penicillin Acylase in Antibiotics Production, *Chim. Oggi.*, 17, 65-68.
- DeRoode, B. M., Van Beek, J., Van Der Padt, A., Franssen, M.C.R., Boom, R.M.** (2001). The integrated Enzymatic Production and Downstream Processing of Hexyl Glucoside, *Enz. Microb. Tech.*, 29, 513-520.

- Doig, S. D., Pickering, S. C. R., Lye, G. J., Woodley, J. M.** (2002). The use of microscale processing technologies for quantification of biocatalytic Baeyer-Villiger oxidation kinetics, *Biotechnol. Bioeng.*, **80**, 42–49.
- Draths, K. M., Pompliano, D. L., Conley, D. L., Frost, J. W., Berry, A., Disbrow, G. L., Staversky, R. J. and Lievens, J. C.** (1992). Biocatalytic Synthesis of Aromatics From D-Glucose: the Role of Transketolase, *Journal of the American Chemical Society* **114**, 3956-3962.
- Du, X., Yuan, Q., Li, Y., Zhou, H.** (2008). Preparative purification of solanesol from tobacco leaf extracts by macroporous resins, *Chem. Eng. Technol*, **31**, No. 1, 87-94.
- Duetz, W. A., Witholt, B.** (2001). Effectiveness of orbital shaking for the aeration of suspended bacterial cultures in square-deepwell microtiter plates, *Biochem. Eng. J.*, **7**, 113–115.
- Elmahdi, I., Baganz, F., Dixon, K., Harrop, T., Sugden, D., Lye, G. J.** (2003). Ph control in microwell fermentations of *S. erythraea* CA340: influence on biomass growth kinetics and erythromycin biosynthesis, *Biochem. Eng. J.*, **16**, 299–310.
- Esabi, B., Kurbanoglu, Zilbeyaz K., Ozdal, M., Taskin, M., Kurbanoglu, N. I.** (2010). Asymmetric reduction of substituted acetophenones using once immobilized *Rhodotorula glutinis* cells, *Bioresource Technology*, **101**, 3825–3829.
- Faber, K.** (2004). *Biotransformations in organic chemistry*, Berlin Heidelberg: Springer- Verlag.
- FDA.** (1992). FDA's Policy Statement for the Development of New Stereoisomeric Drugs, [Http://Www.FDA.Gov/Cder/Guidance/Stereo.Htm](http://www.fda.gov/cder/guidance/stereo.htm).
- Ferreira Vaz, M. R., Soares de França, R. L., Lessa de Andrade, S. S., Sousa Junior, F. C., Santos E. S., Arantes Martins D. R.,; Ribeiro de Macedo, G.** (2011). Influence of culture medium on the production of eif antigen from *Leishmania chagasi* in recombinant *Escherichia coli*, *Braz. J. Microbiol.* vol. **42**, no.4.
- Fischer, R., Hennig, M., Mair, H-J., Oberhauser, T., Rimmler, G., Albiez, T., Bruhin, J., Estermann, H., Gandert, C., Göckel, V., Götzö, S., Hoffmann, U., Huber, G., Janatsch, G., Lauper, S., Röckel-Stäbler, O., Trussardi, R., Zwahlen, A. G.** (1999). Industrial synthesis of the key precursor in the

synthesis of the anti-influenza drug Oseltamivir Phosphate (Ro 64- 0796/002, GS-4104-02): ethyl (3R,4S,5S)-4,5-epoxy-3-(1-ethyl-propoxy)-1-cyclohexene-1-carboxylate. *Org. Proc. Res. Dev.* **3**, 266–274.

Ferreira-Torres, C., Micheletti, M., Lye, G. J., (2005). Microscale process evaluation of recombinant biocatalyst libraries: application to Bayer-Villiger monooxygenase catalysed lactone synthesis, *Bioprocess Biosyst Eng*, **28**, 83-93.

Fernandes, P. (2010). Minutization of biocatalyst, *Int. J. Mol. Sci.*, **11**, 858-879.

Galkin, A., Kulakova L., Yoshimura, T., Soda, K., Esaki, N., (1997). Synthesis of optically active amino acids from alpha-keto acids with *Escherichia coli* cells expressing heterologous genes, *Appl. Environ. Microbiol.*, **63**, 4651-4656.

Gawronski, J., (2006). Asymmetric syntheses and transformations--tools for chirality multiplication in drug synthesis, *Acta Pol Pharm*, **63**, 5, 333-51.

Ghisalba, O., Meyer, H-P., Wohlgemuth, R. (2010). Industrial Biotransformation, *Encyclopedia of Industrial Biotechnology: Bioprocess, Bioseparation, and Cell Technology*, edited by Michael C. Flickinger, John Wiley & Sons, Inc.

Gill, N. K., Appleton, M., Baganaz, F., Lye, G. J. (2008). Design and characterisation of a parallel miniature bioreactor system for rapid fermentation process operation, *Biochem. Eng. J.*, Volume **39**, Issue 1, 164-176.

Gardner, C. R., Almarsson, O., Chen, H. M., Morissette, S., Peterson, M., Zhang, Z., Wang, S., Lemmo, A., Gonzales-Zugasti, J., Monagle, J., Marchionna, J., Ellis, S., McNulty, C., Johnson, A., Levinson, D., Cima, M. (2004). Application of high throughput technologies to drug substance and drug product development, *Comp. Chem. Eng.*, **28**, 6-67, 943-953.

Greenberg, W. A., Varvak, A., Hanson, S. R., Wong, K., Huang, H., Chen, P., Burk, M. J., (2004). Development of an efficient, scaleablaldolase-catalyzed process for enantioselective synthesis of statin intermediates. *Proc. Natl. Acad. Sci. U. S. A.* **101**, 5788–5793.

Greingl, H., Klempier, N., Pochlauer, P., Schmidt, M., Shi, N.Y., Zabelinskakamackova, A.A. (1998). Enzyme Catalysed formation of (S)-Cyanohydrins Derived From Aldehydes and Ketones in a Biphasic Solvent System, *Tetrahedron*, **54** 14477-14486.

- Guo, J. and Frost, J.W.** (2004). Synthesis of aminoshikimic acid. *Org. Lett.* **6**, 1585–1588.
- Guo, J. L., Mu, X-Q., Xu, Y.** (2009a). Integration of newly isolated biocatalyst and resin-based in situ product removal technique for the asymmetric synthesis of (R)-methyl mandelate, *Bioprocess Biosyst Eng*, **33**, **7**, 797-804.
- Guo, J., Mu, X., Zheng, C., Xu, Y.** (2009b). A highly stable whole-cell biocatalyst for the enantioselective synthesis of optically active alpha-hydroxy acids; of *Chemical Technology and Biotechnology*, Volume **84**, Issue 12, 1787–1792.
- Gutman, A. L, Meyer, E, Kalerin, E., Polyak, F., Sterling, J.** (1992). Enzymatic resolution of racemic amines in a continuous reactor in organic solvents, *Biotechnol Bioeng*, **40**, 760-767.
- Hama, H., Shimamoto, T., Tsuda, M., Tsuchiya, T.** (1988). Characterization of a Novel L-Serine Transport System in *Escherichia coli*, *Journal of Biotechnology*, Vol. **170**, No. 5, 2236-2239.
- Hanson, R. L., Davis, B. L., Chen, Y., Goldberg, S. L., Parker, W. L., Tully, T. P., Montana, M. A., Patel, R. N.** (2008). Preparation of (R)-amines from racemic amines with an (S)-amine transaminase from *Bacillus megaterium*, *Adv Synth Catal*, **350**, 1367–1375.
- Hatch, S.D., Khalil, D.A., Kosa, M.B., Lubbehusen, P.P., Muesing, M.A., Patick, A.K., Reich, S.H., Su, K.S., Tatlock, J.H.** (1997). Viracept (Nefinavir Mesylate, Ag1343): A Potent, Orally Available inhibitor of HIV-1 Protease, *J.Med.Chem.* **40**, 3979-3985.
- Held, M., Schmid, A., van Beilen, J. B., Witholt, B.** (2000). Biological systems for the production of chemicals, *Pure Appl. Chem.*, Vol. **72**, No. 7, 1337–1343.
- Heijbel.** (2003). Purification of a protein tagged with (His)₆ at its N-terminus, C-terminus, and both N- and C-termini using different metal ions, *Life Science News* **15**, Amersham Biosciences.
- Henderson, K. W., Kerr, W. J., Moir, J. H.** (2000), Enantioselective Deprotonation Reactions Using a Novel Homochiral Magnesium Amide Base *Chem Commun*, 479-480.
- Hierro, A., Rojas, A. L., Rojas, R., Murthy, N., Effantin, G., Kajava, A. V., Steven, A. C., Bonifacino, J. S., Hurley, J. H.** (2007). Functional architecture of the retromer cargo-recognition complex, *Nature*, **449**, 1063-106.

- Hohne, M., Kuhl, S., Robins, K., Bornscheuer, U. T.** (2008). Efficient Asymmetric Synthesis of Chiral Amines by Combining Transaminase and Pyruvate Decarboxylase, *Chem BioChem*, **9**, 363.
- Hwang, B.-Y., Cho, B. K., Yun, H., Koteswar, K., Kim, B. G.** (2005). Revisit of aminotransferase in the genomic era and its application to biocatalysis, *J Mol Catal B EnzymE*, **37**, 47–55.
- Hwang, B.-Y., Kim, B. G.** (2004). High-throughput screening method for the identification of active and enantioselective ω -transaminases, *Enzyme and Microbial Technology*, **34**, 429-436.
- Hummel W.** (1999). Large-scale applications of NAD(P)-dependent oxidoreductase: recent developments, *Trends Biotechnol*, **17**, 487-492
- Hummel, W.,** (1990). Enzyme-catalysed synthesis of optically pure R (+)-phenylethanol, *Biotechnology Letters*, Vol **12**, No. **6**, 403-408.
- Illanes, A.** (2008). *Enzyme biocatalysis: principles and applications*, Springer Science + Business Media B.V.
- Ingram, C.U., Bommer, M., Smitch, M. E., Dalby, P. A., Ward, J. M., Hailes, H. C., Lye, G. L.** (2007). One-pot synthesis of amino alcohols using a de-novo transketolase and β -Alanine:Pyruvate Transaminase pathway in *Escherichia coli*, *Biotechnol Bioeng*, **96**, 559-569.
- Ingram, C.U.** (2007b). Biocatalytic synthesis of amino-alcohols using a *de novo* designed transketolase- β -Alanine: pyruvate transaminase pathway in *escherichia coli*, PhD Thesis, University College London.
- Islam, R. S., Tisi, D., Levy, M. S., Lye, G. J.** (2008). Scale-up of *Escherichia coli* growth and recombinant protein expression conditions from microwell to laboratory and pilot scale based on matched $k(L)a$. *Biotechnology and bioengineering*, **99**, 1128-39.
- Jackson, M. A, Labeda, D. P., Becker, L. A.** (1995). Enantioselective hydrolysis of ethyl 2-hydroxyalkanoates by an extracellular esterase from a *Bacillus sphaericus* strain, *Enzyme Microb. Technol.*, **17**, 175-179.
- Jackson, N. B., Liddell, J. M., Lye, G. J.** (2006). An automated microscale technique for the quantitative and parallel analysis of microfiltration operations, *Journal of Membrane Science*, **276**, 31–41.

- Jacques, J., Collett, A., Wilen, S.** (1980). *Enantiomers, Racemates and Resolutions*, New York.
- Jankowski, M. D., Henry, C. S., Broadbelt, L. J., Hatzimanikatis, V.** (2008). Group contribution method for thermodynamic analysis of complex metabolic networks. *Biophys J*, **95**, 1487–1499.
- Jauregi, P., Gilmour, S., Varley, J.** (1997). Characterisation of colloidal gas aphrons for subsequent use for protein recovery, *Chem Eng J.*, **65**, 1-11.
- Jauregi, P., Varley, J.** (1998). Colloidal Gas Aphrons: A novel approach to protein recovery. *Biotechnol Bioeng*, **59**, 471-48.
- Jeong, S., Hwang, B.-Y., Kim, J., Kim, B.-G.** (2000). Lipase-Catalysed Reaction in the Packed Bed Reactor with Continuous Extraction Column to Overcome a Product inhibition, *Journal of Molecular Catalysis B: Enzymatic*, **10**, 597-604.
- Johannes, T. W., Zhao, H.** (2006). Directed evolution of enzymes and biosynthetic pathways, *Curr. Opin. Microbiol.*, **9**, 261-267.
- John, G. T., Klimant, I., Wittmann, C., Heinzle, E.** (2003). Integrated optical sensing of dissolved oxygen in microtitre plates: a novel tool for microbial cultivation, *Biotechnol. Bioeng.*, **81**, 7, 829–836.
- Kaiser, P. M.** (1980). Substrate inhibition as a problem of non-linear steady state kinetics with monomeric enzymes, *J. Mol. Catal.*, **8**, 431-442.
- Kaldor, W. K., Kalish, V.J., Davies, J.F., Shetty, B.V., Fritz, J.E., Appelt, K., Burgess, J.A., Campanale, K.M., Chirgadze, N.Y., Clawson, D.K., Dressman, B.A., Hatch, S.D., Khalil, D.A., Kosa, M.B., Lubbehusen, P.P., Muesing, M.A., Patick, A.K., Reich, S.H., Su, K.S., Tatlock, J.H.** (1997). Viracept (Nefinavir Mesylate, Ag1343): A Potent, Orally Available inhibitor of HIV-1 Protease, *J.Med.Chem.*, **40**, 3979-3985.
- Kaulmann, U., Smithies, K., Smith, M. E. B., Hailes, H. C., Ward, J. M.** (2007). Substrate spectrum of ω -transaminase from chromobacterium violaceum DSM30191 and its potential for biocatalysis, *Enzyme Microb. Technol.*, **41**, 628-637.
- Kelley, M. T., Walson, P. D., Edge, J. H., Cox, S. Mortensen, M. E.** (1992). Pharmacokinetics and Pharmacodynamics of Ibuprofen Isomers and Acetaminophen in Febrile Children, *Clin Pharmacol Ther*, **52**, 181-189.

- Kempf, D. J., Codacovi, L. M., Norbeck, D. W., and Plattner, J. J.** (1991). Retroviral Protease inhibiting Compounds, 5,354,866, Usa.
- Kizaki, N., Yasohara, Y., Hasegawa, J., Wada, M., Kataoka, M., Shimizu, S.** (2001) Synthesis of optically active ethyl 4-chloro-3-hydroxybutanoate by *Escherichia coli* transformant cells coexpressing the carbonylreductase and glucose dehydrogenase genes. *Appl. Microbiol. Biotechnol.*, **55**, 5, 590–595.
- Kim, K. H.** (1964). Purification and properties of a diamine alpha-ketoglutarate transaminase from *Escherichia coli*, *J Biol Chem*, **6**, 239, 783-786.
- Klibanov, A. M.** (1990). Asymmetric transformation catalysed by enzymes in organic solvents, *Acc. Chem. Res.*, **23**, 114.
- Koeller, K. M., Wong, C. H.** (2001). Enzyme for chemical synthesis, *Nature*, **409**, 232-240.
- Koszelewski, D., Tauber, K., Faber, K., Kroutil, W.** (2010). α -Transaminases for the synthesis of non-racemic α -chiral primary amines, *Trends in Biotechnology*, **28**, 324–332.
- Koszelewski, D., Clay, D., Rozell, D., Kroutil, W.** (2009). Deracemisation of α -chiral primary amines by a one-pot, two-step cascade reaction catalysed by ω -transaminases, *Eur. J. Org. Chem*, 2289-2292.
- Koszelewski, D., Lavandera I., Clay, D., Guebitz, G. M., Rozzell, D., Kroutil, W.** (2008). Formal Asymmetric Biocatalytic Reductive Amination, *Angew Chem Int Ed*, **47**, 9337–9340.
- Kulla H. G.,** (1991). Enzymatic hydroxylations in industrial application, *Chimia*, **45**, 81-85.
- Kwon, S. J., Ko, S.Y.** (2002). Synthesis of Statine Employing a General Syn-Amino Alcohol Building Block, *Tetrahedron: Letters*, **43**, 639-641.
- Leffingwell, J. C.** (2003). Chirality & Bioactivity I.: Pharmacology, Vol. **3**, No. 1.
- Lemuth, K., Hardiman, T., Winter, S., Pfeiffer, D., Keller, M. A., Lange, S., Reuss, M., Schmid, R. D., Siemann-Herzberg, M.** (2008). Global Transcription and Metabolic Flux Analysis of *Escherichia coli* in Glucose-Limited Fed-Batch Cultivations[∇], *Appl. Environ. Microbiol.*, vol. **74**, no. 22, 7002-7015.

- Li, T., Kootstra, A. B., Fotheringham, I. G.** (2002). Nonproteinogenic alpha-amino acid preparation using equilibrium shifted transamination, *Org Process Res Dev*, **6**, 533–538.
- Liddell, J. M.** (2009). *Bioprocess Scale Up Product and Process Development Interactions*, Bioprocessing 1.
- Lin, J.H., Ostovic, D., Vacca, J. P.** (1998). The integration of medicinal chemistry, drug metabolism, and pharmaceutical research and development in drug discovery and development. The story of Crixivan, an HIV protease inhibitor, *Pharm. Biotechnol.*, **11**, 233–255.
- Lin, H., Liu, J-Y., Wang, H-B., Ahmed, A. B. Q., Wu, Z-L.** (2011). Biocatalysis as an alternative for the production of chiral epoxides: A comparative review. *Journal of Molecular Catalysis B: Enzymatic.*, **72**, 3–4, 77-89.
- Lye, G. J., Ayazi-Shamlou, P., Baganz, F., Dalby, P. A., Woodley, J. M.** (2003). Accelerated design of bioconversion process using automated microscale processing techniques; *Trends in Biotechnology*, Vol **21**, No.1, 29-37.
- Lye, G. J., Hubbuch, J., Schroeder, T., Willmann, E.** (2009). Shrinking the Costs of Bioprocess Development, *BioProcess International.*, 18-22.
- Lye, G. J., Woodley, J. M.** (1999). Application of in situ product-removal techniques to biocatalytic processes; *Trends of Biotechnology*, Vol **17**, Issue 10, 395-402.
- Lye, G.J. Dalby, P. A., Woodley, J. M.** (2002) Better biocatalytic processes faster: new tools for the implementation of biocatalysis in organic synthesis. *Org. Proc. Res. Dev.*, **6**, 434–440
- W. Marckwald and A. McKenzie**, *Ber. dtsh. chem. Ges.* **32**, 2130 (1899).
- Marques, M. P. C., Magalhães, S., Cabral, J. M. S., Fernandes, P.** (2009). Characterization of 24-well microtiter plate reactors for a complex multistep bioconversion: from sitosterol to androstenedione, *Journal of biotechnology*, **141**, 174-80.
- Matosevic, S., Szita, N., Baganz, F.** (2011). Fundamentals and applications of immobilized microfluidic enzymatic reactors, *Journal of Chemical Technology & Biotechnology*, **86**, 325-334.
- Matosevic, S.** (2009). Design and characterisation of a prototype immobilised enzyme microreactor for the quantification of multi- step enzyme kinetics. PhD Thesis. University College London.

- Matosevic, S., Micheletti, M., Woodley, J. M., Lye, G. J., Baganz, F.** (2008). Quantification of kinetics for enzyme-catalysed reactions: implications for diffusional limitations at the 10 ml scale, *Biotechnology letters*, **30**, 995-1000.
- Micheletti, M., Barrett, T., Doig, S. D., Baganz, F., Levy, M. S., Woodley, J. M., Lye, G. J.** (2006). Fluid mixing in stirred bioreactors: implications for scale-up predictions from microlitre-scale microbial and mammalian cell cultures, *Chem Eng Sci.*, **61**, 2939-2949.
- Micheletti, M., Lye, G. J.** (2006). Microscale bioprocess optimisation; Current Opinion in Biotechnology, **17**, 611–618.
- Mehta, P.K., Hale, T. I., Christen, P.,** (1993). Aminotransferase: demonstration of homology and division into evolutionary subgroups, *Eur. J. Biochem.*, **214**, 259-261.
- Nagasawa, T. and Yamada, H.,** (1990). Application of Nitrile Converting Enzyme for the Production of Useful Compounds. *Pure Appl. Chem.* **62**, 1441-1444.
- Nakamura, K., Fujii, M., Ida, I.,** (2000). Asymmetric reduction of ketones by *Geotrichum candidum* in the presence of Amberlite™ XAD, a solid organic solvent; *J. Chem. Soc., Perkin Trans.*, **1**, 3205 – 3211.
- Nealon, A., Okennedy, R., Titchenerhooker, N., Lye, G. J.** (2006). Quantification and prediction of jet macro-mixing times in static microwell plates. *Chemical Engineering Science*, **61**, 4860-4870.
- Nieuwenhuijzen, J. W., Grimbergen, R. E. P., Koopman, C., Kellogg, R. M., Vries, T. R., Pouwer, K., Echten, E. V., Kaptein, B., Hulshof, L. A., Broxterman, Q. B.** (2002). The role of nucleation inhibition in optical resolutions with families of resolving agents, *Angew Chem Int Ed*, **41**, 4281-4286.
- Nugent, T. C., El-Shazly, M.,** (2010). Chiral amine synthesis -Recent developments and trends for enamide reduction, reductive amination, and imine reduction, *Adv Synth Catal*, **352**, 753–819.
- Panke, S., Held, M., Wubbolts, M.** (2004). Trends and innovation in industrial Biocatalysis for the Production of Fine Chemicals, *Current Opinion in Biotechnology*, **15**, 272-279.
- Pannuri, S., DiSanto, R., Kamat, S.** (2003). Biocatalysis. *Kirk-Othmer Encyclopedia of Chemical Technology*. Hoboken, NJ: Wiley.
- Park, J.-H., Kim, G.-J., Kim, H.-S.** (2002). Complete Conversion of D,L-5-Monosubstituted Hydantoins with a Low Velocity of Chemical Racemisation

- into D-Amino Acids Using Whole Cells of Recombinant *Escherichia coli*, *Biotechnol. Prog.* **18**, 1201-1206.
- Patel, R. N.** (2001). Enzymatic Synthesis of Chiral intermediates for Omapatrilat, an Antihypertensive Drug, *Biomolecular Engineering*, **17**, 167-182.
- Pedro, F.**, (2010). Miniaturization in Biocatalysis, *Int. J. Mol. Sci.*, **11**, 858-879.
- Peters, J.** (2008). Dehydrogenase Characteristics, design of reaction conditions, and applications, In: Rehm H-J, Reed G, Puhler.
- Pollard, D. J., Truppo, M., Pollard, J., Chen, C-Y, Moore, J.** (2006). Effective synthesis of (S)-3,5-bis(trifluoromethyl)phenyl ethanol by asymmetric enzymatic reduction, *Tet. Asymm*, **17**, 554–559.
- Pollard, D. J., Woodley, J. M.** (2006). Biocatalysis for pharmaceutical intermediates: the future is now, *Trends in Biotechnology*, Vol **25**, No. 2.
- Porath, J., Carlsson, J., Olsson, J., Belfrage, G.** (1975). Metal chelate affinity chromatography, a new approach to protein fractionation, *Nature*, **258**, 598-599.
- Rissom, S., Beliczey, J., Giffels, G., Kragl U., Wandrey, C.** (1999). Asymmetric reduction of acetophenone in membrane reactors: comparison of oxazaborolidine and alcohol dehydrogenase catalysed processes, *Tetrahedron: Asymmetry*, **10**, 923-928.
- Rios, S. L., Halim, M., Cázares, A., Morris, P., Ward, J. M., Hailes, H. C., Dalby, P. A., Baganz, F., Lye, G. J.** (2011). A microscale toolbox for rapid evaluation of multi-step enzymatic syntheses comprising a mix and match *E. coli* expression system, *Biocatalysis and Biotransformation*. **29**, 5, 192-203.
- Rogers, R. S.** (1999). Companies turn to biocatalysis, *Chem. Eng. News*, **77**, 29, 87-92.
- Roth, B.D.** (2002). The discovery and development of Atorvastatin, a potent novel hypolipidemic agent, *Prog. Med. Chem.*, **40**, 1–22.
- Rudroff, F., Alphan, V., Furstoss, R., Mihovilovic, M. D.** (2006). Optimizing fermentation conditions of recombinant *Escherichia coli* expressing cyclopentanone monooxygenase, *Organic process research & development*, **10**, 599-604.
- Samsonova, N. N., Smirnov, S. V., Atman, I. B., Ptitsyn, L. R.** (2003). Molecular cloning and characterization of *Escherichia coli* *ygjG* gene, *BMC Microbiol.*, **3**, 2.

- Sanchez, S., Demain, A. L.** (2011). Enzymes and Bioconversions of Industrial, Pharmaceutical, and Biotechnological Significance, *Organic Process Research & Development*, **15**, 224–230.
- Savile, C. K., Janey, J. M., Mundorff, E. C., Moore, J. M., Tam, S., Jarvis, W. R., Colbeck, J. C., Krebber, A., Fleitz, F. J., Brands, J., Devine, P. N., Huisman, G. W., Hughes, G. J.** (2010). Biocatalytic Asymmetric synthesis of chiral amines from ketones applied to Sitagliptin manufacture, *Science*, **329**, 305–309.
- Sayer, C., Michail, N. I., Jennifer, A. L.** (2007). Crystallization and preliminary X-ray diffraction analysis of ω -amino acid:pyruvate transaminase from *chromobacterium violaceum*, *Acta Cryst.*, **F63**, 117-119.
- Schmidt, E., Blaser, H.-U.** (2003). *Asymmetric Synthesis On Industrial Scale: Challenges, Approaches and Solutions*, New York.
- Schmid, A., Dordick, J. S., Hauer, B., Kiener, A., Wubbolts, M. and Witholt, B.** (2001). Industrial Biocatalysis Today and Tomorrow, *Nature*, **409**, 258-268.
- Schindler, J.** (1982). Terpenoids by microbial fermentation, *Ind. Eng. Chem. Prod. Res. Dev.*, **21**, 4, 537-539.
- Schoemaker, H. E., Mink, D. and Wubbolts, M. G.** (2003). Dispelling the Myths--Biocatalysis in Industrial Synthesis, *Science*, **299**, 1694-1697.
- Seo, J. H., Kyong, D., Joo, K., Lee, J., Kin, B. G.** (2011). Necessary and sufficient conditions for the asymmetric synthesis of chiral amines using ω -transaminases, *Biotechnol Bioeng*, **108**, 253–263.
- Sheldon, R. A.** (2007). Enzyme immobilization: The quest for optimum performance, *Adv Synth Catal*, **349**, 1289–1307.
- Sheldon, R. A.** (1996). Chirtechnology: designing economic chiral syntheses, *J Chem Tech Biotechnol*, **67**, 1-14.
- Shimazawa, R., Nagai, N., Toyoshima, S., Okuda, H.** (2008). Present State of New Chiral Drug Development and review in Japan, *Journal of Health Science*, **54**, 1, 23-29.
- Shin, J.S., Kim, B.G.** (2002). Substrate inhibition mode of ω -transaminase from *Vibrio fluvialis* JS17 is dependent on the chirality of substrate, *Biotechnol. Bioeng.*, **77**, 832-837.

- Shin, J.S., Kim, B.G.** (2001). Comparison of the ω -transaminases from different microorganisms and application to production of chiral amines, *Biosci. Biotechnol. Biochem.*, **65**, 1782-1788.
- Shin, J. S, Kim, B.G.,** (1999). Modeling of the kinetic resolution of α -methylbenzylamine with ω -transaminase in a two-liquid-phase system, *Enzyme Microb. Technol.*, **25**, 426-432.
- Shin, J. S., Kim, B.G.** (1998). Kinetic modeling of ω -transamination for enzymatic kinetic resolution of α -methylbenzylamine, *Biotechnol. Bioeng.*, **60**, 534-540.
- Shin, J.S., Kim, B. G.,** (1997). Kinetic resolution of α -methylbenzylamine with ω -transaminase screened from soil microorganisms: Application of biphasic system to overcome product inhibition, *Biotechnol. Bioeng.*, **55**, 348-358.
- Shin, J. S., Kim, B. G.** (1996). Optical Resolution of Racemic 1-Phenylethylamine Catalyzed by Aminotransferase and Dehydrogenase, *Annals of the New York Academy of Sciences*, Volume **799**, 717-724.
- Shin, J.S., Yun, H., Jang, J. W., Park, I., Kim, B.G.** (2003). Purification, characterization, and molecular cloning of a novel amine:pyruvate transaminase from *Vibrio fluvialis* JS17, *Appl. Microbiol. Biotechnol.*, **61**, 463-471.
- Shin, J. S., Kim, B. G., Liese, A., Wandrey, C.** (2001). Kinetic resolution of chiral amines with ω -transaminase using an enzyme-membrane reactor, *Biotechnology and Bioengineering*, Vol **73**, No. 3, 179-187.
- Smith, M. E. B., Chen, B. H., Hibbert, E. G., Kaulmann, U., Smithies, K., Galman, J. L., Baganz, F., Dalby, P. A., Hailes, H. C., Lye, G. J., Ward, J. M., Woodley, J. M., Micheletti, M.** (2010). A Multidisciplinary Approach Toward the Rapid and Preparative-Scale Biocatalytic Synthesis of Chiral Amino Alcohols: A Concise Transketolase-/ ω -Transaminase-Mediated Synthesis of (2S,3S)-2-Aminopentane-1,3-diol, *Organic Process Research & Development*, **14**, 99–107.
- Sonawane, H.R., Bellur, N.S., Ahuja, J.R. Kulkarni, D.G.** (1992). Recent developments in the synthesis of optically active α -arylpropanoic acids: An important class of nonsteroidal anti-inflammatory agents. *Tetrahedron: Asymmetry*, **3**, 163-192.
- Stinson, S. C.** (1994). Chiral Drugs, *Chemical Engineering News*, 38-72.

- Stirling, D. I.** (1992). The use of aminotransferases for the production of chiral amines and amines, In: Collins AN, Sheldrake GN, Crosby J, editors. Chirality in Industry, Uk: John Willey & Sons, 209-222.
- Studier, W. F., Moffatt, B. A.** (1986). Use of bacteriophage T7 RNA polymerase to direct selective high-level expression of cloned genes, *J Mol boil*, **189**, 113-130.
- Sutin, L., Anderson, S., Bergquist, L., Castro, V. M., Danielsson, E., James, S., Henriksson, M., Johansson, L., Kaiser, C., Flyren, K., Williams, M.** (2007). Oxazolones as potent inhibitors of 11 β -hydroxysteroid dehydrogenase type 1, *Bioorg. Med. Chem Lett.* **17**, 4837-4840.
- Taylor, P. P., Pantaleone, D. P., Senkpeil, R. F., Fotheringham, I. G.** (1998). Novel biosynthetic approaches to the production on unnatural amino acids using transaminases, *Trends Biotechnol*, **16**, 412-418.
- Tao, J., Xu, J.-H.** (2009). Biocatalysis in development of green pharmaceutical processes. *Curr. Opin. Chem. Biol.*, **13**, 1, 43-50.
- Truppo, M. D., Turner, N. J.** (2010). Micro-scale process development of transaminase catalysed reactions, *Org. Biomol. Chem.*, **8**, 1280-1283.
- Truppo, M. D., Rozzell, D. J., Moore, J., Turner, N. J.** (2009). Rapid Screening and Scale-up of Transaminase Catalysed Reactions, *Organic and Biomolecular Chemistry*, Volume: **7**, Issue: 2, 395-398.
- Tsai, S. W., Wei, H. J.**, (1994). Enantioselective esterification of racemic naproxen by lipase in organic solvent, *Enzyme Microb Technol*, **16**, 328-333.
- Tufvesson, P., Ramos, J. L., Jensen, J. S., Al-Haque, N., Neto, W., Woodley, J. M.** (2011). Process considerations for the asymmetric synthesis of chiral amines using transaminases; *Biotechnology and Bioengineering*, Volume **108**, Issue 7, 1479-1493.
- Van Sonsbeek, H. M., Beeftink, H. H., Tramper, J.** (1993). Two-liquid-phase bioreactor, *Enzyme Microb. Technol*, **15**, 722-729.
- Vicenzi, J. T., Zmijewski, M. J., Reinhard, M. R., Landen, B. E., Muth, W. L., Marler, P. G.** (1997). Large-scale stereoselective enzymatic ketone reduction with in situ product removal via polymeric adsorbent resins, *Enzyme Microb. Technol*, vol **20**, 495-499.
- Wainer, I. W.** (1993). Stereoisomers in Clinical Oncology: Why It Is Important to Know What the Right and Left Hands Are Doing, *Ann Oncol*, **4**, 7-13.

- Wang, J., Araki, T., Ogawa T., Matsuoka, M., Fukuda, H.** (1999). A method of graphically analysing substrate-inhibition kinetics, *Biotech Bioeng*, **62**, 402-411.
- Watanabe, N., Sakabe, K., Sakabe, N., Higashi, T., Sasaki, K., Aibara, S., Morita, Y., Yonoha, K., Toyama, S., Fukutani, H.** (1989). Crystal structure analysis of ω -amino acid:pyruvate aminotransferase with newly developed weissenberg camera and an imaging plate using synchrotron radiation, *J Biochem*, **105**, 1-3.
- Watson J. D.** (1972). *Molecular Biology of the Gene*, 2nd ed. Saunders, Philadelphia, PA USA.
- Wells, A.** (2006). What Is in a Biocatalyst?, *Organic Process Research & Development*, **10**.
- Wubbolts, M.G., Favre-Bulle, O., Wiltholt, B.** (1996). Biosynthesis of synthons in two-liquid-phase media, *Biotechnol Bioeng.*, **52**, 301-308.
- Yang, Z.- H., Zeng, R., Chang, X., Li, X-K., Wang, G-H.** (2008). Toxicity of aromatic ketone to yeast cell and improvement of the asymmetric reduction of aromatic ketone catalysed by yeast cell with the introduction of resin adsorption, *Food Technol. Biotechnol.*, **46**, 3, 322-327.
- Yang, W. C., Shim, W. G., Lee, J. W., Moon, H.** (2003). Adsorption and desorption dynamics of amino acids in a non-ionic polymeric sorbent XAD-16 column, *Korean J. Chem. Eng.*, **20**, 5, 922-929.
- Yazbeck, D. R., Martinez, C.A., Hu, S., Tao, J.** (2004). Challenges in the Development of an Efficient Enzymatic Process in the Pharmaceutical industry, *Tetrahedron: asymmetry*, 2757-2763.
- Yi, S.S., Lee, C.W., Kim, J., Dohyun, K., Kim, B.G., Lee, Y.T.** (2007). Covalent immobilization of ω -transaminase from *Vibrio fluvialis* JS17 on chitosan beads., **42**, 895-898.
- Yohana, K., Toyama, S., Soda, K.** (1987). ω -Amino acid-pyruvate aminotransferase. 1987, *Methods Enzymol*, **143**, 500-505.
- Yun, H., Kim, J., Kinnera, K., Kim, B. G.** (2005). Synthesis of enantiomerically pure trans-(1R,2R)- and cis-(1S, 2R)-1-amino-2-indanol by lipase and ω -transaminase, *Biotechnol Bioeng*, **93**, 391-395.

- Yun, H., Cho, B-K., Kim, B-G.** (2004). Kinetic resolution of (R,S)-sec-butylamine using omega-transaminase from vibrio fluvialis JS17 under reduced pressure, *Biotechnology and bioengineering*, Vol **87**, No 6, 772-778.
- Yun, H., Hun, Y., Cho, B-K., Hwang, B-Y., Kim, B-G.** (2003). Simultaneous synthesis of enantiomerically pure (R)-1-phenylethanol and (R)- α -methylbenzylamine from racemic α -methylbenzylamine using ω -transaminase/alcohol dehydrogenase/glucose dehydrogenase coupling reaction, *Biotechnology Letters*, **25**, 809-814.
- Zhang, H., Lamping, S. R., Pickering, S. C. R., Lye, G. J., Shamlou, P. A.** (2008). Engineering characterisation of a single well from 24-well and 96-well microtitre plates, *Biochemical Engineering Journal*, **40**, 138-149.
- Zhang, X. P., Loke, K. E., Mital, S., Chahwala, S., Hintze, T. H.** (2002). Paradoxical release of nitric oxide by an L-type calcium channel antagonist, the R+ enantiomer of amlodipine, *J. Cardiovasc. Pharmacol.*, **39**, 2, 208-214.

APPENDIX I

CALIBRATION PLOT OF BIOMASS IN FUNCTION OF OD₆₀₀

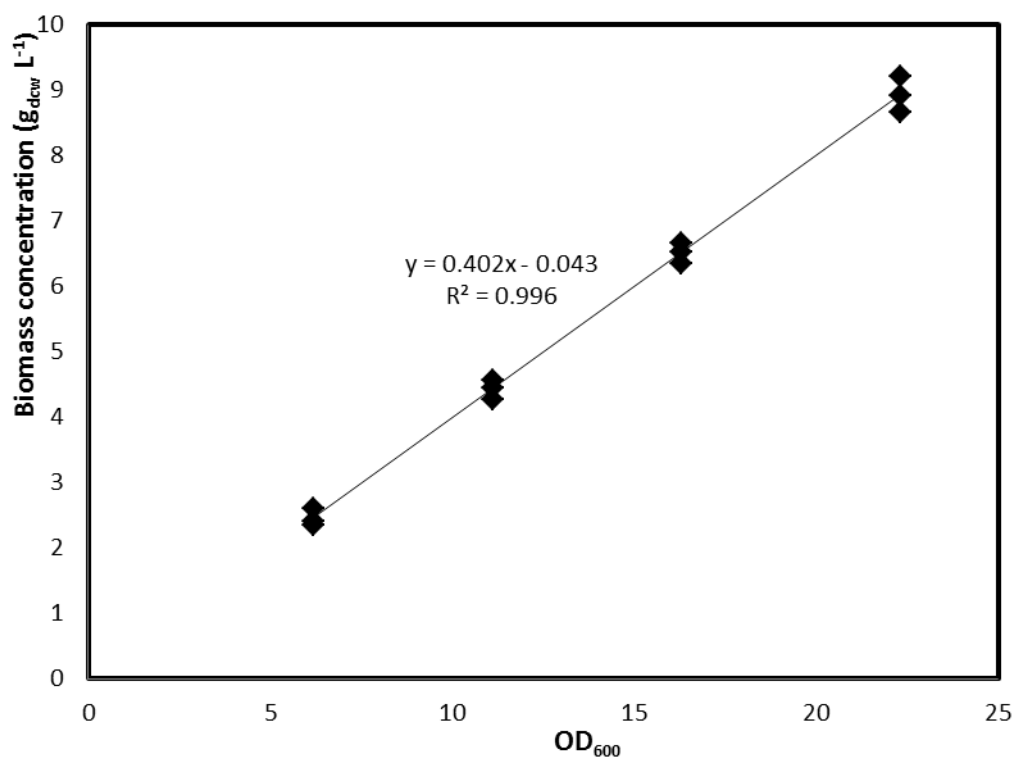


Figure A.I. 1. Calibration graph of biomass in g_{dew} L⁻¹ as a function of OD₆₀₀ (Section 2.6.2).

APPENDIX II

BRADFORD ASSAY: CALIBRATION PLOT OF BSA CONCENTRATION IN FUNCTION OF OD₅₉₅

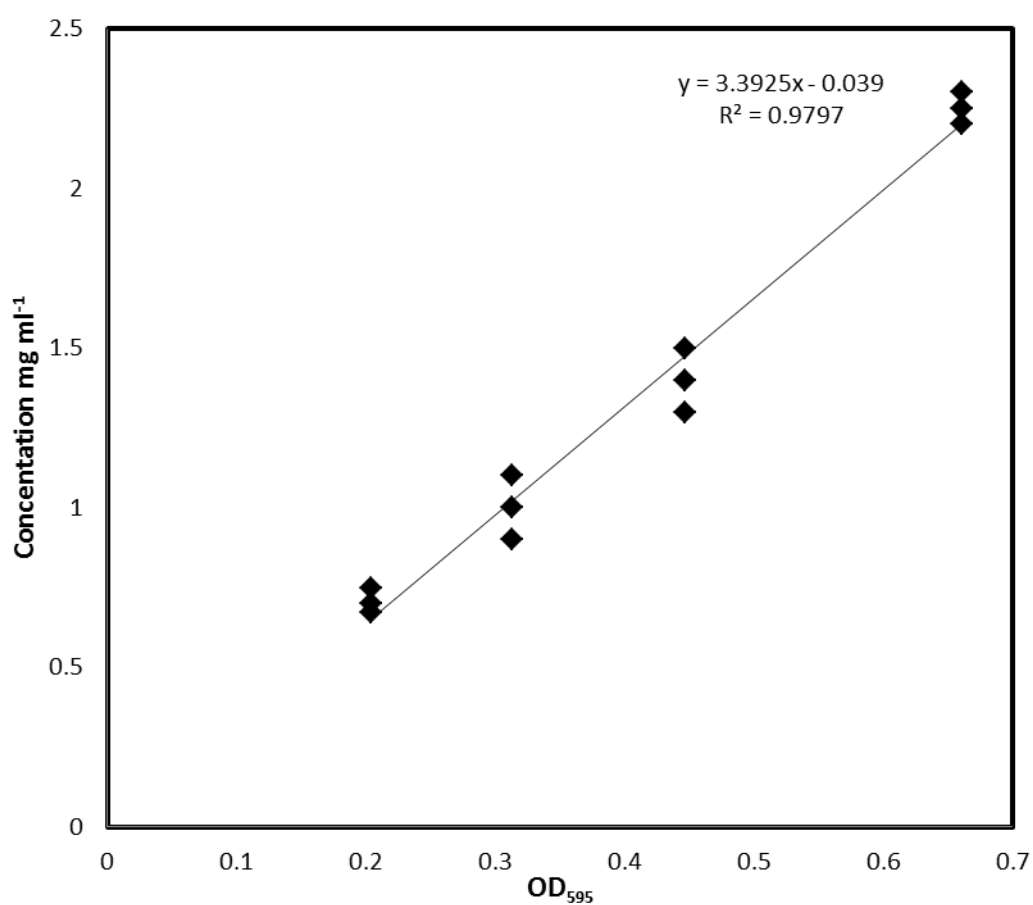


Figure A.II. 1. Standard graph for Bradford assay of BSA concentration as a function of OD₅₉₅ (Section 2.6.3).

APPENDIX III

HPLC STANDARD CALIBRATIONS AND CHROMATOGRAMS

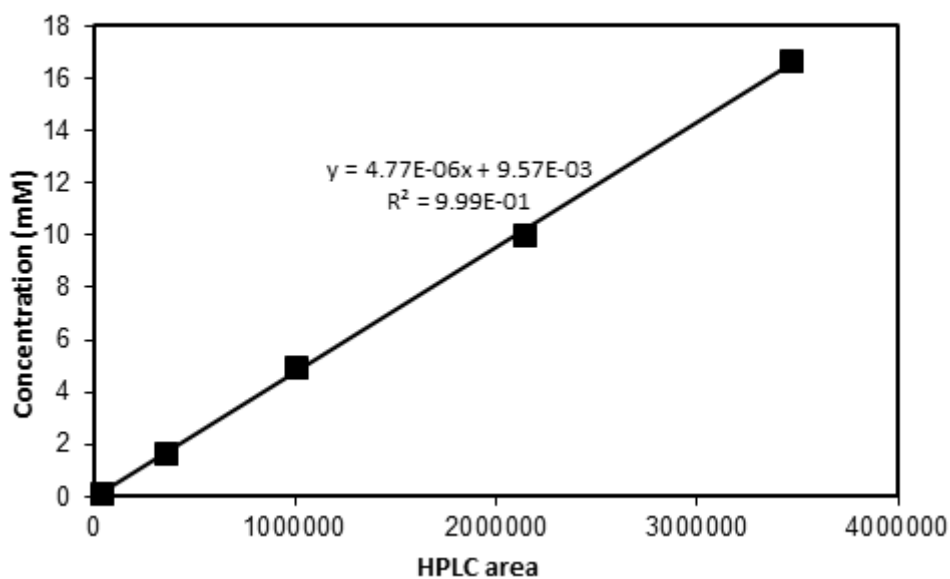


Figure A.III. 1. Calibration graph of L-Erythrulose (Ery) concentration as a function of HPLC area (Section 2.6.6).

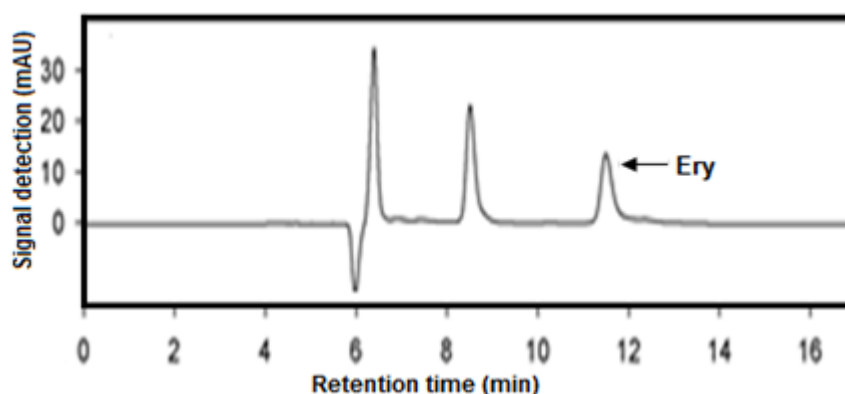


Figure A.III. 2. HPLC chromatogram of Ery. The peak retention time is at 11.63 min. (Section 2.6.6).

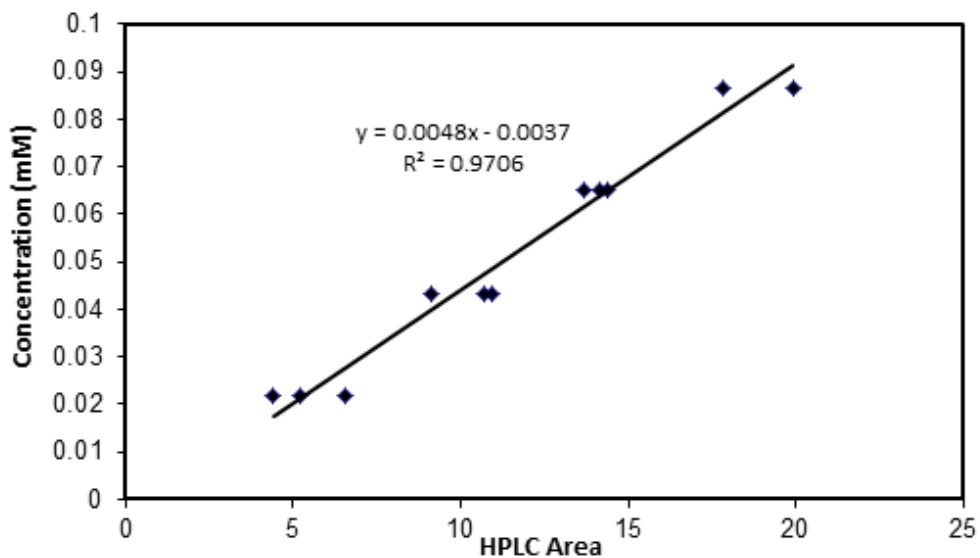


Figure A.III. 3. Calibration graph of derivatized 2-amino-1,3,4-butanetriol (ABT) concentration as a function of HPLC area (Section 2.6.6).

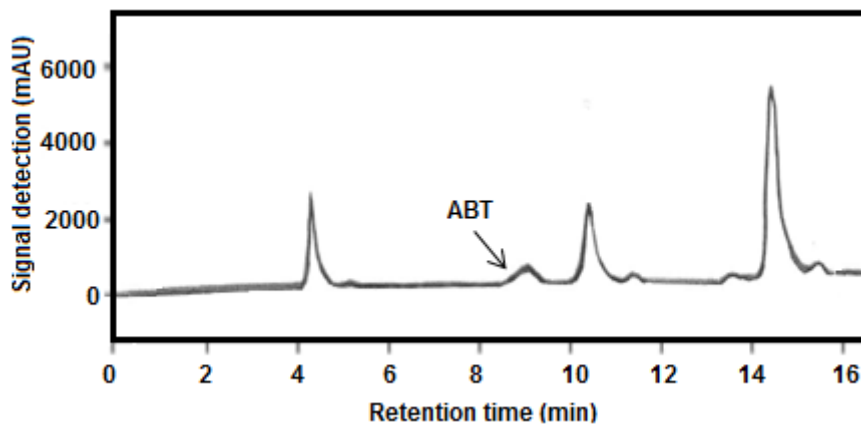


Figure A.III. 4. HPLC chromatogram of derivatized ABT (Section 2.6.6). The peak retention time is at 8.9 min.

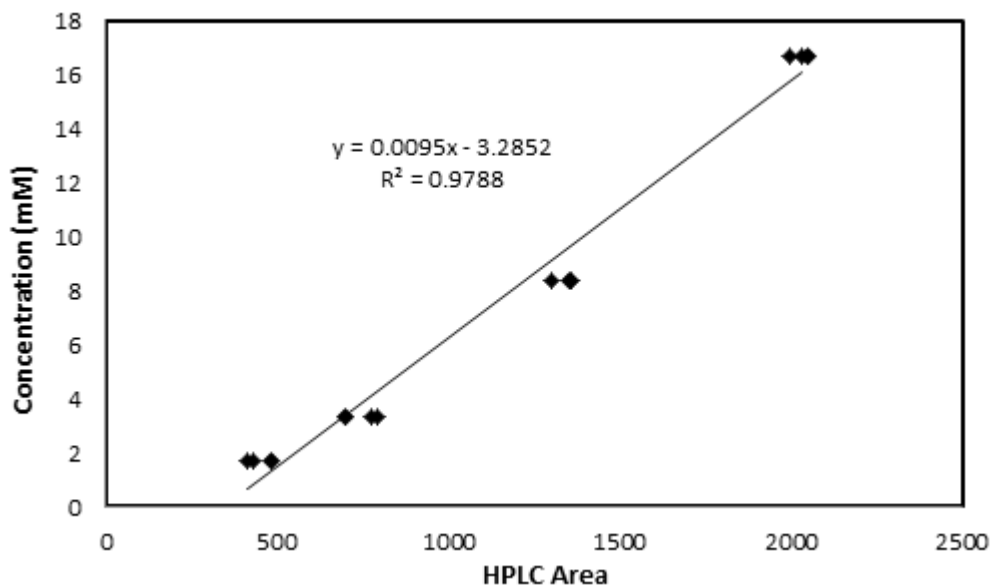


Figure A.III. 5. Calibration graph of derivatized L- α -Serine concentration as a function of HPLC area (Section 2.6.6).

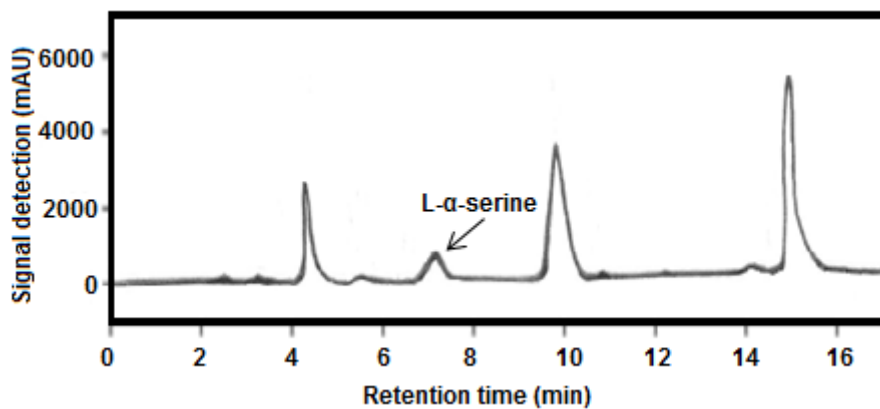


Figure A.III. 6. HPLC chromatogram of derivatized L- α -Serine (Section 2.6.6). The peak retention time is at 7.3 min.

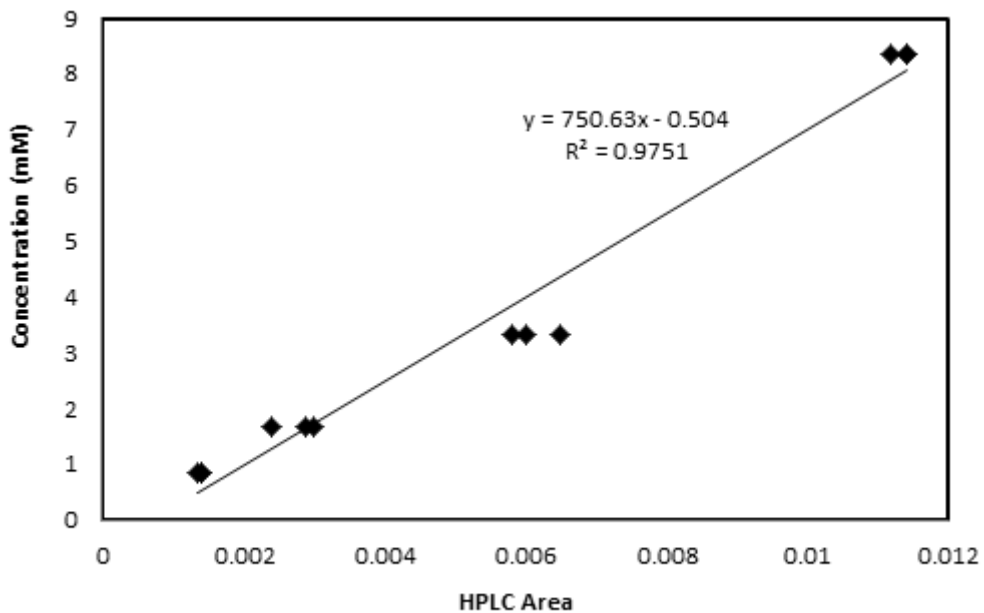


Figure A.III. 7. Calibration graph of Pyruvate concentration as a function of HPLC area (Section 2.6.6).

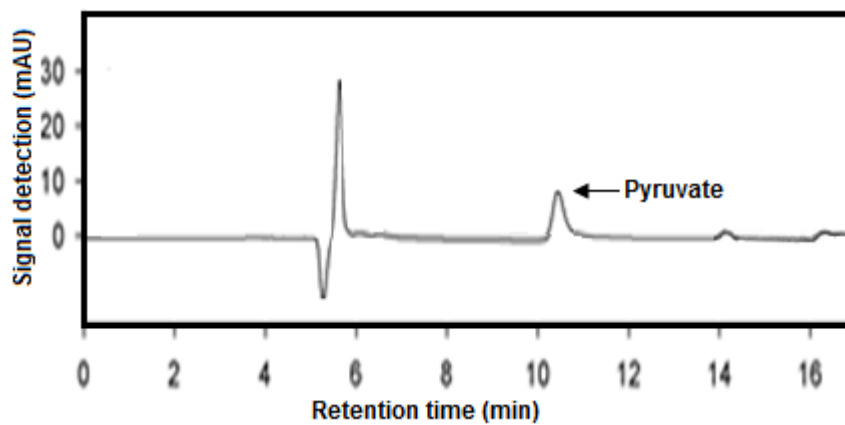


Figure A.III. 8. HPLC chromatogram of pyruvate (Section 2.6.6). The peak retention time is at 10.43 min.

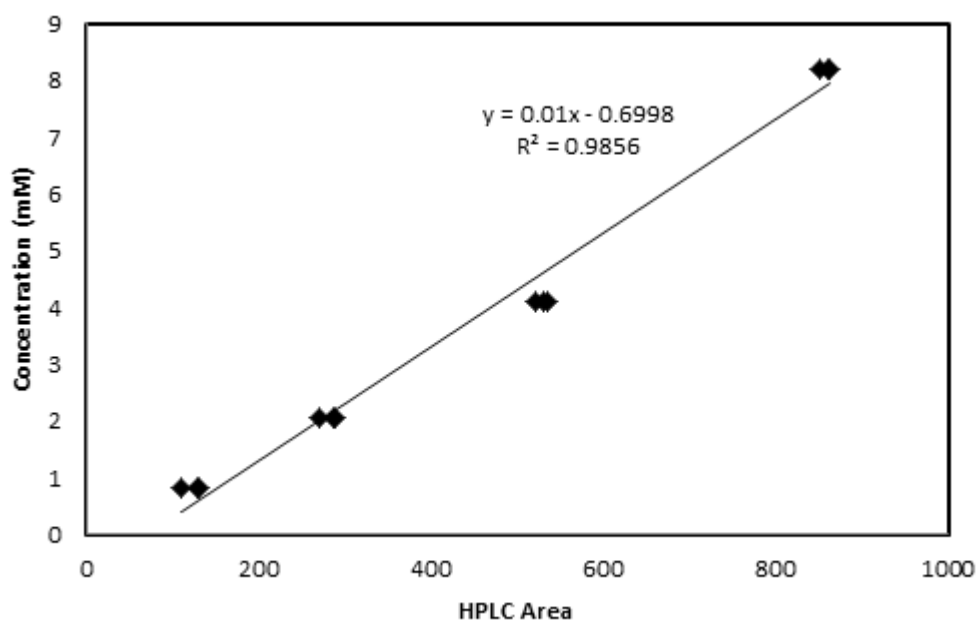


Figure A.III. 9. Calibration graph of Acetophenone (AP) concentration as a function of HPLC area (Section 2.6.6).

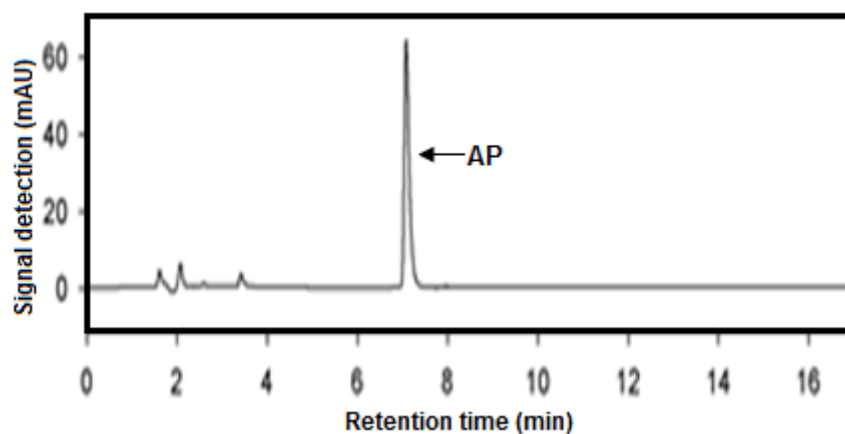


Figure A.III. 10. HPLC chromatogram of AP (Section 2.6.6). The peak retention time is at 7.28 min.

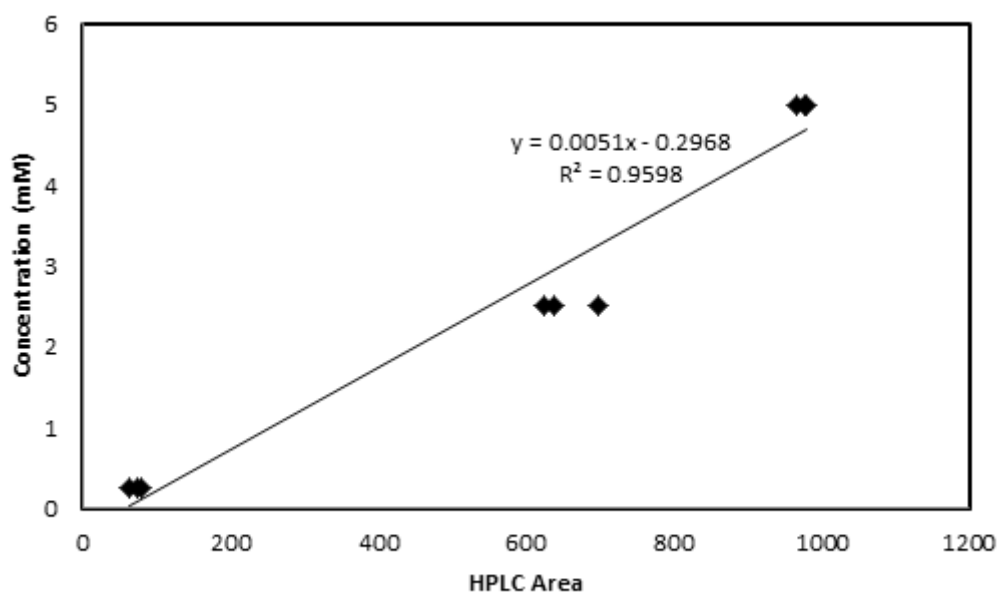


Figure A.III. 11. Calibration graph of (R)-1-phenylethanol concentration as a function of HPLC area (Section 2.6.6).

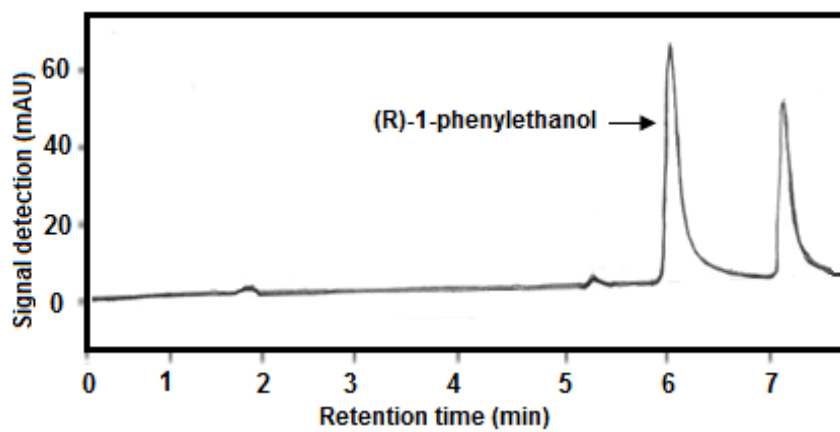


Figure A.III. 12. HPLC chromatogram of (R)-1-phenylethanol (Section 2.6.6). The peak retention time is at 6.45 min.

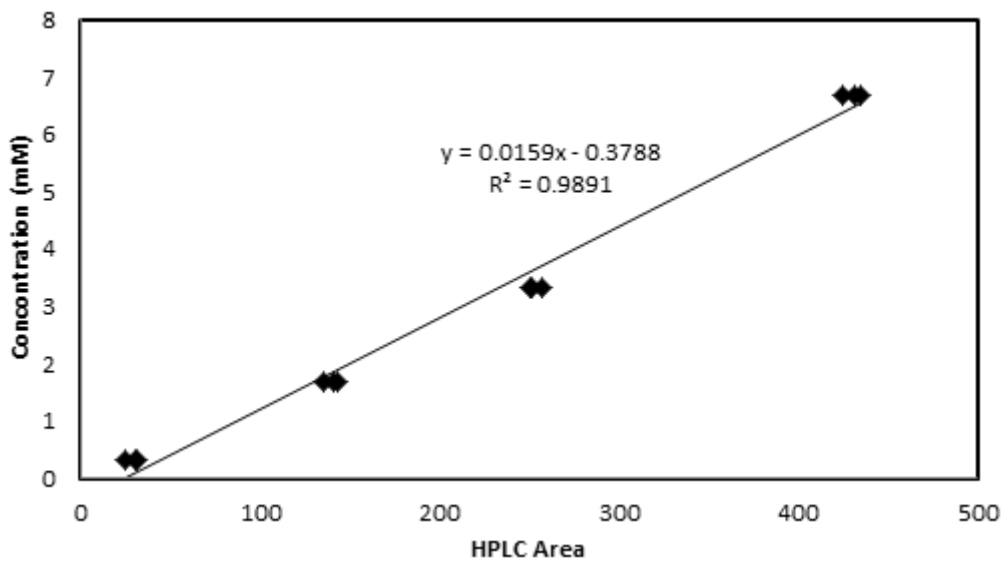


Figure A.III. 13. Calibration graph of (*S*)- α -Methylbenzylamine (MBA) concentration as a function of HPLC area (Section 2.6.6).

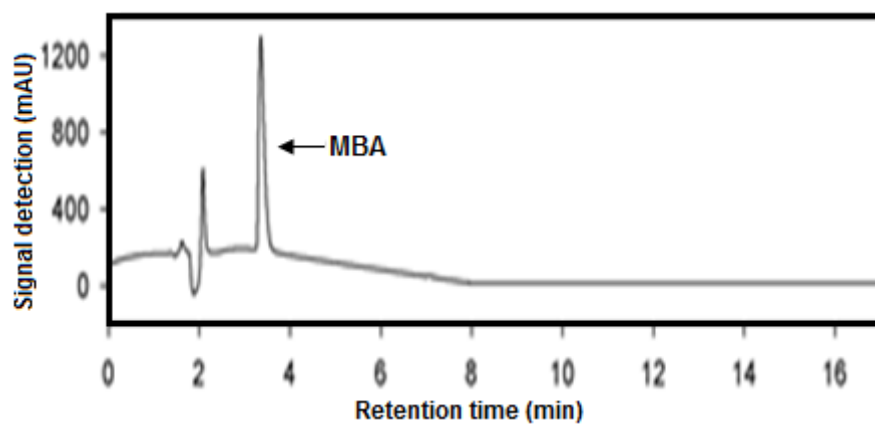


Figure A.III. 14. HPLC chromatogram of MBA (Section 2.6.6). The peak retention time is at 3.4 min.

APPENDIX IV

TECAN SCRIPTS

Figure A.IV. 2. Parallel evaluation of alternative amino donors (Section 5.5)

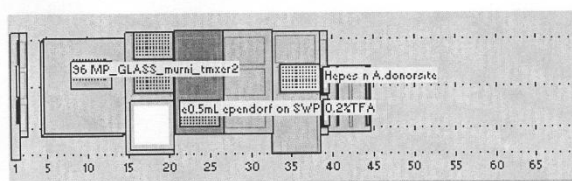
1		Wash Tips		2.0 + 1.0 ml
2		Get DITIs		DITi200, 96 Tips, new tray
3		Comment	Add Enzyme: TAm LYSATES	
4		Begin Loop	6 times "TAm Lysates"	
5		Aspirate		100 µl >> Water << "TAMs lysate" (Col. 1, Rows 1-6)
6		Dispense		100 µl >> Water << "96 MP_GLASS_murni_tmrxer2" (Col. 1, Rows 1-6) , 1 option
7		End Loop	"TAm Lysates"	
8		Wash Tips		2.0 + 1.0 ml
9		Drop DITIs		DITi waste, 1 Pos.
10		Get DITIs		DITi200, 96 Tips, new tray
11		Comment	Add co-factor:PLP	
12		Begin Loop	6 times "PLP"	
13		Aspirate		15 µl >> Water << "PLP n A.donors" (Col. 1, Row 1)
14		Aspirate		15 µl >> Water << "PLP n A.donors" (Col. 1, Row 1)
15		Aspirate		15 µl >> Water << "PLP n A.donors" (Col. 1, Row 1)
16		Aspirate		15 µl >> Water << "PLP n A.donors" (Col. 1, Row 1)
17		Aspirate		15 µl >> Water << "PLP n A.donors" (Col. 1, Row 1)
18		Aspirate		15 µl >> Water << "PLP n A.donors" (Col. 1, Row 1)
19		Dispense		15 µl >> Water << "96 MP_GLASS_murni_tmrxer2" (Col. 1, Rows 1-6) , 1 option
20		Wash Tips		2.0 + 1.0 ml
21		End Loop	"PLP"	
22		Drop DITIs		DITi waste, 1 Pos.
23		Get DITIs		DITi200, 96 Tips, new tray
24		Comment	Add buffer: 50mM HEPES	
25		Begin Loop	6 times "Hepes"	
26		Aspirate		125 µl >> Water << "Hepes" (Col. 1, Rows 1-6)

27		Dispense		125 µl >> Water << "96 MP_GLASS_murni_tmxxer2" (Col. 1, Rows 1-6) , 1 option
28		Wash Tips		2.0 + 1.0 ml
29		End Loop	""	
30		Drop DITIs		DiTi waste, 1 Pos.
31		Comment		Short Incubation of tAM and PLP
32		Start Timer		1
33		Wait Timer		Timer 1 : 1200 sec
34		Comment		Add substrate:ERY (amino acceptor)
35		Get DITIs		DiTi200, 96 Tips, new tray
36		Begin Loop		6 times "Ery"
37		Aspirate		15 µl >> Water << "PLP n A.donors" (Col. 1, Row 2)
38		Aspirate		15 µl >> Water << "PLP n A.donors" (Col. 1, Row 2)
39		Aspirate		15 µl >> Water << "PLP n A.donors" (Col. 1, Row 2)
40		Aspirate		15 µl >> Water << "PLP n A.donors" (Col. 1, Row 2)
41		Aspirate		15 µl >> Water << "PLP n A.donors" (Col. 1, Row 2)
42		Aspirate		15 µl >> Water << "PLP n A.donors" (Col. 1, Row 2)
43		Dispense		15 µl >> Water << "96 MP_GLASS_murni_tmxxer2" (Col. 1, Rows 1-6) , 1 option
44		Wash Tips		2.0 + 1.0 ml
45		End Loop		"Ery"
46		Drop DITIs		DiTi waste, 1 Pos.
47		Get DITIs		DiTi200, 96 Tips, new tray
48		Comment		Add substrate:AMINO DONORS
49		Begin Loop		6 times "Amino donors"
50		Aspirate		45 µl >> Water << "PLP n A.donors" (Col. 1, Row 3) , 1 option
51		Aspirate		45 µl >> Water << "PLP n A.donors" (Col. 1, Row 3) , 1 option
52		Aspirate		45 µl >> Water << "PLP n A.donors" (Col. 1, Row 3) , 1 option

53	Aspirate		45 µl >> Water << "PLP n A.donors" (Col. 1, Row 3) , 1 option
54	Aspirate		45 µl >> Water << "PLP n A.donors" (Col. 1, Row 3) , 1 option
55	Aspirate		45 µl >> Water << "PLP n A.donors" (Col. 1, Row 3) , 1 option
56	Dispense		45 µl >> Water << "96 MP_GLASS_murni_tmxxer2" (Col. 1, Rows 1-6) , 1 option
57	Mix		2 x 150 µl Water "96 MP_GLASS_murni_tmxxer2" (Col. 1, Rows 1-6) , 1 option
58	Drop DITIs		DiTi waste, 1 Pos.
59	Get DITIs		DiTi200, 96 Tips, new tray
60	End Loop	""	
61	Wash Tips		2.0 + 1.0 ml
62	Drop DITIs		DiTi waste, 1 Pos.
63	Get DITIs		DiTi200, 96 Tips, new tray
64	Comment		REACTION SAMPLING
65	Begin Loop		4 times "Sampling"
66	Aspirate		30 µl >> Water << "96 MP_GLASS_murni_tmxxer2" (Col. 1, Rows 1-6)
67	Dispense		30 µl >> Water << "e0.5mL ependorf on SWP" (Col. 1, Rows 1-6)
68	Drop DITIs		DiTi waste, 1 Pos.
69	Get DITIs		DiTi200, 96 Tips, new tray
70	Aspirate		30 µl >> Water << "96 MP_GLASS_murni_tmxxer2" (Col. 2, Rows 1-6)
71	Dispense		30 µl >> Water << "e0.5mL ependorf on SWP" (Col. 2, Rows 1-6)
72	Drop DITIs		DiTi waste, 1 Pos.
73	Get DITIs		DiTi200, 96 Tips, new tray
74	Aspirate		30 µl >> Water << "96 MP_GLASS_murni_tmxxer2" (Col. 3, Rows 1-6)
75	Dispense		30 µl >> Water << "e0.5mL ependorf on SWP" (Col. 6, Rows 1-6)
76	Drop DITIs		DiTi waste, 1 Pos.
77	Get DITIs		DiTi200, 96 Tips, new tray
78	Aspirate		30 µl >> Water << "96 MP_GLASS_murni_tmxxer2" (Col. 4, Rows 1-6)

79	Dispense		 30 µl >> Water << "e0.5mL ependorf on SWP" (Col. 7, Rows 1-6)
80	Drop DITIs		DiTi waste, 1 Pos.
81	Get DITIs		DiTi200, 96 Tips, new tray
82	Aspirate		 30 µl >> Water << "96 MP_GLASS_murni_tmxxr2" (Col. 5, Rows 1-6)
83	Dispense		 30 µl >> Water << "e0.5mL ependorf on SWP" (Col. 11, Rows 1-6)
84	Drop DITIs		DiTi waste, 1 Pos.
85	Get DITIs		DiTi200, 96 Tips, new tray
86	Aspirate		 30 µl >> Water << "96 MP_GLASS_murni_tmxxr2" (Col. 6, Rows 1-6)
87	Dispense		 30 µl >> Water << "e0.5mL ependorf on SWP" (Col. 12, Rows 1-6)
88	Drop DITIs		DiTi waste, 1 Pos.
89	Get DITIs		DiTi1000, 96 Tips, new tray
90	Comment		Add: 0.2 % TFA
91	Aspirate		 270 µl >> Water << "0.2%TFA" (Col. 1, Rows 1-6)
92	Dispense		 270 µl >> Water << "e0.5mL ependorf on SWP" (Col. 1, Rows 1-6)
93	Drop DITIs		DiTi waste, 1 Pos.
94	Get DITIs		DiTi1000, 96 Tips, new tray
95	Aspirate		 270 µl >> Water << "0.2%TFA" (Col. 1, Rows 1-6)
96	Dispense		 270 µl >> Water << "e0.5mL ependorf on SWP" (Col. 2, Rows 1-6)
97	Drop DITIs		DiTi waste, 1 Pos.
98	Get DITIs		DiTi1000, 96 Tips, new tray
99	Aspirate		 270 µl >> Water << "0.2%TFA" (Col. 1, Rows 1-6)
100	Dispense		 270 µl >> Water << "e0.5mL ependorf on SWP" (Col. 6, Rows 1-6)
101	Drop DITIs		DiTi waste, 1 Pos.
102	Get DITIs		DiTi1000, 96 Tips, new tray
103	Aspirate		 270 µl >> Water << "0.2%TFA" (Col. 1, Rows 1-6)
104	Dispense		 270 µl >> Water << "e0.5mL ependorf on SWP" (Col. 7, Rows 1-6)

105	Drop DITIs		DiTi waste, 1 Pos.
106	Get DITIs		DiTi1000, 96 Tips, new tray
107	Aspirate		270 µl >> Water << "0.2%TFA" (Col. 1, Rows 1-6)
108	Dispense		270 µl >> Water << "e0.5mL ependorf on SWP" (Col. 11, Rows 1-6)
109	Drop DITIs		DiTi waste, 1 Pos.
110	Get DITIs		DiTi1000, 96 Tips, new tray
111	Aspirate		270 µl >> Water << "0.2%TFA" (Col. 1, Rows 1-6)
112	Dispense		270 µl >> Water << "e0.5mL ependorf on SWP" (Col. 12, Rows 1-6)
113	Drop DITIs		DiTi waste, 1 Pos.
114	Wash Tips		2.0 + 1.0 ml
115	Start Timer	1	
116	Wait Timer	Timer 1 : 25200 sec	
117	End Loop	""	



TECAN SCRIPTS

Figure A.IV. 2. Optimization of second enzyme reaction condition (Section 5.6)

1	 Wash Tips	 2.0 + 1.0 ml
2	 Get DITIs	 DiTi200, 96 Tips, new tray
3	 Comment	Add Enzyme: CV2025 TAM LYSATES
4	 Begin Loop	6 times "TAM:CV2025"
5	 Aspirate	 90 µl >> Water << Epdf_2ml_3 sites_murni (Col. 1, Rows 1-5)
6	 Dispense	 90 µl >> Water << 96 MP_GLASS_murni (Col. 1, Rows 1-5) , 1 option
7	 End Loop	"TAM:CV2025"
8	 Comment	Add Co-Factor: PLP
9	 Begin Loop	6 times "PLP"
10	 Aspirate	 15 µl >> Water << Epdf_2ml_3 sites_murni (Col. 1, Rows 1-5)
11	 Dispense	 15 µl >> Water << 96 MP_GLASS_murni (Col. 1, Rows 1-5) , 1 option
12	 End Loop	"PLP"
13	 Wash Tips	 2.0 + 1.0 ml
14	 Comment	TAm and PLP short incubation
15	 Start Timer	1
16	 Wait Timer	Timer 1 : 1200 sec
17	 Comment	Add 2nd Enzyme: ADH (various concentrations)
18	 Begin Loop	6 times "ADH"
19	 Aspirate	 45 µl >> Water << Epdf_2ml_3 sites_murni (Col. 1, Rows 1-5)
20	 Dispense	 45 µl >> Water << 96 MP_GLASS_murni (Col. 1, Rows 1-5) , 1 option
21	 End Loop	"ADH"
22	 Wash Tips	 2.0 + 1.0 ml
23	 Comment	Add 3rd Enzyme: GDH (various concentrations)
24	 Begin Loop	6 times "GDH"
25	 Aspirate	 15 µl >> Water << Epdf_2ml_3 sites_murni (Col. 1, Rows 6-10)
26	 Dispense	 15 µl >> Water << 96 MP_GLASS_murni (Col. 1, Rows 1-5) , 1 option

27	End Loop	""	
28	Wash Tips	 2.0 + 1.0 ml	
29	Comment	Add buffer: 1.5 M HEPES	
30	Begin Loop	5 times "Hepes"	
31	Aspirate	 51 µl >> Water << Trough 100ml JB (Col. 1, Rows 1-5)	
32	Dispense	 51 µl >> Water << 96 MP_GLASS_murni (Col. 1, Rows 1-5) , 1 option	
33	End Loop	"Hepes"	
34	Comment	Add substrate:ERYTHRULOSE	
35	Begin Loop	5 times "Ery"	
36	Aspirate	 15 µl >> Water << Epdrf_2ml_3 sites_murni (Col. 1, Rows 6-10)	
37	Dispense	 15 µl >> Water << 96 MP_GLASS_murni (Col. 1, Rows 1-5) , 1 option	
38	End Loop	"Ery"	
39	Wash Tips	 2.0 + 1.0 ml	
40	Drop DITIs	 DiTi waste, 1 Pos.	
41	Get DITIs	 DiTi200, 96 Tips, new tray	
42	Comment	Add substrate:GLUCOSE and NADPH	
43	Begin Loop	2 times "70mM glucose and NADPH"	
44	Aspirate	 24 µl >> Water << Epdrf_2ml_3 sites_murni (Col. 1, Row 6)	
45	Aspirate	 24 µl >> Water << Epdrf_2ml_3 sites_murni (Col. 1, Row 6)	
46	Aspirate	 24 µl >> Water << Epdrf_2ml_3 sites_murni (Col. 1, Row 6)	
47	Aspirate	 24 µl >> Water << Epdrf_2ml_3 sites_murni (Col. 1, Row 6)	
48	Aspirate	 24 µl >> Water << Epdrf_2ml_3 sites_murni (Col. 1, Row 6)	
49	Dispense	 24 µl >> Water << 96 MP_GLASS_murni (Col. 1, Rows 1-5) , 1 option	
50	End Loop	"70mM glucose and NADPH"	
51	Wash Tips	 2.0 + 1.0 ml	
52	Drop DITIs	 DiTi waste, 1 Pos.	

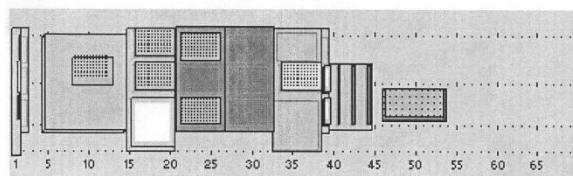
53		Get DITIs		DiTi200, 96 Tips, new tray
54		Begin Loop	2 times "50mM glucose and NADPH"	
55		Aspirate		24 µl >> Water << Epdrf_2ml_3 sites_murni (Col. 1, Row 7)
56		Aspirate		24 µl >> Water << Epdrf_2ml_3 sites_murni (Col. 1, Row 7)
57		Aspirate		24 µl >> Water << Epdrf_2ml_3 sites_murni (Col. 1, Row 7)
58		Aspirate		24 µl >> Water << Epdrf_2ml_3 sites_murni (Col. 1, Row 7)
59		Aspirate		24 µl >> Water << Epdrf_2ml_3 sites_murni (Col. 1, Row 7)
60		Dispense		24 µl >> Water << 96 MP_GLASS_murni (Col. 3, Rows 1-5) , 1 option
61		End Loop	"50mM glucose and NADPH"	
62		Wash Tips		2.0 + 1.0 ml
63		Drop DITIs		DiTi waste, 1 Pos.
64		Get DITIs		DiTi200, 96 Tips, new tray
65		Begin Loop	1 times "25mM glucose and NADPH"	
66		Aspirate		24 µl >> Water << Epdrf_2ml_3 sites_murni (Col. 1, Row 8)
67		Aspirate		24 µl >> Water << Epdrf_2ml_3 sites_murni (Col. 1, Row 8)
68		Aspirate		24 µl >> Water << Epdrf_2ml_3 sites_murni (Col. 1, Row 8)
69		Aspirate		24 µl >> Water << Epdrf_2ml_3 sites_murni (Col. 1, Row 8)
70		Aspirate		24 µl >> Water << Epdrf_2ml_3 sites_murni (Col. 1, Row 8)
71		Dispense		24 µl >> Water << 96 MP_GLASS_murni (Col. 5, Rows 1-5)
72		End Loop	"25mM glucose and NADPH"	
73		Wash Tips		2.0 + 1.0 ml
74		Drop DITIs		DiTi waste, 1 Pos.
75		Get DITIs		DiTi200, 96 Tips, new tray
76		Comment	Add substrate:50mM MBA	
77		Begin Loop	2 times "MBA_for reactions with 70mM glucose"	
78		Aspirate		45 µl >> Water << Epdrf_2ml_3 sites_murni (Col. 1, Rows 9-12)

79	Aspirate		45 µl >> Water << Epdrf_2ml_3 sites_murni (Col. 1, Row 12)
80	Dispense		45 µl >> Water << 96 MP_GLASS_murni (Col. 1, Rows 1-5) , 1 option
81	Mix		2 x 150 µl Water 96 MP_GLASS_murni (Col. 1, Rows 1-5) , 1 option
82	End Loop	""	
83	Drop DITIs		DiTi waste, 1 Pos.
84	Get DITIs		DiTi200, 96 Tips, new tray
85	Begin Loop		2 times "MBA_for reactions with 50mM glucose"
86	Aspirate		45 µl >> Water << Epdrf_2ml_3 sites_murni (Col. 1, Rows 9-12)
87	Aspirate		45 µl >> Water << Epdrf_2ml_3 sites_murni (Col. 1, Row 12)
88	Dispense		45 µl >> Water << 96 MP_GLASS_murni (Col. 3, Rows 1-5) , 1 option
89	Mix		2 x 150 µl Water 96 MP_GLASS_murni (Col. 3, Rows 1-5) , 1 option
90	End Loop		"MBA_for reactions with 50mM glucose"
91	Drop DITIs		DiTi waste, 1 Pos.
92	Get DITIs		DiTi200, 96 Tips, new tray
93	Begin Loop		1 times "MBA_for reactions with 25mM glucose"
94	Aspirate		45 µl >> Water << Epdrf_2ml_3 sites_murni (Col. 1, Rows 9-12)
95	Aspirate		45 µl >> Water << Epdrf_2ml_3 sites_murni (Col. 1, Row 12)
96	Dispense		45 µl >> Water << 96 MP_GLASS_murni (Col. 5, Rows 1-5) , 1 option
97	Mix		2 x 150 µl Water 96 MP_GLASS_murni (Col. 5, Rows 1-5) , 1 option
98	End Loop		"MBA_for reactions with 25mM glucose"
99	Wash Tips		2.0 + 1.0 ml
100	Drop DITIs		DiTi waste, 1 Pos.
101	Comment		SAMPLING # 1
102	Get DITIs		DiTi200, 96 Tips, new tray
103	Start Timer		1
104	Wait Timer		Timer 1 : 3600 sec

105		Begin Loop	2 times "Seventy1"
106		Aspirate	 40 µl >> Water << 96 MP_GLASS_murni (Col. 1, Rows 1-5) , 1 option
107		Dispense	 40 µl >> Water << SWP_0.5eppendorf_carrier Murni (Col. 1, Rows 1-5) , 1 option
108		End Loop	"Seventy1"
109		Drop DITIs	 DiTi waste, 1 Pos.
110		Get DITIs	 DiTi200, 96 Tips, new tray
111		Begin Loop	2 times "Fifty1"
112		Aspirate	 40 µl >> Water << 96 MP_GLASS_murni (Col. 3, Rows 1-5) , 1 option
113		Dispense	 40 µl >> Water << SWP_0.5eppendorf_carrier Murni (Col. 6, Rows 1-5) , 1 option
114		End Loop	"Fifty1"
115		Drop DITIs	 DiTi waste, 1 Pos.
116		Get DITIs	 DiTi200, 96 Tips, new tray
117		Begin Loop	1 times "Twenty Five1"
118		Aspirate	 40 µl >> Water << 96 MP_GLASS_murni (Col. 5, Rows 1-5) , 1 option
119		Dispense	 40 µl >> Water << SWP_0.5eppendorf_carrier Murni (Col. 11, Rows 1-5) , 1 option
120		End Loop	"Twenty Five1"
121		Drop DITIs	 DiTi waste, 1 Pos.
122		Get DITIs	 DiTi200, 96 Tips, new tray
123		Start Timer	2
124		Wait Timer	Timer 2 : 3600 sec
125		Begin Loop	3 times "Sampling"
126		Comment	SAMPLING #2, 3, 4
127		Begin Loop	2 times "Seventy"
128		Aspirate	 40 µl >> Water << 96 MP_GLASS_murni (Col. 1, Rows 1-5) , 1 option
129		Dispense	 40 µl >> Water << SWP_0.5eppendorf_carrier Murni (Col. 1, Rows 1-5) , 1 option
130		Drop DITIs	 DiTi waste, 1 Pos.

131	Get DITIs		DiTi200, 96 Tips, new tray
132	End Loop	""	
133	Begin Loop	2 times "Fifty"	
134	Aspirate		40 µl >> Water << 96 MP_GLASS_murni (Col. 3, Rows 1-5) , 1 option
135	Dispense		40 µl >> Water << SWP_0.5eppendorf_carrier Murni (Col. 6, Rows 1-5) , 1 option
136	Drop DITIs		DiTi waste, 1 Pos.
137	Get DITIs		DiTi200, 96 Tips, new tray
138	End Loop	"Fifty"	
139	Begin Loop	1 times "Twenty Five"	
140	Aspirate		40 µl >> Water << 96 MP_GLASS_murni (Col. 5, Rows 1-5) , 1 option
141	Dispense		40 µl >> Water << SWP_0.5eppendorf_carrier Murni (Col. 11, Rows 1-5) , 1 option
142	Drop DITIs		DiTi waste, 1 Pos.
143	End Loop	"Twenty Five"	
144	Get DITIs		DiTi1000, 96 Tips, new tray
145	Comment	Add: 0.2 % TFA	
146	Begin Loop	2 times "70"	
147	Aspirate		360 µl >> Water << Trough 100ml (Col. 1, Rows 1-5)
148	Dispense		360 µl >> Water << SWP_0.5eppendorf_carrier Murni (Col. 1, Rows 1-5) , 1 option
149	End Loop	"70"	
150	Drop DITIs		DiTi waste, 1 Pos.
151	Get DITIs		DiTi1000, 96 Tips, new tray
152	Begin Loop	2 times "50"	
153	Aspirate		360 µl >> Water << Trough 100ml (Col. 1, Rows 1-5)
154	Dispense		360 µl >> Water << SWP_0.5eppendorf_carrier Murni (Col. 6, Rows 1-5) , 1 option
155	End Loop	"50"	
156	Drop DITIs		DiTi waste, 1 Pos.

157	Get DITIs		DiTi1000, 96 Tips, new tray
158	Begin Loop		1 times "25"
159	Aspirate		360 µl >> Water << Trough 100ml (Col. 1, Rows 1-5)
160	Dispense		360 µl >> Water << SWP_0.5eppendorf_carrier Murni (Col. 11, Rows 1-5) , 1 option
161	End Loop		"25"
162	Drop DITIs		DiTi waste, 1 Pos.
163	Wash Tips		2.0 + 1.0 ml
164	Start Timer		2
165	Wait Timer		Timer 2 : 36000 sec
166	End Loop		""



TECAN SCRIPTS

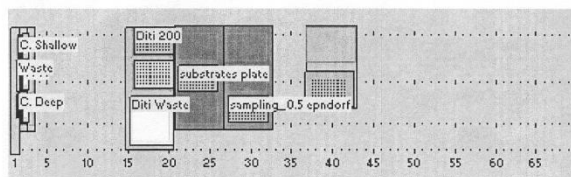
Figure A.IV. 3. Parallel evaluation of reduced pressure reactvion (Section 5.7).

1		Wash Tips		2.0 + 1.0 ml
2		Get DITIs		DiTi1000, 96 Tips, new tray
3		User Prompt	"Add 0.5 ependorf on SWP_carrier MH (G27/ S3)" sound : three times	
4		Comment	Add : 0.2% TFA	
5		Begin Loop	2 times "tfa"	
6		Aspirate		360 µl Water "TFA" (Col. 1, Rows 1-3)
7		Dispense		360 µl Water "sampling_0.5 ependorf" (Col. 1, Rows 1-3) , 1 option
8		End Loop	"tfa"	
9		Drop DITIs		"Diti Waste"
10		Get DITIs		DiTi200, 96 Tips, new tray
11		User Prompt	"Place COVER PLATE for Vac on Carrier MH (G21/S1)" sound : three times	
12		Comment	Add Enzyme: TAm	
13		Aspirate		100 µl Water "substrates plate" (Col. 1, Rows 1-3)
14		Dispense		100 µl Water 96 MP_GLASS_VACUUM_murni (Col. 7, Rows 4-6)
15		Comment	Add co-factor:PLP	
16		Aspirate		15 µl Water "substrates plate" (Col. 2, Rows 1-3)
17		Dispense		15 µl Water 96 MP_GLASS_VACUUM_murni (Col. 7, Rows 4-6)
18		Comment	Add substrate:50mM HEPES	
19		Aspirate		125 µl Water "HEPES" (Col. 1, Rows 1-3)
20		Dispense		125 µl Water 96 MP_GLASS_VACUUM_murni (Col. 7, Rows 4-6)
21		Start Timer	1	
22		Wait Timer	Timer 1 : 10 sec	
23		Comment	Add substrate:Ery	
24		Aspirate		15 µl Water "substrates plate" (Col. 3, Rows 1-3)
25		Dispense		15 µl Water 96 MP_GLASS_VACUUM_murni (Col. 7, Rows 4-6)

27	Aspirate		45 µl Water "substrates plate" (Col. 4, Row 1)
28	Aspirate		45 µl Water "substrates plate" (Col. 4, Row 1)
29	Aspirate		45 µl Water "substrates plate" (Col. 4, Row 1)
30	Dispense		45 µl Water 96 MP_GLASS_VACUUM_murni (Col. 7, Rows 4-6)
31	Mix		3 x 100 µl Water 96 MP_GLASS_VACUUM_murni (Col. 7, Rows 4-6)
32	Drop DITIs		"Diti Waste"
33	Get DITIs		DiTi200, 96 Tips, new tray
34	Comment		SAMPLING TIME = 0
35	Aspirate		40 µl Water 96 MP_GLASS_VACUUM_murni (Col. 7, Rows 4-6)
36	Dispense		40 µl Water "sampling_0.5 epndorf" (Col. 1, Rows 1-3)
37	Wash Tips		2.0 + 1.0 ml
38	Drop DITIs		"Diti Waste"
39	ROMA Vector		Vector "White plastic plate_carrier MH", Grid 21, Site 1 (ROMA 1) open, from Safe to End Position, grip, from End to Safe Position
40	ROMA Vector		Vector "SPE Block plate_murni", Grid 37, Site 2 (ROMA 1) from Safe to End Position, open, from End to Safe Position
41	Move ROMA		Move to home position (ROMA 1)
42	Comment		APPLY VACUUM (@ T=0 for 1 hours)
43	Vac. Separator		Grid 37 Apply vacuum to block 2, 30 mbar
44	Start Timer		1
45	Wait Timer		Timer 1 : 3600 sec
46	Vac. Separator		Grid 37 Vent block 2
47	Vac. Separator		Grid 37 Deactivate system
48	ROMA Vector		Vector "SPE Block plate_murni", Grid 37, Site 2 (ROMA 1) open, from Safe to End Position, grip, from End to Safe Position
49	ROMA Vector		Vector "White plastic plate_carrier MH", Grid 21, Site 1 (ROMA 1) from Safe to End Position, open, from End to Safe Position
50	Move ROMA		Move to home position (ROMA 1)
51	Comment		SAMPLING TIME=1 hours
52	Get DITIs		DiTi200, 96 Tips, new tray

53		Aspirate	  40 µl Water 96 MP_GLASS_VACUUM_murni (Col. 7, Rows 4-6)
54		Dispense	  40 µl Water "sampling_0.5 epndorf" (Col. 2, Rows 1-3)
55		Drop DITIs	 "Diti Waste"
56		User Prompt	"pipette water of evaporation control" sound : three times
57		ROMA Vector	Vector "White plastic plate_ carrier MH", Grid 21, Site 1 (ROMA 1) open, from Safe to End Position, grip, from End to Safe Position
58		ROMA Vector	Vector "SPE Block plate_murni", Grid 37, Site 2 (ROMA 1) from Safe to End Position, open, from End to Safe Position
59		Move ROMA	Move to home position (ROMA 1)
60		Comment	APPLY VACUUM (@ T=1 for 14 hours)
61		Vac. Separator	Grid 37 Apply vacuum to block 2, 30 mbar
62		Start Timer	1
63		Wait Timer	Timer 1 : 50400 sec
64		Vac. Separator	Grid 37 Vent block 2
65		Vac. Separator	Grid 37 Deactivate system
66		ROMA Vector	Vector "SPE Block plate_murni", Grid 37, Site 2 (ROMA 1) open, from Safe to End Position, grip, from End to Safe Position
67		ROMA Vector	Vector "White plastic plate_ carrier MH", Grid 21, Site 1 (ROMA 1) from Safe to End Position, open, from End to Safe Position
68		Move ROMA	Move to home position (ROMA 1)
69		Comment	SAMPLING TIME= 15 hours
70		Get DITIs	 DiTi200, 96 Tips, new tray
71		Aspirate	  40 µl Water 96 MP_GLASS_VACUUM_murni (Col. 7, Rows 4-6)
72		Dispense	  40 µl Water "sampling_0.5 epndorf" (Col. 3, Rows 1-3)
73		Drop DITIs	 "Diti Waste"
74		User Prompt	"pipette water of evaporation control" sound : three times
75		ROMA Vector	Vector "White plastic plate_ carrier MH", Grid 21, Site 1 (ROMA 1) open, from Safe to End Position, grip, from End to Safe Position
76		ROMA Vector	Vector "SPE Block plate_murni", Grid 37, Site 2 (ROMA 1) from Safe to End Position, open, from End to Safe Position
77		Move ROMA	Move to home position (ROMA 1)
78		Comment	APPLY VACUUM (@ T=2 for 3 hours)

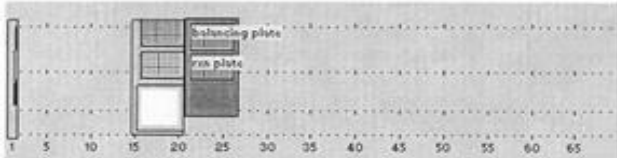
79		Vac. Separator	Grid 37 Apply vacuum to block 2, 30 mbar
80		Start Timer	1
81		Wait Timer	Timer 1 : 10800 sec
82		Vac. Separator	Grid 37 Vent block 2
83		Vac. Separator	Grid 37 Deactivate system
84		ROMA Vector	Vector "SPE Block plate_murni", Grid 37, Site 2 (ROMA 1) open, from Safe to End Position, grip, from End to Safe Position
85		ROMA Vector	Vector "White plastic plate_carrier MH", Grid 21, Site 1 (ROMA 1) from Safe to End Position, open, from End to Safe Position
86		Move ROMA	Move to home position (ROMA 1)
87		Comment	SAMPLING TIME=19hours
88		Get DITIs	 DiTi200, 96 Tips, new tray
89		Aspirate	 40 µl Water 96 MP_GLASS_VACUUM_murni (Col. 7, Rows 4-6)
90		Dispense	 40 µl Water "sampling_0.5 epndorf" (Col. 4, Rows 1-3)
91		Drop DITIs	 "Diti Waste"

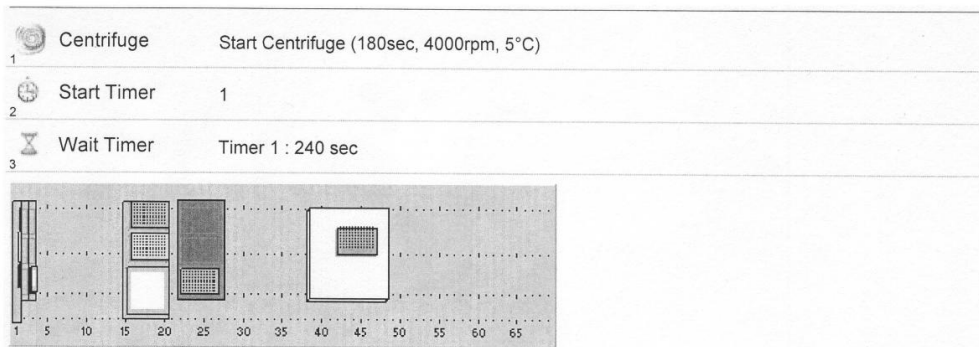


TECAN SCRIPTS

Figure A.IV. 4. Bioconversion reactions samples centrifugation step prior HPLC analysis (Sections 5.5, 5.6 and 5.7).

1	Comment	Pick up reaction plate from carrier 1 site 2
2	ROMA Vector	Vector "White DEEP plate_carrier MH", Grid 21, Site 2 (ROMA 1) open, from Safe to End Position, grip, from End to Safe Position
3	Centrifuge	Open Hatch
4	Centrifuge	Move Rotor to Position 1
5	ROMA Vector	Vector "Centrifuge_Load_MH", Grid 1, Site 1 (ROMA 1) from Safe to End Position, open, from End to Safe Position
6	Comment	Pick up balancing plate from carrier 1 site 1
7	ROMA Vector	Vector "White DEEP plate_carrier MH", Grid 21, Site 1 (ROMA 1) open, from Safe to End Position, grip, from End to Safe Position
8	Centrifuge	Move Rotor to Position 3
9	ROMA Vector	Vector "Centrifuge_Load_MH", Grid 1, Site 1 (ROMA 1) from Safe to End Position, open, from End to Safe Position
10	Centrifuge	Close Hatch
11	Sub-Routine	C:\Program Files\Gemini\Data\Murni\vectors\centrifuge\centrifuge_cond.gem Execute sub-routine and wait for it to finish
12	Centrifuge	Open Hatch
13	Centrifuge	Move Rotor to Position 1
14	Comment	Pick up reaction plate from centrifuge
15	ROMA Vector	Vector "Centrifuge_Load_MH", Grid 1, Site 1 (ROMA 1) open, from Safe to End Position, grip, from End to Safe Position
16	ROMA Vector	Vector "White DEEP plate_carrier MH", Grid 21, Site 2 (ROMA 1) from Safe to End Position, open, from End to Safe Position
17	Centrifuge	Move Rotor to Position 3
18	Comment	Pick up balancing plate from centrifuge
19	ROMA Vector	Vector "Centrifuge_Load_MH", Grid 1, Site 1 (ROMA 1) open, from Safe to End Position, grip, from End to Safe Position
20	ROMA Vector	Vector "White DEEP plate_carrier MH", Grid 21, Site 1 (ROMA 1) from Safe to End Position, open, from End to Safe Position
21	Centrifuge	Close Hatch



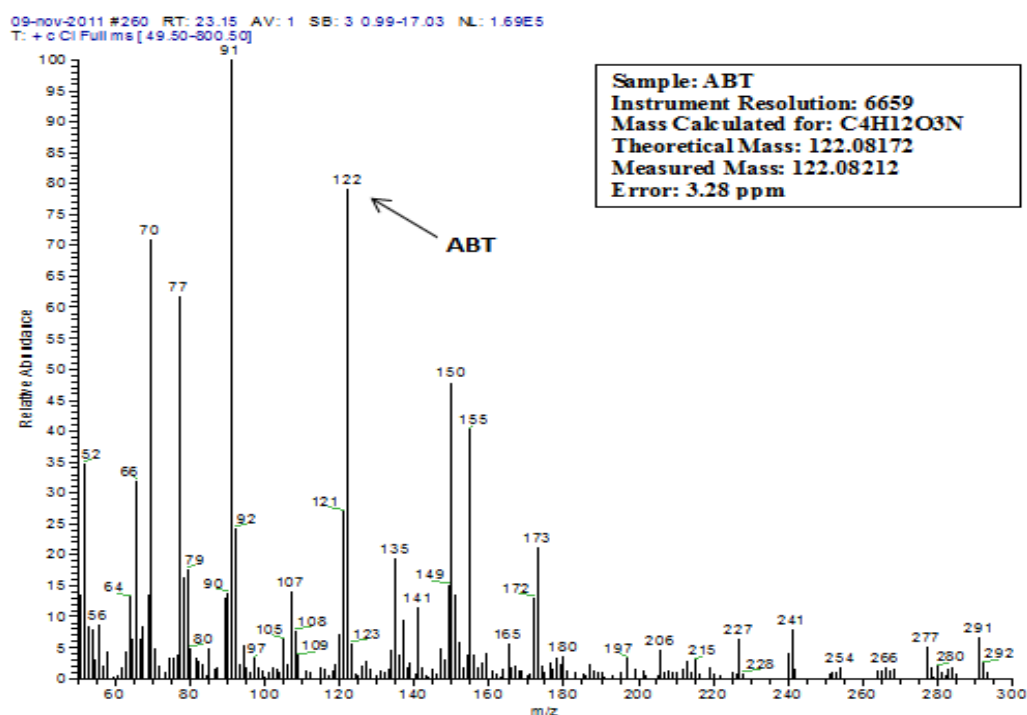


APPENDIX V

MASS SPECTROMETRY

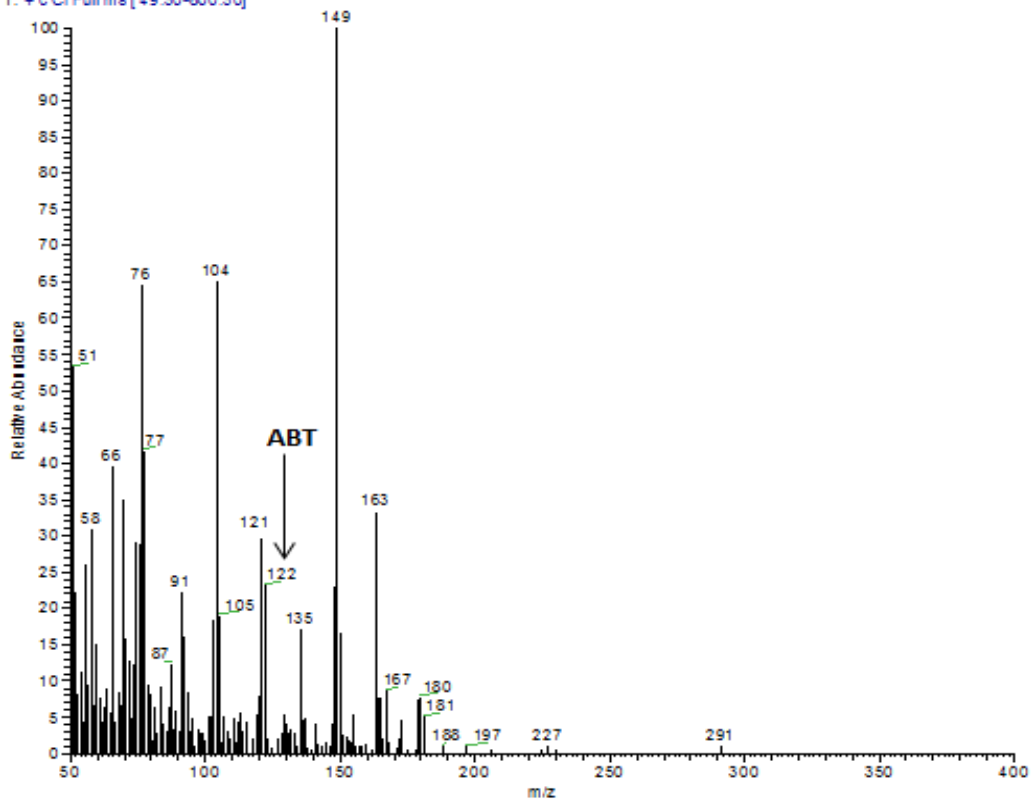
CHROMATOGRAMS

Chemical ionization (CI) mass spectrometry analyses were carried out on reaction mixture with ABT produced from CV2025 ω -TAM bioconversion of MBA and Ery with second enzyme reaction (Figure A.V.1), and BSU09260_1971 ω -TAM bioconversion of L- α -serine and ERY (Figure A.V.2). Results were compared with previous ABT MS-MS standards (Ingram, 2007).



Appendix A.V.1. Chemical ionization (CI) mass spectrometry analysis for reaction mixture with ABT produced from CV2025 ω -TAM bioconversion of MBA and Ery with second enzyme reaction using ADH from *Lactobacillus kefir* (Section 6.3).

09-nov-2011 #341 RT: 31.54 AV: 1 SB: 3 0.99-17.03 NL: 1.14E5
T: + c CI Full ms [49.50-300.50]



Appendix A.V.2. Chemical ionization (CI) mass spectrometry analysis for reaction mixture with ABT produced from BSU09260_1971 ω -TAm bioconversion of L- α -serine and ERY (Section 6.4.1).